# CARBON NANOTUBE PRODUCTION

A THESIS SUBMITTED TO
THE GRADUATE SCHOOL OF NATURAL AND APPLIED SCIENCES
OF
MIDDLE EAST TECHNICAL UNIVERSITY

BY

CANER HOCAOĞLU

IN PARTIAL FULFILLMENT OF THE REQUIREMENTS
FOR
THE DEGREE OF MASTER OF SCIENCE
IN
CHEMICAL ENGINEERING

NOVEMBER 2011

Approval of the thesis:

**CARBON NANOTUBE PRODUCTION**

submitted by **CANER HOCAOĞLU** in partial fulfillment of the requirements for the degree of Master of Science in **Chemical Engineering Department, Middle East Technical University** by,

Prof. Dr. Canan ÖZGEN _____
Dean, Graduate School of **Natural and Applied Sciences**

Prof. Dr. Deniz ÜNER _____
Head of Department, **Chemical Engineering**

Assoc. Prof. Dr. Naime Aslı SEZGİ _____
Supervisor, **Chemical Engineering Dept., METU**

Prof. Dr. H. Önder ÖZBELGE _____
Co-Supervisor, **Chemical Engineering Dept., METU**

**Examining Committee Members:**

Prof. Dr. Timur DOĞU _____
Chemical Engineering Dept., METU

Assoc. Prof. Dr. Naime Aslı SEZGİ _____
Chemical Engineering Dept., METU

Prof. Dr. H. Önder ÖZBELGE _____
Chemical Engineering Dept., METU

Prof. Dr. Göknur BAYRAM _____
Chemical Engineering Dept., METU

Prof. Dr. Suna BALCI _____
Chemical Engineering Dept., Gazi University

**Date:** **03.11.2011**

**I hereby declare that all information in this document has been obtained and presented in accordance with academic rules and ethical conduct. I also declare that, as required by these rules and conduct, I have fully cited and referenced all material and results that are not original to this work.**

Name, Last Name: Caner HOCAOĞLU

Signature :

# ABSTRACT

CARBON NANOTUBE PRODUCTION

Hocaoğlu, Caner

M.Sc., Department of Chemical Engineering

Supervisor: Assoc. Prof. Dr. Naime Aslı Sezgi

Co-Supervisor: Prof. Dr. H. Önder Özbelge

November 2011, 188 pages

Carbon nanotubes (CNTs), allotropes of carbon with a cylindrical nanostructure, are one of the most attractive research subjects for scientists and industry because of their extraordinary chemical, electrical, optical, mechanical and thermal properties, and their wide range of potential application areas. Mainly, there are two types of carbon nanotubes: single-walled carbon nanotubes (SWNTs) and multi-walled carbon nanotubes (MWNTs).

The most commonly used methods for carbon nanotube production are arc discharge, laser ablation, and chemical vapor deposition (CVD). In the CVD method, CNTs are produced from thermal decomposition of the carbon-containing molecules on a suitable transition metal catalyst. CVD method enables large scale production of

high-quality CNTs with low cost compared to other methods. The growth and morphology of CNTs can be controlled by adjusting the reaction parameters.

In this study, Co and Mo impregnated $CaCO_3$ catalysts were synthesized at different Co:Mo weight ratios and calcined at different temperatures. XRD results showed that there was mainly $CaCO_3$ compound in the catalysts calcined at 500ºC whereas the catalysts calcined at 700 and 750 ºC were mainly composed of CaO and $Ca(OH)_2$ compounds. In addition to these, $CaMoO_4$, CoO, $CoMoO_4$ and $Mo_2C$ were the other solid phases mainly observed in all catalysts.

The production of CNTs was performed by chemical vapor deposition of acetylene at a temperature range of 500-700˚C using Co-Mo/$CaCO_3$ catalysts. The synthesized nanotubes were purified with a single-step purification process in diluted nitric acid solution.

SEM and TEM results showed that the synthesized materials were multi-walled carbon nanotubes with outer diameter ranging from 13 to 138 nm. MWNTs were mostly closed-end.

The CNT yield was increased with an increase in the catalyst calcination and reaction temperatures. The rise in the Co:Mo weight ratio also resulted in higher CNT yields. The highest CNT yield was obtained at a reaction temperature of 700˚C using the catalyst with a Co:Mo weight ratio of 6 and a calcination temperature of 750ºC.

An increase in nanotube diameters was observed with an increase in synthesis temperature. Thermal analyses revealed that the oxidation temperatures of MWNTs were around 700ºC and the purity of MWNTs was generally higher than 96%. On the other hand, Raman spectroscopy results showed the presence of structural defects in CNTs.

Purified MWNTs showed Type II isotherms for nitrogen adsorption. Multi-point BET surface areas of purified nanotubes were in the range of 24.8-89.9 $m^2/g$.

**Keywords:** Carbon Nanotubes, Chemical Vapor Deposition, Cobalt, Molybdenum, Calcium Carbonate.

# ÖZ

KARBON NANOTÜP ÜRETİMİ

Hocaoğlu, Caner

Yüksek Lisans, Kimya Mühendisliği Bölümü

Tez Yöneticisi: Doç. Dr. Naime Aslı Sezgi

Ortak Tez Yöneticisi: Prof. Dr. H. Önder Özbelge

Kasım 2011, 188 sayfa

Silindirik nanoyapısı ile, bir karbon alotropu olan karbon nanotüpler; sıradışı kimyasal, elektriksel, optik, mekanik ve termal özellikleri ve geniş potansiyel uygulama alanlarından dolayı bilim adamları ve endüstri için en ilgi çekici araştırma konularından biridir. Esas olarak, iki tip karbon nanotüp vardır: tek duvarlı karbon nanotüpler ve çok duvarlı karbon nanotüpler.

Karbon nanotüp üretimi için en çok kullanılan metotlar ark boşalma, lazer ablasyon ve kimyasal buhar biriktirmedir. Kimyasal buhar biriktirme metodunda, karbon nanotüpler, karbon içeren moleküllerin uygun geçiş metal katalizörü üzerinde ısıl ayrışmasından üretilirler. Kimyasal buhar biriktirme yöntemi, diğer metotlara nazaran ucuz maliyetle yüksek kaliteli karbon nanotüplerin büyük miktarda

üretilmesine imkan verir. Karbon nanotüplerin oluşumu ve morfolojileri reaksiyon parametrelerinin ayarlanması ile kontrol edilebilir.

Bu çalışmada, Co ve Mo emdirilmiş $CaCO_3$ katalizörler farklı Co:Mo ağırlık oranlarında sentezlenmiş ve farklı sıcaklıklarda kalsine edilmiştir. XRD sonuçları, 500ºC'de kalsine edilmiş katalizörlerde başlıca $CaCO_3$ bileşiği varken, 700 ve 750ºC'de kalsine edilmiş katalizörlerin başlıca, CaO ve $Ca(OH)_2$ bileşiklerinden oluştuğunu göstermiştir. Bunlara ek olarak; $CaMoO_4$, CoO, $CoMoO_4$ ve $Mo_2C$ bütün katalizörlerde gözlenmiş diğer başlıca katı fazlarıdır.

Karbon nanotüp üretimi, Co-Mo/$CaCO_3$ katalizörleri kullanarak 500-700ºC sıcaklık aralığında, asetilenin kimyasal buhar biriktirilmesiyle yapılmıştır. Üretilen nanotüpler, seyreltik nitrik asit çözeltisi içinde tek aşamalı saflaştırma işlemi ile saflaştırılmıştır.

SEM ve TEM sonuçları, sentezlenen malzemelerin, dış yarıçapları 13 nm'den 138 nm'ye değişen, çok duvarlı karbon nanotüpler olduğunu göstermiştir. Çok duvarlı karbon nanotüpler çoğunlukla kapalı uçludur.

Karbon nanotüp verimi, katalizör kalsinasyon ve reaksiyon sıcaklıkları ile artmıştır. Co:Mo ağırlık oranındaki artış da daha yüksek karbon nanotüp verimliliğine neden olmuştur. En yüksek karbon nanotüp verimi; 700ºC reaksiyon sıcaklığında, Co:Mo oranı 6 ve kalsinasyon sıcaklığı 750ºC olan katalizör ile elde edilmiştir.

Sentez sıcaklığındaki artış ile nanotüp çaplarında bir artış gözlenmiştir. Termal analizler, çok duvarlı karbon nanotüplerin oksidasyon sıcaklığının 700ºC civarında olduğunu ve çok duvarlı karbon nanotüplerin saflığının genelde %96'dan yüksek olduğunu göstermiştir. Öte yandan, Raman spektroskopi sonuçları karbon nanotüplerde yapısal bozuklukların olduğunu göstermiştir.

Saflaştırılmış nanotüpler, nitrojen adsorbsiyonu için Tip II izotermi göstermiştir. Saflaştırılan karbon nanotüplerin çok nokta BET yüzey alanları 24,8-89,9 $m^2/g$ aralığındadır.

**Anahtar Kelimeler**: Karbon Nanotüpler, Kimyasal Buhar Biriktirme, Kobalt, Molibden, Kalsiyum Karbonat.

**To my family and my love,**

# ACKNOWLEDGEMENTS

First, I want to express my deepest appreciation to my supervisor Assoc. Prof. Dr. Naime Aslı Sezgi for her guidance, her humanity, her kindly attitude toward me, her continuous support and encouragement throughout this study. I also express my thanks and appreciations to my co-supervisor Prof. Dr. Hilmi Önder Özbelge for his kindly attitude, help and suggestions.

I also would like to thank Dr. Zeynep Obalı, Seval Gündüz, Sultan Orman, Gökhan Çelik, Canan Şener, Hakan Demir, Ceren Kasapoğlu, Ayça Arınan, K. Cem Tokay, Buğçe Aydemir, Özge Mercan and Birce Pekmezci for their help and friendship.

I wish to thank METU Central Laboratory, METU Metallurgical and Materials Department and METU Chemical Engineering Department for the analyses of the catalysts and products. I also want to thank the technicians of Chemical Engineering Department for their help during the preparation of the experimental setup.

Finally, I would like to present my greatest and deepest thanks to my family and Deniz for their continuous support, encouragement and patience throughout this study.

# TABLE OF CONTENTS

# LIST OF TABLES

## TABLES

# LIST OF FIGURES

**FIGURES**

# NOMENCLATURE

| | |
|---|---|
| I | Intensity |
| m | Weight (g) |
| $m_C$ | Weight of catalyst after decomposition reaction (g) |
| $m_T$ | Total weight of material after synthesis (g) |
| MW | Molecular weight (g/gmol) |
| n | Number of moles (moles) |
| $R_C$ | Carbon deposition rate (g/min) |
| $T_{cal}$ | Calcination temperature (°C) |
| $T_{rxn}$ | Reaction temperature (°C) |
| $t_{rxn}$ | Reaction time (min) |
| $w_x$ | Weight percent (%) |
| Y | Yield (%) |

**Greek Letters**

| | |
|---|---|
| 2θ | Bragg angle (°) |

**Abbreviations**

| | |
|---|---|
| AFM | Atomic Force Microscope |
| BDDT | Brauner-Deming-Deming-Teller |
| BET | Brunauer, Emmett and Teller |
| CNT | Carbon Nanotube |
| CVD | Chemical Vapor Deposition |
| DTA | Differential Thermal Analysis |
| EDS | Energy Dispersive X-ray Spectroscopy |
| MWNT | Multi-walled Carbon Nanotube |
| PECVD | Plasma Enhanced Chemical Vapor Deposition |
| SEM | Scanning Electron Microscopy |
| SWNT | Single-walled Carbon Nanotube |
| TEM | Transmission Electron Microscopy |
| TGA | Thermal Gravimetric Analysis |
| XPS | X-ray Photoelectron Spectroscopy |
| XRD | X-Ray Diffraction |

# CHAPTER 1

# INTRODUCTION

Nanotechnology which is an interdisciplinary field including chemistry, physics, material science and biology enables to observe and manufacture structures at nanometer scale. Since first introduction of nanotechnology as a concept in 1959 [1], it has been considered to be one of the revolutionary technologies due to its great potential to change the future and improve standards of humanity. Nanotechnology has gained a huge interest and become one of the most popular research areas in recent years with its potential to effect every part of life. Great improvements in health, agriculture, new materials, electronics, energy resources, automobile and aerospace industries, and construction are possible with the help of nanotechnology [2]. One of the results of the advancement in nanotechnology is the capability of manufacturing nano-sized materials which have novel chemical, physical and biological properties due to their small size and large surface area. Buckministerfullerene ($C_{60}$) and carbon nanotubes (CNTs) are examples for these materials with superior properties.

Carbon nanotubes, an allotrope of carbon with a cylindrical shape, have become the main building block of the entire nanotechnology since their discovery in 1991 [1]. The scientific and industrial attention to CNTs grow dramatically due to their extraordinary mechanical, electrical, thermal and chemical properties. Although CNTs are more lighter they are much stronger than steel. They have a current capacity 1000 times higher than copper while their thermal capacity is twice that of diamond [2]. Because of these terrific properties they have a wide range of potential application areas some of which are automotive and aerospace industries, electronics,

biotechnology, medical fields, sensors, and fuel cells [3]. However, the use of nanotubes was limited today because of their low production quantity and quality.

Carbon nanotubes are generally produced by three methods, namely, arc discharge, laser ablation, and chemical vapor deposition (CVD) [4]. Arc discharge and laser ablation require special equipment and high amount of energy which limits the large scale production of CNTs. On the contrary, CVD seems to be the most promising method for the production of high quality nanotubes in large quantities. It is considered as an easy and relatively cheap production method for CNTs. CVD method involves the decomposition of a carbon-containing gas over suitable catalysts at high temperatures. The reaction parameters such as synthesis temperature and time, pressure, gaseous carbon source, catalyst, can be controlled in the CVD technique.

In this study, an experimental setup for the production of carbon nanotubes by CVD method was designed and constructed. The catalysts used for the CNT production were synthesized with different Co:Mo weight ratios and calcination temperatures. Carbon nanotubes were produced over Co:Mo binary metal catalyst supported over calcium carbonate ($CaCO_3$) from the thermal decomposition of acetylene which was the carbon precursor. The reaction temperature for the nanotube growth was in the range of 500-1000˚C. The synthesized nanotubes were purified in one single-step purification with diluted nitric acid. Finally, purified carbon nanotubes and synthesized catalysts were characterized in order to understand the relationship between the catalyst and carbon nanotube growth. The effect of Co:Mo weight ratio in catalysts, reaction and catalyst calcination temperatures on the CNT yield was investigated. Additionally, the effect of the acetylene inlet composition in argon was also observed.

# CHAPTER 2

# CARBON NANOTUBES

## 2.1 Nanotechnology

Nanotechnology is one of the key technologies of the 21$^{st}$ century and considered to be a revolutionary technology. It is an interdisciplinary field including chemistry, physics, biology, material science, medicine, and engineering.

Nanotechnology is the term used for the research and development of materials, devices, and systems at nanometer scale [2]. It enables the observation, measurement, manipulation and manufacture things on molecular scale in today's world. The prefix "nano" originates from the Greek word "nanos" which means dwarf and corresponds to $10^{-9}$ meters. A nanometer (nm) is one-billionth of a meter (m) [5]. As a concept, nanotechnology was first mentioned by Richard Feynman in 1959 with his famous word: "There is plenty of room at the bottom [1]."

The area of interest of nanotechnology is materials having a size in the range of 1-100 nm at least in one dimension. These materials are called nanomaterials. Nanomaterials have unique and extraordinary chemical, mechanical, electrical, optical, thermal and magnetic properties due to their size and surface effect properties which make them ideal for the use in composite materials, drug delivery, chemical energy storage [2].

Nanotechnology has a great potential to change the future and to improve the life of humanity. It is able to impact the key scientific and technological activities

positively. Additionally, it has a promising potential to solve the problems related to other science and technology. According to the predictions of the US National Science Foundation, nanotechnology will become a big industry for many countries and the worth of nanotechnology market can be one trillion dollars by 2015 [2].

Some of the major application areas of nanotechnology are electronics and semiconductor industry, automotive and aerospace industries, agriculture, biotechnology and bioengineering, solar energy, materials science, medical fields, pharmaceuticals, military science and technology, fuel cells and batteries, and sport equipment.

## 2.2 Carbon Materials

Carbon in different forms has been used in the science and technology throughout history. Carbon in the solid phase has several allotropes which have different molecular structures and properties. The mostly known allotropes of carbon are graphite, diamond and amorphous carbon. There are also new discovered forms of carbon, namely fullerenes and carbon nanotubes (CNTs). The properties of carbon allotropes vary according to the arrangement of carbon atoms. Some properties of the allotropes of carbon are briefly mentioned below.

Diamond which is known to be the hardest substance is purely composed of $sp^3$ hybridized bonds. In the crystalline structure of diamond, each $sp^3$ hybridized carbon atom is bonded to other four carbon atoms in a tetrahedral arrangement. The hardness and excellent heat conduction properties of diamond result from this crystalline network. Furhermore, these $sp^3$ hybridized bonds are associated with electrically insulating property and optical transparency of diamond [3]. The structure of diamond is represented in Figure 2.1.

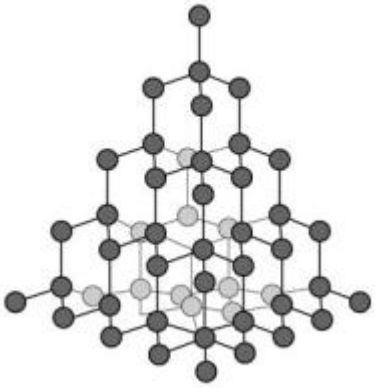

**Figure 2.1** Structure of diamond **[2].**

The structure of graphite (Figure 2.2) consists of layered planar sheets of $sp^2$ hybridized carbon atoms which are bonded to only three other carbon atoms in a hexagonal network. Due to this different bond geometry graphite is soft, opaque and slippery. It is a semi-metal and electrically conductive because of the electrons moving freely. Graphite consists of graphene sheets with an interplanar spacing of 3.354 Å . These sheets scan slide upon each other due to the weak interplanar bond spaced at this distance [6].

The structure of graphene is one-atom-thick planar sheets of $sp^2$ bonded carbon atoms. These atoms are densely packed in a honeycomb crystal lattice. Some carbon allotropes like graphite, fullerenes and carbon nanotubes have graphene as the basic structural element [7].

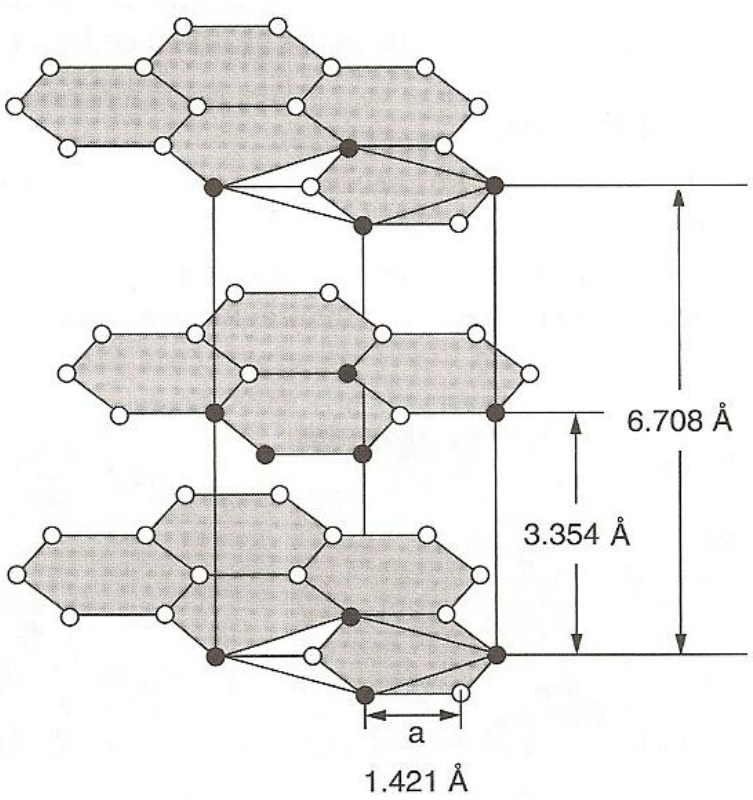


**Figure 2.2** Structure of graphite **[6].**

Amorphous carbon (Figure 2.3) which is another allotrope of carbon does not have any crystalline structure. The term "amorphous" has a meaning of lacking a definite form or having no specific shape. Amorphous carbon is generally abbreviated to aC and is composed of a highly disordered network of carbon atoms which mostly have $sp^2$ bonding [8].

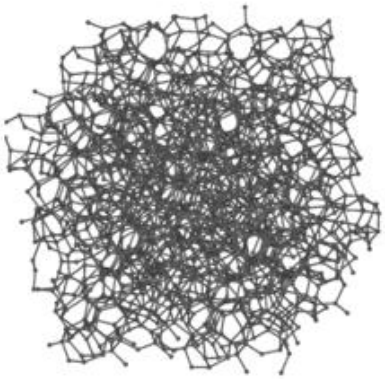

**Figure 2.3** Amorphous carbon **[8]**.

Only three allotropes of carbon which are diamond, graphite, and amorphous carbon were known in 1980's. Then in 1985, fullerenes were discovered by Kroto, Smalley, and Curl [1]. For this discovery, they were awarded the Nobel Prize in Chemistry in 1996. Fullerenes (Figure 2.4) are spheroidal molecules composed of entirely carbon atom. The most common fullerenes are $C_{60}$ and $C_{70}$. $C_{60}$ fullerene (Buckminsterfullerene) was the first fullerene discovered. It is a hollow, cage-like fullerene molecule with 60 carbon atoms arranged in a spherical shape. The bonding in $C_{60}$ is actually $sp^2$ and each carbon is joined to three neighbours. However, there are also a small amount of $sp^3$-bonded atoms because of the curvature [5]. Buckminsterfullerene molecules are one of the most popular discoveries in nanotechnology and subjected to intense research due to their unique chemistry and potential technological applications. Later on, fullerenes with larger number of carbon atoms ($C_{76}$, $C_{80}$, $C_{240}$, etc.) were also discovered [6].

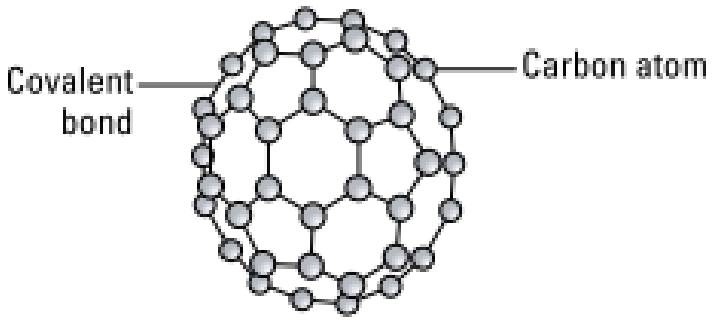


**Figure 2.4** Structure of a fullerene **[9].**

## 2.3 Carbon Nanotubes (CNTs)

Carbon nanotubes are one-dimensional nanomaterials with a high aspect ratio which were discovered by Iijima in 1991 using an electron microscope while he was producing fullerenes in an electric arc-evaporation reactor. With the discovery of CNTs a new era in nanotechnology has started. After the discovery of CNTs, carbon nanotechnology can be thought as the main building block of the entire nanotechnology [1]. There have been plenty of studies and a large number of researches carried out on the carbon nanotubes since their discovery.

Carbon nanotubes (Figure 2.5) are the cylindrical forms of fullerenes. They are hollow cylinders consisting of rolled graphite sheets. A CNTs are quasi-one dimensional structures and can be considered as single molecule. The diameters of CNTs are in nanometers while their lengths can reach centimeters [2, 3]. A carbon nanotube consists of graphene sheets appropriately rolled into a cylinder with a diameter in nanometer size. Therefore, it can be expected that the planar $sp^2$ bonding which is the characteristic of graphite plays a significant role in CNTs [10].

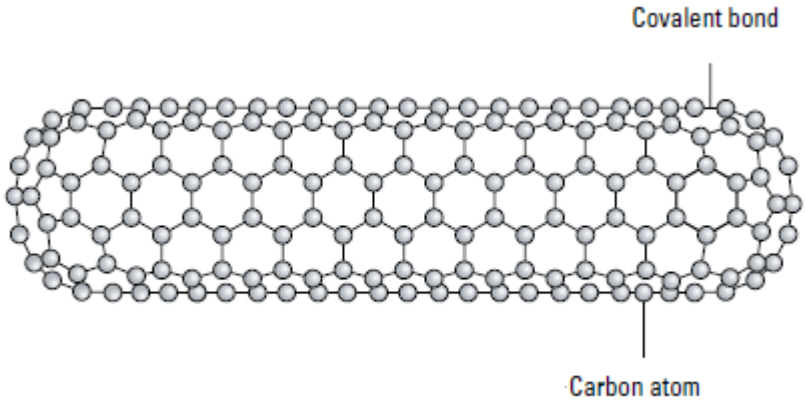


**Figure 2.5** Illustration of a carbon nanotube **[9].**

There are numerous experimental and theoretical studies about CNTs since they have extraordinary mechanical strength, stiffness, and elasticity characteristics, electronic properties ranging from semiconductors to metals, thermal and chemical properties. Carbon nanotubes have great potential for a wide range of applications, such as nanoelectronic devices, high performance composite materials, field emission displays [11].

### 2.3.1 The Structure of Carbon Nanotubes

The structure of an individual nanotube can be conceptualized by rolling a layer of graphite with a thickness of one atom into a hollow cylinder. Hence, carbon nanotubes can be classified in terms of the way how the graphene sheet is rolled.

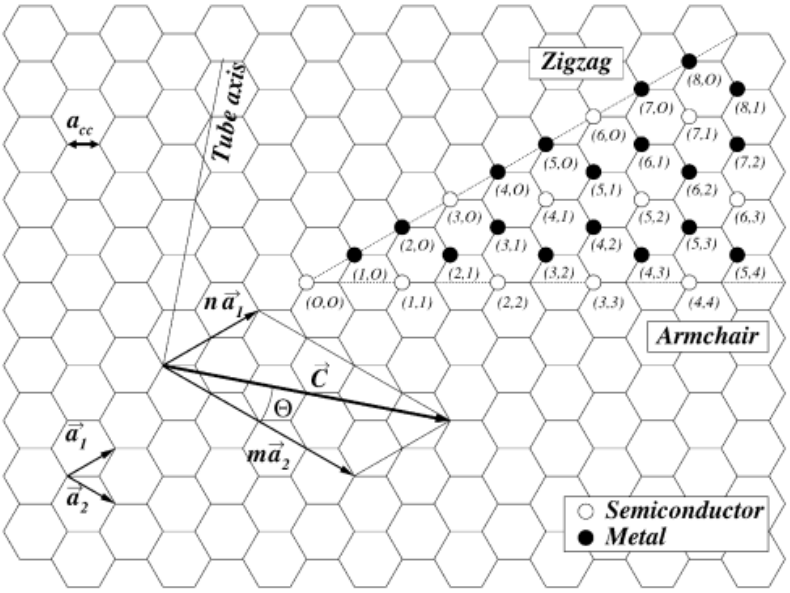


**Figure 2.6** Schematic representation of a graphene sheet **[12].**

Graphene lattice vectors (Figure 2.6) are mostly used for specifying the exact structure of an individual nanotube because of the fact that CNTs have microscopic structure similar to that of graphene. The way of wrapped graphene sheet can be described by a single vector $\vec{C}$ which is called chiral vector. Two atoms in a planar graphene sheet one of which is used as origin are selected. As the chiral vector $\vec{C}$ is pointed from the origin toward the second atom the relation is defined as

$$\vec{C} = n\vec{a}_1 + m\vec{a}_2$$

where n and m are integers whereas $\vec{a}_1$ and $\vec{a}_2$ are unit vectors of the two-dimensional lattice which is generated by the graphene sheets. The angle between the chiral vector and the tube axis is called the chiral angle θ [12].

There are three different types of CNTs because of the different rolling ways of graphene sheets. If n=m (θ=30º), nanotubes are called armchair tubes while m=0

(θ=0º) for all zigzag nanotubes. All other nanotubes are chiral (0<θ<30º) [3]. Armchair, zig-zag and chiral configurations of carbon nanotubes are illustrated in Figure 2.7.

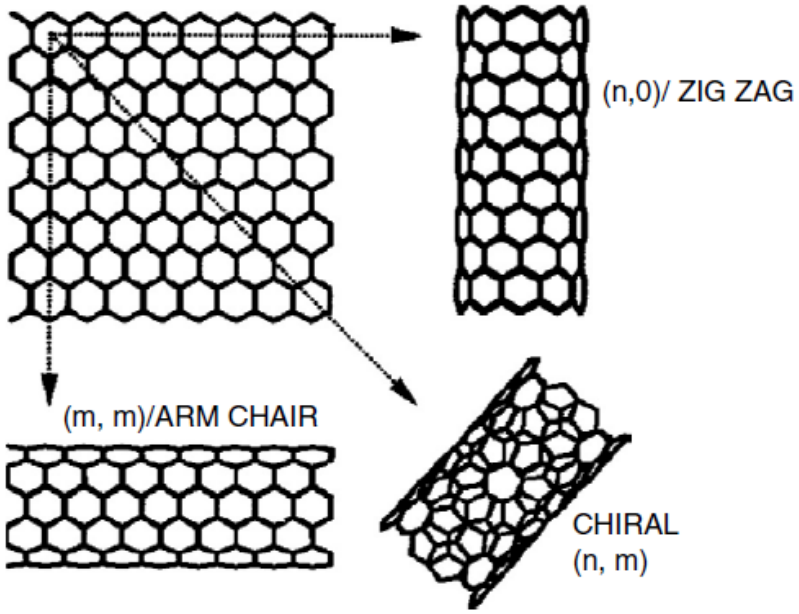


**Figure 2.7** Armchair, zig-zag and chiral configurations of CNTs **[11].**

These different structures of CNTs (zigzag, armchair, and chiral) can be understood by analyzing the pattern across the diameter of nanotubes and their cross-sectional structure. Armchair and zig-zag terms correspond to the arrangement of hexagons around the circumferences. These structures have a high degree of symmetry. On the other hand, chiral which is the most common one can exist in two mirror-related forms. The properties of CNTs such as mechanical strength and electrical conductivity differ because of these different chiral vectors [12].

Carbon nanotubes can also be classified with respect to the number of walls. According to the number of concentric cylindrical walls, there are mainly two types of carbon nanotubes: single-walled nanotubes (SWNTs) or multi-walled nanotubes

(MWNTs). There are also two-atom-thick CNTs called double-walled carbon nanotubes (DWNTs).

#### 2.3.1.1 Single-walled Nanotubes (SWNTs)

Single-walled carbon nanotubes (Figure 2.8) discovered in 1993 are a class of carbon nanotubes with only a single layer of graphite which is wrapped into a hollow cylindrical structure [3]. They have one dimensional structure with an axial symmetry. Most SWNTs have a diameter of close to one nanometer whereas their length can reach the value of centimeters .

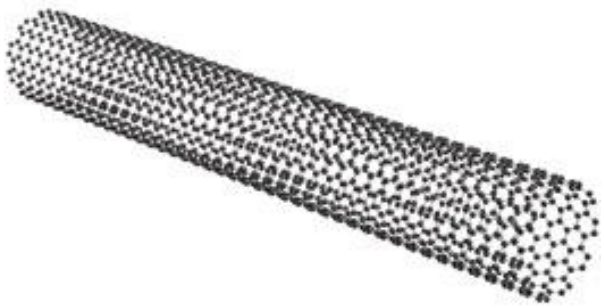

**Figure 2.8** A single-walled carbon nanotube **[5].**

Specific types of SWNTs are essential for more advance use of nanotubes. SWNTs are potentially appropriate candidates for a variety of applications especially for the electrical nanodevices.

#### 2.3.1.2 Multi-walled Nanotubes (MWNTs)

Multi-walled carbon nanotubes (Figure 2.9) discovered in 1991 by Iijima are a class of carbon nanotubes [13]. MWNTs have similar properties to that of graphite and

same distance between two graphene sheets which is 3.354 Å as the interlayer distance in graphite [6]. MWNTs have similar lengths to SWNTs; on the other hand, the diameters of MWNTs are much larger than that of SWNTs. They have inner and outer diameters of around 5 and 100 nm, respectively. Their properties also differ from those of SWNTs. Multi-walled carbon naotubes are more complex than SWNTs due to the number of walls and the interaction between them, nonuniformity and disorderliness [6].

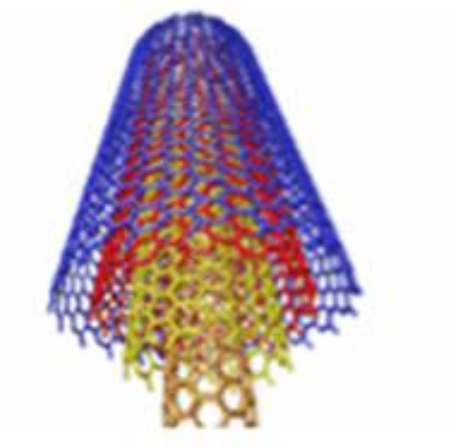

**Figure 2.9** A multi-walled carbon nanotube **[13].**

Most of the manufacturers prefer to produce MWNTs since it is easier to synthesize them when compared to SWNTs. Although MWNTs differ in length, width, and number of walls they are mostly added in bulk to have stronger polymers in products such as vehicle chassis and sport goods.

### 2.3.2 Properties of Carbon Nanotubes

The properties of CNTs including density, lattice structure, electrical, mechanical, and thermal conductivity are dependable on their structure. Type and diameter of nanotubes are also important factors affecting their structures. CNTs having wider diameters behave like graphite. As the diameter of a nanotube becomes smaller its characteristic properties depend more on its specific type. Carbon nanotubes have high surface area and high aspect ratio (i.e., length/diameter). The aspect ratio of CNTs is more than 1000:1. Additionally, the density of nanotubes with a value of 1.33 $g/cm^3$ is lower than that of aluminum (2.7 $g/cm^3$). Furthermore, carbon nanotubes are almost chemically inert; therefore, they do not react with other materials [2].

Other important and extraordinary properties of nanotubes are briefly explained below:

#### 2.3.2.1 Electrical Properties:

Carbon nanotubes have outstanding electrical properties. Depending on their specific structure they can be metallic or semiconducting. Whereas some CNTs can be semiconducting and behave like silicon, others can be metallic with a conductivity of higher than that of copper. The electrons in nanotubes can travel much faster than in metals such as copper, and they do not dissipate or scatter. A copper wire has a current capacity of 1 $MAmps/cm^2$; on the other hand, this value can reach 1 $GAmps/cm^2$ for carbon nanotubes. This makes nanotubes ideal candidates to replace copper wires [2].

There is great interest for constructing nanoscale electronic devices from nanotubes, and some progress is being made in this area. The electrical conductivity of the nanotubes could be useful in absorbing static noise, storing energy, or in replacing silicon circuits in computer chips [2].

### 2.3.2.2 Thermal Properties:

The highest measured thermal conductivity among all known materials belongs to crystalline carbon. Heat capacity and thermal conductivity of graphite and diamond are remarkable. The value of the thermal conductivity is 2000-2500 W $m^{-1}K^{-1}$ for pure diamond whereas it is 2000 W $m^{-1}K^{-1}$ for graphite [5].

CNTs have a better thermal conductivity when compared to that of diamond. Nanotube test results showed that its thermal conductivity is at least as twice as that of diamond. It was also found that CNTs have a thermal conductivity of about 6000 $Wm^{-1}K^{-1}$ at room temperature whereas copper well known for its good conductivity has a thermal conductivity of 385 $Wm^{-1}K^{-1}$. The exceptional thermal properties of nanotubes are based on their graphitic nature and their unique structure and size [11].

The thermal stability of CNTs is 750°C in the air and 1800°C in the inert atmosphere. SWNTs and MWNTs have different thermal behaviors. SWNTs are more stable than MWNTs. Although carbon nanotubes are very good thermal conductors along the tube, they are good insulators laterally to the tube axis [1].

### 2.3.2.3 Mechanical Properties:

As well as their electronic and thermal properties, carbon nanotubes have also attracted much interest owing to exceptional mechanical properties. It is a known fact that CNTs are the stiffest, strongest, and toughest fiber known and ever produced. They have extraordinary mechanical properties because of the strength of the $sp^2$ carbon-carbon bonds present in its structure [5].

The Young's modulus represents the stiffness of a material which is the rate of stress change with applied strain. Both theoretical calculations and experimental studies showed that MWNTs have higher Young's modulus than SWNTs. The highest Young's modulus of a carbon nanotube was recorded as 1.3 TPa [11]. This value is approximately five hundred times higher than that of steel. CNTs are much more

stronger than steel although they are six times lighter [2]. They can have a tensile strength of 150 GPa with an extraordinary elastic response to deformation of 15%. When these properties are combined with the lightness of CNTs, it is possible for them to have a terrific potential in applications such as aerospace [11].

Thanks to their exceptional mechanical properties carbon nanotubes have a notable potential to replace copper wires or to create superstrong plastics. There is also a great amount of research to produce composite materials containing CNTs. Nanotube/polymer composites having extraordinary mechanical properties were produced by several researchers [5].

### 2.3.3 Application Areas of Carbon Nanotubes

Carbon nanotubes have a variety of potential application areas due to their remarkable and unique electrical, magnetic, mechanical, thermal, and chemical properties. It can be said that CNTs with their nano sizes and lightness are able to replace plenty of materials in an amazing range of different areas. Because of the fact that different types of carbon nanotubes have distinct properties, their application areas also differ.

Today, carbon nanotubes are commercially available and already being used in several technological areas some of which are flat-panel displays, scanning probe microscopes, AFM tips [2]. In order to increase the range of their application areas some improvements in the growth and purification techniques of nanotubes must be fulfilled.

Due to their amazing properties they can be used in chemical-biological separation and purification, biomedical applications, energy and hydrogen storage, fuel cells, probe and sensors, transistors, field emission device, supercapacitors, battery electrodes, membrane filters, artificial muscles, drug delivery, and biosensors. Furthermore, carbon nanotubes are good candidates for structural applications due to

their stiffness. They can be used as reinforcements in high strength, low weight and high performance composites. CNTs are also considered to be ideal for applications in automative and aerospace industries thanks to their mechanical properties and lightness [2].

## 2.4 Production Methods of Carbon Nanotubes

There are three main methods for the CNT production with a high yield and quality, namely arc discharge, laser ablation, and chemical vapor deposition (CVD). The general principles of these techniques are briefly described below.

### 2.4.1 Arc Discharge

The arc discharge technique which was initially used for the production of $C_{60}$ fullerenes is a widely used method for the growth of carbon nanotubes. It is possible to produce both SWNTs and MWNTs with a high quality using this technique.

In the arc discharge method, a power supply with a low voltage (12-25 V) and a high current having a value between 50 and 120A is utilized to create a high temperature discharge between two high-purity graphite electrodes with a diameter of 5-20 mm and a separation distance of 1 mm. He or Ar are used as an inert gas for the reaction atmosphere at a pressure between 100 and 1000 torr. The high temperature (>3000ºC) generated by the arc vaporizes carbon from the anode during the discharge and plasma of carbon is produced. At the end, carbon nanotubes are produced from the condensation and deposition of carbon on the cathode. The length of the anode reduces during the CNT synthesis [14, 15]. A schematic representation of arc discharge is illustrated in Figure 2.10.

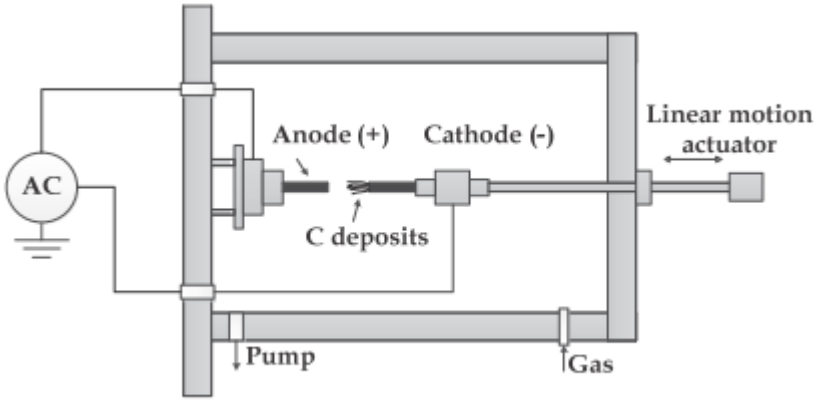


**Figure 2.10** Schematic drawing of set-up for arc discharge **[4].**

Although Iijima was the first person who observed MWNTs during the production of fullerenes by arc discharge method in 1991, the first CNT production in large quantities was achieved by Ajayan and Ebbesen in 1992 using this technique. In 1993, Bethune and coworkers reported the first synthesized SWNTs by arc discharge. In their experiments, a carbon anode containing cobalt catalysts was used [16]. In arc discharge method, no catalyst is required for the synthesis of MWNTs. On the contrary, metal catalysts are necessary for the formation of SWNTs which can be synthesized using transition metals such as Fe, Ni, Co and rare earth metals such as Y and Gd. The binary catalysts such as Fe-Ni, Co-Ni and Co-Pt can be employed for the production of SWNT ropes [17].

### 2.4.2 Laser Ablation

Another method for the CNT production is laser ablation which utilizes a focused laser beam with high energy to generate carbon vapor species ( e.g. $C_2$, $C_3$ and C) [17]. This technique has been used for the production of fullerene clusters. In 1995, Smalley and coworkers reported the synthesis of SWNTs by laser ablation [1]. A

schematic drawing of set-up for laser ablation is represented in Figure 2.11. A laser ablation apparatus is made up of an oven in which a quartz tube is present. This internal quartz tube possess a cooling device where carbon nanotubes are collected [4]. In the laser ablation method, a high-power laser is used to vaporize carbon at the graphite target in an oven which is held at 1200˚C while an inert gas (Ar or He) is fed into the chamber. Then, vaporized carbon species are carried by the flowing inert gas from the high temperature zone to the cooler surface the location of which is at the exit of the oven. The condensation of the vaporized carbon on the cooler surface of the reactor results in the formation of carbon nanotubes [14, 15].

In the laser ablation method, MWNTs can be synthesized without catalyst. The presence of the pure graphide electrodes is sufficient for their growth. On the contrary; for the synthesis of SWNTs, a mixture of Fe, Ni, Co or Y metals with the graphite target is required. No catalyst particle or amorphous carbon is present in the resulting SWNTs. The disadvantage of this technique is its high cost. However, the purity of CNTs produced by this method is higher when compared to arc discharge technique [13].

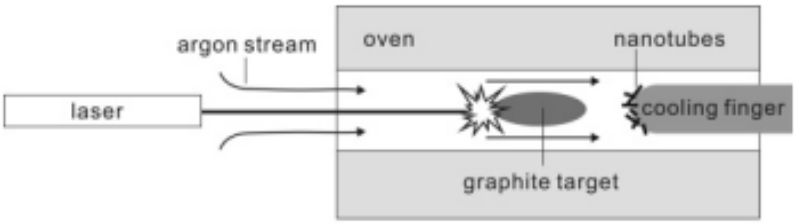


**Figure 2.11** Schematic drawing of set-up for laser ablation apparatus **[4].**

### 2.4.3 Chemical Vapor Deposition

Chemical vapor deposition is a widely used method for the production of carbon fiber, filament and nanotubes. Nowadays, most of the CNT manufacturing companies use CVD method in which a gaseous carbon source passes over metal catalyst particles [18].

During the chemical vapor deposition method which is a heterogeneous catalyst process, the solid catalyst is heated to a high temperature in a tube furnace under an inert atmosphere. Then, a carbon precursor (hydrocarbon gas or CO) flows through a tube reactor for an appropriate time required for CNT growth. Carbon source in the gas phase decomposes on the metal catalyst in the reactor at the high temperature. Products which are grown over the catalyst are collected after the cooling of the system to a room temperature [19]. A schematic experimental set-up of CVD is shown in Figure 2.12.

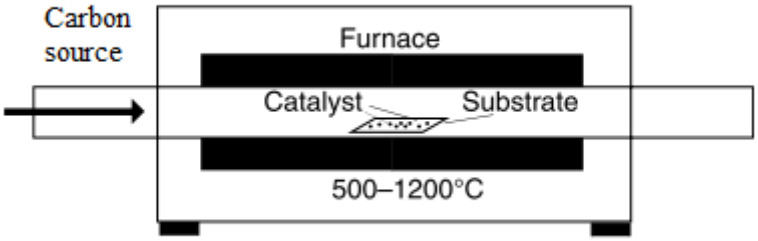


**Figure 2.12** Schematic drawing of experimental set-up for CVD **[3].**

In recent years, different CVD techniques for the production of nanotubes have been developed while keeping the basic principles same. Some of them are plasma enhanced CVD (PECVD), laser-assisted thermal CVD and vapor phase growth CVD [1]. In the plasma enhanced CVD, a glow discharge is generated by a high-

frequency power source in a reaction chamber which is applied to two electrodes. A substrate (Si, $SiO_2$ or glass) is present on a grounded electrode. Metal particles (Fe, Ni or Co) are placed on the substrate. During the discharge, a carbon source ($C_2H_2$, $CH_4$, $C_2H_4$ or CO) is fed into the chamber from the opposite electrode and CNTs are formed on the metal particles over the substrate. In the laser-assisted CVD, a $CO_2$ laser with a medium power and continuous wave is targeted to a substrate and used to pyrolyse a mixture of metal precursor and carbon source in a flow reactor. The growth of nanotubes takes place on metal particles. In the vapor-phase growth, also known as the floating catalyst method, metal nanoparticles in gas phase are generated when volatile organometallic precursors are fed into a high-temperature reaction zone. The decomposition of hydrocarbons on these metal nanoparticles leads to the formation on CNTs. Then, nanotubes are transported from the reaction zone with the help of a gas flow and collected on a cold plate [1].

Metal catalyst particles are very crucial in CNT production since they are active sites for the growth of CNTs. Therefore, catalyst preparation is an important part of the CVD synthesis of CNTs. The metal-support interaction, metal particle size and morphology are key factors affecting the catalytic properties of metals [19].

Catalysts used for the CNT growth are generally transition metals such as Ni, Fe, Co; and other metals such as Mo, Cu, etc. In order to increase the yield and the quality of carbon nanotubes bimetallic particles are used such as Fe-Co, Fe-Ni, Fe-Mo, Co-Mo. The reasons for the use of these metals as catalyst are that carbon is highly soluble in these metals at high temperatures and the diffusion rate of carbon is high in these metals [20, 21].

Metal particles are generally deposited on the surface of the support materials. Supports are mostly porous materials with high surface area. They are also thermostable. The most commonly used support materials for CNT synthesis are silica ($SiO_2$), alumina ($Al_2O_3$), magnesium oxide (MgO), and zeolites. The advantages of these supports are high surface area, porosity, cost, and high thermal

stability. Their main disadvantage is that they are hardly removed from the product because of their insolubility problems [20, 22].

The support materials play a key role in the activity of the catalyst. The decomposition temperature and the surface area of the support are important factors for the CNT growth process. The interaction between metal and support materials is also important since this interaction controls the size of the catalyst particle and the sintering potential of the catalyst. The removal of support materials is critical for pure carbon nanotubes. Supports with high surface area such as $SiO_2$, $Al_2O_3$, MgO and zeolites can not be easily removed because of their nature. Therefore, several acidic/oxidation steps are essential for complete purification of CNTs. These steps cause damage in the structures of CNTs [23]. On the other hand, calcium carbonate ($CaCO_3$) is a good support for transition metal particles due to the catalyst activity. In addition, it is environmentally friendly. Around the temperature of 700˚C, calcium carbonate decomposes into lime (CaO) and carbon dioxide ($CO_2$). CaO can easily be dissolved in dilute acids such as $HNO_3$ and HCl. As a conclusion, $CaCO_3$ as a support can be easily removed together with metal catalyst particles from the products. Furthermore, $CaCO_3$ is cheap. The use of this support leads to production of CNTs with a high quality, high yield, and high purity [19, 21, 24].

Methane, acetylene, ethylene, carbon monoxide, benzene, toluene, and short chain alcohols are commonly used as carbon precursors for the formation of carbon nanotubes by the chemical vapor deposition method. These compounds are cracked into reactive carbon atoms by an energy source. This energy source is generally a high temperature furnace [11, 25].

Acetylene ($C_2H_2$) is most widely used as carbon precursor for MWNT synthesis whereas methane ($CH_4$) is mostly used for SWNTs and DWNTs production. Acetylene is able to decompose at lower temperatures which makes it a good candidate for the growth of MWNTs. Additionally, it can be concluded that there is a relationship between the graphitic layers of CNTs and hydrocarbon gas. SWNTs or

DWNTs can be favorably synthesized using short chain molecules like $CH_4$. Longer chain molecules such as $C_2H_2$ and $C_2H_4$ lead to MWNT growth in CVD [19].

Reaction parameters affecting CNT growth such as reaction (synthesis) temperature and time, carbon precursors, flow rate of gases, metal particles, and support material can be easily controlled in the CVD method when compared to the arc discharge and laser ablation methods. The yield and type of CNTs can be controlled by optimizing these parameters. Additionally, the properties of synthesized CNTs such as length, orientation, and diameter can also be controlled by changing reaction conditions [19].

The temperature range for CNT production is between 500 and 1200˚C depending on the type of support material and carbon source. Melting point of supports and the stability of hydrocarbons used are main major factors affecting the optimum temperature range. Additionally, the quality of carbon nanotubes changes with the synthesis time. In the case of long reaction times, the formation of other carbon species may take place and the quality of CNTs decreases [3, 19].

Both arc-discharge and laser ablation methods need for special equipment for CNT synthesis. Furthermore, because of large energy consumption and less control on the reaction parameters in these methods they are not appropriate candidates for large scale CNT production. Hence, they are restricted to be used in laboratories only. On the contrary, CVD which enables a control over reaction parameters is a very promising method for the production of high-quality carbon nanotubes in large quantities. In order to achieve this goal, there must be some improvements in the growth and purification techniques [2, 19, 20].

The price of carbon nanotubes produced using chemical vapor deposition decreased dramatically because of the improvements in large-scale production. This results in a decrease in CNT prices. Other methods (arc discharge, laser ablation) are not able to produce CNTs in such large quantities. Currently, manufacturers focus on the developing more efficient CVD methods and also on the better control over the nanotube types. Furthermore, CNTs can be synthesized in desired arrangements by catalytic CVD method [5].

### 2.4.4 Growth Mechanism of CNTs

There are several mechanisms suggested for the CNT growth from the pyrolysis of carbon sources over metal particles. A schematic representation of the CNT growth mechanism is illustrated in Figure 2.13. In the first step, reactive species such as carbon monoxide (CO) or hydrocarbons ($C_nH_m$) in the gas phase are transported to the reaction zone. In the second step, carbon containing molecules decompose on the metal surface. These molecules are cracked into reactive carbon atoms when they contact with the hot metal surface. In the third step, carbon diffuses through the metal particle. In the last step, carbon precipitates out after carbon solubility limit in the metal is reached. The precipitation of carbon from the saturated metal particle results in the formation of tubular carbon solids with $sp^2$ structure. The reason why tubular formation is favored instead of other carbon forms such as graphitic sheets with open edges is that a tube contains no dangling bonds, therefore, it is energetically stable [1, 3, 4].

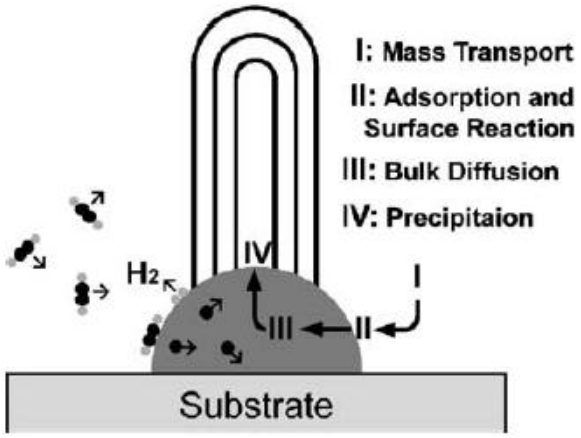


**Figure 2.13** Schematic representation of the CNT growth mechanism **[26]**.

Depending on the metal-substrate interaction the growth of nanotubes can occur either below or above the metal catalyst. In the case of weak metal particle-subsrate interaction, the decomposition of carbon precursors occurs on the top surface of the metal particle. Then, the diffusion of carbon through the metal takes place. The metal bottom serves as a place where nanotubes precipitate out and the whole metal particle is pushed up which causes the separation of metal and substrate. The nanotube end remains stuck to the metal surface while hydrocarbon continues to decompose. The nanotube length extends as long as the top of the metal is appropriate for further hydrocarbon decomposition. When the metal particle is compeletely covered, the activity of metal catalyst stops and the growth of nanotubes finishes [27]. This is known as "tip-growth model" (Figure 2.14).

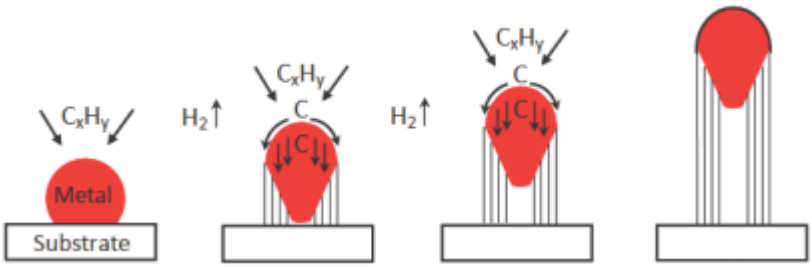


**Figure 2.14** An illustration of the tip-growth mechanism **[27].**

In the case of strong metal particle-substrate interaction, the initial decomposition of hydrocarbon and the diffusion of carbon through the metal is similar to that in the tip-growth model. On the contrary, the precipitation of carbon nanotubes can not push the metal particle up. The metal particle remains attached to the substrate surface. In the first step, hydrocarbon precipitates at metal top and forms a hemispherical structure which is a favorable closed carbon structure on a spherical nanoparticle. Then, it continues to extend up as a graphitic cylinder. The lower

peripheral surface of the metal particle serves as a place for the next decomposition of carbon precursor as carbon diffuses upward [27]. Meanwhile, a metal particle becomes a base for a nanotube, therefore the mechanism is known as “base-growth model” (Figure 2.15).

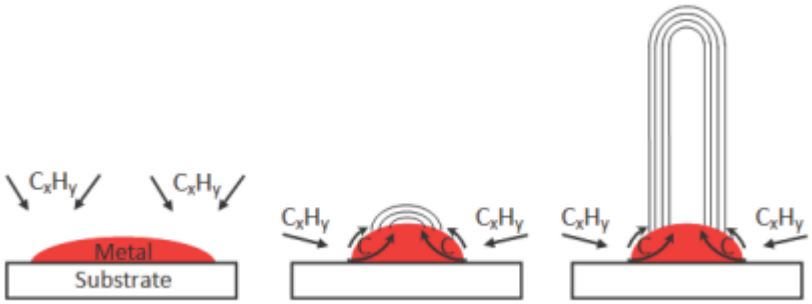


**Figure 2.15** An illustration of the base-growth mechanism **[27].**

Tip-growth mechanism is found to be dominant during MWNT growth while base-growth is dominant for SWNT formation [1].

## 2.5 Purification of Carbon Nanotubes

All methods for the CNT production such as arc discharge, laser ablation, and CVD techniques mostly contain various impurities such as residual metal particles, support material, carbon nanoparticles, amorphous carbon, and other undesired particles [13, 15]. These impurities present in CNT sample depend on the growth method and reaction parameters. The performance of CNTs can be influenced by these impurities. It is important to remove these impurities completely from nanotubes using appropriate purification techniques for a high quality CNT sample. To achieve a complete purification, a combination of some chemical and physical techniques is

essential depending on the nature of impurities. The important techniques for the purification of CNTs are oxidation, ultrasonication, acid treatment, annealing, magnetic purification, filtration, functionalization, and centrifugation [13].

**Oxidation:** Oxidative treatment can be used to remove carbonaceous impurities such as amorphous carbon from carbon nanotubes and to clean the metal surface. The dry oxidation can be performed under an oxidative atmosphere such as air at high temperatures (500-750ºC). Liquid-phase (wet) oxidation of nanotubes in strong acids such as $HNO_3$, $H_2O_2$, $HClO_4$, $HNO_3$+$H_2SO_4$, $H_2SO_4$+$KMnO_4$ is another oxidation method. In wet oxidation, CNTs are usually refluxed in concentrated $HNO_3$, $H_2SO_4$ or $KMnO_4$ solutions at room temperature for 24 hours. The strong oxidation in $HNO_3$+ $H_2SO_4$ is also possible [1, 13, 20].

The impurities present in the product have more defects or a more open structure compared to nanotubes; therefore, the damage in impurities is more than that in CNTs during oxidative treatment. There are some parameters affecting the efficiency and yield of the purification such as metal content, oxidation time and environment, temperature, and oxidizing agent [13].

**Ultrasonication:** In this purification method, products are placed into an acid solution, toluene or distilled water and vibrated in an ultrasonic bath. Ultrasonic vibrations separate nanotubes from other particles. After agglomerates of different nanoparticles are vibrated, they become more dispersed. The purity of CNTs is dependable on the exposure time when using acid as a solvent. The nanotubes are also affected when exposing to the acid for a long time, on the other hand, only metal particles solvate in a short exposure time [13].

**Acid treatment:** In this technique, metal particles and support material are removed by an acid treatment after the metal surface is exposed to oxidation or sonication. Metal particles present in the catalyst are exposed to acid and solvated whereas nanotubes remain in a suspended form. Mostly used acids are nitric acid ($HNO_3$), hydrofluoric acid (HF) and hydrochloric acid (HCl). When products are treated in nitric acid only metal particles are affected while there is no effect on the nanotubes

and other carbon particles. The use of nitric acid is an inexpensive and effectice method for removing metal particles. On the other hand, the acid slightly affects CNTs and other carbon particles when hydrochloric acid is used [13].

**Annealing:** In this method, high temperatures (900-1600˚C) result in the rearrangement of CNTs and the removal of defects. The graphitic carbon and short fullerenes also decompose due to high temperature. Additionally, vacuum treatment at high temperature can melt the metal particles and remove them [13].

**Magnetic Purification:** This method is used for removing ferromagnetic catalytic particles from their graphitic shells. The CNT suspension is mixed with inorganic nanoparticles which are generally $ZrO_2$, $NHCl_4$, or $CaCO_3$ in an ultrasonic bath. The ferromagnetic particles are then trapped with permanent magnetic poles. Nanotubes with a high purity can be obtained after a chemical treatment [13].

**Filtration:** This separation technique is based on the size or particle separation. A filter can trap nanotubes and a small quantities of carbon nanoparticles. Other nanoparticles such as metal nanoparticles, nanospheres, and fullerenes are able to pass through the filter [13].

**Functionalization:** In this technique, other groups are attached to carbon nanotubes and CNTs are made more soluble than the impurities such as metal particles. This results in the easy separation of nanotubes from less soluble impurities by filtration. The remaining nanoparticles and amorphous carbon can be removed by a slow precipitation process which includes the addition of diethyl ether to a chloroform solution of nanotubes. This leads to the precipitation of impurities. The purified CNTs can be easily recovered by removing the functional groups using thermal treatment at 350˚C and subsequent annealing to 900˚C [13].

**Centrifugation:** Low-speed centrifugation is effective in the suspending of amorphous carbon which leaves nanotubes in the sediment. On the other hand, high-speed centrifugation is effective in sedimenting carbon nanoparticles whereas it leaves nanotubes suspended in aqueous media [13].

## 2.6 Literature Survey

In the study of Kibria et al. [28], carbon nanotubes were synthesized using Co-Mo/MgO catalyst at three different reaction temperatures (500˚C, 700˚C and 900˚C). These catalysts were calcined at 400ºC and then reduced in $H_2$ atmosphere at 450ºC. The synthesized nanotubes were multi-walled carbon nanotubes which were grown from the decomposition of $C_2H_2$ for 30 minutes by the chemical vapor deposition method. It was observed that the growth temperature influenced the growth density and diameter of nanotubes. The highest yield and the lowest diameter of CNTs were observed at 700˚C and 900˚C, respectively. Furthermore, the highest and lowest densities of nanotubes were synthesized at 700˚C and 500˚C, respectively. It was reported that the origins of Co particles which play an important role in the growth of nanotubes at 500˚C, 700˚C and 900˚C were $Co_3O_4$, $CoMoO_4$, and CoO-MgO solid solution, respectively. It was also realized that carbon yield increased with an increase in reaction time. SEM images indicated carbon nanotubes with white spots at their ends which were attributed to catalytic metal particles. These white spots were an indicator for the tip growth mechanism.

In the study of Shajahan et al. [29], MgO supported catalysts including Co and Mo metals (5-40 wt.%) with a ratio of 1:1 were prepared by using impregnation method. The synthesized catalysts were calcined at 400ºC and then reduced in $H_2$ atmosphere at 450ºC. CNTs were synthesized over these catalysts using $C_2H_2$ as carbon source at 800˚C for 30 min. Results showed that the amount of metal loading highly affected the production of SWNTs and MWNTs. Products synthesized using 5 and 10 wt.% Co-Mo/MgO catalysts were SWNTs whereas Co-Mo/MgO catalysts with 20, 30 and 40 wt.% produced MWNTs. It was also found that Mo/MgO catalyst was inactive for CNT synthesis whereas Co-Mo/MgO catalysts yielded a large amount of carbon nanotubes. The yield of MWNTs grown over 40 wt.% Co-Mo/MgO catalyst was 576%. In Co-Mo/MgO catalyst, large cobalt clusters originated from $Co_3O_4$ phase during nanotube growth stage produced MWNTs. On the other hand, SWNTs were grown over small clusters of cobalt which may be generated from decomposition of $CoMoO_4$ during the nanotube growth stage.

In the study of Couteau et al. [30], $CaCO_3$ was used as a catalyst support for the growth of multi-walled carbon nanotubes. MWNTs were produced in a fixed-bed flow reactor at 720˚C from the decomposition of acetylene by CVD. In addition to mono-metallic salt of Co(II), Fe(II) and Fe(III) they also used bimetallic combinations of Fe(II), Co(II) and Fe(III), Co(II) as a catalyst over $CaCO_3$ support with a total catalyst concentration of 5 wt.%. Except for Fe(II)/$CaCO_3$, remarkable amounts of CNTs were obtained using all catalysts. TEM images showed that samples contained nanotubes, catalyst, and support material. No amorphous carbon or carbonaceous particles were found in the products. MWNTs produced had well-graphitized wall structure with a few defects which are characteristic for the growth by chemical vapor deposition. One of the advantages of $CaCO_3$ support was the ability to be removed in one-step purification. Both metallic particles and catalyst support were dissolved in diluted nitric acid (30 v/v % $HNO_3$) which prevented multi-step purification processes.

Kitiyanan et al. [31] synthesized SWNTs using Co-Mo catalysts with a high selectivity depending on Co:Mo ratio. They used CO as a carbon precursor to produce SWNTs at a temperature of 700˚C. In the study it was reported that the reaction time and temperature were important parameters affecting the selectivity towards SWNTs. The Co-Mo/$SiO_2$ catalyst with a total metal loading of 6 wt % and a Co:Mo molar ratio of 1:2 showed a high selectivity towards SWNTs. On the contrary, Co metal alone was not selective for SWNT production. A considerable amount of MWNTs was produced over the catalyst including only Co as catalyst metal particles. On the other hand, the catalyst including only Mo metal particles could not produce any carbon nanotubes. It was concluded that the synergism between Co and Mo resulted in high-yield CNT synthesis as they were present together in the catalyst.

Alvarez and his coworkers [32] studied the effects of the change in catalyst composition and reaction conditions in order to increase the selectivity for SWNTs using CO as carbon source. The support material used for the catalyst was $SiO_2$ and the reaction temperature was 700˚C. The calcination temperature for the catalysts

was 500ºC. Metallic Co and Mo particles present in the catalyst were also investigated. In the case of simultaneous presence of both metals, especially in the excess amount of Mo, the catalyst was very effective for nanotube synthesis. As only Mo was present in the catalyst it was inactive for the production of nanotubes. X-ray absorption spectroscopy revealed that Co was reduced to the metallic form with time although it was in the oxidic state at the beginning of CNT formation. In addition, Mo was converted to the carbidic form during the formation. It was also concluded that the reaction temperature and the CO concentration in the gas phase strongly influenced the yield and the selectivity of SWNTs. Furthermore, it was realized that the carbon yield declined with a rise in reaction temperature due to rapid deactivation of the catalyst at higher temperatures. The amount of carbon deposit at lower temperatures was higher than that of carbon deposit at higher temperatures. It was also observed that the main product was amorphous carbon at low CO concentrations. The formation of SWNTs started with an increase in the CO concentration and was observed at longer reaction times.

Li and his coworkers [21] investigated the effects of active species Fe-Co composition on the formation of nanotubes. CNTs were synthesized from the pyrolytic decomposition of $C_2H_2$ over Fe-Co/$CaCO_3$ catalysts at a temperature of 720˚C. The catalyst was calcined at 500ºC in order to remove acetates and nitrates from the catalyst. It was concluded that carbon deposition rate and the characteristics of nanotube crystallinity were greatly affected by the catalysts stoichiometry. Nanotubes synthesized over catalysts containing Fe metals had less amorphous carbon when compared to nanotubes produced by monometallic Co/$CaCO_3$ catalysts. It was also reported that the bimetallic Fe-Co/$CaCO_3$ catalyst had higher yield of high-quality CNTs when compared to Fe or Co monometallic catalyst under the same reaction conditions. The maximum yield was achieved at the Fe/Co atomic ratio of 2:1. No encapsulated particles were observed in the nanotubes which were synthesized on the bimetallic catalyst Fe-Co/$CaCO_3$ whereas the nanotubes grown over monometallic catalysts often included encapsulated particles. In addition, the crystallinity of CNTs also increased with an increase in the Fe amount of catalyst.

In the study of Smajda and coworkers [33], a rotary tube furnace is used for a continuous mass production of high quality CNTs at a low cost. Multi-walled carbon nanotubes were produced at 650-700˚C by chemical vapor deposition of acetylene and carbon dioxide over supported Fe, Co, Ni catalysts alloys. In order to decrease the cost, naturally occurring calcite was used as a support. It was reported that bimetallic $Fe_2Ni$ and $Fe_2Co$ alloys showed a higher activity than mono metallic Fe, Co or Ni for a large scale CNT production. The reaction yield for $Fe_2Ni$ and $Fe_2Co$ catalysts was 4 times higher than that for Ni and Co catalysts. They produced about 1.2 kg of CNTs per day with a cost of less than $1 per gram. They synthesized CNTs using sea urchin shell collected in Bodrum as a support material. Carbon nanotubes synthesized had a diameter smaller than 10 nm. It was concluded that CNTs had good mechanical properties with a Young's modulus of 1 TPa.

Li et al. [25] produced MWNT bundles with Ni-Mo/MgO catalyst using methane-hydrogen mixture in a CVD process. The operation temperature for nanotube synthesis was 1000˚C while $N_2$ was used as an inert gas. The yield was 80 times more than the amount of the catalyst before the synthesis. Results indicated that the purity of as-prepared MWNTs was over 97% as the reaction time was over 60 minutes. The diameters of CNTs were in the range of 9-20 nm. It was also reported that the main reason for the high yield was the synergism between Ni and Mo. Ni-Mo/MgO catalyst increased carbon diffusion in the catalyst metal particles and resulted in a high yield. This catalyst was found to be suitable for the large-scale CVD production of MWNTs with high quality.

Dervishi et al. [34] produced high-quality MWNTs on Fe-Co catalyst using CVD method. They used $CaCO_3$ and acetylene as a support material and carbon precursor, respectively. Carbon nanotubes were synthesized at 720˚C in a nitrogen atmosphere. It was reported that partial decomposition of $CaCO_3$ resulted in two groups of MWNTs with different outer diameter distributions. $CaCO_3$ decomposed into CaO and $CO_2$ at the temperature which was close to the growth temperature of MWNTs. Due to this thermal decomposition, Fe-Co/$CaCO_3$ and Fe-Co/CaO were together in the synthesis process. Since the surface areas of CaO and $CaCO_3$ were different from

each other metal clusters with two different sizes formed. CNTs with smaller diameter were synthesized over Fe-Co/CaO whereas nanotubes with larger diameter were grown over Fe-Co/$CaCO_3$ catalyst. Furthermore, only a single-step acid washing required for high-purity MWNTs made Fe-Co/$CaCO_3$ catalyst very effective for a large scale production of high-quality MWNTs at low cost.

Qingwen et al. [22] studied the importance of the catalyst and support interaction for the CNT production by the CVD method. They used porous MgO as a catalyst support for the synthesis of SWNTs at 850˚C under an Ar atmosphere. Methane, hydrocarbon source, was fed into the system for 30 min. Different metal particles (Co, Fe, Cu, Mo, Mn and Ni) were used in this study. SWNTs could be produced with desired diameters, less impurities and higher yields by controlling the synthesis conditions such as temperature, gas flow rate, and catalyst and support materials. It was reported that the quality of SWNTs synthesized over MgO support was higher than other support materials such as $SiO_2$, $ZrO_2$, $Al_2O_3$ and CaO, etc. With the treatment of products in 4 M HCl, high purity CNTs were obtained (90%). In this study, MgO was found to be a promising support in terms of low cost and easy purification in mild acids which resulted in less damage in CNTs.

Colomer and his coworkers [35] reported a large-scale production of single-walled carbon nanotubes by catalytic decomposition of methane at 1000˚C over well-dispersed metal particles (Co, Fe and Co-Fe) supported on MgO. Hydrogen was the carrier gas in this catalytic chemical vapor deposition (CCVD). In order to obtain high-purity SWNTs the support material was easily removed by a simple acidic treatment. After purification process, the purity of SWNTs was found to be 70-80%. In the experiments, 1 g of SWNTs was produced per day. Small amounts of impurities like MWNTs, amorphous carbon, and metal particles encapsulated in nanotubes were observed in SWNTs. The diameters of SWNTs were in the range of 1-5 nm.

In the study of Murakami et al. [36], catalytic activities of Co and Fe in the formation of SWNTs at 800˚C using the CVD technique were analyzed and compared. Ethanol

and $SiO_2$ were the carbon source and support material, respectively. The synthesis time was 30 minutes. The changes in catalyst precursors (Co- and Fe acetate) were analyzed at three different stages. The first stage was after oxidation in air at 400˚C but before the synthesis temperature (800˚C). The second stage was after heating to the synthesis temperature in Ar and $H_2$ flows, but before starting the CNT synthesis. The last stage was after the growth of CNTs. XRD results revealed that, Co and Fe precursors converted to $Co_3O_4$ and $Fe_2O_3$ at the first stage, respectively. At the second stage, they were in the phases of β-Co and CoO, and $Fe_2O_3$. At the final stage, they changed to β-Co and $Fe_2SiO_4$, respectively. Raman and TEM results revealed that Fe catalyst had a poor yield of SWNTs while Co catalyst was very effective in the production of SWNTs with a high yield. The catalytic activity was prevented as Fe reacted with the supporting material $SiO_2$ to form the silicate. In addition, both Co and Fe catalysts were able to synthesize SWNTs with high yield when catalyst support was MgO. In the light of this, it could be said that the catalytic ability was influenced by the reactions between catalyst precursors and support materials.

Gulino et al. [37] reported a large scale production of high-quality CNTs by CVD method using ethane as a carbon source over $Fe/Al_2O_3$ catalyst. Synthesized catalysts were calcined in air atmosphere at 450ºC to obtain oxidic form of the catalyst precursor. The metal loading was 20 wt.% and the synthesis temperature was 650˚C. It was reported that 20 grams of CNTs were synthesized per one gram of catalyst in one hour. These products did not contain any other impurities such as amorphous carbon and consisted of only MWNTs having homogeneous diameters between 20 and 40 nm. The lengths of CNTs were several hundred nanometers. In this study, it was observed that ethane was an active carbon precursor for the production of MWNTs with a high yield and selectivity at relatively low temperatures (650-750˚C). As the reaction temperature was higher than 750˚C there were amorphous soot and carbon nanoparticles present together with carbon nanotubes. It was also observed that $H_2$ was an important factor in the formation of nanotubes because graphite could not encapsulate the catalytic site in the presence of hydrogen which

prevented deactivation of catalytic sites during the synthesis. A mixture of metastable iron carbide ($Fe_3C$) and α-Fe was found to be the active phase for CNT production. Furthermore, the specific surface area of MWNTs after purification was in the range of 100-160 $m^2g^{-1}$.

Magrez et al. [38] synthesized multi-walled carbon nanotubes at 750˚C using acetylene and argon as carbon source and inert gas, respectively. It was concluded that $Fe_2Co$ and $Fe_2Ni$ were the most effective catalysts among the family of $Fe_{1-x}M_x$ (M = Co and Ni) alloys. The growth of CNTs was significantly affected by the $CO_2$ produced by the thermal decomposition of $CaCO_3$ which was used as a support material. The growth of nanotubes was enhanced by the interaction between $C_2H_2$ and $CO_2$. This interaction also caused the growth of nanotubes over unfavorable substrate materials and at relatively lower temperatures. In the lack of $CO_2$, only amorphous carbon was observed in the thermal decomposition of $C_2H_2$ below 600˚C. In this study, it was also reported that catalytic efficiency was enhanced by water-assisted growth. The water-assisted growth resulted in dense CNTs with narrower diameter distribution and thus in a higher average bending modulus. It was also reported that $CaCO_3$ is an appropriate support material for both high yield MWNTs and SWNTs.

Mortazavi et al. [39] studied the effects of the reaction temperature and Pd addition to Fe as a co-catalsyt on the CNT production. Carbon nanotubes were produced at 920 and 970˚C using methane as carbon source. It was observed that as Pd was added to Fe as a co-catalyst the yield of CNTs increased whereas the quality decreased. It was also realized that nanotubes and fibers in different types were synthesized with an increase in the Pd/Fe ratio. Moreover, TEM images showed that the addition of Pd into the catalyst led to the tip-growth of nanotubes. Raman spectroscopy results revealed that the $I_G/I_D$ ratio of the products which indicated the structural quality of sample increased as the reaction temperature decreased. The products were SWNTs which were produced at 920˚C at higher concentration of Fe metal.

In the study of Lyu and his coworkers [40], high-quality SWNTs were produced in large quantities using Fe-Mo/MgO bimetallic catalyst by the CVD method. Ethylene was the carbon precursor and decomposed at a temperature of 800˚C. The products were mainly composed of SWNTs with a diameter of 0.7-2.8 nm, a few DWNTs and a small amount of amorphous carbon. The yield of the as-synthesized SWNTs was high with a value of 550%. These results revealed that ethylene was an appropriate candidate for the synthesis of nanotubes with a high quality. Furthermore, they could not achieve a high yield of SWNTs using Fe or Mo metals separately as a catalyst at the same reaction conditions. It was mentioned that Fe and Mo mixture was much more effective in the SWNTs growth. The weight ratio of Fe:Mo in the catalyst structure was 1:0.1. XRD results indicated that metal oxide catalysts were effective in the large-scale SWNT production.

In the study of Lee and his coworkers [41], the effects of the catalyst on the CNT production by chemical vapor deposition were studied. The catalyst influenced the grow rate, nanotube diameter and crystallinity. As a result, it could be said that the activity of catalysts was in the order of Ni>Co>Fe whereas the average diameter of synthesized CNTs was in the order of Fe>Co>Ni. The crystallinity of carbon nanotubes were significantly affected by the catalyst used while nanotubes had almost the same morphology. CNTs synthesized by Fe-containing catalyst had a higher crystallinity than that by Ni or Co catalysts. In addition, the size of catalyst particles and especially the diffusion rate of carbon in the catalyst were two important factors determining the growth rate of CNTs.

Liu and his coworkers [42] synthesized high-quality SWNTs using Fe-Mo bimetallic catalyst supported over MgO by the catalytic decomposition of acetylene at a temperature range of 800-950˚C. The CNTs produced included few defects and small amount of amorphous carbon coating. The yield was about 29%. The diameters of SWNTs were in the range of 0.80-2.43 nm. Compared to $Al_2O_3$ support the large-scale and high-quality synthesis of SWNTs with smaller diameters was possible with the use of MgO support by the decomposition of acetylene. In addition, it was

concluded that the increase in the temperature slightly increased the yield of SWNTs; on the other hand, it did not affect the morphology of the as-synthesized SWNTs.

In the study of Kathyayini and his coworkers [43], a mixture of Fe-Co catalysts over aluminum hydroxide support was used to find out the right combination of catalyst and support to produce CNTs with high quality and quantity. The activity of catalyst and support material was investigated in the synthesis of nanotubes by catalytic chemical vapor deposition. They produced nanotubes in a horizontal tubular furnace at 700˚C. Nitrogen was used as a carrier gas while acetylene was the carbon-containing gas. Results showed that the preparation method of the support and catalyst-support mixture significantly affected the yield and the nature of nanotubes grown. Also, the surface properties of the support played an important role in the quality of CNTs. It was realized that a large surface area for catalyst-support mixture is not sufficient to synthesize high-quality CNTs. The yield of carbon products was between the values of 24 and 319 % with respect to the initial weight of the catalyst. TEM images showed that CNTs produced were MWNTs. Furthermore, they suggested that commercial crystalline $Al(OH)_3$ owing low surface area and porosity could be an appropriate candidate as a support material for Fe and Co salts for a large-scale high-quality CNT production.

In the study of Kathyayini et al. [44], the role of Ca and Mg oxides, hydroxides and carbonates as catalyst supports by the catalytic chemical vapor deposition (CCVD) was studied for a large-scale CNT synthesis. Fe, Co and Fe-Co mixture were catalysts used in this study. Ethylene and acetylene were two different carbon sources while $N_2$ was used as a carrier gas in a horizontal tubular furnace. The reaction temperature was 700˚C. Results showed that almost all of catalyst-support combinations were active for CNT synthesis. On the other hand, different CNT synthesis conditions such as carbon source, the nature of interaction between metal particles and support resulted in different quantity and quality of nanotubes. Co-Fe metal particles supported either $CaCO_3$ or MgO gave the highest yield. However, the yield of Fe metal particles supported on these supports was very low. It was observed that Co was more active than Fe. After the experiments, the products contained only

MWNTs. The support material and metal particles could be easily removed from the sample by a simple HCl treatment for pure CNTs.

Li et al. [45] compared different catalyst systems and hydrocarbons to optimize the production of carbon nanotubes in their study. They used $CaCO_3$ supported Fe-Mo, Co-Mo or Ni-Mo metals as catalyst. Synthesized catalysts were calcined at 500ºC to remove nitrates from the catalysts. In this work, the highest CNT yield was obtained by chemical vapor deposition of acetylene at 720˚C using Co-Mo metal particles supported on $CaCO_3$. On the other hand, catalysts containing Fe-Mo metals gave a better crystallinity of nanotubes. It was also reported that higher CNT yields were achieved by unsaturated hydrocarbons such as acetylene whereas highly graphitized nanotubes having fewer walls were formed by saturated hydrocarbons such as methane. The purification of the as-produced MWNTs was carried out by one single step using diluted HCl solution with sonication. Additionally, phenomenological growth mechanisms for CNTs were suggested. Before reaction, Co and Mo existed in their oxide forms. After hydrocarbon was fed into the reactor, Co became metallic while Mo became carbide. The large Co metal particles participate in the formation of MWNTs. Co was the active metal whereas Mo played two different roles in the nanotube formation. It took part in the breakup of hydrocarbon molecules. Also, it behaved like a secondary support for active metals (Co, Fe or Ni).

## 2.7 Objectives of the Present Study

In most of the literature studied, a variety of production methods for the synthesis of CNTs were utilizied. In addition, different types of metals and support materials are used for the preparation of catalysts which are employed for the growth of carbon nanotubes by the CVD method. However, studies related with Co-Mo/$CaCO_3$ catalyst and the effect of the Co/Mo weight ratio on the CNT production are very rare in the literature. Also, there is not any published information in the literature related to the effects of the catalyst calcination temperature on the growth and morphology of nanotubes. Moreover, surface characteristics of CNTs are barely studied in the literature.

The objectives of this study were:

- To design and construct an experimental set-up to produce carbon nanotubes
- To synthesize Co-Mo/$CaCO_3$ catalysts at different calcination temperatures and Co:Mo weight ratios
- To produce carbon nanotubes using acetylene gas as a carbon source over Co-Mo/$CaCO_3$ catalysts
- To purify the synthesized CNTs
- To investigate the effects of reaction temperature, catalyst calcination temperature, Co:Mo weight ratio in catalyst and inlet acetylene composition in argon on the yield and the morphology of nanotubes
- To characterize Co-Mo/$CaCO_3$ catalysts and synthesized carbon nanotubes using X-ray Diffraction (XRD), Energy Dispersive X-ray Spectroscopy (EDS), Scanning Electron Microscopy (SEM), Transmission Electron Microscopy (TEM), X-ray Photoelectron Spectroscopy (XPS), multi-point BET, Thermogravimetric Analysis (TGA) and Raman spectroscopy methods

# CHAPTER 3

# EXPERIMENTAL

The aims of this study were to synthesize Co-Mo/$CaCO_3$ binary catalyst at different Co:Mo weight ratios and calcination temperatures, to characterize the synthesized catalysts, to produce carbon nanotubes using Co-Mo/$CaCO_3$ catalyst from chemical vapor deposition of acetylene gas at different reaction temperatures and inlet acetylene compositions, to purify the synthesized CNTs, and to characterize purified CNTs. The experimental parts of this study were summarized in 4 groups:

i. The synthesis of Co-Mo/$CaCO_3$ catalysts
ii. The production of CNTs
iii. The purification of CNTs
iv. The characterization of purified CNTs and synthesized catalysts

In the first part of the experimental work, the catalysts for the CNT production were synthesized at different Co:Mo weight ratios and calcination temperatures. In the second part, carbon nanotubes were produced over the synthesized Co-Mo/$CaCO_3$ binary catalysts from the catalytic decomposition of acetylene at different reaction temperatures and inlet acetylene compositions. The third part of the experimental work covered the purification of the synthesized nanotubes. The last part focused on the characterization of the purified CNTs with XRD, SEM-EDS, TGA-DTA, TEM, Raman spectroscopy and multi-point BET surface measurement and the synthesized catalysts with XRD, SEM-EDS, TGA-DTA and XPS.

## 3.1 Catalyst Preparation

Catalyst preparation is one of the most important parts of the carbon nanotube production since the catalyst greatly affects the nature and the yield of CNTs. The type, the morphology, the length, and the diameter of nanotubes significantly depend on the catalyst used for synthesis.

In our study, bimetallic Co-Mo catalyst over calcium carbonate ($CaCO_3$) (Sigma-Aldrich, ≥99.0%) support was chosen to be used for the CNT production. The source of cobalt was cobalt (II) acetate tetrahydrate [$(CH_3COO)_2Co{\cdot}4H_2O$] (Sigma-Aldrich, 98%) whereas ammonium molybdate tetrahydrate [$(NH_4)_6Mo_7O_{24}{\cdot}4H_2O$] (Fluka, ≥99.0%) was used as a molybdenum source.

An impregnation method was used to prepare bimetallic Co-Mo/$CaCO_3$ catalysts in which the Co:Mo weight ratio was kept at three desired ratios (0.44, 2.30 and 6) whereas total metal loading was kept at 9.29 wt.%. According to the desired Co:Mo weight ratios, determined amounts of $(CH_3COO)_2Co{\cdot}4H_2O$ and $(NH_4)_6Mo_7O_{24}{\cdot}4H_2O$ were separately dissolved in 10 ml distilled water and stirred by a magnetic stirrer at 500 rpm and 30˚C for 30 minutes. The amounts of the $(CH_3COO)_2Co{\cdot}4H_2O$ and $(NH_4)_6Mo_7O_{24}{\cdot}4H_2O$ compounds used are given in Appendix A. After this step, the solutions were mixed drop by drop and stirred together for 60 minutes to have a homogeneous mixture. Then, this mixture was added into a beaker in which 19 g of $CaCO_3$ was dissolved in 80 ml distilled water and stirred at 500 rpm and 30˚C for 2 hours. The resulting mixture was placed on a hot plate and evaporated for 60˚C under continuous stirring at a rate of 500 rpm for 1 day. Moreover, the catalyst was further dried in an oven at 120˚C overnight in order to remove the excess water. Finally, it was calcined at three different temperatures (500, 700 and 750˚C). Calcination was performed in a tubular furnace. The catalyst was heated from room temperature to the calcination temperature with a heating rate of 1ºC/min under dry air flow and kept at this temperature for 8 hours at dry air atmosphere. Synthesis parameters for Co-Mo/$CaCO_3$ catalyst are given in Table 3.1.

**Table 3.1** Synthesis parameters for Co-Mo/$CaCO_3$ catalyst

| **Co wt.%** | **Mo wt.%** | **$T_{cal}$ (˚C)** |
|---|---|---|
| 2.82 | 6.47 | 500 |
| 2.82 | 6.47 | 700 |
| 2.82 | 6.47 | 750 |
| 6.47 | 2.82 | 500 |
| 6.47 | 2.82 | 700 |
| 6.47 | 2.82 | 750 |
| 7.96 | 1.33 | 500 |
| 7.96 | 1.33 | 700 |
| 7.96 | 1.33 | 750 |

## 3.2 Experimental Set-Up

The production of carbon nanotubes was carried out in the experimental setup shown in Figure 3.1. In the CNT synthesis, argon (Oksan, ≥99.99) was used as an inert gas while $C_2H_2$ (Oksan, ≥99.9) was the hydrocarbon source. The inlet flow rates of these gases were adjusted using mass flow controllers which were calibrated and related calibration curves were given in Appendix B. To measure the actual inlet and outlet volumetric flow rates of argon and acetylene two soap bubble meters were located in the system before and after the quartz reactor. These gases were connected to a vertical quartz tube through copper tubing with a diameter of ¼ in. The pressure of argon and acetylene gases were adjusted to desired pressures using regulators. The CNT growth took place on a porous glass located at the center of the vertical quartz reactor. The length of the quartz reactor was 114 cm while its diameter was 22 mm. The catalyst was placed on the porous glass. The desired reaction temperature was reached with the help of the tubular furnace (Protherm PTF 16/50/450). The inner temperature of the reactor was measured using a ceramic thermocouple placed at the center of the reactor. Through a temperature readout connected to the thermocouple the temperature was observed. A 3-way valve was used to by-pass and adjust the inlet volumetric flow rate of acetylene gas just before the reaction started. A water bath was utilized to cool both ends of the reactor.

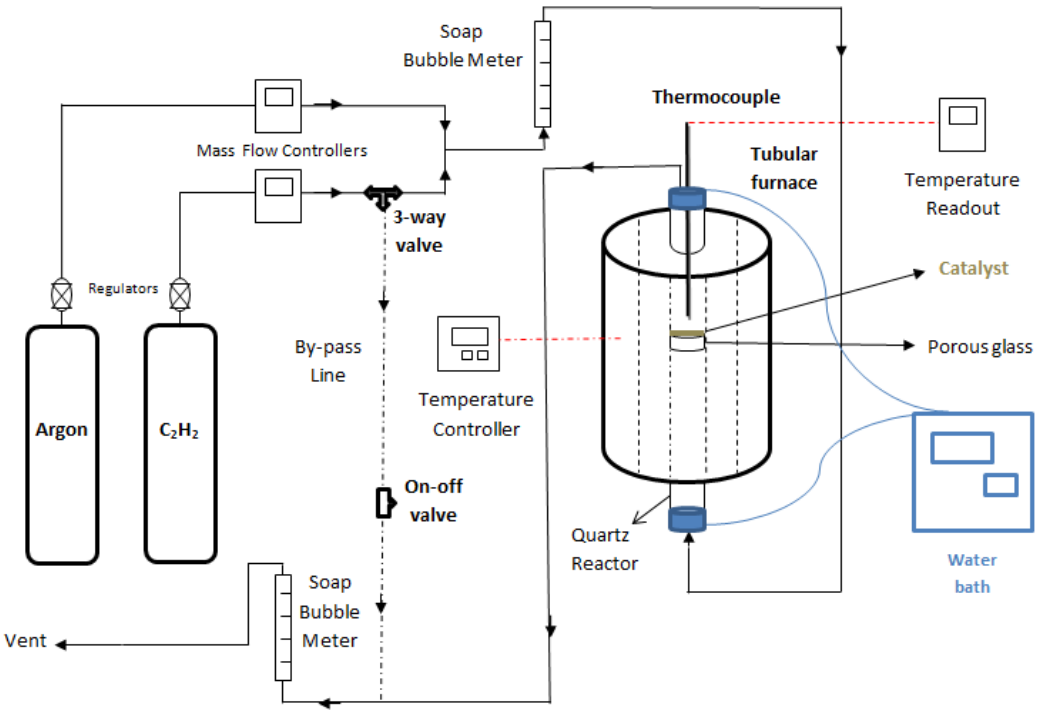


**Figure 3.1** Schematic representation of the experimental setup

### 3.3 Experimental Procedure

In this work, carbon nanotubes were synthesized using Co-Mo/$CaCO_3$ binary catalysts by the chemical vapor deposition. The CVD growth of nanotubes was carried out in a temperature range of 500-1000˚C for 150 minutes at atmospheric pressure.

For the CNT synthesis, 50 mg of catalyst was weighed and uniformly placed on the porous glass. Before and after each run, the experimental system was purged with high-purity argon gas with a flow rate of 100 ml/min in order to remove oxygen from the system until the reaction temperature was reached. The pressure of the argon and acetylene gases was set to 3 bar with the help of the regulators. Meanwhile, the furnace was heated to the desired reaction temperature with a heating rate of 8˚C/min. The acetylene gas was fed into the reactor with the help of the three-way

valve at desired volumetric flow rates as the furnace temperature reached the reaction temperature. The argon flow rate was decreased to ensure a total inlet flow rate of 100 ml/min during the reaction. After a reaction time of 150 minutes, the acetylene gas was shut off and argon was fed into the system again with a volumetric flow rate of 100 ml/min in order to purge the system after the reaction. Then, the furnace was cooled down to the room temperature with a rate of 5˚C/min. Finally, the products were collected and weighted.

Experimental conditions for the synthesis of carbon nanotubes are given in Table 3.2.

**Table 3.2** Experimental conditions for CNT synthesis

| **Run No.** | **Co:Mo wt. ratio** | **$T_{cal}$ (˚C)** | **$T_{rxn}$ (˚C)** | **Inlet acetylene composition in argon (%)** |
|---|---|---|---|---|
| 1 | 0.44 | 750 | 750 | 20 |
| 2 | 0.44 | 750 | 750 | 50 |
| 3 | 0.44 | 750 | 750 | 30 |
| 4 | 0.44 | 750 | 700 | 25 |
| 5 | 0.44 | 750 | 800 | 25 |
| 6 | 0.44 | 750 | 1000 | 25 |
| 7 | 0.44 | 750 | 500 | 25 |
| 8 | 0.44 | 750 | 600 | 25 |
| 9 | 0.44 | 500 | 700 | 25 |
| 10 | 0.44 | 700 | 500 | 25 |
| 11 | 0.44 | 700 | 600 | 25 |
| 12 | 0.44 | 700 | 650 | 25 |
| 13 | 0.44 | 700 | 700 | 25 |

**Table 3.2** Experimental conditions for CNT synthesis (cont'd)

| Run No. | Co:Mo wt. ratio | $T_{cal}$ (˚C) | $T_{rxn}$ (˚C) | Inlet acetylene composition in argon (%) |
|---|---|---|---|---|
| 14 | 2.30 | 500 | 700 | 25 |
| 15 | 2.30 | 700 | 500 | 25 |
| 16 | 2.30 | 700 | 600 | 25 |
| 17 | 2.30 | 700 | 650 | 25 |
| 18 | 2.30 | 700 | 700 | 25 |
| 19 | 2.30 | 750 | 500 | 25 |
| 20 | 2.30 | 750 | 600 | 25 |
| 21 | 2.30 | 750 | 650 | 25 |
| 22 | 2.30 | 750 | 700 | 25 |
| 23 | 6 | 500 | 700 | 25 |
| 24 | 6 | 700 | 700 | 25 |
| 25 | 6 | 750 | 500 | 25 |
| 26 | 6 | 750 | 600 | 25 |
| 27 | 6 | 750 | 650 | 25 |
| 28 | 6 | 750 | 700 | 25 |
| 29 | 6 | 750 | 700 | 10 |
| 30 | 6 | 750 | 700 | 15 |
| 31 | 6 | 750 | 700 | 20 |
| 32 | 6 | 750 | 700 | 30 |
| 33 | 6 | 750 | 700 | 25 |

Blank experiments were also carried out in order to determine the actual weight loss of the catalyst. These experiments were performed under the argon atmosphere without a carbon source by following the procedure given above.

### 3.4 Purification of CNTs

The as-synthesized carbon nanotubes were purified in one single-step purification process according to the procedure described by Li et al. [21] to remove impurities such as metal particles and support material. This purification process was modified. CNT sample was placed in a diluted nitric acid ($HNO_3$) [Merck, 65% extra pure] solution and sonicated for 1 hour at room temperature. The concentration of $HNO_3$ was kept at around 20 (v/v) % by adding 100 ml of $HNO_3$ solution into 200 ml of distilled water. The mixture was then filtered and washed with distilled water. Lastly, it was dried at 120˚C overnight.

### 3.5 Characterization of Carbon Nanotubes and Synthesized Catalysts

Characterization techniques are very significant for carbon nanotechnology to investigate the physical and chemical properties of materials and to evaluate their potential in applications.

The synthesized catalysts and CNTs were characterized using XRD, SEM-EDS, TEM, TGA, XPS, multi-point BET and Raman spectroscopy analyses to determine the crystalline structures, chemical compositions, the shapes and dimensions of nanotubes, thermal behaviors, surface areas, pore size distributions and nitrogen adsorption-desorption isotherms of the CNTs.

#### 3.5.1 X-Ray Diffraction (XRD)

The crystal structure of synthesized catalysts and carbon nanotubes before and after purification was identified using XRD. It is also very useful to determine sample purity. The success of synthesized CNTs' purification is also understood by XRD.

XRD analyses of purified CNTs and synthesized catalysts were performed in a Bragg angle range of 10-100˚ using Rigaku D/MAX2200 diffractometer with a $CuK_{\alpha}$

radiation source and a scan speed of 2°/min. The voltage and the current were 40 kV and 40 mA during the analysis, respectively.

### 3.5.2 Scanning Electron Microscope (SEM) and Energy Dispersive X-ray Spectroscopy (EDS)

SEM analyses were performed for imaging purified CNTs and synthesized catalysts. Moreover, morphological properties of carbon nanotubes and their dimensions were studied using SEM. Energy Dispersive X-ray Spectroscopy (EDS or EDX) is a chemical analysis technique used for the elemental analysis or chemical [20, 46].

SEM and EDS analyses of the purified carbon nanotubes and synthesized catalysts were conducted using a QUANTA 400F Field Emission SEM instrument. The samples were uniformly placed on a carbon tape and coated with Au-Pd alloy before the analysis to have an electrically conductive surface. Diameter range of CNTs was found by using a set of 20 CNT diameter data.

### 3.5.3 Transmission Electron Microscope (TEM)

TEM analysis enables to determine the type, structure, and size of carbon nanotubes. TEM images of the purified CNTs were obtained using JEOL JEM 2100F 200kV HRTEM instrument. Before the analysis, CNTs were dispersed in ethanol and sonicated for 15 minutes. Then, a few drops of suspension were placed on the holey carbon-coated copper grid and dried.

### 3.5.4 Thermal Analysis (TGA and DTA)

TGA measures the change in the mass of a sample as a function of temperature or time. In differential thermal analysis (DTA), the sample and an inert reference are exposed to the same thermal cycles. Then, temperature difference between the sample and the reference are recorded. The amount of impurities, i.e. residual metal catalysts, amorphous carbon present in carbon nanotube samples can be quantitatively determined using TGA. In addition, thermal analyses can be used to obtain the thermal behavior and thermal stability of the purified CNTs and synthesized catalysts [21].

Thermal analyses of purified carbon nanotubes and synthesized catalysts were carried out using Shimadzu DTG-60H instrument. Under an air flow of 100 ml/min, nanotubes were heated to 800°C from room temperature with a rate of 8°C/min. Thermal analyses of the catalysts were performed under air atmosphere with a flow rate of 100 ml/min. The temperature was raised from room temperature to 900˚C with a temperature rate of 10˚C/min.

### 3.5.5 X-ray photoelectron spectroscopy (XPS)

The chemical state of the catalysts and the compounds present on the catalyst surface after calcination were characterized using X-ray photoelectron spectoscopy. XPS data of synthesized catalysts were recorded on SPECS EA 300 with monochromatic $AlK_{\alpha}$ X-rays. The spot size used was 100 μm and the value of the pass energy was 117.40 eV.

### 3.5.6 Multi-point BET Surface Analysis

Physical properties of the CNTs, such as pore size distribution, multi-point BET surface area, nitrogen adsorption-desorption isotherms, average pore diameter and pore volume are obtained with nitrogen adsorption technique [47].

Multi-point BET surface analyses of carbon nanotubes were conducted using a Quantachrome Autosorb-6 instrument. Before the analysis, 50 mg of sample was dried at 120˚C overnight and degassed for 4 hours at 300°C to remove moisture from sample pores. Nitrogen adsoption/desorption were obtained in a relative pressure range of $10^{-4}$ to 0.99 at liquid nitrogen temperature of 77K.

### 3.5.7 Raman Spectroscopy

Raman is frequently used for the determination of the presence of different carbon types (diamond, graphite, amorphous carbon, nanotubes, etc.) and their relative proportions. It is a qualitative tool used for the detection of CNTs in bulk samples and for the study of the nanotube structure. All allotropes of carbon are such as diamond, amorphous carbon, fullerenes and CNTs are Raman active. The vibrational frequency of molecular allotropes of carbon can be determined using Raman spectroscopy. According to the $sp^3$ and $sp^2$ configurations of carbon the position, width and relative intensity of Raman peaks are modified [20, 22, 25, 28, 48].

Three spectral regions are important to characterize CNTs. These regions are the radial breathing mode (RBM), the tangential mode (G-band) and the disorder-induced mode (D-band). The RBM peak is characteristic peak for the SWNTs and corresponds to tube diameter of 0.8-1.2 nm. Radial Breathing Mode is usually located between 75 and 300 $cm^{-1}$. The D-band corresponds to the defects and impurities in the CNTs while the G-band is associated with the stretching mode of the C-C bond in the graphite plane. The D-band is usually located between 1280 and 1360 $cm^{-1}$ whereas the G-band is usually present between 1500 and 1605 $cm^{-1}$. By

deconvoluting the G peak, another band (D') can be observed between 1605 and 1610 $cm^{-1}$. The origins of the D' band are disorders induced in the crystalline structure and the finite size of the crystalline domains. In the Raman spectrum of MWNTs, another observed band located between 2450 and 2800 $cm^{-1}$ is 2D band which is second-order harmonic of the D-band. The 2D band is highly dispersive and attributed to nanotubes' degree of crystallinity. It is consideed to be characteristic of MWNTs [20, 22, 24, 29, 49].

The ratio between G-band and D-band ($I_D/I_G$) is a good indicator of the quality of carbon products and it can be considered as a direct measure of well-structured morphology of CNTs. In the case of similar intensity values of these two bands it can be said that there is a high quantity of structural defects. The low $I_D/I_G$ value represents a well-graphitic structure of CNTs. On the other hand, the presence of well-graphitized CNTs can be observed in the case of a higher G-band intensity than that of D-band. The presence of a strong D-band is either associated with amorphous carbon on the CNT surface or relatively low crystallization degree of CNT arrays [20, 28].

In this study, Raman spectroscopy analyses of purified nanotubes were performed using FRA 106/S Ramanscope II equipped with a laser (532 nm ) as excitation source.

# CHAPTER 4

# RESULTS AND DISCUSSION

In this study, bimetallic Co-Mo loaded $CaCO_3$ catalysts were synthesized using impregnation method and characterized using XRD, SEM-EDS, thermal analyses (TGA-DTA) and XPS techniques. Carbon nanotubes were also produced at different reaction temperatures and acetylene inlet compositions in argon over Co-Mo/$CaCO_3$ catalysts. The synthesized nanotubes were purified and characterized using XRD, SEM-EDS, TEM, thermal analyses (TGA-DTA), multi-point BET and Raman spectroscopy techniques.

## 4.1 Characterization Results of Catalysts

### 4.1.1 Thermal Analysis Results

The thermal behavior and stability of pure and metal loaded $CaCO_3$ catalysts were characterized using TGA and DTA techniques in order to determine appropriate calcination temperatures for the synthesized catalysts.

Figure 4.1 illustrates the weight loss profile of pure $CaCO_3$ as a function of temperature. At lower temperatures, a minor weight loss was observed. This weight loss starting at a temperature of around 135˚C is associated with the evaporation of water present in the $CaCO_3$ material. This corresponded to a weight loss of approximately 3.1 wt.%. A major weight loss between 600 and 740˚C was attributed to the thermal decomposition of the $CaCO_3$ the products of which were $CO_2$ and CaO

[30]. The weight loss profile indicates that the mass drop in the catalyst is approximately 44 wt.%.

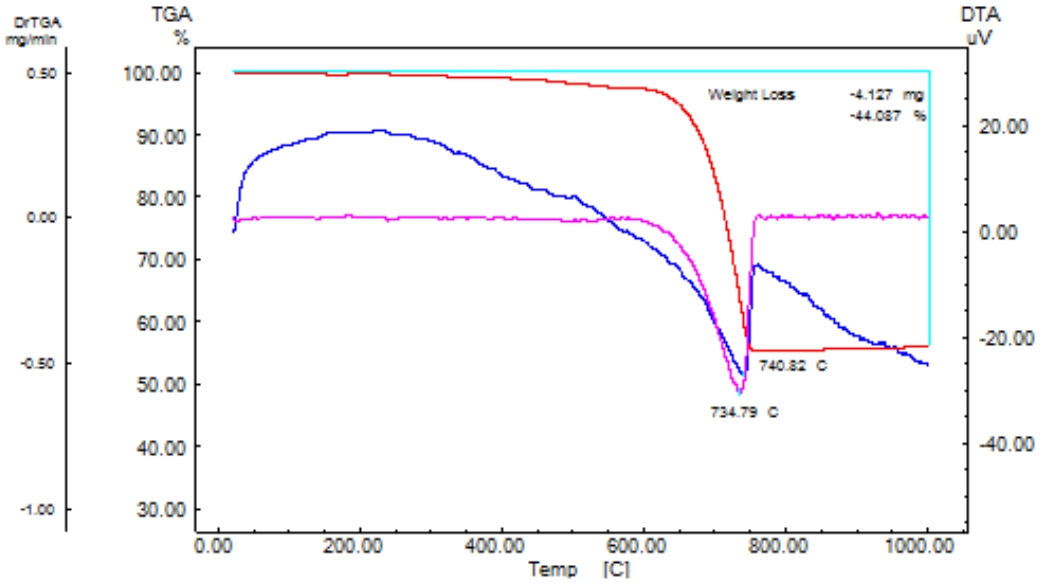


**Figure 4.1** TGA and DTA profiles of the pure $CaCO_3$ (red: TGA; blue: DTA).

Figure 4.2 gives the weight loss profile of the catalyst synthesized at a Co:Mo ratio of 6 which was calcined at 500˚C. It showed a similar weight loss profile to that of the pure $CaCO_3$. The minor drop in the weight of the catalyst corresponding to the water removal was observed up to a temperature of 300˚C [24]. The main weight loss of the catalyst occurred between the temperatures of 610 and 740˚C because of the decomposition of $CaCO_3$ into CaO and $CO_2$. This decomposition resulted in a weight loss of 39.3 wt.%.

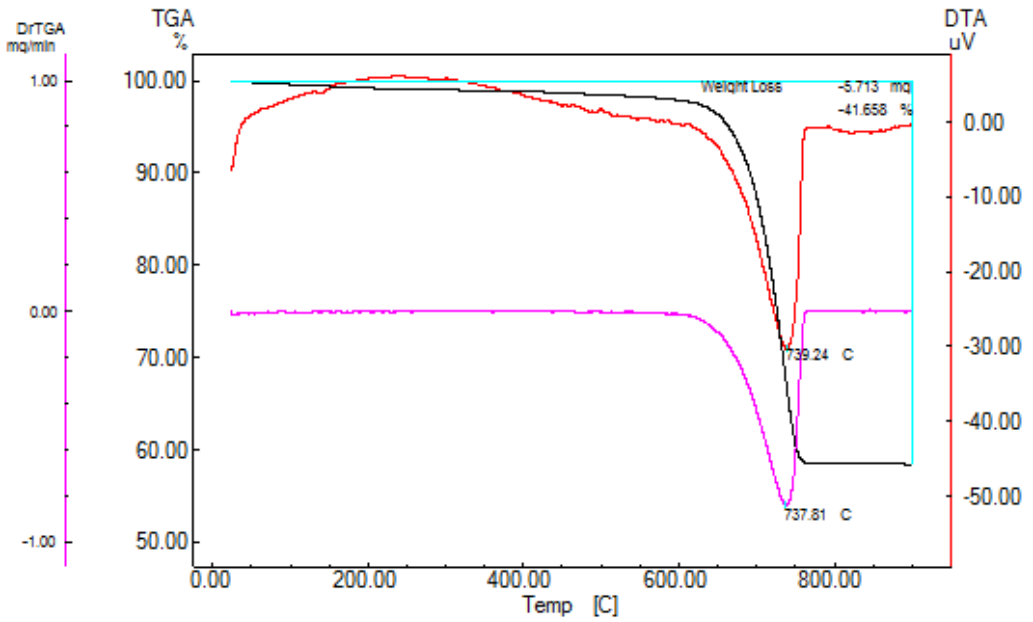


**Figure 4.2** TGA and DTA profiles of the catalyst with a Co:Mo ratio of 6 and a calcination temperature of 500˚C (black: TGA; red: DTA).

The weight loss profile of the catalyst with a Co:Mo ratio of 6 which was calcined at 700˚C is illustrated in Figure 4.3. An additional weight loss was present between 330˚C and 420˚C. This weight loss in the catalyst was associated with removal of acetate from Co source and nitrates from Mo source [24]. This led a weight loss of approximately 18.5 wt.%. Furthermore, the weight loss profile indicated that the weight of the catalyst was reduced by 3.5 wt.% between 500 and 650˚C. This was due to decomposition of $CaCO_3$.

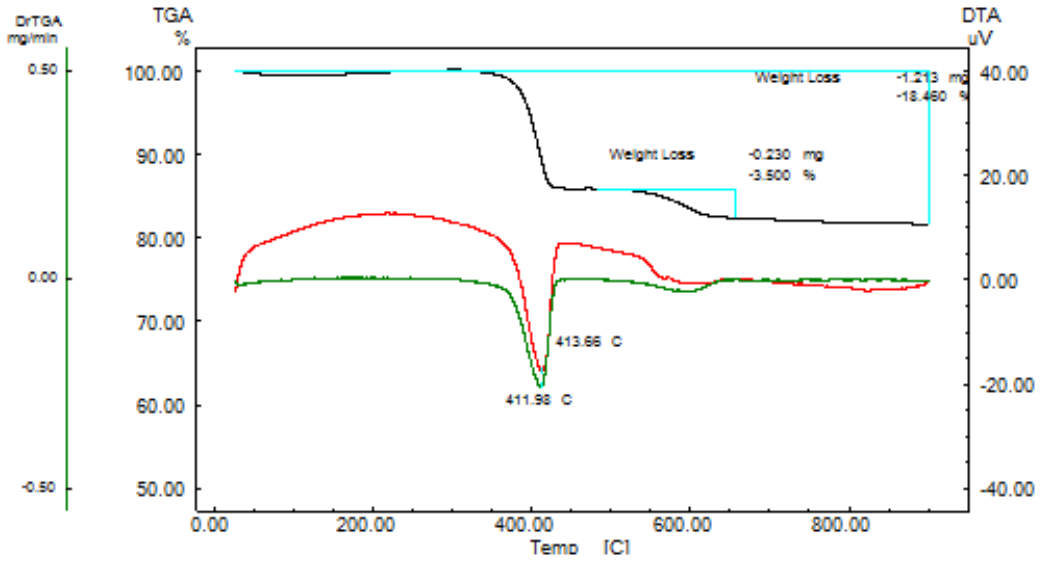


**Figure 4.3** TGA and DTA profiles of the catalyst with a Co:Mo ratio of 6 and a calcination temperature of 700˚C (black: TGA; red: DTA).

Figure 4.4 reveals the weight loss profile of the catalyst with a Co:Mo ratio of 6 which was calcined at 750˚C. This catalyst has a weight loss profile similar to the catalyst with a Co:Mo ratio of 6 which was calcined at 700˚C. The first weight loss originating from the evaporation of water up to 300˚C was about 1.5 wt.%. The second peak attributed to the weight loss up to 410˚C was due the acetate and nitrate exhaustion from the catalyst. The mass of the catalyst is decreased by approximately 18.5 wt.%.

TGA and DTA profiles of the other synthesized catalysts are given in Appendix C. Similar weight loss profiles were observed for these materials with the same calcination temperatures.

Based on these results, the synthesized catalysts with different Co:Mo weight ratios were calcined at three temperatures (500, 700 and 750ºC) in dry air to investigate the effect of catalyst calcination temperature on the yield of CNTs.

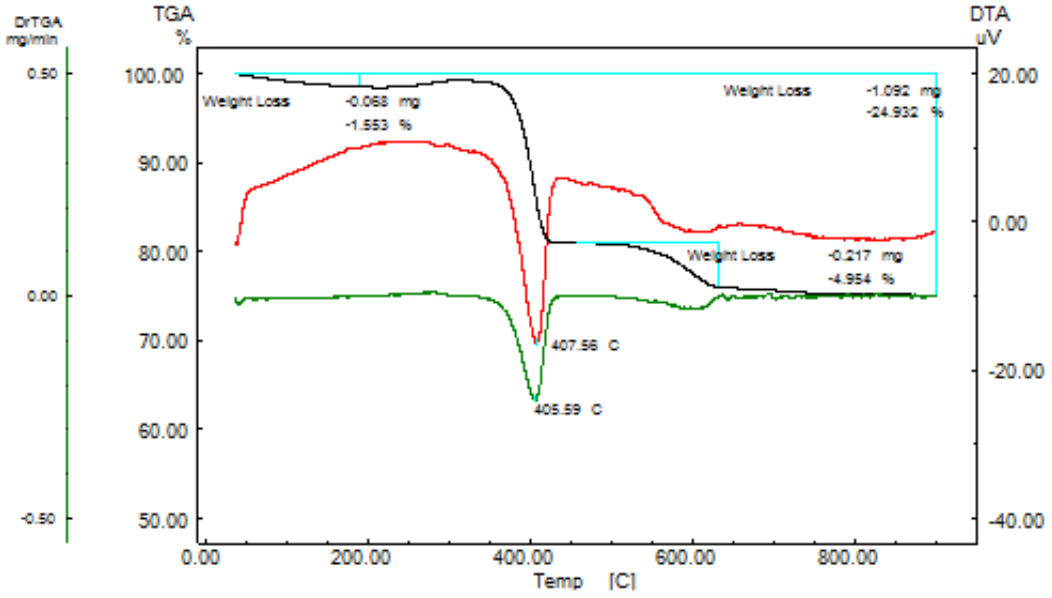


**Figure 4.4** TGA and DTA profiles of the catalyst with a Co:Mo ratio of 6 and a calcination temperature of 750˚C (black: TGA; red: DTA).

### 4.1.2 XRD Analysis Results

X-ray diffraction pattern and data of pure calcium carbonate are given in Appendix D.1.1 and D.3.1 to get information about its crystal structure and compare it with the catalysts synthesized at three different Co:Mo ratios and calcined at three different temperatures. XRD patterns of the Co and Mo impregnated $CaCO_3$ catalysts are given in Figures 4.5-4.8.

In Figure 4.5, XRD pattern of the catalyst having a Co:Mo ratio of 6 which was calcined at 500˚C is shown. The peaks at Bragg angle values of 23.22˚, 29.56˚, 36.14˚, 39.57˚, 43.33˚, 47.65˚, 48.66˚ and all the peaks after the Bragg angle values

of 60º belonged to $CaCO_3$. The peaks observed at Bragg angle values of 18.54˚, 28.90˚, 47.33˚, and 58.18˚ was attributed to the presence of $CaMoO_4$ (29-0351) in the catalyst structure. CoO (75-0419) which was considered to be one of the Co source candidates in this catalyst was observed at 2θ values of 34.00˚, 39.57˚, and 57.57˚ [36]. The peak appearing at 28.90˚ might be associated with the presence of $CoMoO_4$ (25-1434) [50]. Moreover, $Mo_2C$ (71-0242) might have a peak at a Bragg angle of 39.57˚ [28, 32]. XRD data of $CaMoO_4$, CoO, $CoMoO_4$, and $Mo_2C$ are given in Appendix D.3.

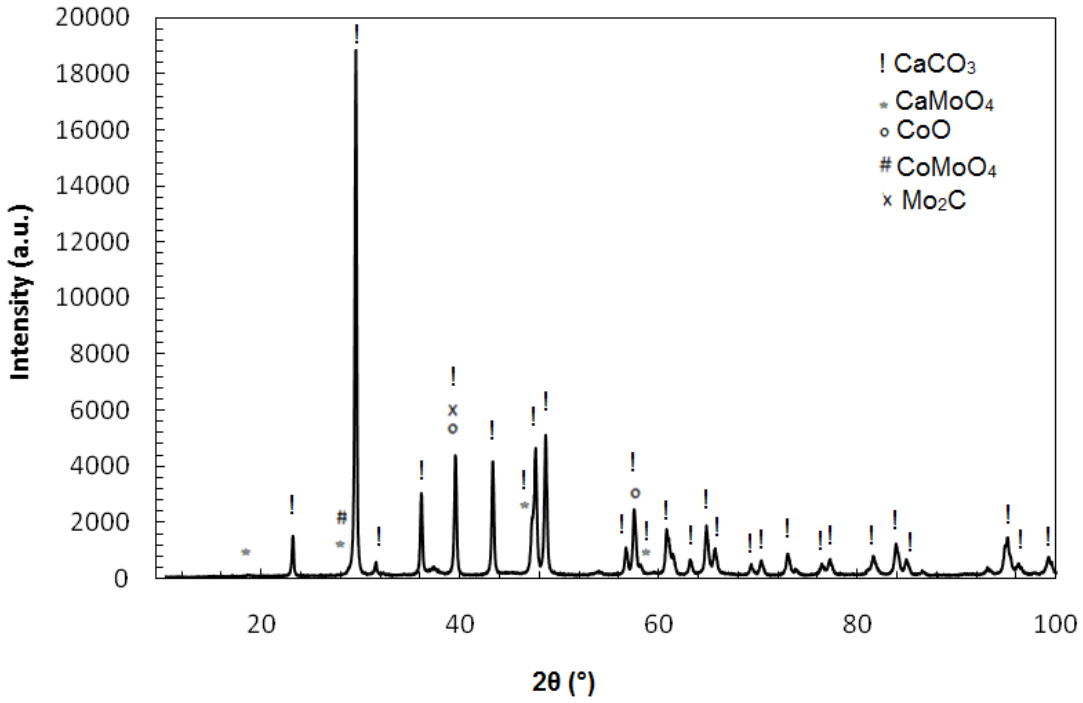


**Figure 4.5** XRD pattern of the catalyst with a Co:Mo ratio of 6 and a calcination temperature of 500˚C.

The Figure 4.6 represents the XRD pattern of the catalyst with a Co:Mo ratio of 0.44 which was calcined at 700˚C. The peaks at 2θ values of 23.08˚, 29.40˚, 36.02˚, 39.42˚, 43.20˚, 47.10˚, 47.46˚, 48.50˚, 57.44º, 60.70º, 64.72˚, 84.82˚, 94.96º and

some peaks in Bragg angle range of 60-100º corresponded to $CaCO_3$ peaks. Besides $CaCO_3$; $Ca(OH)_2$ (04-0733) the origin of which is the transformation of CaO due to easy water absroption of CaO in air was observed at Bragg angle values of 18.00˚, 28.74˚, 34.12˚, 47.10˚, 50.80˚, 54.40˚, 62.60˚, 64.10˚, 71.60˚, 84.54˚, 93.00˚, and 99.16º. On the other hand, CaO (48-1467) might be also present at 37.36º [21, 30, 38]. The peaks observed at Bragg angles 18.66˚, 28.74˚, 31.24º, 34.12˚, 39.42˚, 45.48˚, 47.10˚, 49.28˚, 54.12˚, 58.04˚, 59.50˚, 75.78˚, and 79.54˚ were associated with $CaMoO_4$ (29-0351). The peaks appearing at 2θ values of 34.12˚, 39.42˚, and 57.44˚ corresponded to the presence of CoO (75-0419) in the catalyst. In addition to cobalt oxides, metallic Co (89-4308) might be present at 47.46˚ [44]. $Mo_2C$ (71-0242) might have a peak at a Bragg angle value of 39.42º. The peak appearing at a 2θ value of 23.08˚ might be attributed to $MoO_3$ (89-1554) [28, 50]. XRD data of $Ca(OH)_2$, CaO, and $MoO_3$ are given in Appendix D.3.

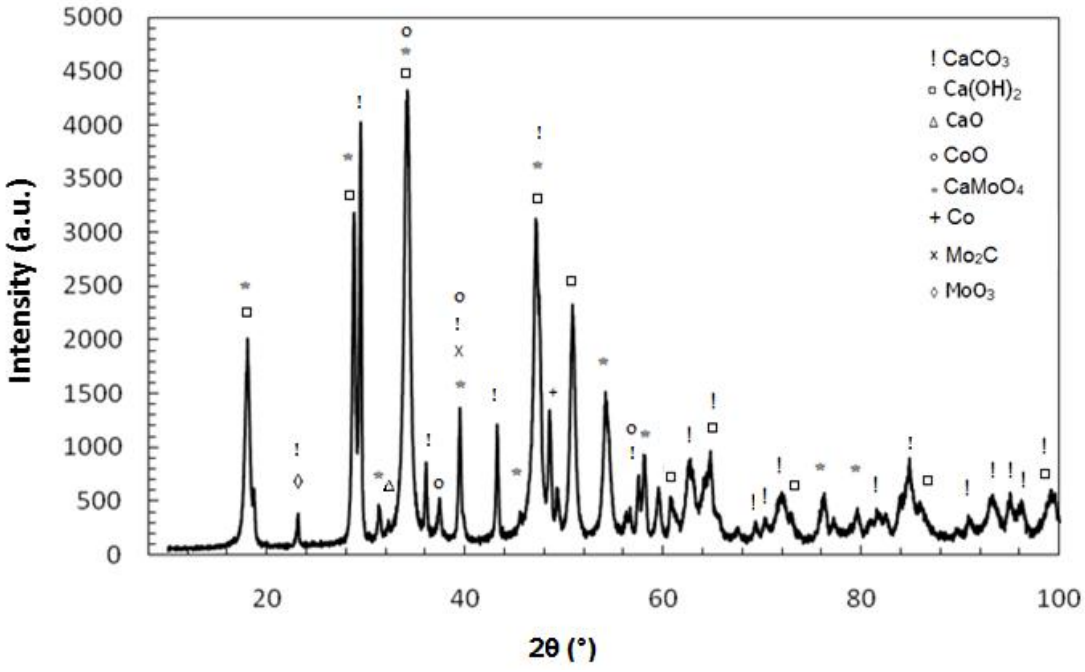


**Figure 4.6** XRD pattern of the catalyst with a Co:Mo ratio of 0.44 and a calcination temperature of 700˚C.

In Figure 4.7, XRD pattern of the catalyst with a Co:Mo ratio of 2.30 which was calcined at 700˚C is represented. The peaks appearing at Bragg angle values of 23.00˚, 29.44˚, 35.98˚, 39.42˚, 43.18˚, 47.12˚, 47.40˚, 48.52˚, 57.36˚, 60.56˚, 64.66˚, 84.80˚, 94.86˚ and some peaks in Bragg angle range of 60-100º were associated with $CaCO_3$ peaks. $Ca(OH)_2$ (04-0733) was also observed at Bragg angle values of 18.04˚, 28.74˚, 34.14˚, 47.12˚, 50.82˚, 54.32˚, 62.62˚, 64.04˚, 71.76˚, 93.06˚ and 98.68˚. The peaks belonging to $CaMoO_4$ (29-0351) were observed at 18.52˚, 28.74˚, 34.14˚, 39.42˚, 47.12˚, 54.32˚, 58.04˚, and 75.96˚. CoO (75-0419) might have a peak at 2θ value of 34.14˚, 39.42˚ and 57.36˚. Cobalt might also exist in the form of metallic Co (89-4308) which had a peak at 47.40˚. The peak observed at 28.74º might be associated with the presence of $CoMoO_4$ (25-1434). The peak at a Bragg angle value of 39.42˚ might be attributed to the presence of $Mo_2C$ (89-3014) in the catalyst structure. The peak appearing at a 2θ value of 23.00˚ might be associated with $MoO_3$ (89-1554).

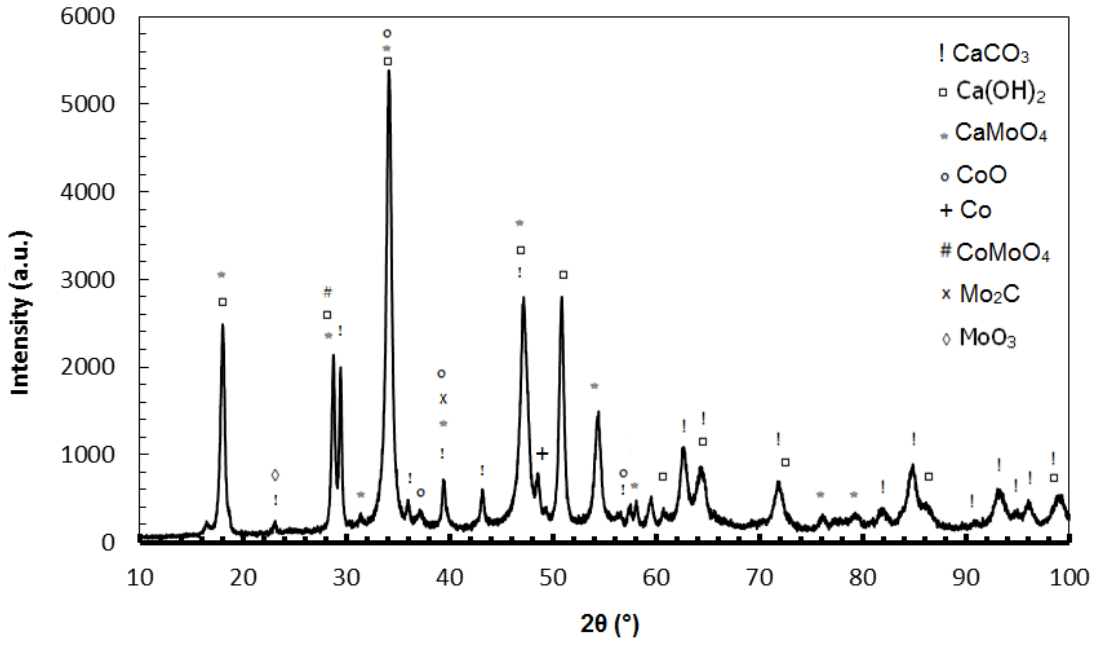


**Figure 4.7** XRD pattern of the catalyst with a Co:Mo ratio of 2.30 and a calcination temperature of 700˚C.

In Figure 4.8, XRD pattern of the catalyst with a Co:Mo ratio of 6 which was calcined at 750˚C is indicated. The peaks at Bragg angle values of 32.28˚, 37.44˚, 53.94˚, 64.22˚, 67.44˚, 79.72˚, 88.58˚ and 91.46˚ belonged to CaO (48-1467) compound. In addition to CaO, $Ca(OH)_2$ (04-0733) peaks were observed at 2θ values of 18.02˚, 28.76˚, 34.16˚, 47.14˚, 50.86˚, 62.60˚, 84.66˚, and 93.66˚. $CaMoO_4$ (29-0351) had peaks at 18.72º, 28.76˚, 34.16º, 47.14˚, 49.26º, and 59.50º. The peak which appeared at a 2θ value of 28.76˚ could be related with $CoMoO_4$ (25-1434) compound. Furthermore, CoO (75-0419) was observed at 34.16˚. The peak at a Bragg value of 47.14˚ could be associated with metallic Co (89-4308). Additionally, $Mo_2C$ (89-2669) might have a peak at 39.60º.

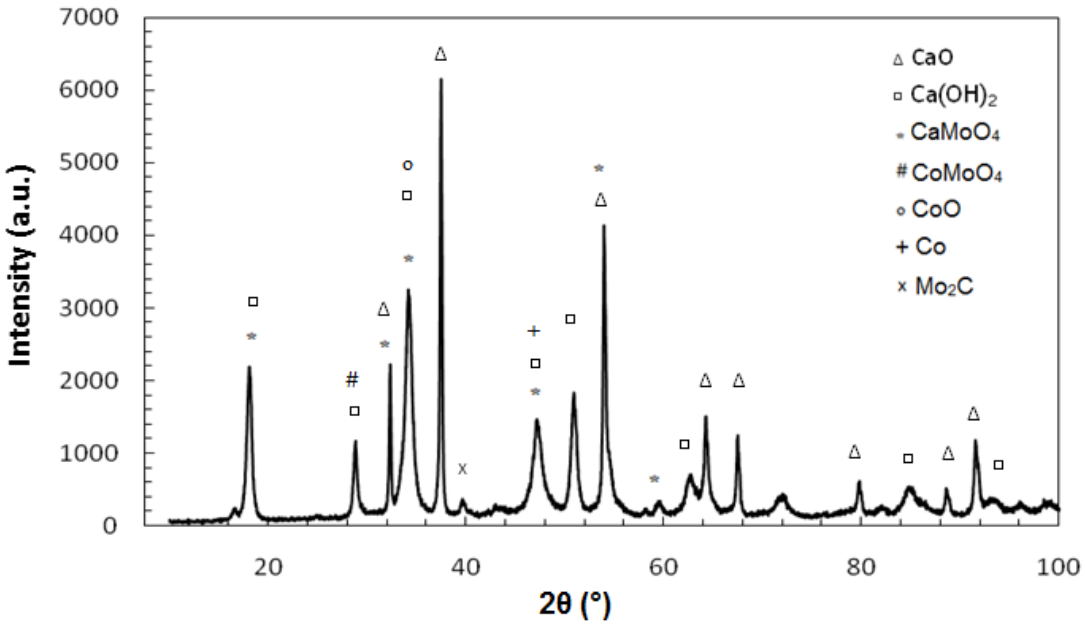


**Figure 4.8** XRD pattern of the catalyst with a Co:Mo ratio of 6 and a calcination temperature of 750˚C.

XRD patterns of the other synthesized catalysts are given in Appendix D.1. The catalysts showed similar XRD patterns to the patterns given in Figures 4.5-4.8. They were mainly composed of $CaCO_3$, CaO and/or $Ca(OH)_2$ compounds. In addition to

these, $CaMoO_4$, CoO, $CoMoO_4$ and $Mo_2C$ were the other solid phases mainly observed in all catalysts.

### 4.1.3 SEM and EDS Analysis Results

SEM images of catalyst with a Co:Mo ratio of 6 and a calcination temperature of 700ºC is illustrated in Figure 4.9. From this figure, uniform distribution of materials and large metal clusters formed during catalyst synthesis can be seen.

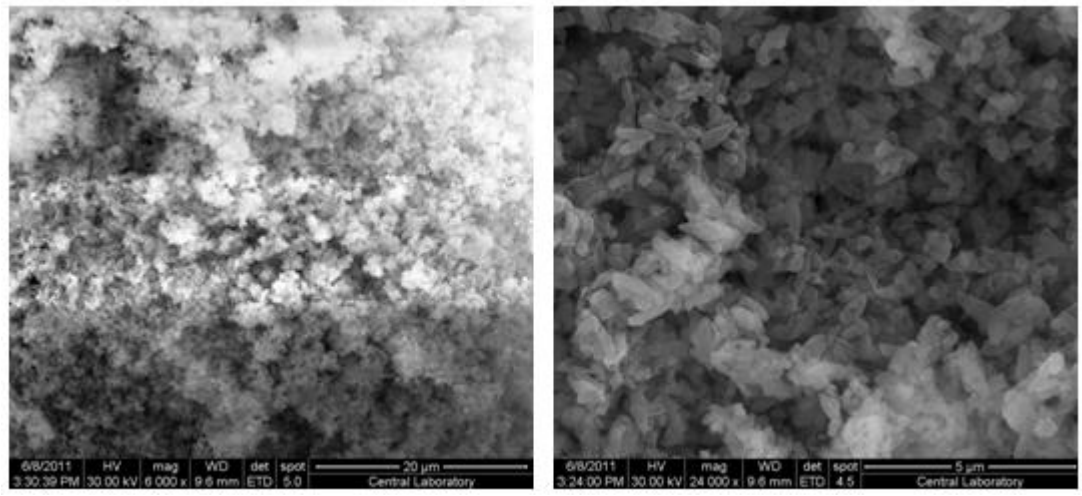


**(a)** **(b)**

**Figure 4.9** SEM images of the synthesized catalyst with a Co:Mo ratio of 6 and a calcination temperature of 700ºC (a) 6,000x and (b) 24,000x magnification.

The success of the metal loading was verified by the EDS analysis. EDS spectrum for the catalyst with a Co:Mo ratio of 0.44 and a calcination temperature of 750˚C is illustrated in the Figure 4.10.

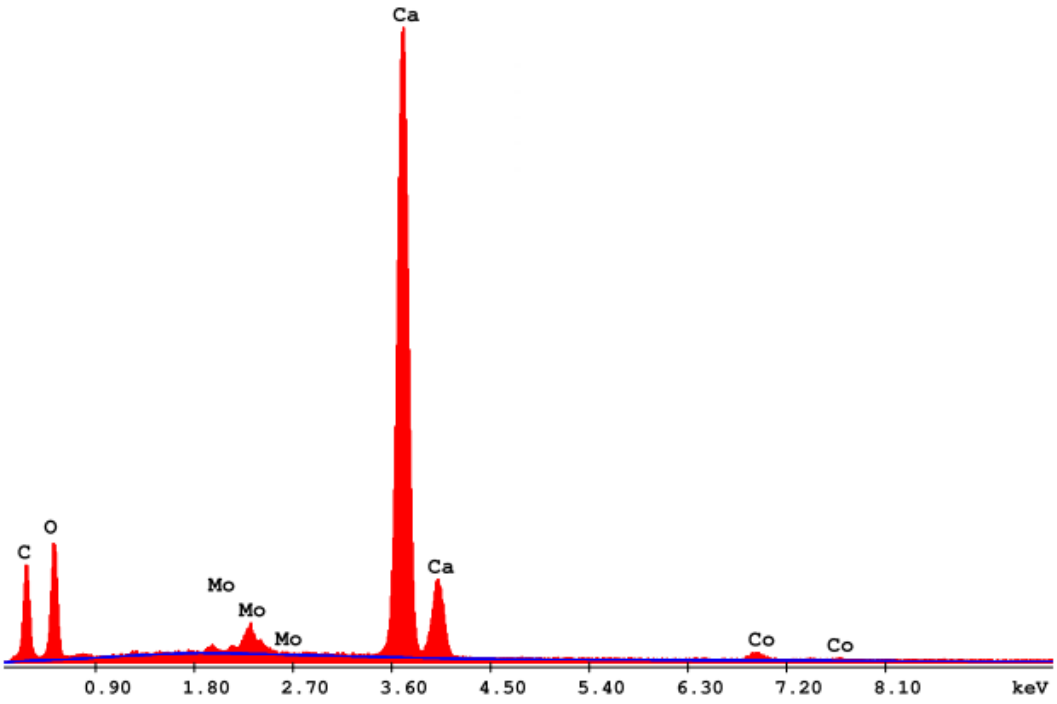


**Figure 4.10** EDS spectrum of the catalyst with a Co:Mo ratio of 0.44 and a calcination temperature of 750˚C.

EDS analysis showed that the elements present in the catalyst were carbon, oxygen, calcium, molybdenum and cobalt. EDS analysis results of Co-Mo impregnated $CaCO_3$ materials are given in Table 4.1. It was observed that metal loading was successfully done. The values of Co:Mo weight ratio were found to be close to that of the calculated Co:Mo weight ratio of 0.44. The weight concentration of Ca was close to 90 wt.%.

**Table 4.1** Weight concentrations of Ca, Co and Mo, and Co:Mo weight ratio for the catalyst with a Co:Mo ratio of 0.44.

| $T_{cal}$ (˚C) | Ca wt.% | Co wt.% | Mo wt.% | Co:Mo wt. ratio (EDS) | Co:Mo wt. ratio (in the initial solution) |
|---|---|---|---|---|---|
| 500 | 88.43 | 3.12 | 8.45 | 0.37 | 0.44 |
| 700 | 90.51 | 3.28 | 6.21 | 0.53 | 0.44 |
| 750 | 90.13 | 2.98 | 6.89 | 0.43 | 0.44 |

Figure 4.11 illustrates EDS spectum for the catalyst with a Co:Mo ratio of 2.30 and a calcination temperature of 750˚C. EDS revealed that Co and Mo elements were successfully incorporated into the $CaCO_3$ support.

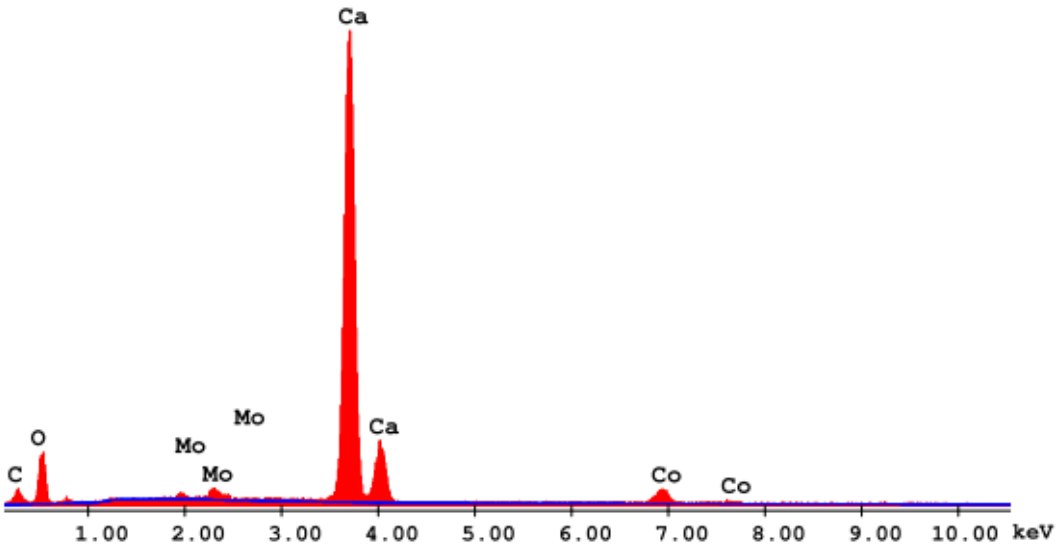


**Figure 4.11** EDS spectrum of the catalyst with a Co:Mo ratio of 2.30 and a calcination temperature of 750˚C.

Table 4.2 gives the weight concentrations for the elements Ca, Co, and Mo and the Co:Mo ratios of the catalyst at three calcination temperatures. From Table 4.2, it was observed that EDS results were consistent with the value of Co:Mo ratio of 2.30 in the initial solution. It could be concluded that Co and Mo elements were successfully incorporated into the $CaCO_3$ support.

**Table 4.2** Weight concentrations of Ca, Co and Mo, and Co:Mo weight ratio for the catalyst with a Co:Mo ratio of 2.30.

| $T_{cal}$ (˚C) | Ca wt.% | Co wt.% | Mo wt.% | Co:Mo wt. ratio (EDS) | Co:Mo wt. ratio (in the initial solution) |
|---|---|---|---|---|---|
| 500 | 90.21 | 6.71 | 3.08 | 2.18 | 2.30 |
| 700 | 88.74 | 8.16 | 3.09 | 2.64 | 2.30 |
| 750 | 88.75 | 7.37 | 3.88 | 1.90 | 2.30 |

In Figure 4.12, EDS spectrum for the catalyst with a calculated Co:Mo ratio of 6 and a calcination temperature of 750˚C is illustrated. The presence of the Co and Mo elements in the catalyst was verified by the EDS analysis.

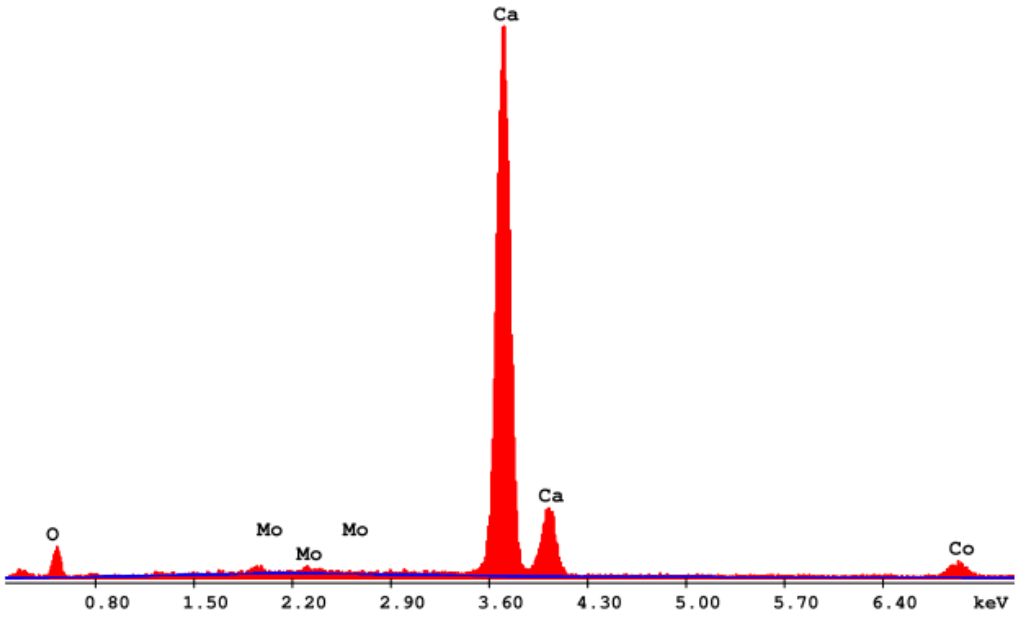


**Figure 4.12** EDS spectrum of the catalyst with a Co:Mo ratio of 6 and a calcination temperature of 750˚C.

Table 4.3 shows the weight concentrations for the elements Ca, Co, and Mo and the Co:Mo ratios of the catalyst at different calcination temperatures. From Table 4.3, it was observed that EDS results were consistent with the value of Co:Mo ratio in the initial solution.

**Table 4.3** Weight concentrations of Ca, Co and Mo, and Co:Mo weight ratio for the catalyst with a Co:Mo ratio of 6.

| $T_{cal}$ (˚C) | Ca wt.% | Co wt.% | Mo wt.% | Co:Mo wt. ratio (EDS) | Co:Mo wt. ratio (in the initial solution) |
|---|---|---|---|---|---|
| 700 | 84.95 | 13 | 2.05 | 6.34 | 6 |
| 750 | 91.24 | 7.15 | 1.61 | 4.44 | 6 |

The difference between weight values for Co, Mo and Ca elements in all synthesized catalysts obtained from EDS and the initial solution might be because of random analysis of different parts of the sample.

The remaining EDS spectra for the catalysts synthesized at three different Co:Mo ratios and calcined at different temperatures are given in Appendix E.

### 4.1.4 XPS Analysis Results

To get information about the chemical state of the catalysts and the compounds present on the catalyst surface, synthesized catalysts were characterized using XPS. The XPS spectrum for the catalyst with a Co:Mo ratio of 0.44 and a calcination temperature of 500ºC is shown in Figure 4.13.

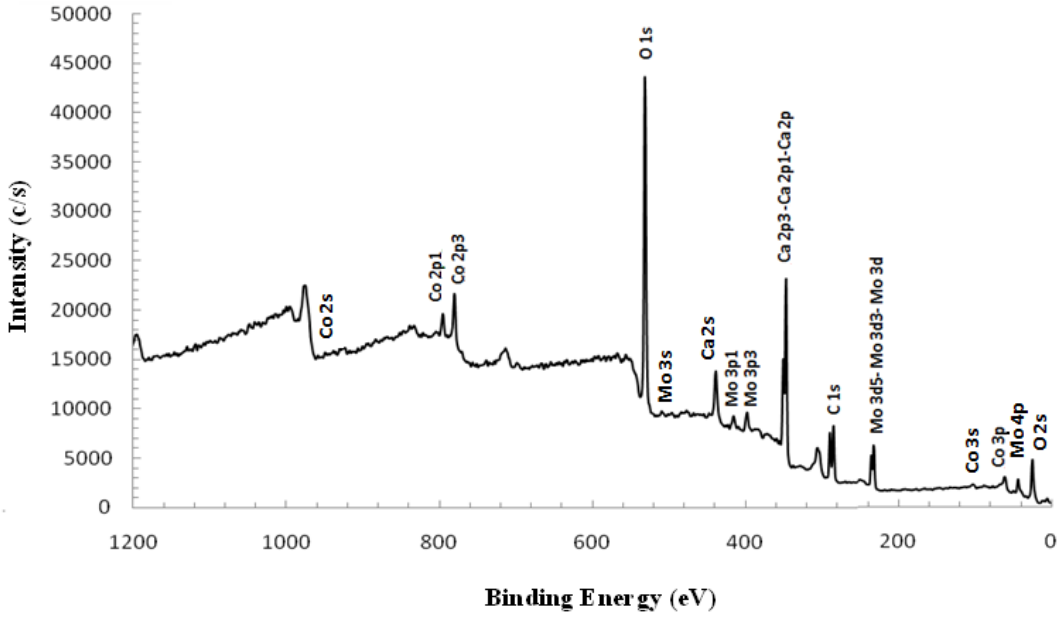


**Figure 4.13** XPS spectrum of the catalyst with a Co:Mo ratio of 0.44 and a calcination temperature of 500ºC.

XPS spectrum (Figure 4.13) showed that cobalt, molybdenum, and calcium elements were present on the surface of the catalyst. In addition to these elements, there were also carbon and oxygen elements on the catalyst surface.

In the XPS analysis of the catalysts, the C 1s peak at a binding energy value of 284.5 eV was taken as a reference. The BE shifts were corrected according to this BE value of C 1s. XPS analysis showed that Co was present in the form of Co oxide phase. In Figure 4.13, Co 2p3 peak observed at a BE value of 780.5 eV and Co 3p peak at a BE value of 60.5 eV were attributed to the presence CoO. XRD results showed that Co mostly had a CoO form in the catalyst. The peak appearing at the Mo 3d5/Mo 3d3/Mo 3d BE value of 232.5 eV might be associated with the formation of $MoO_3$, $CaMoO_4$ and/or $CoMoO_4$ compounds. Mo 3p3 peak at a BE value of 398.5 eV and Mo 3p1 peak at 415.5 eV might correspond to the presence $MoO_3$. Furthermore, the peak of O 1s at 531.5 eV BE also verified the formation of $MoO_3$, $CaMoO_4$ and/or

$CoMoO_4$. In the light of these results, it may be concluded that the decomposition of Mo nitrates led to formation of $Mo^{+6}$ in the form of $MoO_3$, $CaMoO_4$ and $CoMoO_4$ in the catalyst [51]. No metallic Co or Mo was detected during XPS measurements. In addition, the Ca 2p3/Ca 2p1/Ca 2p BE at 346.5 eV was assigned to the presence of $CaCO_3$. These results agree well with XRD results.

In Figure 4.14, XPS spectrum of the catalyst with a Co:Mo ratio of 0.44 and a calcination temperature of 700˚C is given.

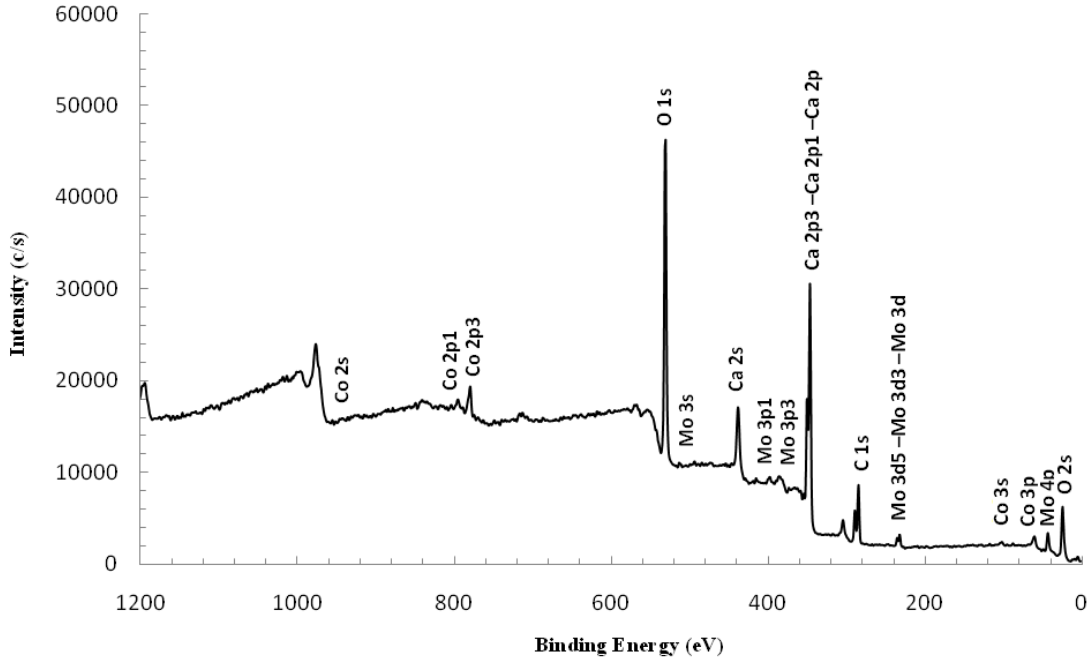


**Figure 4.14** XPS spectrum of the catalyst with a Co:Mo ratio of 0.44 and a calcination temperature of 700˚C.

In Figure 4.14, Co 2p3 peak observed at a BE value of 780.5 and Co 3p peak at a BE value of 60.5 were assigned to the presence CoO. XRD results showed that CoO was present in synthesized catalyst, too. The peak appearing at the Mo 3d5/Mo 3d3/Mo

3d BE value of 232.5 eV might correspond to the presence of $MoO_3$, $CaMoO_4$ and/or $CoMoO_4$ compounds. Mo 3p3 peak at a BE value of 398.5 eV and Mo 3p1 peak at 415.5 eV might be associated with $MoO_3$. Furthermore, the peak of O 1s at 531.5 eV BE also showed the formation of $MoO_3$, $CaMoO_4$ and/or $CoMoO_4$. Futhermore, the Ca 2p3/Ca 2p1/Ca 2p BE at 346.5 eV was attributed to the $Ca(OH)_2$ and CaO. These results agree well with XRD results. The XPS spectrum for the catalyst calcined at 700˚C with Co:Mo ratio 2.30 is given in Appendix F.

## 4.2 Synthesis of Carbon Nanotubes

### 4.2.1 XRD Analysis Results

XRD pattern of the as-synthesized CNT at 700˚C over the catalyst with a Co:Mo ratio of 6 and a calcination temperature of 750ºC is given in Figure 4.15. For this non-purified sample, it was seen from the figure that corresponding peaks to carbon were observed at 2θ value of around 25.9˚ and 43˚ [24, 28]. Additionally, the peaks around 53˚ and 79˚ were also associated with carbon. The peaks appearing at 2θ values of 32.16˚, 37.32˚, 53.80˚, 64.08˚, 67.32˚, 79.54˚, 88.44˚, and 91.40˚ were associated with CaO (48-1467) which originated from the decomposition of $CaCO_3$ at a calcination temperature of around 700˚C. The peaks observed at Bragg angle values of 18.66˚, 28.70˚, 34.24˚, 46.94˚, and 57.96˚ corresponded to the presence of $CaMoO_4$ (29-0351) compound. Furthermore, CoO (75-0419) had a small peak at 2θ value of 34.24˚. The peak at a Bragg angle value of 39.39˚ might be attributed to the presence of $Mo_2C$ (89-3014) in the catalyst structure.

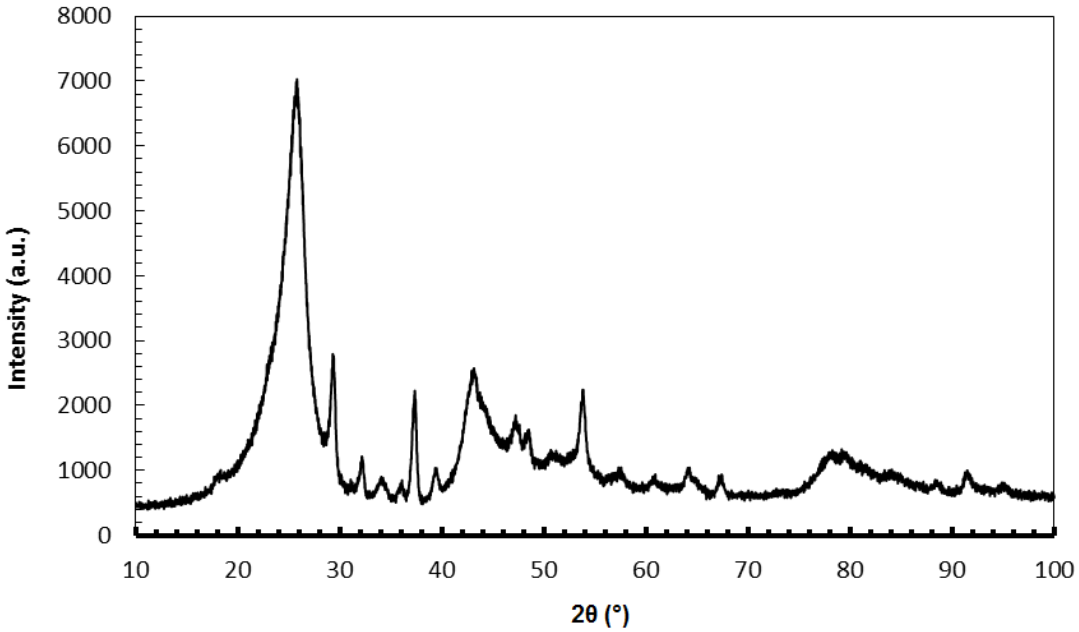


**Figure 4.15** XRD pattern of synthesized CNTs produced at 700˚C on the catalyst with a Co:Mo ratio of 6 and a calcination temperature of 750˚C before purification.

In Figure 4.16, XRD pattern of the purified CNTs which were synthesized over the catalyst with a Co:Mo value of 6 and a calcination temperature of 750ºC is shown. After a single step purification process, all peaks corresponding to the catalytic impurities were diminished. Peaks at 2θ values of 26.11˚ and 43.14˚ were characteristic peaks of nanotubes. Other two small peak observed around 53.40º and 77.89˚ were also attributed to carbon. XRD patterns of the CNTs synthesized at different temperatures and inlet $C_2H_2$ compositions in Ar over Co-Mo/$CaCO_3$ catalyst with different Co:Mo ratios and calcination temperatures are given in Appendix D.2.

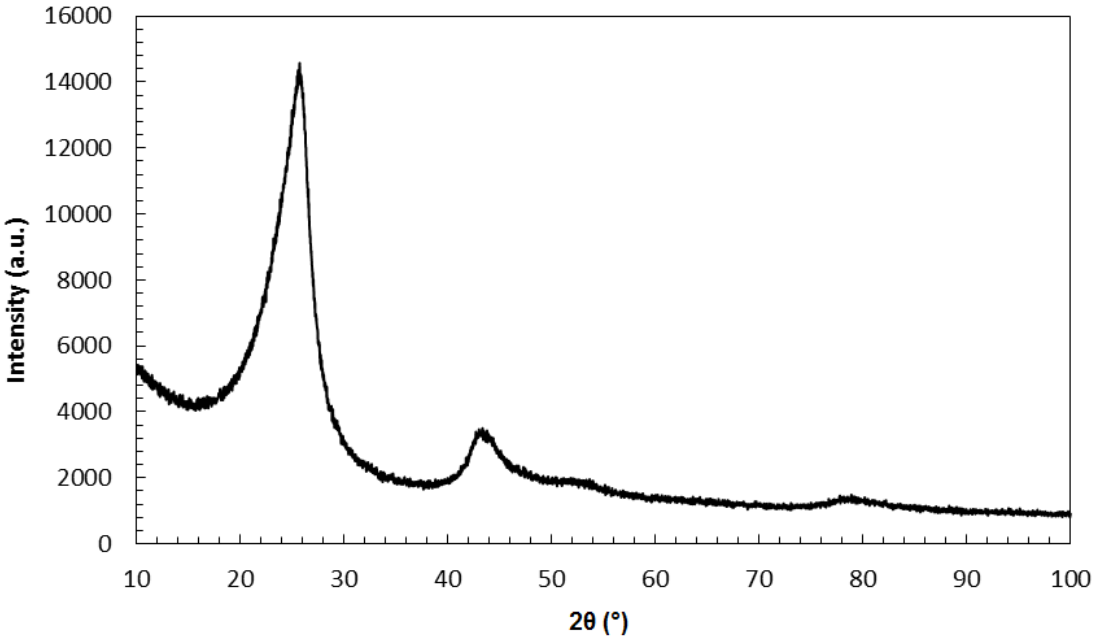


**Figure 4.16** XRD pattern of purified CNTs produced at 700˚C on the catalyst with a Co:Mo ratio of 6 and a calcination temperature of 750˚C

### 4.2.2 SEM and EDS Analysis Results

In Figure 4.17, SEM images of purified CNTs synthesized at 600˚C on the catalyst with a Co:Mo ratio of 0.44 and a calcination temperature of 750˚C are shown. As seen from figure, purified nanotubes produced did not contain impurities or other carboneous nanoparticles. CNTs were agglomerated and had noodle-like shapes with random orientations. They had diameters in the range of 24-36 nm. EDS results showed only C (94.94 wt.%) and O (5.06 wt.%) elements in the products (Figure E.6).

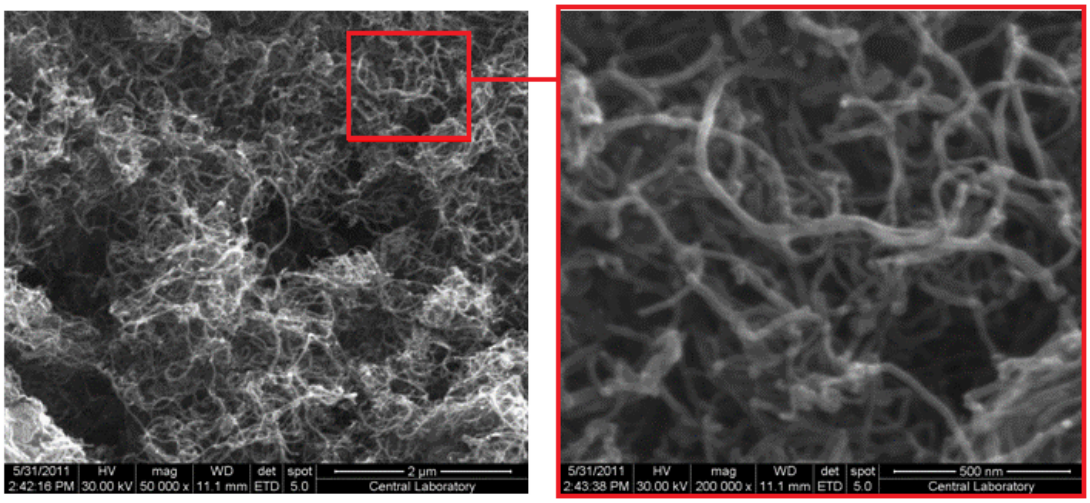


(a) (b)

**Figure 4.17** SEM images of carbon nanotubes produced at 600˚C over the catalyst with a Co:Mo ratio of 0.44 and a calcination temperature of 750˚C at an inlet $C_2H_2$ composition of 25% in Ar (a) 50,000x magnification (b) 200,000x magnification.

SEM images of carbon nanotubes produced at a synthesis temperature of 700˚C on the catalyst with a Co:Mo ratio of 0.44 and a calcination temperature of 750˚C are shown in Figure 4.18. It was observed that purified products mostly contained CNTs with large amounts of impurities (shown in circle). XRD results (Figure D.2.1) showed that these impurities were mostly composed of CaO. The diameters of nanotubes varied from 80 nm to 125 nm. The shape of CNTs was not aligned, but randomly oriented.

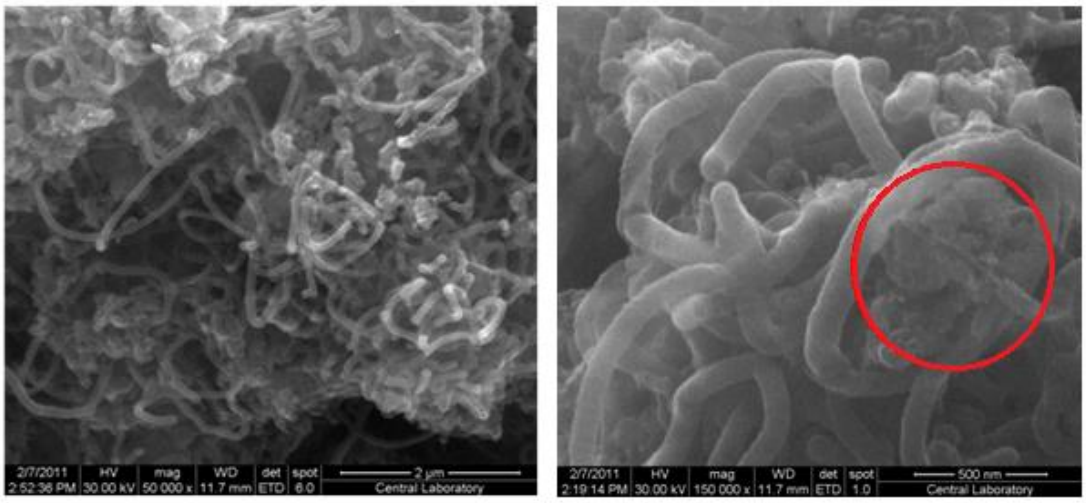


(a) (b)

**Figure 4.18** SEM images of carbon nanotubes produced at 700˚C on the catalyst with a Co:Mo ratio of 0.44 and a calcination temperature of 750˚C at an inlet $C_2H_2$ composition of 25% in Ar (a) 50,000x magnification (b) 150,000x magnification.

As the inlet composition of acetylene in argon was reduced to a value of 20% at 700ºC the products were in nanotube structure. The purified nanotubes were thick and short some of which were open-ended. The outer diameters of nanotubes were in the range of 55-85 nm. As seen from Figure 4.19, nanotubes were highly agglomerated. No other particles were observed in the sample. The inner and outer diameters of the carbon nanotube circled in Figure 4.19 (b) were 28 and 85 nm, respectively.

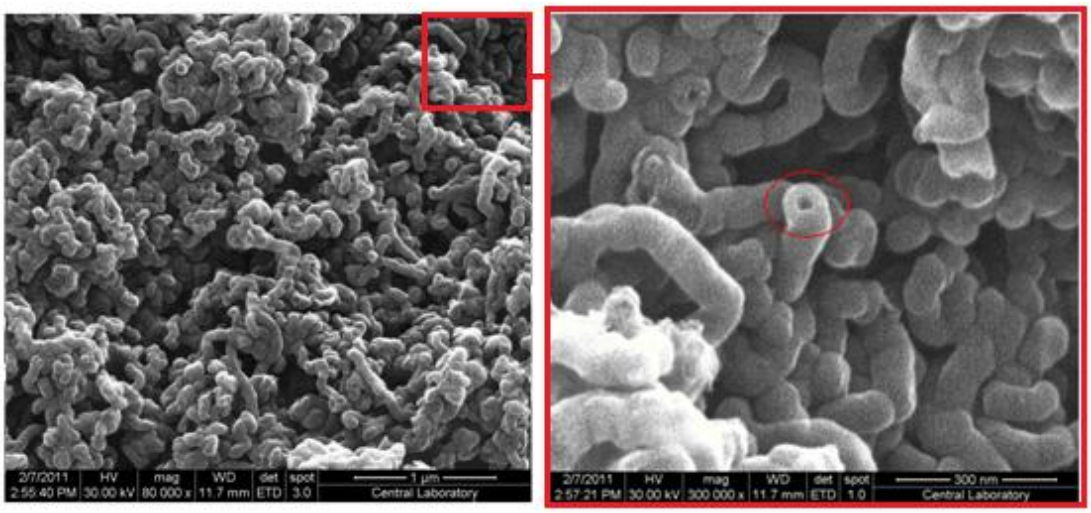


(a) (b)

**Figure 4.19** SEM images of carbon nanotubes produced at 700˚C on the catalyst with a Co:Mo ratio of 0.44 and a calcination temperature of 750˚C at an inlet acetylene composition of 20% in Ar (a) 80,000x magnification (b) 300,000x magnification.

At a relatively higher inlet composition of acetylene (30%) in argon, two different structures (Figure 4.20) were observed in the sample. Whereas globular structures (Figure 4.20-a) with an average diameter of 3.637 µm were present there were also highly agglomerated CNTs (Figure 4.20-b) having diameters varying from 124 nm to 205 nm.

As the inlet acetylene composition in argon was further increased to 50% products were only carbon nanospheres (Figure 4.21). The diameter of nanospheres was approximately uniform with a value of around 550 nm.

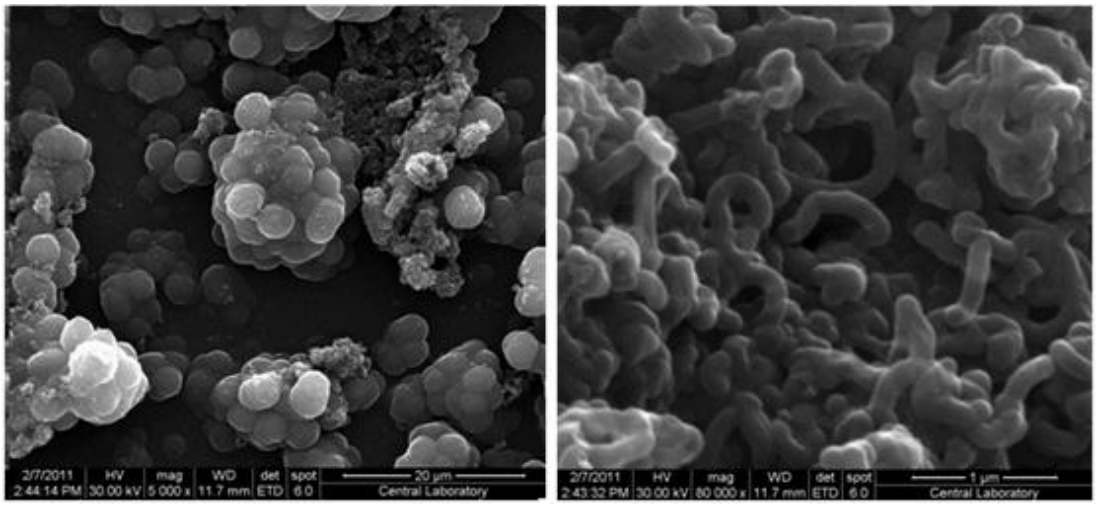


(a) (b)

**Figure 4.20** SEM images of carbon products produced at 700˚C on the catalyst with a Co:Mo ratio of 0.44 and a calcination temperature of 750˚C at an inlet acetylene composition of 30% in Ar (a) 5,000x magnification (b) 80,000x magnification.

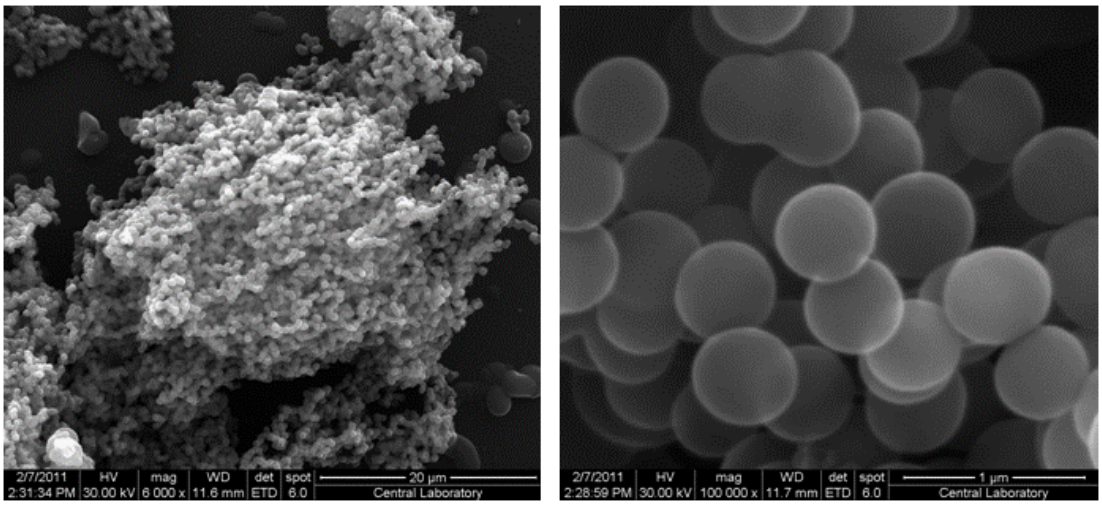


(a) (b)

**Figure 4.21** SEM images of carbon nanospheres produced at 700˚C on the catalyst with a Co:Mo ratio of 0.44 and a calcination temperature of 750˚C at an inlet acetylene composition of 50% in Ar (a) 6,000x magnification (b) 100,000x magnification.

Figure 4.22 shows the products at 800˚C and 1000˚C over the catalyst with a Co:Mo ratio of 0.44 and a calcination temperature of 750˚C. The inlet acetylene composition in argon was 25%. SEM results revealed that the products contained no nanotubes at relatively higher temperatures (800 and 1000˚C). In Figure 4.22 (a) and (b), globular carbon nanoparticles were observed. The average diameters of globular particles at 800 and 1000ºC were 387 and 338 nm, respectively. The globular structures produced at 1000ºC had holes which might result from the blow out (explosion) of globular structures at higher temperatures when compared to that produced at 800ºC. Globular structures might result from the rapid rate of carbon nucleation at high reaction temperatures leading to the encapsulation of catalytic metal particles [19]. EDS results showed that the sample produced at 1000ºC contained catalytic impurities such as Mo (2.86 wt.%), Co (0.40 wt.%) and Ca (1.33 wt.%) elements in addition to C (94.61 wt.%).

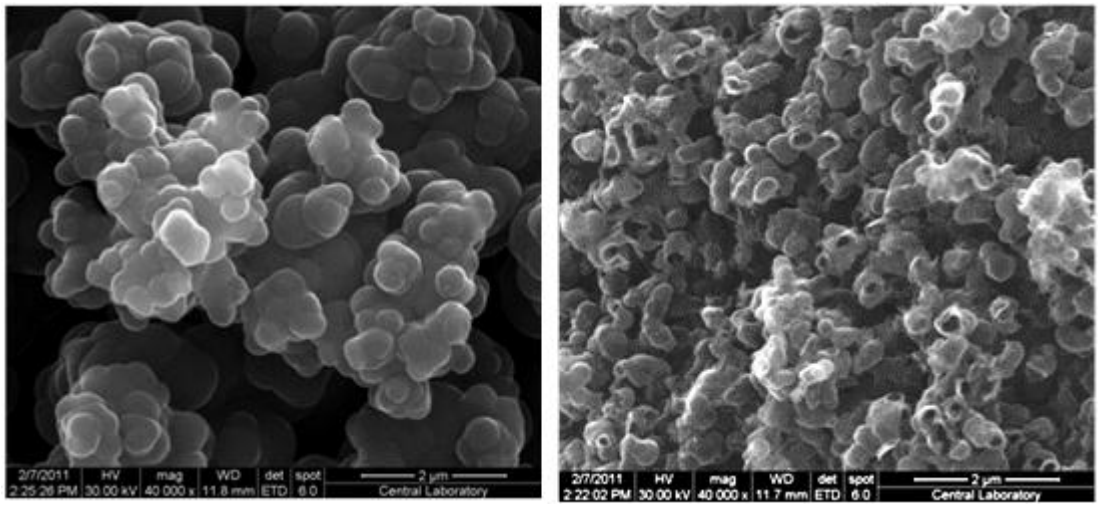


(a) (b)

**Figure 4.22** SEM images of carbon products produced at (a) 800˚C (40,000x magnification) and (b) 1000˚C (40,000x magnification) on the catalyst with a Co:Mo ratio of 0.44 and a calcination temperature of 750˚C (25% $C_2H_2$ in Ar).

In Figure 4.23, SEM images of the nanotubes grown at a synthesis temperature of 700˚C over the catalyst with a Co:Mo ratio of 0.44 and a calcination temperature of 700˚C are illustrated. It could be seen from the figure that CNTs were highly agglomerated (Figure 4.23-a). The diameter of nanotubes measured ranged from 78 to 137 nm. Moreover, deposition of a small amount of amorphous carbon was observed on the outer surface of nanotubes.

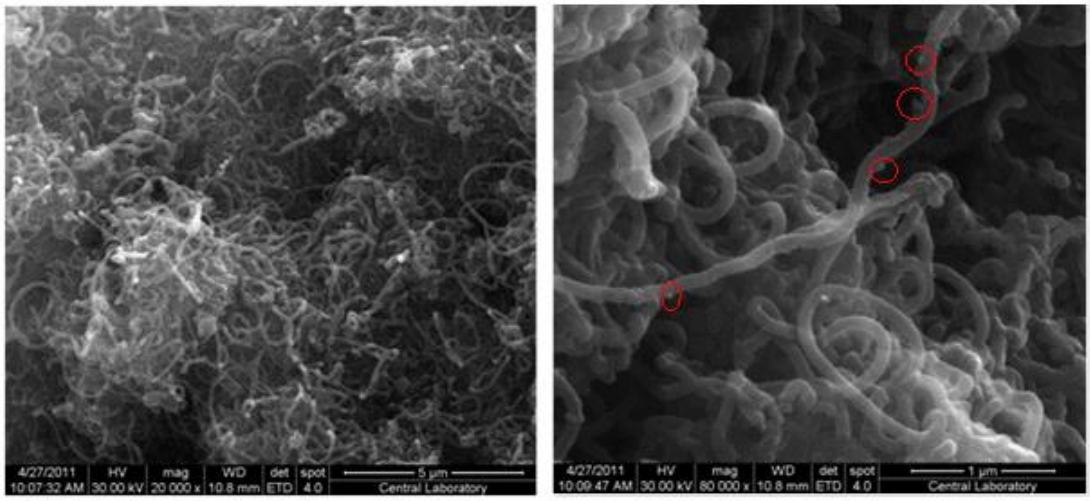


(a) (b)

**Figure 4.23** SEM images of CNTs grown at 700˚C over the catalyst with a Co:Mo ratio of 0.44 and a calcination temperature of 700˚C (25% $C_2H_2$ in Ar) (a) 20,000x magnification (b) 80,000x magnification.

SEM images of the carbon nanotubes produced over the catalyst with a Co:Mo ratio of 0.44 and calcined at 700˚C at different reaction temperatures (500, 600 and 650˚C) are indicated in Figures G.1-G.3. All products synthesized at different reaction temperatures contained entangled CNTs. The average diameters of nanotubes synthesized at 500, 600 and 650˚C were 21, 26 and 47 nm, respectively. It

was observed that diameters of nanotubes increased with an increase in reaction temperature. EDS results (Figure E.7) revealed that CNTs produced at 500ºC contained a small amount of impurities such as Co (1.23 wt.%) and O (4.20 wt.%) elements. The weight percent of C was determined as 94.57%. It was also observed from Figure G.3 (a) that the length of CNTs synthesized at 650˚C reached a length value of 6 μm.

In Figure 4.24, carbon nanotubes grown at a synthesis temperature of 700˚C over the catalyst with a Co:Mo ratio of 0.44 and a calcination temperature of 500˚C are shown. In addition to highly agglomerated nanotubes with noodle-like shapes, some catalyst residues were also observed in SEM images because the products were not purified. However, no other carbon particles were present in the sample. EDS results (Figure E.8) revealed that the products contained impurities such as Ca (8.74 wt.%) and O (6.95 wt.%) elements. The weight percent of C element was determined as 84.31%. CNTs had a diameter range of 67-138 nm.

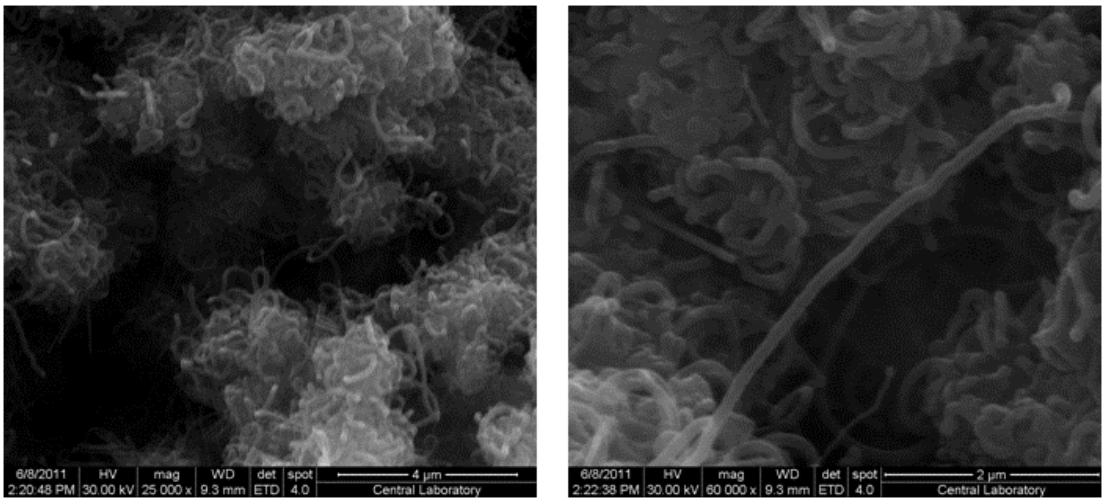


(a) (b)

**Figure 4.24** SEM images of unpurified CNTs grown at 700˚C over the catalyst with a Co:Mo ratio of 0.44 and a calcination temperature of 500˚C (25% $C_2H_2$ in Ar) (a) 25,000x magnification (b) 60,000x magnification.

In Figure 4.25, high density of nanotubes grown at 700˚C over the catalyst with a Co:Mo ratio of 2.30 and a calcination temperature of 750˚C can be observed in SEM images. Purified nanotubes were entangled and higly agglomerated. The diameters of nanotubes changed from 38 nm to 100 nm. No catalytic impurities or other carbonaceous paticles were observed in products.

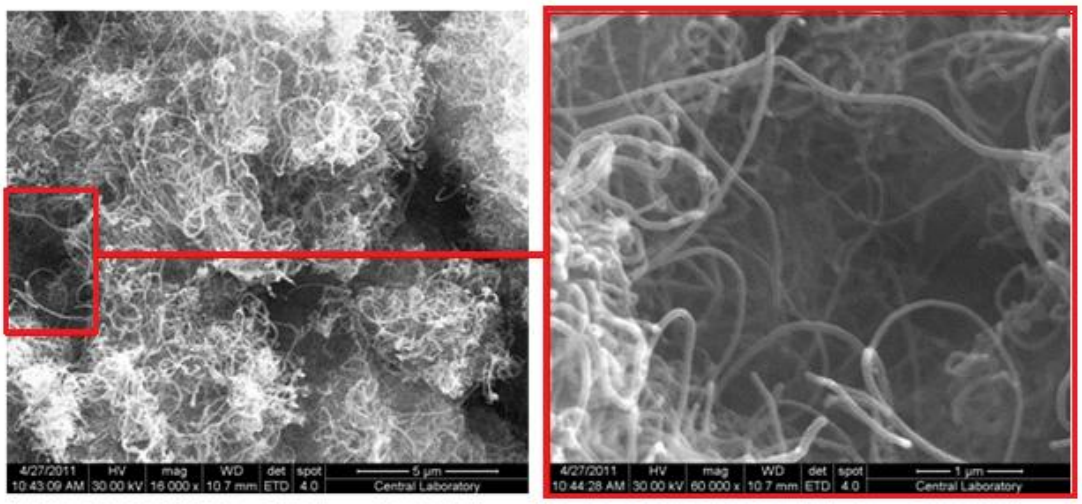


(a) (b)

**Figure 4.25** SEM images of CNTs synthesized at 700˚C on the catalyst with a Co:Mo ratio of 2.30 and a calcination temperature of 750˚C (25% $C_2H_2$ in Ar) (a) 16,000x magnification (b) 60,000x magnification.

SEM images of carbon nanotubes produced on the catalyst with a Co:Mo ratio of 2.30 and a calcination temperature of 750˚C at a synthesis temperature of 500, 600 and 650˚C are illustrated in Figures G.4-G.6. The purified samples contained only noodle-like CNTs. EDS results ( Figure E.9-E.11) showed that no element other than C (100 wt.%) was present in all porducts. The nanotubes synthesized at these temperatures had average diameters close to each other in the range of 31-45 nm.

SEM images of CNTs produced at 700˚C on the catalysts with a Co:Mo ratio of 2.30 which was calcined at 700˚C are indicated in Figure 4.26. The diameters of these nanotubes were measured between 81 and 136 nm.

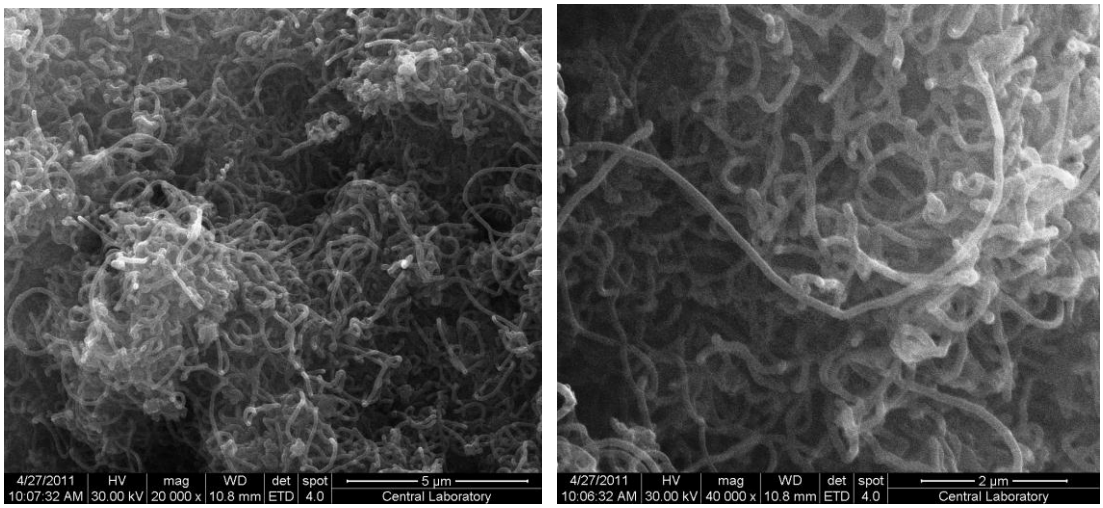


(a) (b)

**Figure 4.26** SEM images of CNTs synthesized at 700˚C on the catalyst with a Co:Mo ratio of 2.30 and a calcination temperature of 700˚C (25% $C_2H_2$ in Ar) (a) 20,000x magnification (b) 40,000x magnification.

From Figures G.7-G.9, it was observed that CNTs synthesized at 500, 600 and 650ºC over the catalyst with a Co:Mo ratio of 2.30 and a calcination temperature 700˚C contained a small amount of amorphous carbon. Furthermore, SEM images revealed that the diameter of nanotubes increased with the increasing reaction temperature. The diameter distribution of nanotubes grown at 500˚C was between 13 and 27 nm while that of CNTs grown at 600˚C was between 13 and 36 nm. Moreover, the diameters of nanotubes grown at 650˚C ranged from 26 nm to 49 nm. Therefore, it

was concluded that the diameters of carbon nanotubes increased with a rise in reaction temperature because of an increase in carbon deposition.

SEM images of CNTs produced at 700˚C on the catalysts with a Co:Mo ratio of 2.30 which was calcined at 500˚C are indicated in Figure 4.27. SEM images revealed thick CNTs with a diameter range of 85-125 nm. Some of nanotubes were longer than 3.6 µm. At higher magnifications, it could be clearly seen that the surface of CNTs was rough. The reason of this might be the deposition of amorphous carbon on the outer surface of nanotubes.

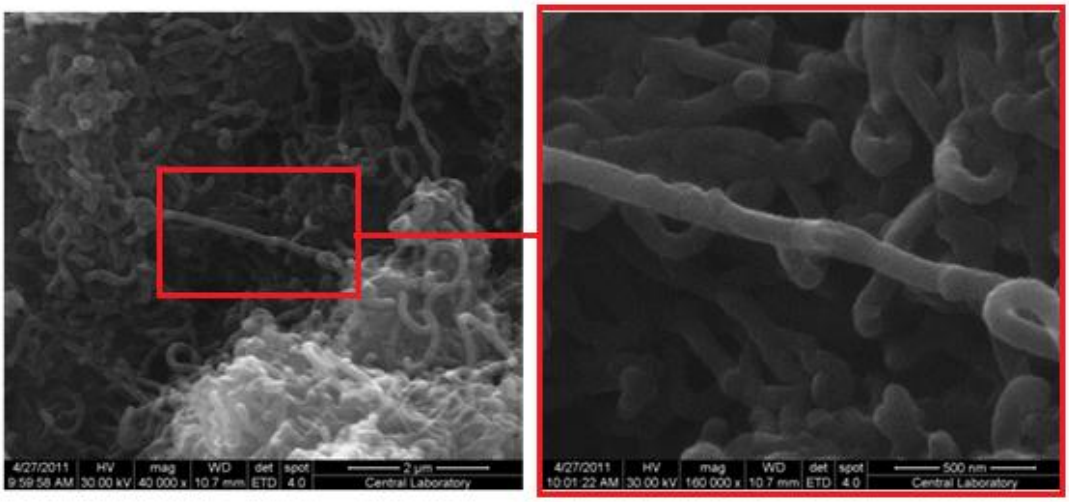

(a) (b)

**Figure 4.27** SEM images of CNTs synthesized at 700˚C on the catalyst with a Co:Mo ratio of 2.30 and a calcination temperature of 500˚C (25% $C_2H_2$ in Ar) (a) 40,000x magnification (b) 160,000x magnification.

In Figure 4.28, SEM images of nanotubes synthesized at 700˚C on the catalyst with a Co:Mo ratio of 6 and a calcination temperature of 750˚C are shown. The sample did

not contain any other carbon nanoparticles. Only dense carbon nanotube regions were observed. The diameters of nanotubes varied from 42 to 106 nm. The length of some nanotubes was around 4 μm.

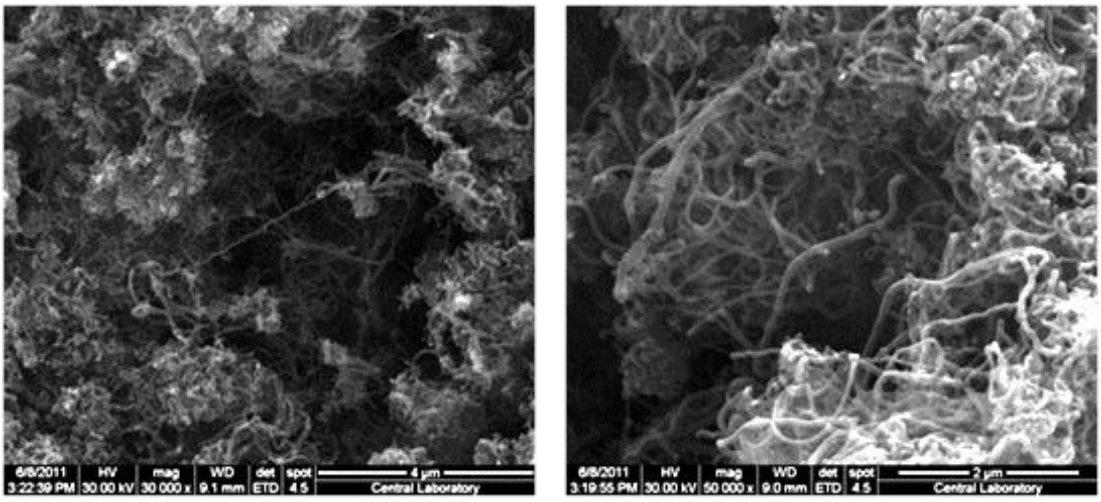


(a) (b)

**Figure 4.28** SEM images of CNTs grown at 700˚C over the catalyst with a Co:Mo ratio of 6 and a calcination temperature of 750˚C (25% $C_2H_2$ in Ar) (a) 30,000x magnification (b) 50,000x magnification.

SEM images of carbon nanotubes produced on the catalyst with a Co:Mo ratio of 6 and a calcination temperature of 750˚C at a synthesis temperatures of 500, 600 and 650˚C are illustrated in Figures G.10-G.12. All CNTs synthesized at these three temperatures were agglomerated and had random orientations. Besides nanotubes, some impurities were observed in the sample synthesized at 500ºC. EDS results (Figure E.12) showed that these impurities composed of Co (0.83 wt.%), Mo (0.31 wt.%) and O (11.14 wt.%) elements. The weight percent of C in this sample was

87.72 %. On the other hand, the products synthesized at 600 and 650˚C included only carbon nanotubes without catalytic impurities.

Figure 4.29 indicates SEM images of nanotubes grown at 700˚C over the catalyst with a Co:Mo ratio of 6 and a calcination temperature of 700˚C. Intensive CNT formation with a noodle-like shape was observed in this sample. The diameter of nanotubes varied from 52 to 82 nm while their length could reach 7 μm. This corresponded to a calculated aspect ratio of 85. Again, random orientation of nanotubes was observed. There was no unwanted products, but only CNTs with high agglomeration. However, EDS results revealed small amount of impurities with a weight percent of 1.96% in the sample.

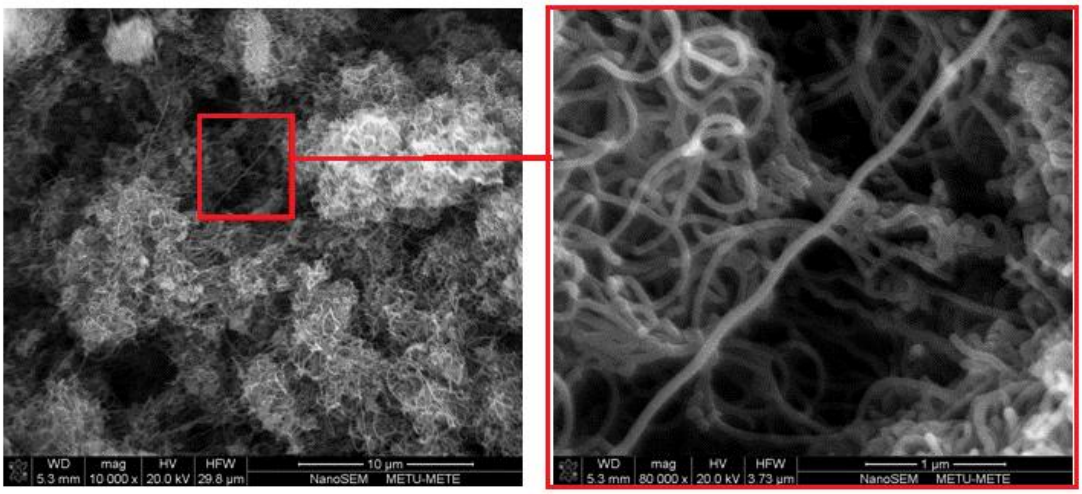


(a) (b)

**Figure 4.29** SEM images of CNTs grown at 700˚C over the catalyst with a Co:Mo ratio of 6 and a calcination temperature of 700˚C (25% $C_2H_2$ in Ar) (a) 10,000x magnification (b) 80,000x magnification.

SEM images of CNTs produced at 700˚C on the catalyst with a Co:Mo ratio of 6 and a calcination temperature of 500˚C are shown in Figure 4.30. SEM images revealed that the longest nanotubes were produced on this catalyst with a length of approximately 32 μm. The diameters of these CNTs were in the range of 81-112 nm. The aspect ratio was calculated as 400. In the sample, no other carbonaceous or catalyst particles were observed which suggested a high selectivity to CNTs. The purified carbon nanotubes were noodle-like and randomly entangled.

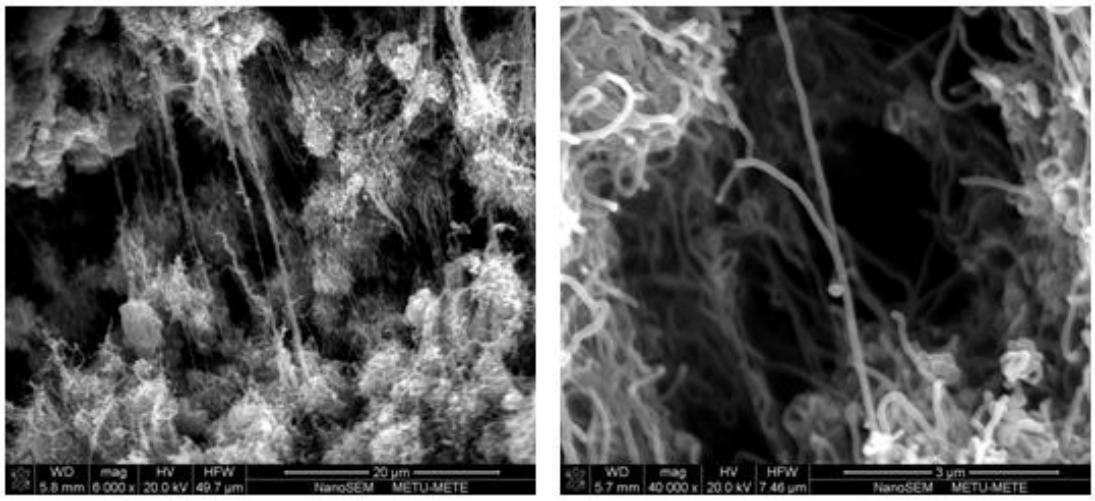


(a) (b)

**Figure 4.30** SEM images of CNTs grown at 700˚C over the catalyst with a Co:Mo ratio of 6 and a calcination temperature of 500˚C (25% $C_2H_2$ in Ar) (a) 6,000x magnification (b) 40,000x magnification.

As a result, it was observed that the reaction temperature was also an important factor on nanotube diameters. An increase in the nanotube diameter could be observed as the reaction temperature increased. On the other hand, it was concluded that the calcination temperature of catalyst did not have a significant effect on the nanotube diameter. The diameters of CNTs synthesized over the catalysts with different calcination temperatures were close to each other.

Figure 4.31 shows the morphological changes in CNTs synthesized at 700˚C over the catalyst with a Co:Mo ratio of 6 and a calcination temperature of 750˚C at different compositions of acetylene. It was observed that all samples only included entangled carbon nanotubes. EDS results (Figure E.13-E.14) showed that samples contained only carbon (100 wt.%). No metallic particles or support material were present in these samples. On the contrary, a little amount of amorphous carbon could be observed on the outer surface of nanotubes. The diameters of CNTs synthesized at an acetylene composition of 10% ranged between 21 and 39 nm. The range of nanotube diameter produced at a composition of 15% and 20% was 30-45 nm and 39-71 nm, respectively. A nanotube was observed at the inlet acetylene composition of 15% in argon with its huge size compared to that of the other CNTs present in the sample. The diameter of this nanotube was 344 nm in average while its length was longer than 64 μm (Figure 4.31-b). This means an aspect ratio of greater than 186. Additionally, the diameter of carbon nanotubes grown at a acetylene composition of 30% varied from 71 to 119 nm. From SEM measurements, it was concluded that the diameters of nanotubes increased with an increase in acetylene composition.

All SEM images showed that CNTs had noodle-like shapes. They were not straight, but bended. This bending might result from relatively low synthesis temperature in chemical vapor deposition method when compared to physical methods such as arc-discharge or laser ablation. Low synthesis temperature in CVD leads to the formation of structural defects in nanotubes. These defects may cause bending or twisting of nanotubes [19]. It could be clearly seen that CNTs were not damaged after the single-step purification in diluted $HNO_3$.

XRD analysis are in agreement with the SEM results. Only carbon element was in the products. There were no other elements detected. This also proved the effectiveness of the single step purification.

SEM images of CNTs produced over Co-Mo/$CaCO_3$ catalysts were given in Appendix G.

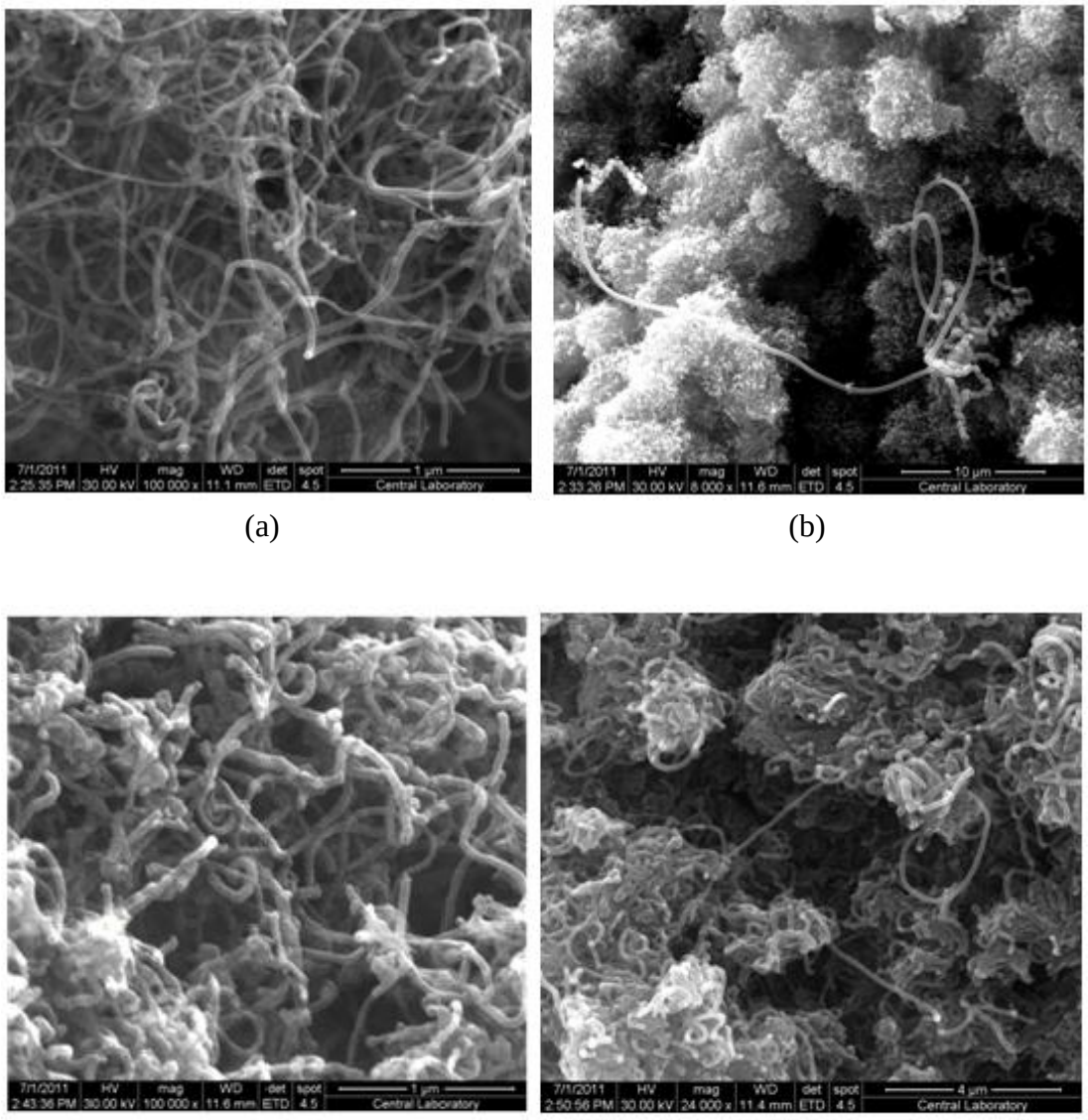


(a) (b)

(c) (d)

**Figure 4.31** SEM images of CNTs grown at 700˚C over the catalyst with a Co:Mo ratio of 6 and a calcination temperature of 750˚C at different $C_2H_2$ compositions in Ar : (a) 10%, (b) 15%, (c) 20%, and (d) 30%.

### 4.2.3 Carbon Deposition Rate and Yield of CNTs

The production of carbon nanotubes was performed at different reaction over Co-Mo/$CaCO_3$ catalysts with different calcination temperatures. Weights of materials after the CNT synthesis experiments and the catalysts after the blank experiments are given in Appendix H. Carbon deposition rate was calculated using the following equation:

$$R_C = \frac{m_T - m_{CB}}{t_{rxn}}$$

where $m_T$ is the total weight of material after CNT synthesis, $m_{CB}$ is the mass of the catalyst after thermal decomposition reaction and $t_{rxn}$ is the reaction time.

In Figure 4.32, the carbon deposition rates at a reaction temperature of 700ºC over the synthesized catalysts at different calcination temperatures and Co:Mo weight ratios are given. It was seen from the figure that carbon deposition rate increased with an increase in catalyst calcination temperature. It was also observed that carbon deposition rate increased with an increase in Co:Mo weight ratio. The highest carbon deposition rate was observed at a catalyst calcination temperature of 750ºC with a Co/Mo ratio of 6 whereas the lowest rate was determined at 500ºC with a Co/Mo ratio of 0.44.

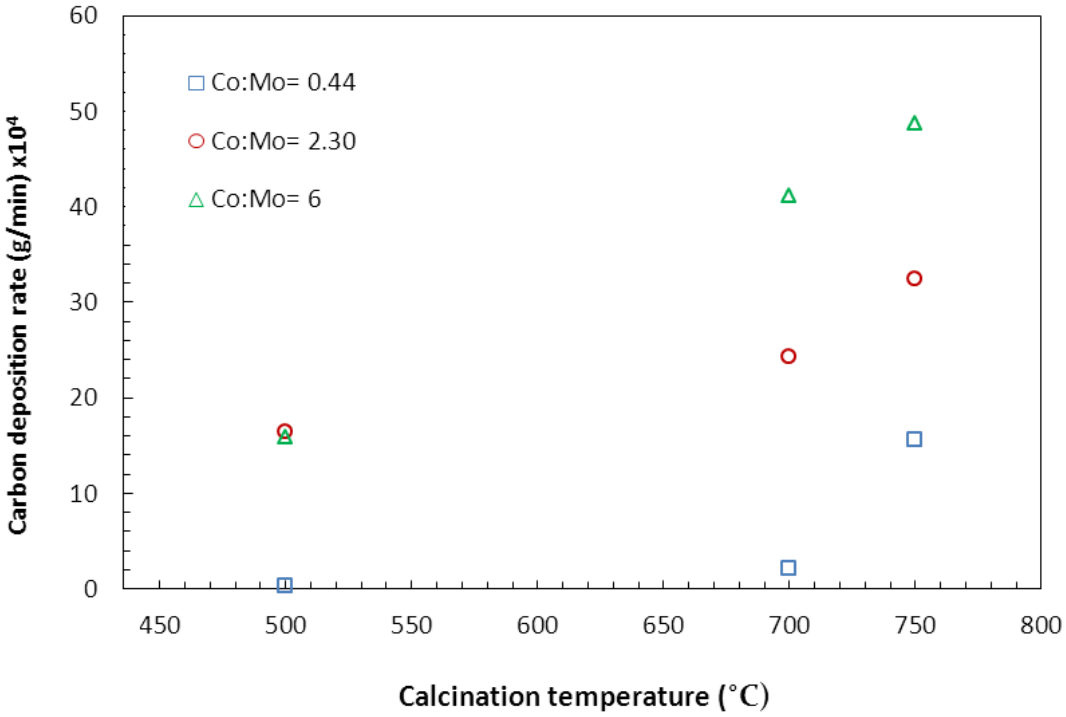


**Figure 4.32** Change of carbon deposition rate with respect to catalyst calcination temperature and Co:Mo weight ratio ($T_{rxn}$=700ºC; 25% $C_2H_2$ in Ar).

In Figure 4.33, carbon deposition rates at different reaction temperatures using the catalyst synthesized with a Co:Mo ratio of 0.44 and a calcination temperature of 750ºC are given. It was observed that carbon deposition rate increased until 700ºC with an increase in reaction temperature. After 700ºC, the increase in the reaction temperature resulted in a decrease in deposition rates because deposition occurred as amorphous carbon as it was observed in SEM images. It was also observed that the CNT yield increased with an increase in Co:Mo weight ratio. This showed that Co was more active than Mo for carbon deposition.

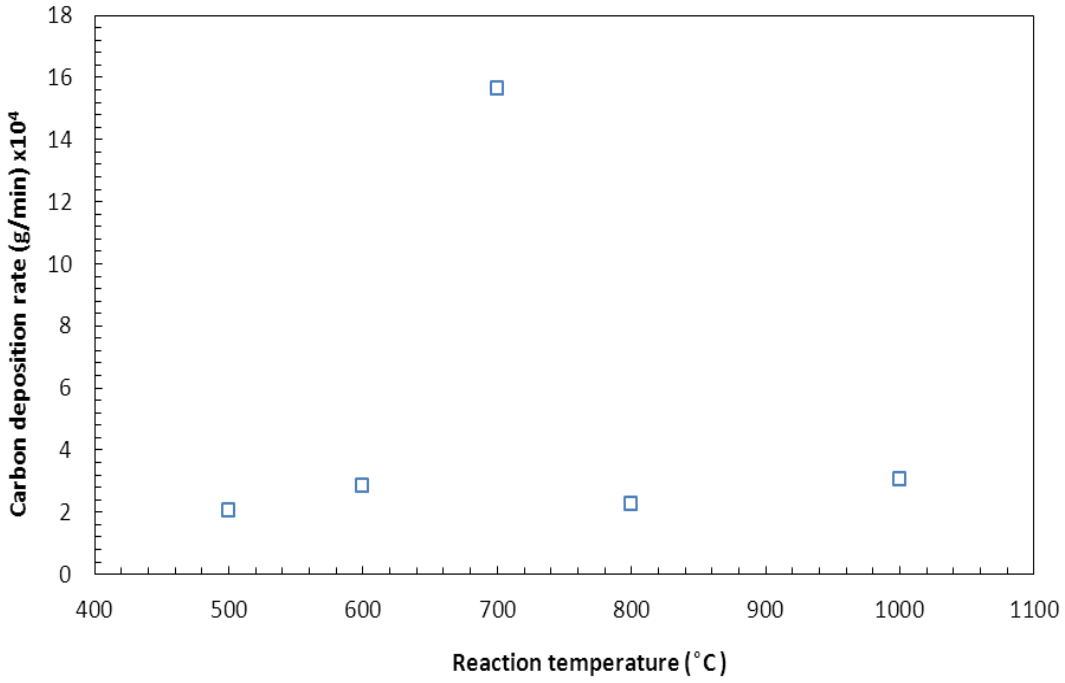


**Figure 4.33** Effect of reaction temperature on carbon deposition rate (Co/Mo: 0.44; $T_{cal}$=750ºC; 25% $C_2H_2$ in Ar).

Figure 4.34 shows carbon deposition rates at different reaction temperatures over the synthesized catalysts with different Co:Mo weight ratios. The calcination temperature for all catalysts was 700ºC. It was observed that there was an increase in carbon deposition rate as the reaction temperature increased as expected. The highest deposition rate was obtained using the catalyst with a Co:Mo ratio of 6 whereas the lowest deposition rate was obtained using the catalyst with a Co:Mo ratio of 0.44. Moreover, deposition rates of the catalyst with a Co:Mo ratio of 0.44 were close to each other at different reaction temperatures. In other words, it did not change as reaction temperature increased.

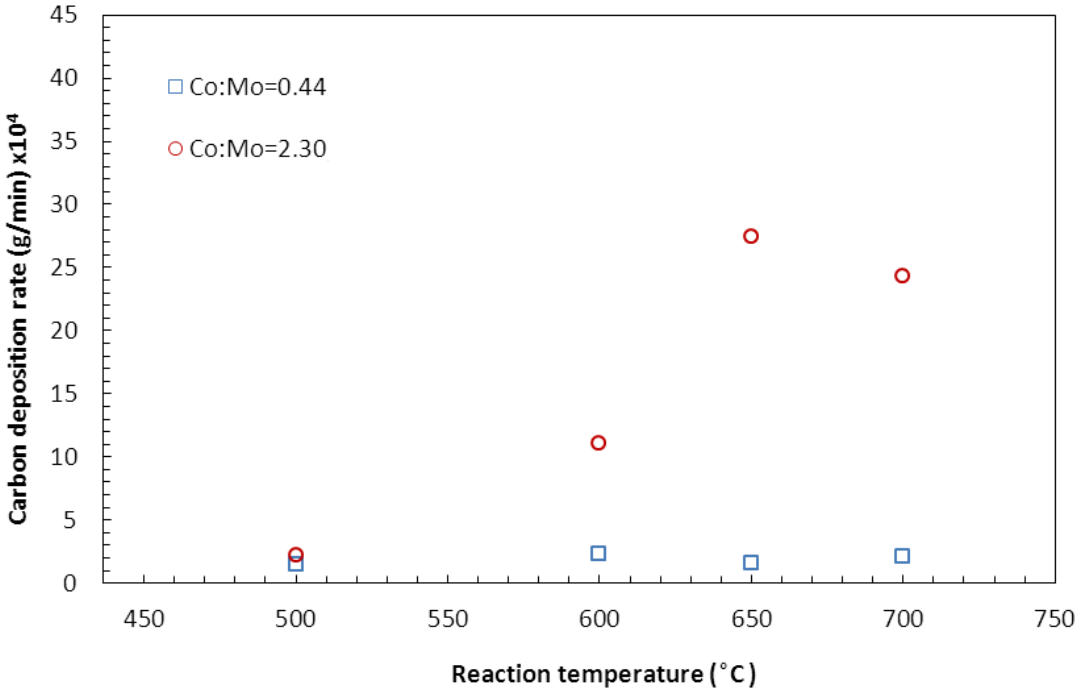


**Figure 4.34** Change of carbon deposition rate as a function of reaction temperature and Co:Mo weight ratio ($T_{cal}$= 700ºC; 25% $C_2H_2$ in Ar).

Carbon deposition rates at different reaction temperatures over the synthesized catalysts at different Co:Mo weight ratios are given in Figure 4.35. The calcination temperature for all catalysts was 750ºC. From the figure it was seen that deposition rates increased with an increase in the reaction temperature as expected. The highest deposition rate was obtained at 700º using the catalyst with a Co:Mo ratio of 6. For the catalyst with a Co:Mo ratio of 2.30, deposition rates at 650 and 700ºC were close to each other. The lowest carbon deposition rate was obtained using the catalyst with a Co:Mo ratio of 0.44. It was observed that there was an increase in deposition rates as the Co:Mo weight ratio increased.

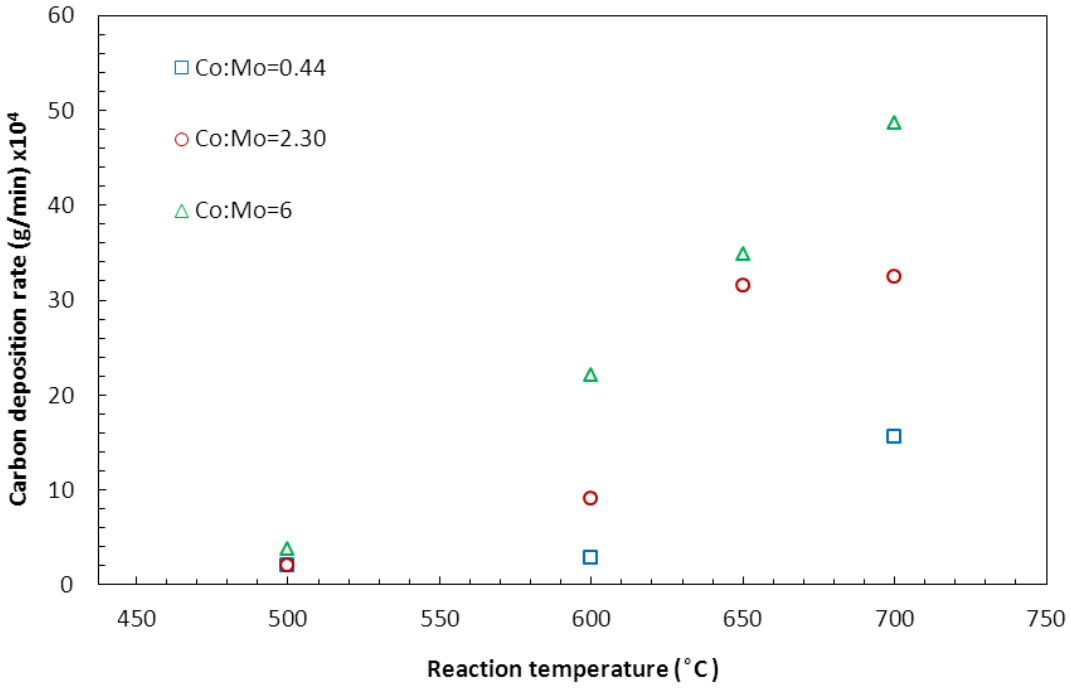


**Figure 4.35** Carbon deposition rates at different reaction temperatures over the synthesized catalysts with different Co:Mo weight ratios ($T_{cal}$= 750ºC; 25% $C_2H_2$ in Ar).

In Figure 4.36, carbon deposition rates obtained using the catalyst with a Co:Mo ratio of 6 and a calcination temperature of 750˚C are given at different acetylene inlet compositions in argon. The synthesis temperature was 700ºC. It can be seen from the figure that there was a slight rise in carbon deposition rates between inlet acatylene compositions of 10% and 20%. Then, deposition rate dramatically increased at inlet acetylene compositions of 25% and 30%. It could be concluded that carbon deposition rate increased with an increase in inlet acetylene composition in argon.

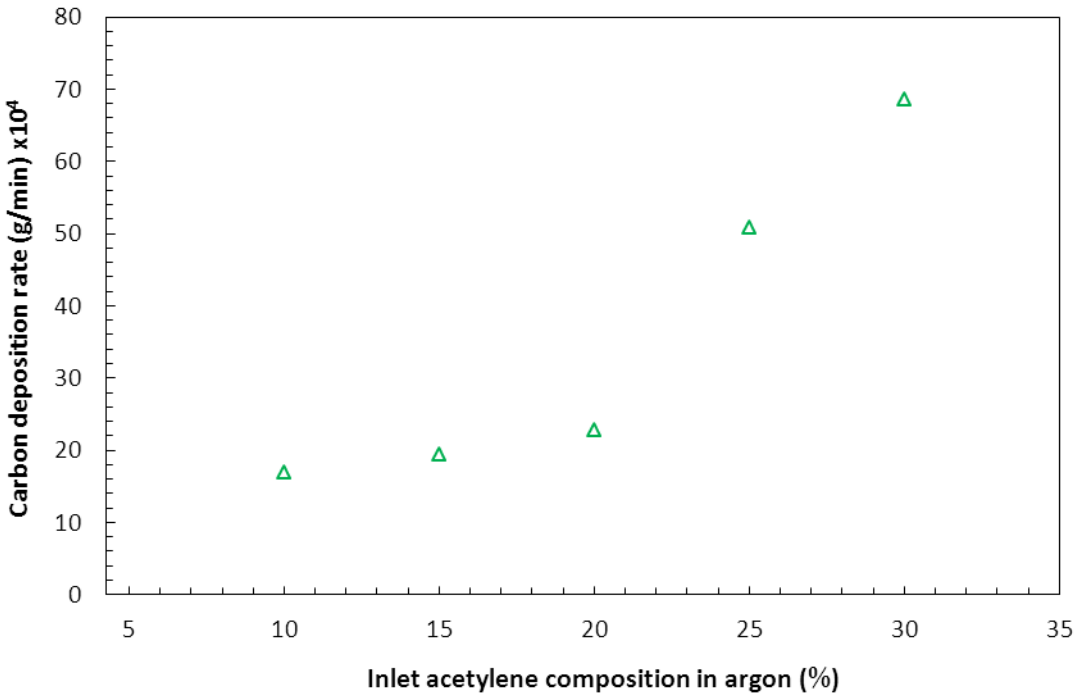


**Figure 4.36** Effect of inlet acetylene composition in Ar on the carbon deposition rate (Co:Mo= 6; $T_{cal}$=750ºC; $T_{rxn}$= 700ºC).

The weight of the catalyst after the blank experiment was used to calculate the yield of the carbon nanotubes after each CNT synthesis. The yield of CNTs was calculated according to the formula given below:

$$Y(\%) = \frac{m_T - m_{CB}}{m_C} X100$$

where $m_T$ is the total weight of the material after synthesis, $m_{CB}$ is the mass of the catalyst after thermal decomposition reaction (blank experiment) and $m_C$ is the initial amount of catalyst used in the CNT synthesis [45].

Yields of CNTs synhesized over Co-Mo/$CaCO_3$ catalysts at different reaction temperatures, calcination temperatures and inlet acetylene compositions in Ar are

given in Figures 4.37-4.40. The yields of CNTs synthesized at a reaction temperature of 700ºC over Co-Mo/$CaCO_3$ catalysts with different calcination temperatures and Co:Mo weight ratios are shown in Figure 4.37. For all catalysts synthesized at different Co:Mo weight ratios, the highest yields were obtained at a calcination temperature of 750ºC. An increase in the CNT yield was clearly seen with an increase in catalyst calcination temperature. The lowest yield was observed at 500ºC. In addition, the increase in Co:Mo weight ratio led to an increase in the CNT yield which showed that Co was more active than Mo for the CNT synthesis. For the catalsyts synthesized with Co:Mo ratios of 2.30 and 6, there was a small difference in the CNT yields at a calcination temperature of 500ºC

There was an increase in the yields of CNTs grown over the catalyst with a Co/Mo ratio of 2.30 as the reaction temperature increases (Figure 4.38). The yields of the catalyst with a Co:Mo weight ratio of 0.44 were low and did not change with reaction temperature significantly. The catalyst with a higher Co:Mo ratio resulted in higher yields. This revealed that Co was more active than Mo for the CNT growth.

Yields of CNTs synthesized at different reaction temperatures over Co-Mo/$CaCO_3$ catalysts with a calcination temperature of 750ºC and different Co:Mo ratios are illustrated in Figure 4.39. The lowest CNT yield was observed at 500ºC for all catalysts. The increase in the reaction temperature resulted in an increase in CNT yields. There was a sharp increase in yields for the catalysts with a Co:Mo ratio of 2.30 and 6 until the reaction temperature of 650ºC. Between 650 and 700ºC, the increase was slow. Moreover, there was also an increase in the CNT yield as the Co:Mo weight ratio increased.

In Figure 4.40, the change in the yields of CNTs synthesized at a reaction temperature of 700ºC over Co-Mo/$CaCO_3$ catalyst (Co:Mo=6; $T_{cal}$= 750ºC) at different acetylene inlet compositions in Ar is shown. A slight increase in the CNT yield was observed between inlet acetylene compositions of 10 and 20% in Ar. After 20%, there was a sharp increase in yields of nanotubes. The highest CNT yield was achieved at 30%.

The yield results revealed that the CNT yield increased as the weight percent of Co increased with respect to Mo. Therefore, it can be concluded that Co is more active than Mo for the CNT growth [45].

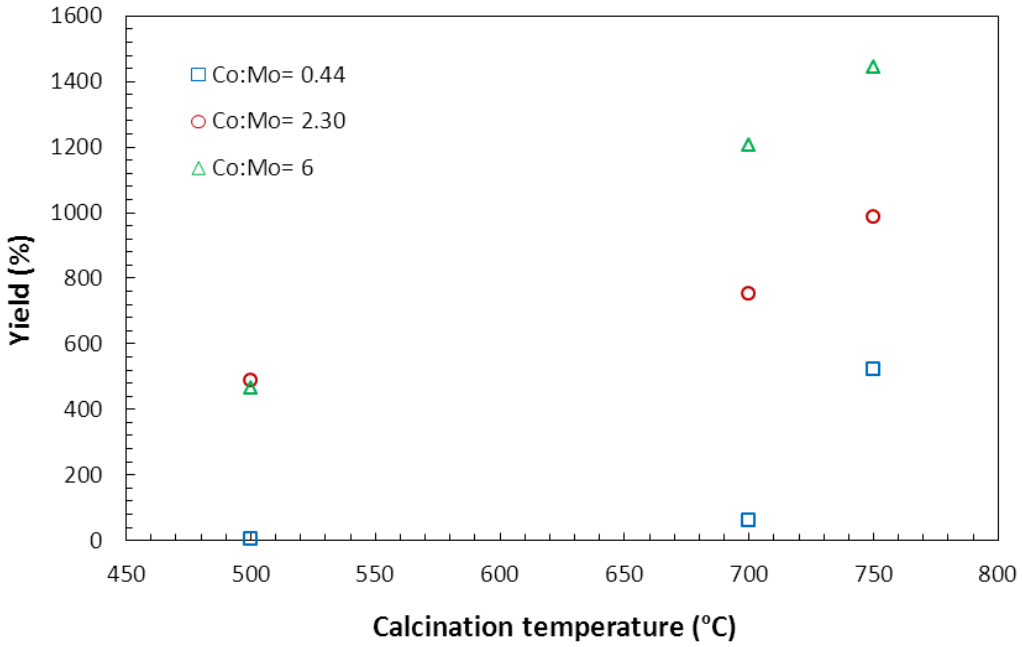


**Figure 4.37** Yields of CNTs synthesized over Co-Mo/$CaCO_3$ catalysts with different calcination temperatures and Co:Mo ratios ($T_{rxn}$= 700ºC; 25% $C_2H_2$ in Ar).

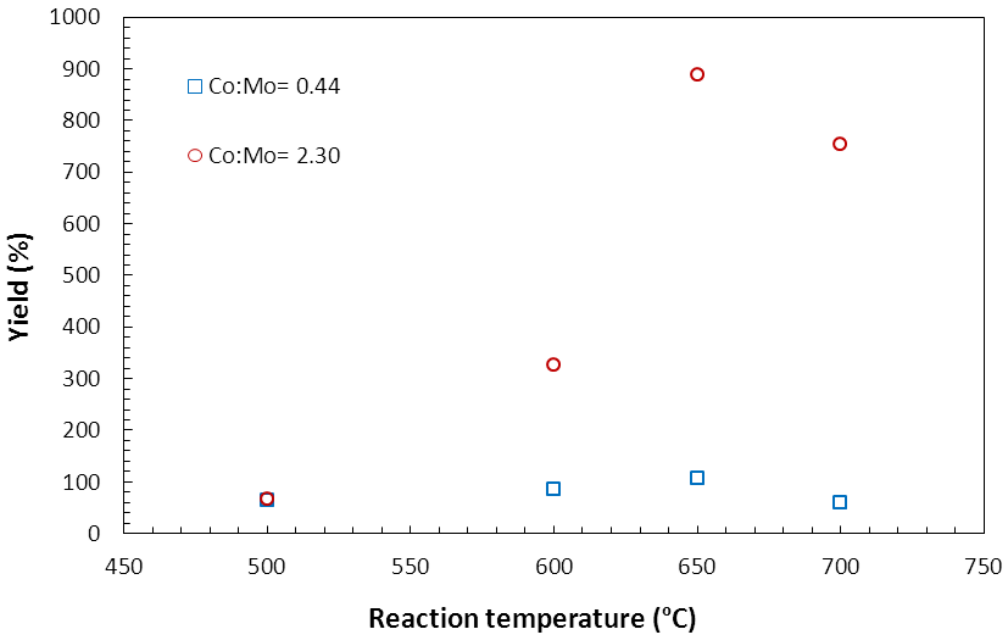


**Figure 4.38** Yields of CNTs synthesized at different reaction temperatures over Co-Mo/$CaCO_3$ catalysts with different Co:Mo ratios ($T_{cal}$=700ºC; 25% $C_2H_2$ in Ar).

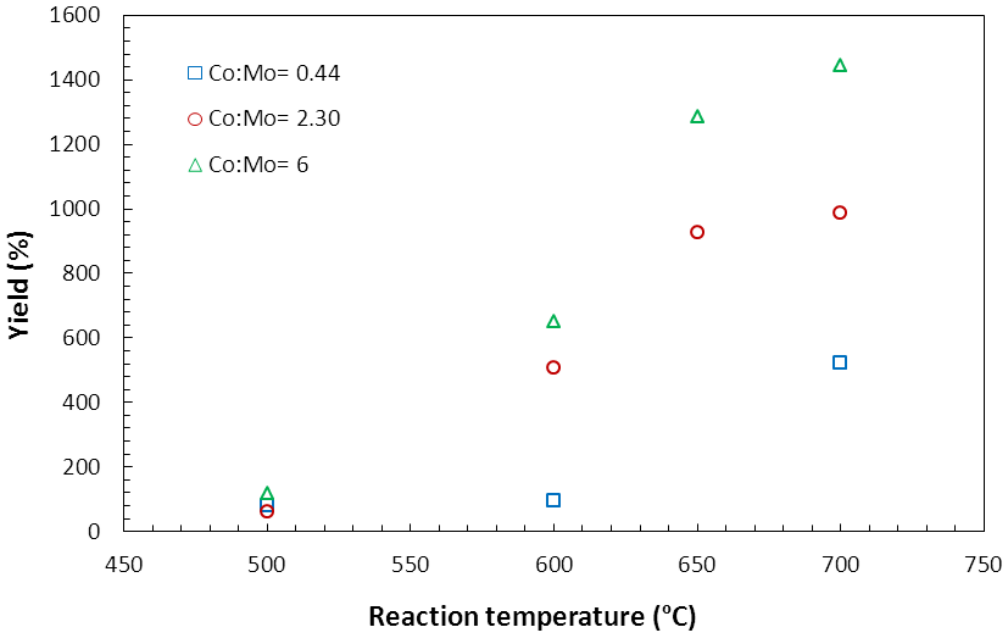


**Figure 4.39** Yields of CNTs synthesized at different reaction temperatures over Co-Mo/$CaCO_3$ catalysts with different Co:Mo ratios ($T_{cal}$=750ºC; 25% $C_2H_2$ in Ar).

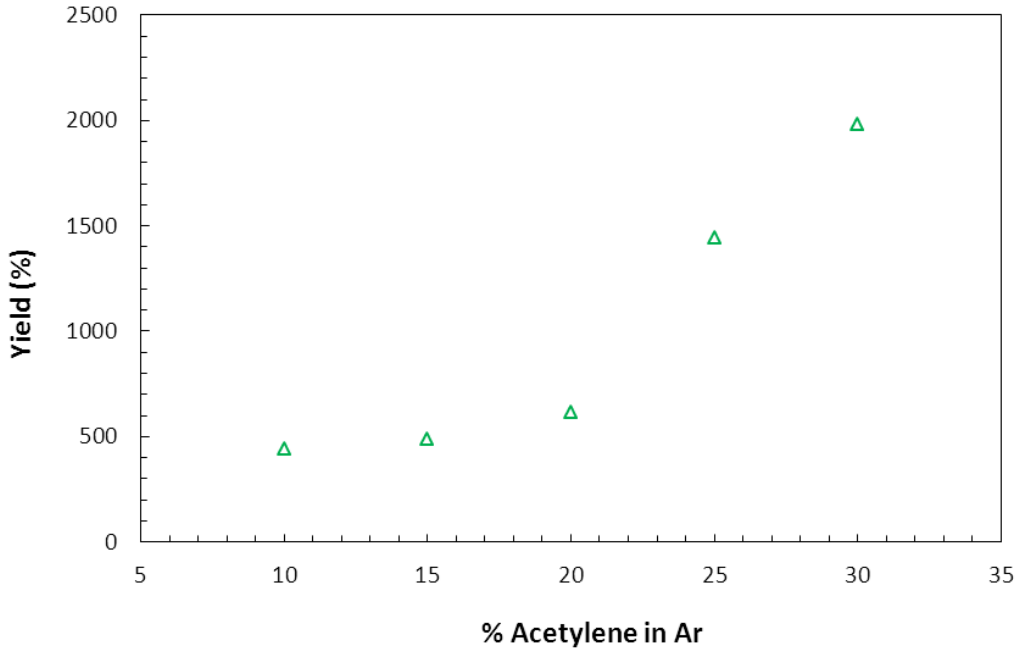


**Figure 4.40** Yields of CNTs synthesized at a reaction temperature of 700ºC over Co-Mo/$CaCO_3$ catalyst (Co:Mo=6; $T_{cal}$= 750ºC) at different acetylene inlet compositions in Ar.

### 4.2.4 TEM Analysis Results

The high resolution TEM image in the Figure 4.41 illustrates a typical tubular wall structure of a MWNT with a central channel. The central channel is an evidence for the CNT structure and used to distinguish them from carbon nanofibers (CNFs) which are also graphitic structures.

As seen from Figure 4.41 the graphitic structure of the CNT was not affected by the purification process. However, there were some defects in the structure of nanotubes. The inner diameter was approximately 7 nm while the outer diameter is 14 nm in average. In addition, high resolution TEM images revealed that MWNT was composed of 8 walls at the left side and 12 walls at the right side. The distance between the graphene sheets was measured as approximately 0.340 nm. This value is

close to the interplanar distance between two adjacent graphene planes in graphite which is 0.3354 nm. Interlayer distance determines the degree of graphitization for graphite-like carbons. In this sample, the graphitization degree was low because of its interlayer distance value. The reason of the low graphitization level might be the curvature of the graphene layers [37].

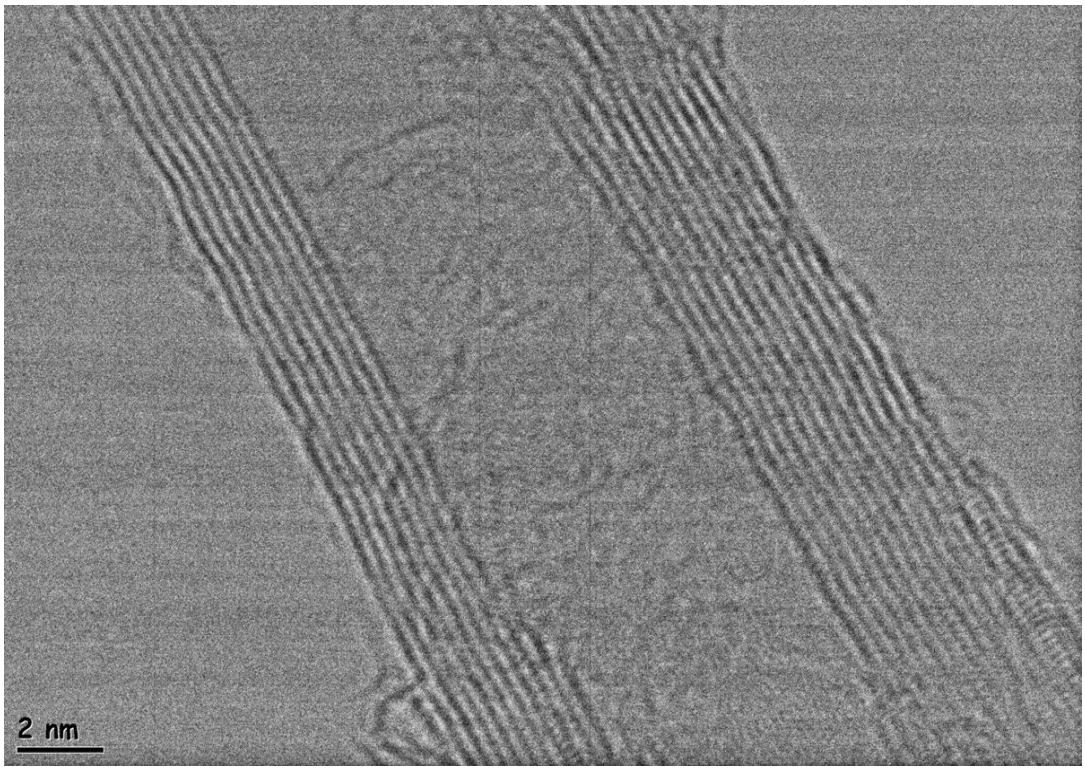


**Figure 4.41** High Resolution TEM image of multi-walled nanotube grown at 700˚C over the catalyst with a Co:Mo ratio of 6 and a calcination temperature of 750˚C.

In Figure 4.42, a TEM image of a multi-walled carbon nanotube with a hollow cylindrical shape which was synthesized at a temperature of 700˚C over the catalyst with a Co:Mo ratio of 6 and a calcination temperature of 750˚C is illustrated. It was

clearly seen that a significant amount of amorphous carbon was deposited on the outer surface of the carbon nanotube. The hollow shape of the CNT with closed tip was also observed. The nanotube has an outer diameter of 11 nm and an inner diameter of 6 nm. The further deposition of carbon on already-formed CNTs may result in the formation of amorphous carbon regions. This deposition might cause thickening and fragmentation of nanotubes [19]. The nanotube diameter was 35 nm in average with amorphous region in Figure 4.42. In this study, the prevention of amorphous carbon and other undesired species formation was aimed using $CaCO_3$ as a support material which is non-porous. Moreover, it was easily dissolved in diluted acids and removed from the sample. Besides, the amount of support material was reduced by the decomposition of $CaCO_3$ into CaO and $CO_2$ at the reaction temperatures above 700˚C which also simplified the purification process of nanotubes.

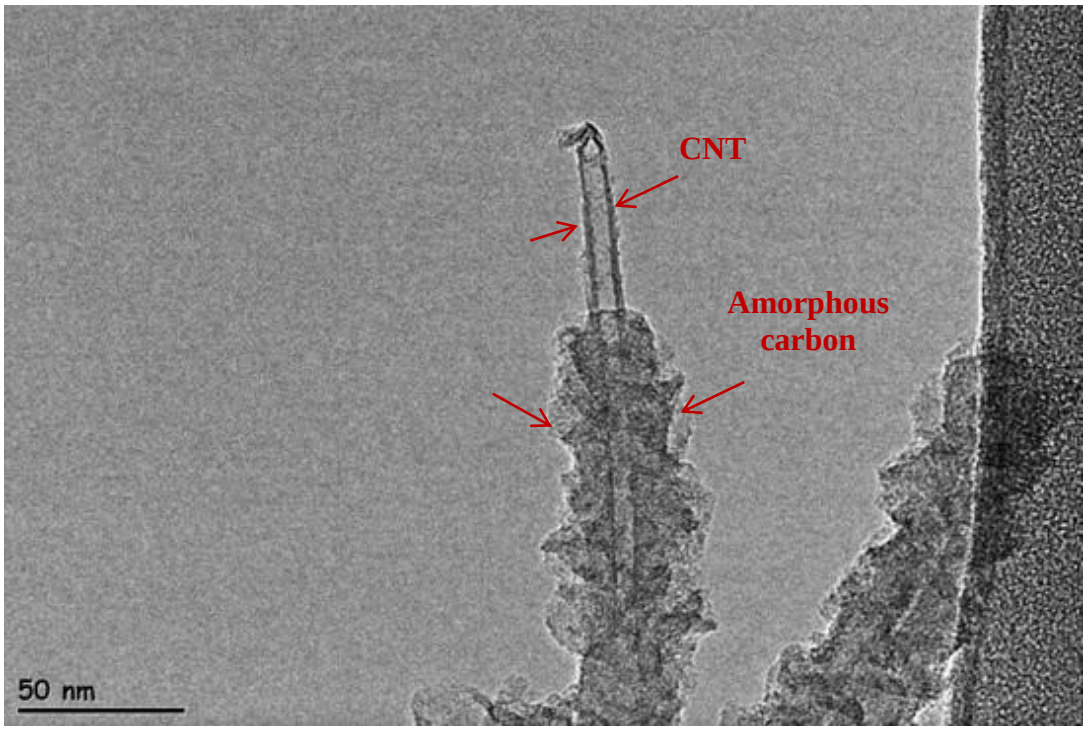


**Figure 4.42** TEM image of a MWNT grown at 700˚C over the catalyst with a Co:Mo ratio of 6 and a calcination temperature of 750˚C.

In Figure 4.43, some CNTs grown over the catalyst (Co/Mo:6; $T_{cal}$=750ºC) at a relatively lower temperature of 600˚C are shown. It was observed that products contained large amounts of MWNTs in bundles. No SWNT was observed in the sample. In addition, other carbonaceous particles were not present in the sample. The inner cavities of CNTs were clearly seen. The origin of the dark spots may be nanotube endings seen with the tube-axis parallel to the beam direction [30].

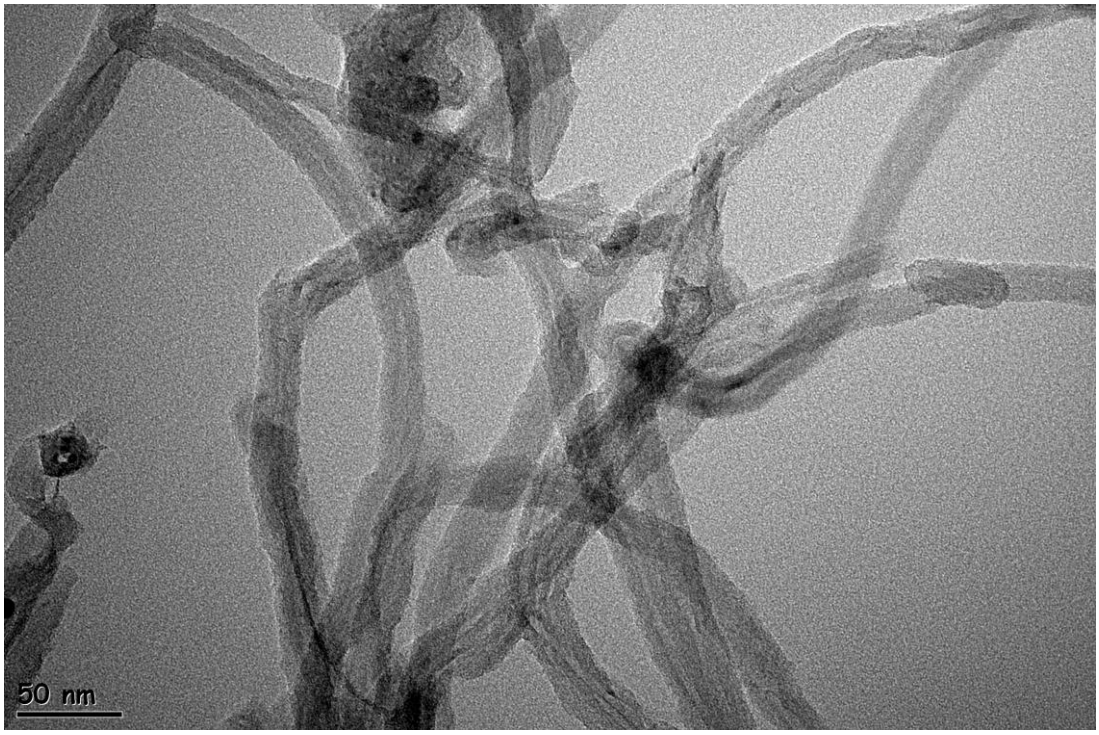


**Figure 4.43** TEM image of CNT bundles grown at 600˚C over the catalyst with a Co:Mo ratio of 6 and a calcination temperature of 750˚C.

The Figure 4.44 illustrates a High Resolution TEM image of the internal structure of a MWNT the walls of which were defective. The walls of this CNT were not well-graphitized. The inner and outer diameters of the nanotube were 3 nm and 16 nm in

average, respectively. TEM image revealed that no metal catalyst particles were encapsulated in the MWNTs which had a closed tip. This might suggest the formation of CNTs by the base growth mechanism.

Figure 4.45 indicates a MWNT with an outer diameter of about 20 nm and an inner diameter of 4 nm. It can be clearly seen that the nanotube had a closed tip. On the outer surface of the nanotube some defects were observed. The central channel and amorphous carbon deposited on the outer surface of the nanotube were clearly seen. TEM images of CNTs are given in Appendix I.

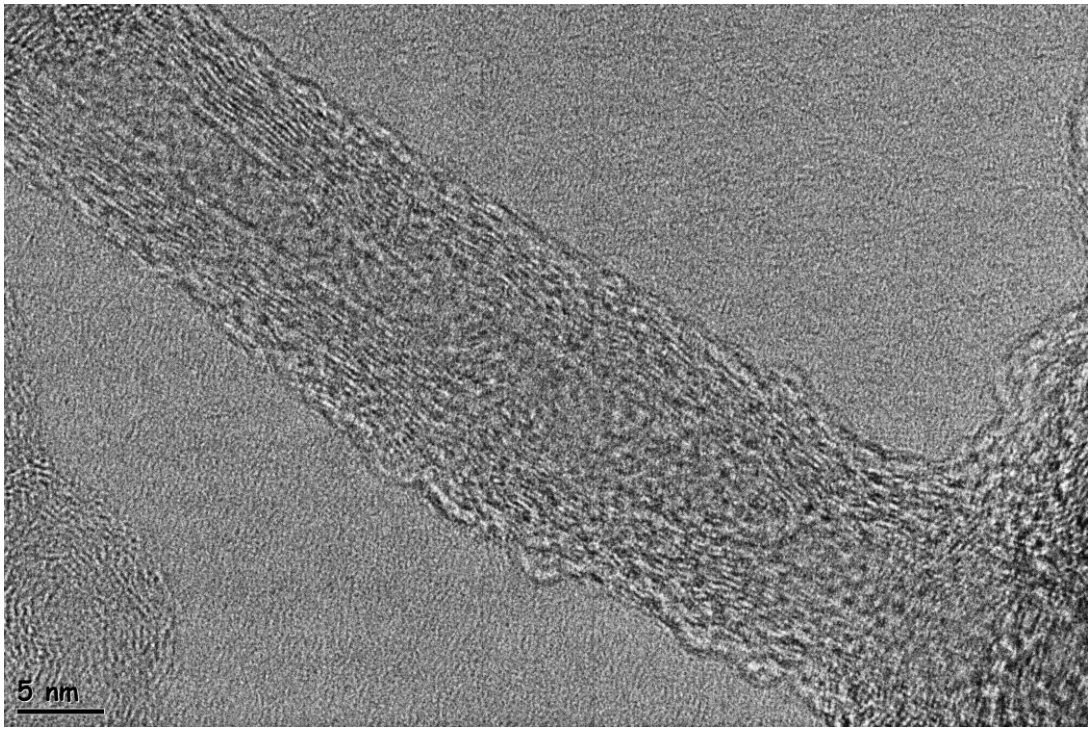


**Figure 4.44** High Resolution TEM image of a MWNT grown at 600˚C over the catalyst with a Co:Mo ratio of 6 and a calcination temperature of 750˚C.

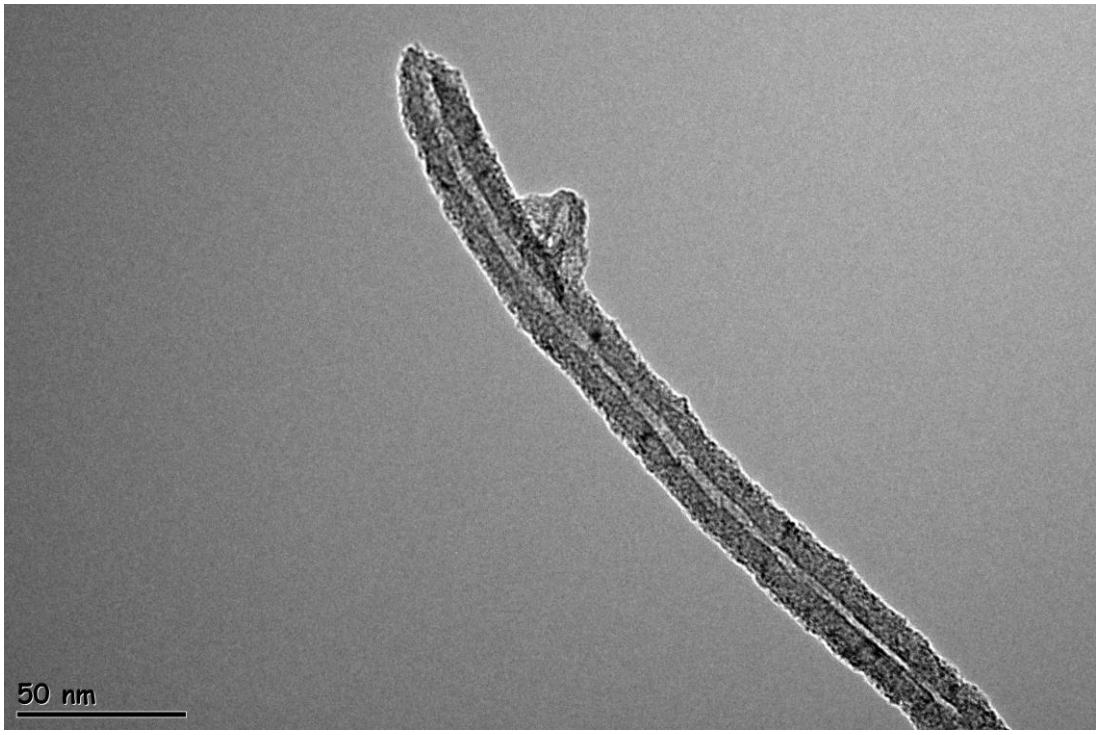


**Figure 4.45** TEM image of a MWNT with a close end grown at 600˚C over the catalyst with a Co:Mo ratio of 6 and a calcination temperature of 750˚C.

### 4.2.5 Thermal Analysis Results

The oxidation behavior in air and the overall purity of the CNTs were evaluated by thermogravimetric analyses. In Figure 4.46, TGA and DTA profiles of MWNTs synthesized at a temperature of 700˚C on the catalyst with a Co:Mo ratio of 6 and a calcination temperature of 500˚C are illustrated. The weight loss at lower temperatures up to around 400˚C was 1.8 wt.% and attributed to the oxidation of the amorphous carbon which was present together with CNTs in the sample. On the other hand, carbon nanotubes oxidizes at higher temperatures up to 800˚C. The higher thermal stability of MWNTs than that of SWNTs might result from the strong interaction between graphene layers in MWNTs. The oxidation of the nanotubes in

this sample started around 400˚C and finished at 751˚C which was in agreement with the studies in literature [20, 28, 30]. A significant weight loss was observed between 400 and 750˚C which originates from the decomposition of MWNTs. This corresponded to a weight loss of 96.6%. According to this quantitative analysis, the purity of MWNTs was determined as around 96%. TGA curve indicated that the amount of amorphous carbon was negligible. The accumulation of large amount of amorphous carbon was prevented by the use of non-porous $CaCO_3$ in catalysts instead of porous supports. Therefore, the selective formation of CNTs was favored.

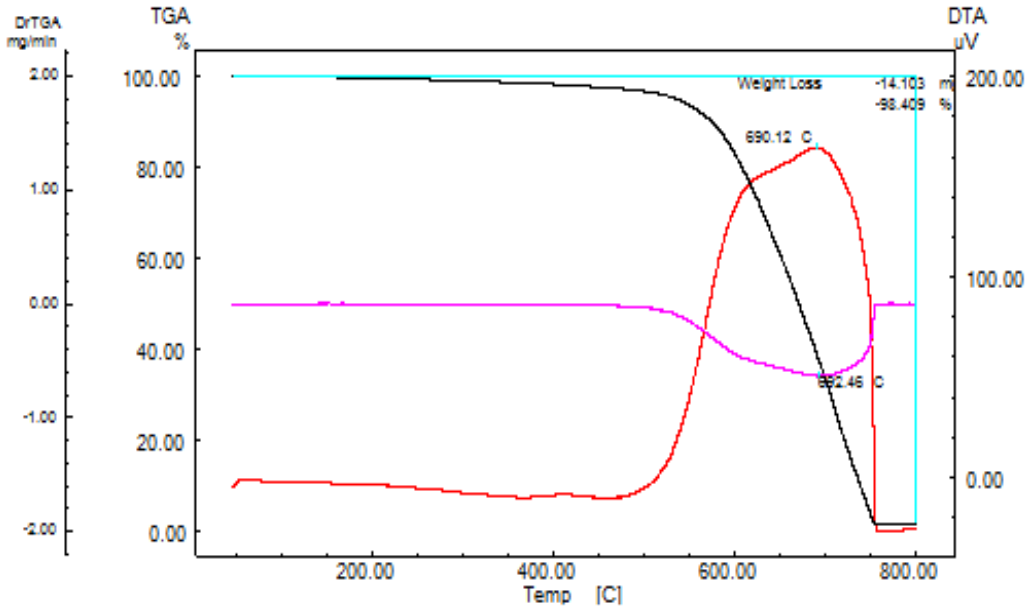


**Figure 4.46** TGA and DTA profiles of MWNTs grown at 700˚C (25% $C_2H_2$ in Ar) over the catalyst with a Co:Mo ratio of 6 and a calcination temperature of 500˚C (black: TGA; red: DTA).

Figure 4.47 indicates the weight loss profile of the MWNTs produced at a temperature of 700˚C on the catalyst with a Co:Mo ratio of 6 and a calcination temperature 700˚C. The weight loss due to combustion of amorphous carbon up to

400 ˚C was determined as 1.8 wt.%. The weight loss between 400 and 765.7˚C was attributed to a decrease in the mass around 97% which might correspond to the overall purity of CNTs.

Figure 4.48 shows the oxidation curve for MWNTs produced at 700˚C on the catalyst with a Co:Mo ratio of 6 and a calcination temperature of 750˚C. A slight loss (1.8 wt.%) in product weight was observed before 400˚C which might be attributed to the combustion of amorphous carbon. It could be also seen from Figure 4.48 that there was a considerable weight loss between 400 and 735˚C. This loss in mass corresponded to 97.3 wt.%. The TGA result revealed that the overall purity of MWNTs was approximately 97 %.

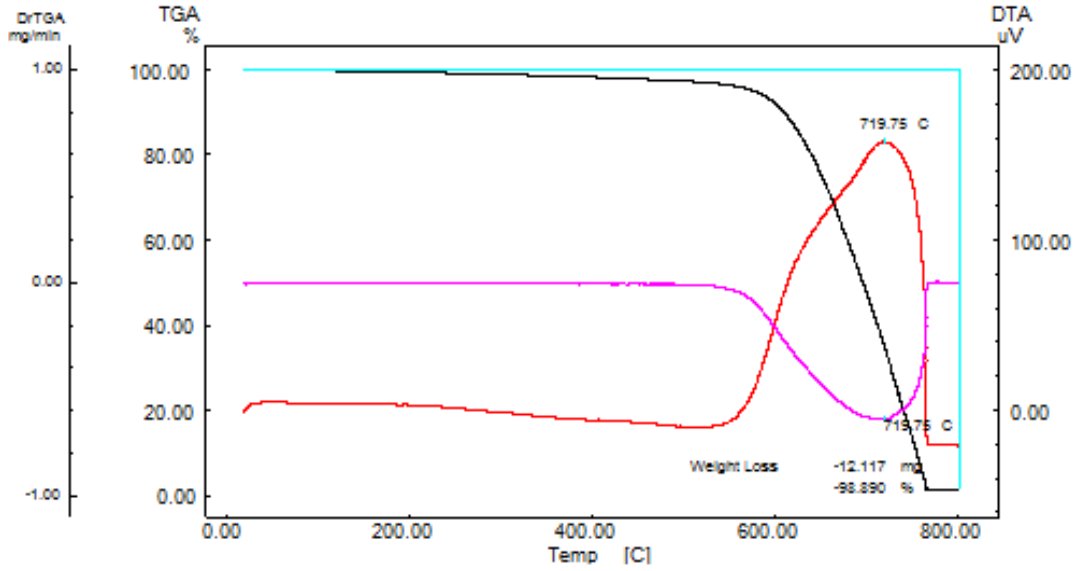


**Figure 4.47** TGA and DTA profiles of MWNTs grown at 700˚C (25% $C_2H_2$ in Ar) over the catalyst with a Co:Mo ratio of 6 and a calcination temperature of 700˚C (black: TGA; red: DTA).

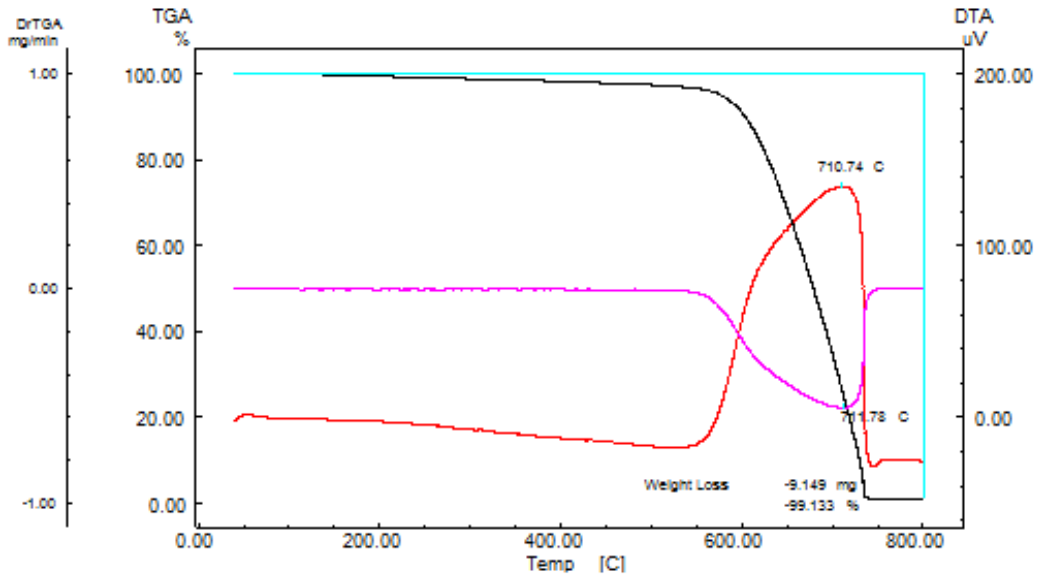


**Figure 4.48** TGA and DTA profiles of MWNTs grown at 700˚C (25% $C_2H_2$ in Ar) over the catalyst with a Co:Mo ratio of 6 and a calcination temperature of 750˚C (black: TGA; red: DTA).

In the light of thermal analyses, it was concluded that the weight loss in the samples was increased with an increase in catalyst calcination temperature. It was also said that the overall purity of nanotubes increased with an increase in the reaction temperature.

The TGA and DTA profiles (Figure 4.49) of carbon nanotubes synthesized at 600˚C over the catalyst with a Co:Mo ratio of 6 and a calcination temperature of 750˚C indicated a decline in the mass up to 400˚C. This weight loss was determined as 5.8 wt.% and associated with the amount of amorphous carbon in the sample. Additionally, the weight loss between 400 and 682˚C was 93.3 wt.%. Thus, the purity was determined as around 93%.

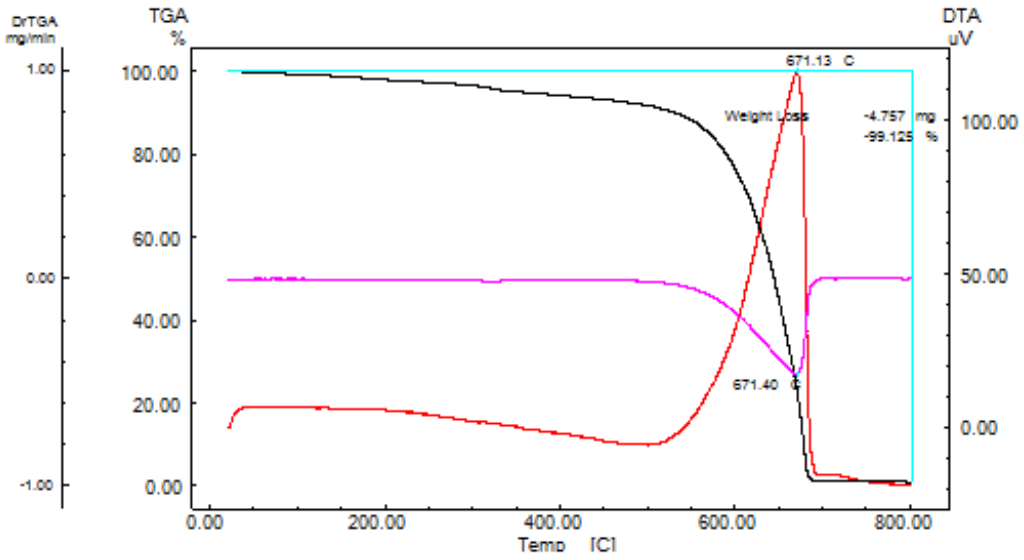


**Figure 4.49** TGA and DTA profiles of MWNTs grown at 600˚C (25% $C_2H_2$ in Ar) over the catalyst with a Co:Mo ratio of 6 and a calcination temperature of 750˚C (black: TGA; red: DTA).

The weight loss profile for CNTs grown at 500˚C over the catalyst with a Co:Mo ratio of 6 and a calcination temperature of 750˚C is illustrated in Figure 4.50. The weight loss up to 400˚C is around 2.9 wt.% because of the oxidation of amorphous carbon. There was also a significant weight loss between 400 and 709˚C with a value of 93.8 wt.% which was attributed to the oxidation of MWNTs. This concluded that the purity of the CNTs was approximately 94%.

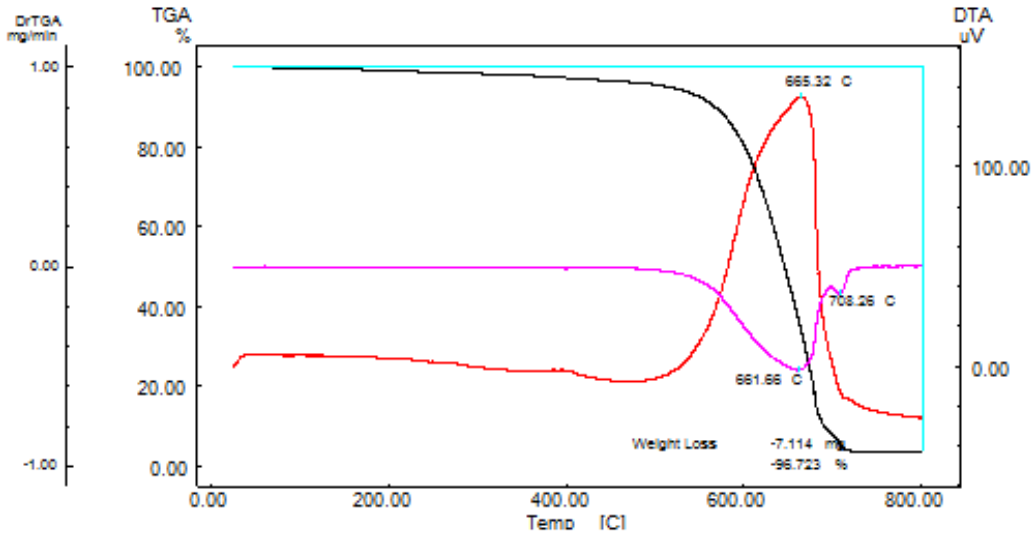


**Figure 4.50** TGA and DTA profiles of MWNTs grown at 500˚C (25% $C_2H_2$ in Ar) over the catalyst with a Co:Mo ratio of 6 and a calcination temperature of 750˚C (black: TGA; red: DTA).

TGA results indicated that the oxidation temperature of nanotubes increased with an increase in the synthesis temperature. It was also observed that the purity of CNTs produced at lower temperatures such as 500 and 600˚C was lower than that of nanotubes produced at a relatively higher reaction temperature of 700˚C using the same catalyst.

### 4.2.6 BET Analysis Results

In Figure 4.51, nitrogen adsorption/desorption isotherms of MWNTs produced at different reaction temperatures over Co-Mo/$CaCO_3$ catalyst with a Co:Mo ratio of 6 and a calcination temperature of 750˚C are shown. Carbon nanotubes exhibited isotherm of Type II according to the Brauner-Deming-Deming-Teller (BDDT) classification. This behavior is observed when the adsorption occurs on the non-

porous powders or on the powders having pore diameters larger than micropores [47].

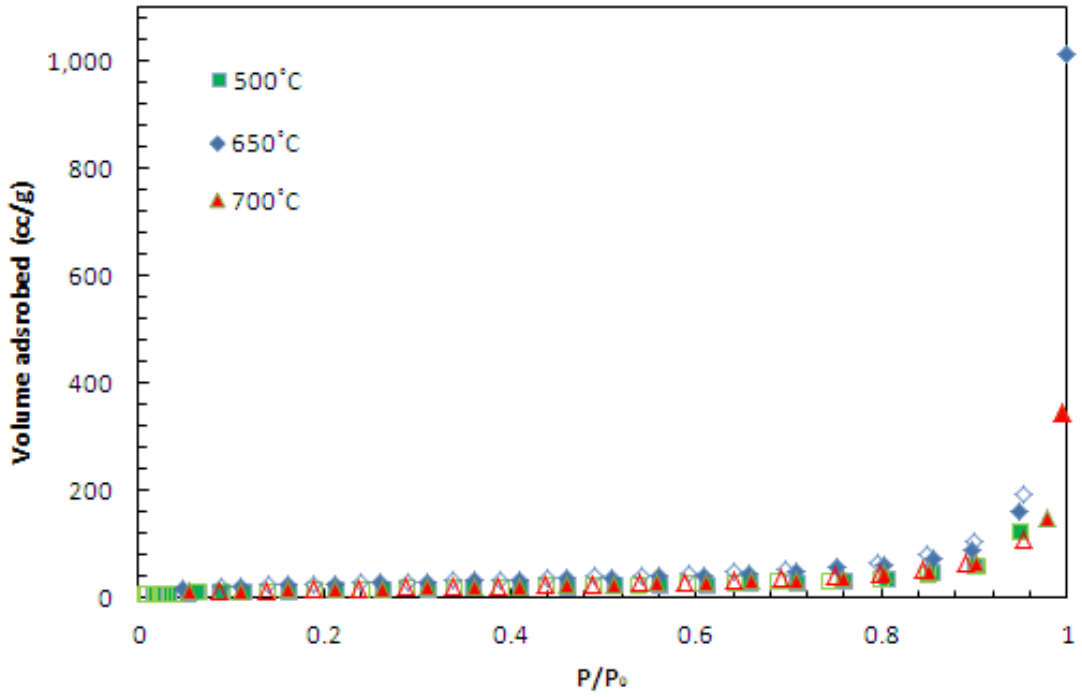


**Figure 4.51** Nitrogen adsorption/desorption isotherms of MWNTs produced at different reaction temperatures (25% $C_2H_2$ in Ar) over the Co-Mo/$CaCO_3$ catalysts with a Co:Mo ratio of 6 and a calcination temperature of 750˚C (Filled symbols: adsorption; empty symbols: desorption).

The volumes of the adsorbed nitrogen for MWNTs produced at 700˚C on the catalyst with a Co:Mo ratio of 6 and a calcination temperature of 750˚C were 12.2 and 110.1 cc/g at P/P0 value of 0.01 and 0.96, respectively. The adsorbed gas volume at microporous region was 11.1% of the adsorbed gas volume at $P/P_0$ of 0.96. For the MWNTs produced at 650˚C, a sharp increase in the adsorbed volume at a relative pressure value of around 0.90 was observed and attributed to macroporosity range. The amount of nitrogen adsorption in the relative pressure range of 0.9-0.99 exhibits

a dramatic rise from 103.89 cc/g to 1013.39 cc/g. This can be a result of the enhanced condensation in larger aggregated pores which corresponds to approximately 89.75% of the total amount of adsorption. The volume of the adsorbed nitrogen for MWNTs produced at 500˚C was determined as 125 cc/g at $P/P_0$ value of 0.95 whereas the volume of the adsorbed nitrogen was 7.5 cc/g at $P/P_0$ value of 0.01. Thus, adsorbed gas volume at microporous region was 6%. Except for MWNTs produced at 500ºC, there was a sharp increase after a relative pressure of 0.96 which revealed the macropores in the synthesized materials. These macropores might result from aggregated pores among MWNTs.

Figure 4.52 indicates nitrogen adsorption/desorption isotherms of MWNTs produced at 700˚C over the Co-Mo/$CaCO_3$ catalysts with different Co:Mo ratios and a calcination temperature of 750˚C. From Figure 4.52, the volume of the adsorbed nitrogen was determined as 37.3 cc/g at $P/P_0$ value of 0.95 whereas the volume of the adsorbed nitrogen was 3.3 cc/g at $P/P_0$ value of 0.01 for MWNTs grown over the Co-Mo/$CaCO_3$ catalysts with a Co:Mo ratio of 0.44. This corresponded to an adsorbed gas volume of 8.8% at microporous region ($P/P_0<0.01$).

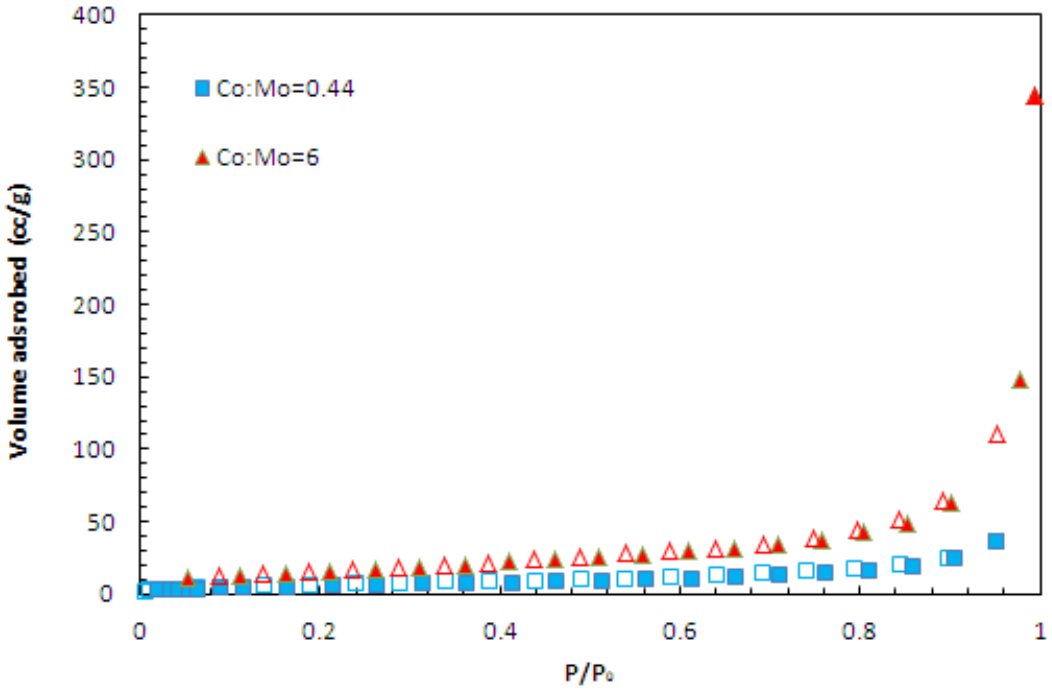


**Figure 4.52** Nitrogen adsorption/desorption isotherms of MWNTs produced at 700˚C over the Co-Mo/$CaCO_3$ catalysts with different Co:Mo ratios ($T_{cal}$= 750˚C) (Filled symbols: adsorption; empty symbols: desorption).

In all isotherms, a sharp increase in adsorbed nitrogen volume after the relative pressure of 0.96 was observed. This showed the presence of macropores in materials.

BET analysis revealed that the purified multi-walled carbon nanotubes synthesized at 500, 650 and 700˚C had a specific surface area of 55.4, 89.9 and 59.3 $m^2/g$, respectively. The highest surface area of purified nanotubes was observed at a reaction temperature of 650ºC. On the other hand, the surface area decreased to a value of 24.8 $m^2/g$ as the Co:Mo ratio in the catalyst declined to 0.44. The surface areas of purified MWNTs in all samples were determined to be close that of MWNTs in the literature [37].

The pore size distribution for MWNTs grown at 700˚C over the catalyst with a Co:Mo ratio of 0.44 and a calcination temperature of 750˚C is given in Figure 4.53.

Most of the pores had a diameter in the mesoporous region. There were also macropores (50 nm≤d) which might be aggregated pores among MWNTs.

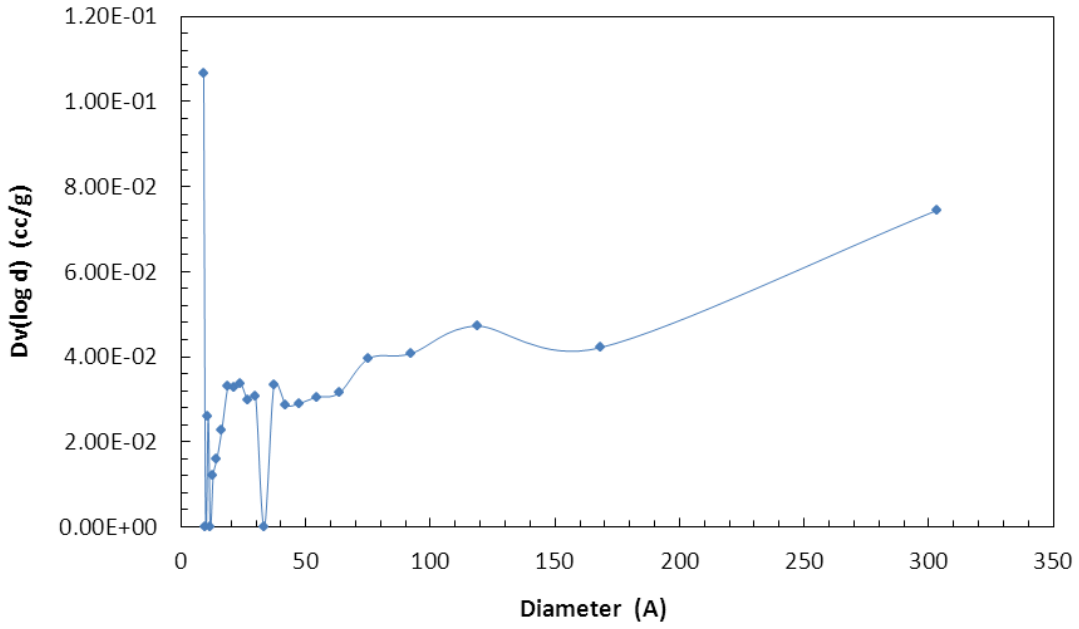


**Figure 4.53** Pore size distribution of MWNTs produced at 700˚C on the catalyst with a Co:Mo ratio of 0.44 and a calcination temperature of 750˚C.

The Figures 4.54-4.56 illustrate the pore size distributions for MWNTs grown at 750, 650 and 500˚C over the catalyst with a Co:Mo ratio of 6 and a calcination temperature of 750˚C. For all samples, the presence of macropores was also observed.

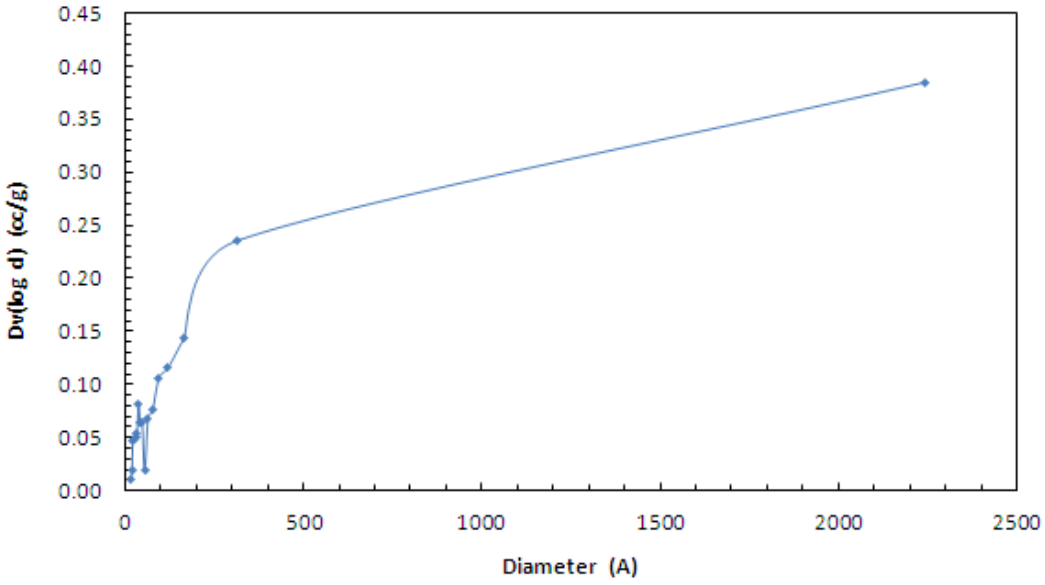


**Figure 4.54** Pore size distribution of MWNTs produced at 700˚C on the catalyst with a Co:Mo ratio of 6 and a calcination temperature of 750˚C.

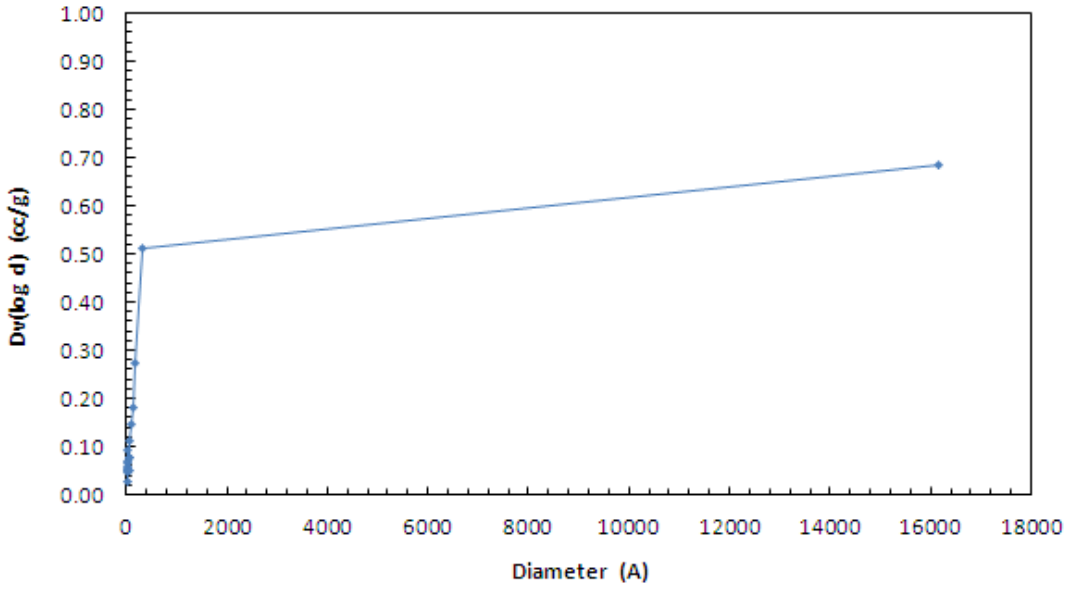


**Figure 4.55** Pore size distribution of MWNTs produced at 650˚C on the catalyst with a Co:Mo ratio of 6 and a calcination temperature of 750˚C.

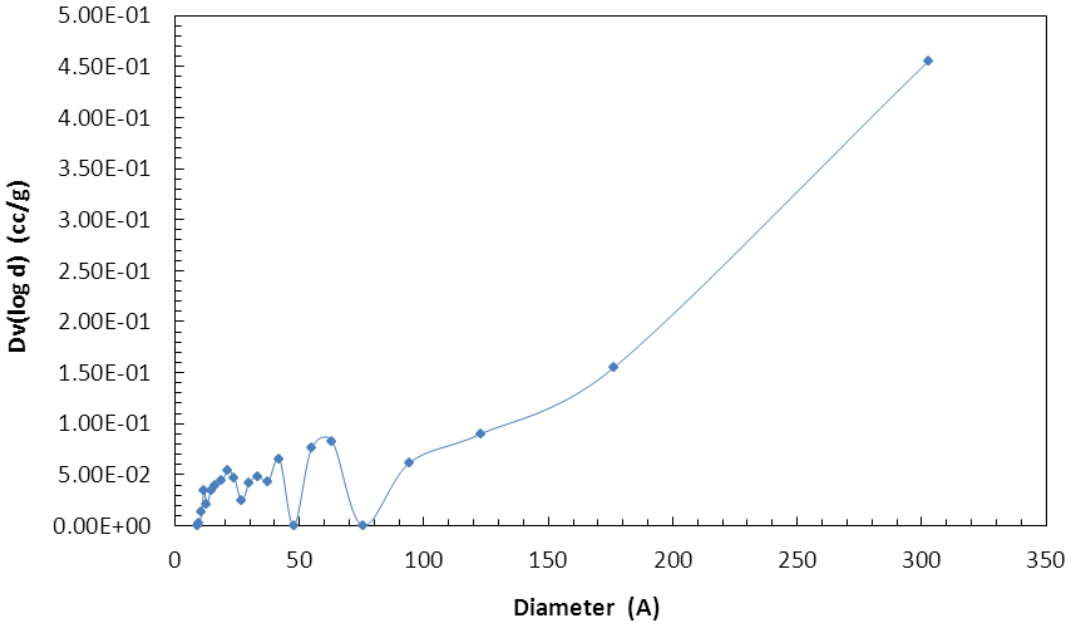


**Figure 4.56** Pore size distribution of MWNTs produced at 500˚C on the catalyst with a Co:Mo ratio of 6 and a calcination temperature of 750˚C.

### 4.2.7 Raman Spectroscopy Results

Figure 4.57 indicates the Raman spectrum for the multi-walled carbon nanotubes grown over the catalyst with a Co:Mo ratio of 6 and a calcination temperature of 750˚C. Two narrow peaks were observed in the spectrum at 1339 and 1579 $cm^{-1}$. These peaks were attributed to the disordered carbonaceous products (D-band) and tangential graphitized products (G-band), respectively. The peak observed at 1339 $cm^{-1}$ reveals the existence of defective graphitic layers on the wall surfaces of nanotubes. Another peak at 2666 $cm^{-1}$ was associated with 2D band. These were characteristics peaks of MWNTs. RBM band which indicates presence of single-walled carbon nanotubes was not observed in this sample. This was an evidence for no SWNT formation.

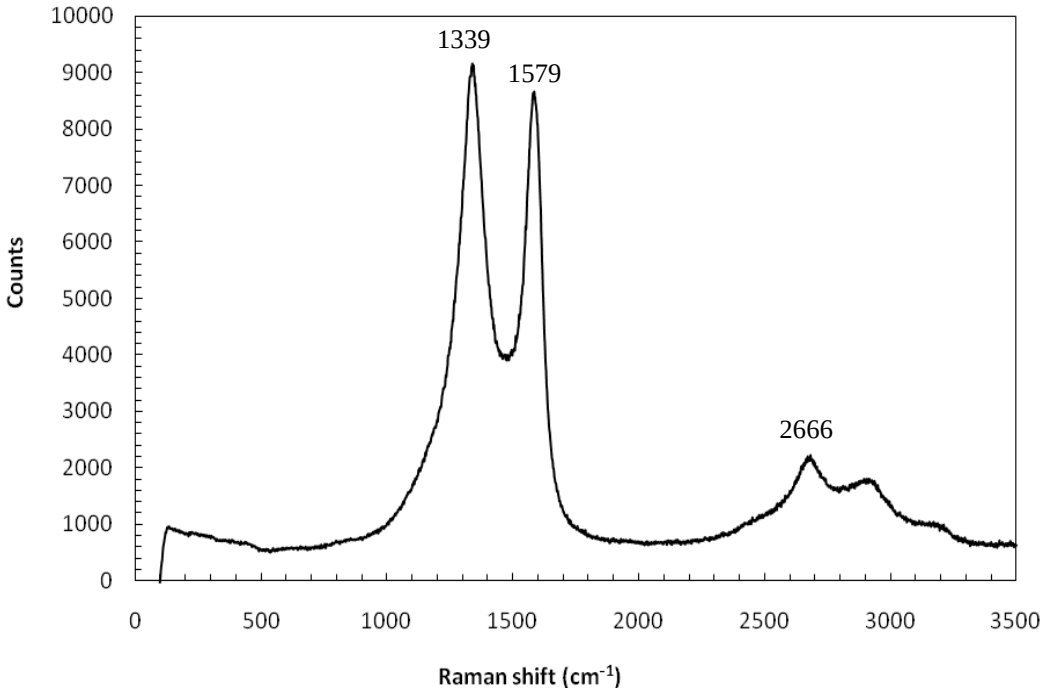


**Figure 4.57** Raman spectrum of the MWNTs produced at 700˚C on the catalyst with a Co:Mo ratio of 6 and a calcination temperature of 750˚C (25% $C_2H_2$ in Ar).

The Raman spectra of CNTs produced at different reaction temperatures over the catalyst with different Co/Mo weight ratios and different calcination temperatures are given in Appendix J. Similar spectra were observed for all samples. Raman spectroscopy results were in agreement with TEM and SEM results.

To get information about the quality of nanotubes, Raman active D-band and G-band intensity ratio ($I_D/I_G$) was calculated. Intensity ratio of D to G bands was found to be 1.06 for MWNTs grown at 700ºC over the catalyst with a Co:Mo ratio of 6 and a calcination temperature of 750ºC. This value showed the presence of nanotubes with high disorder and less graphitic structure. In other words, this shows existence of high defect level in the carbon structure of CNTs [25, 28]. The $I_D/I_G$ ratios for MWNTs are tabulated in Table 4.4. It was observed that CNTs were not in a good crystalline quality.

**Table 4.4** $I_D/I_G$ ratio values for purified CNTs

| Run No. | Co:Mo wt. ratio in catalyst | $T_{cal}$ (˚C) | $T_{rxn}$ (˚C) | Inlet $C_2H_2$ composition in Ar (%) | $I_D/I_G$ ratio |
|---|---|---|---|---|---|
| 4 | 0.44 | 750 | 700 | 25 | 0.99 |
| 22 | 2.30 | 750 | 700 | 25 | 0.97 |
| 25 | 6 | 750 | 500 | 25 | 0.84 |
| 26 | 6 | 750 | 600 | 25 | 1.12 |
| 28 | 6 | 750 | 700 | 25 | 1.06 |
| 29 | 6 | 750 | 700 | 10 | 0.83 |

Raman results revealed that the $I_D/I_G$ ratio decreased as the reaction temperature was decreased. Moreover, a decrease in the composition of acetylene in argon led to decrease in the $I_D/I_G$ ratio. The effect of Co:Mo weight ratio in the catalyst composition was also investigated. The effect of Co:Mo weight ratio on the $I_D/I_G$ ratio was not observed.

### 4.2.8 Reproducibility Results

In order to check the reliability of the experimental data the reproducibility experiments are essential. Some experiments were carried out at the same conditions to examine the reproducibility of the experimental results. XRD and yield results were used to check the reproducibilty of experiments. XRD patterns of CNTs produced at the same reaction temperature of 700ºC using the same catalyst with a Co:Mo ratio of 6 and a calcination temperature of 750ºC are given in Figure 4.58. In Figure 4.58 (a), peaks appearing at Bragg angle values of 26.11º, 43.14º, 53.40º and 77.98º were attributed to carbon. On the other hand, the same peaks corresponding to carbon were also observed at 2θ values of 26.14º, 43.58º, 53.09º and 78.38º in Figure 4.58 (b). As a result, the formation of carbon products was observed for the reproducibility experiments. The CNT yields were 1444.2 and 1430.1 %.

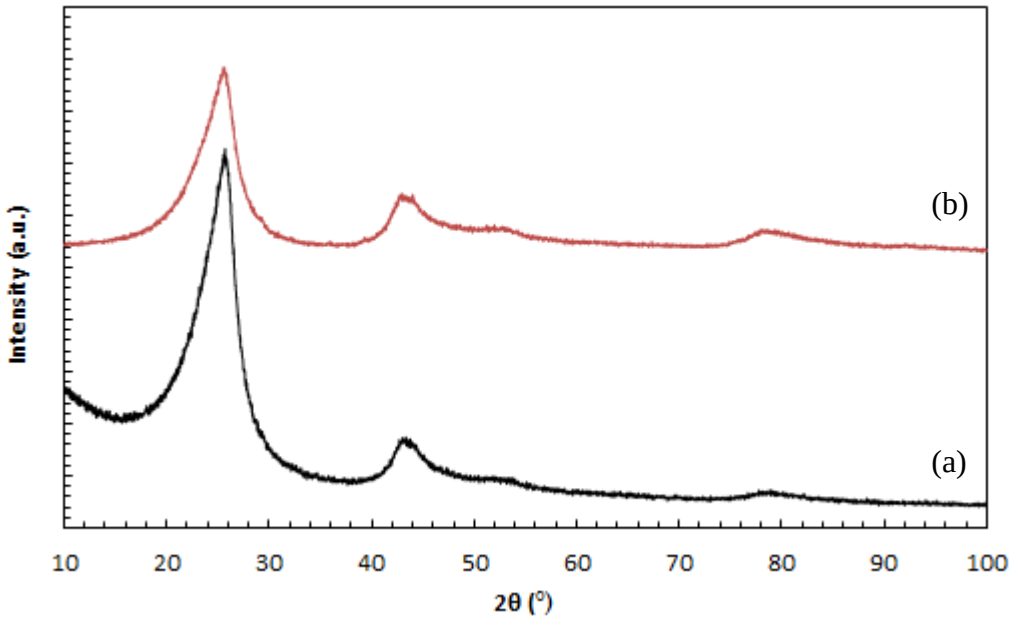


**Figure 4.58** XRD patterns of CNTs produced at 700ºC using the catalyst with a Co:Mo ratio of 6 and a calcination temperature of 750ºC and at different days (a) and (b).

# CHAPTER 5

# CONCLUSIONS AND RECOMMENDATIONS

An experimental setup for CNT production was designed and constructed. Co-Mo/$CaCO_3$ binary catalysts were successfully prepared using impregnation method.

CNTs were successfully synthesized in the temperature range of 500-700ºC. XRD results showed that carbon was the only solid phase. No catalytic metal particles or support material were present in almost all samples.

All samples were purified well. Purified CNTs contained entangled carbon nanotubes to a large extent. They had random orientations and noodle-like shape. Only a small amount of amorphous carbon deposited on the outer surface of nanotubes. The synhesized CNTs were multi-walled with variable outer diameters between 13 and 138 nm. At reaction temperature higher than 800℃, no formation of nanotubes over the catalyst with a Co/Mo ratio of 0.44 and a calcination temperature of 750ºC was observed. In addition, no nanotube was grown at an inlet acetylene composition of 50%. Products synthesized were only carbon nanospheres.

The yield of CNTs and carbon deposition rate increased when there was a rise in the reaction temperature. The catalyst calcination temperature also enhanced CNT yield and carbon deposition rate. Futhermore, there was an increase in the yield and deposition rate with increasing Co:Mo ratio. This showed that Co was more active than Mo for the CNT growth. The highest yield and carbon deposition rate were observed at reaction temperature of 700ºC using a catalyst with a Co:Mo weight ratio of 6 and a calcination temperature of 750ºC.

The oxidation temperature of CNTs was around 700ºC. The oxidation temperature of nanotubes increased with an increase in the synthesis temperature. The purity of CNTs was generally higher than 96%. It was also observed that the purity of CNTs produced at temperatures lower than 650˚C was lower than that of nanotubes produced at temperatures higher than 650˚C.

Purified MWNTs exhibited Type II isotherms. Multi-point BET surface areas of purified nanotubes were in the range of 24.8-89.9 $m^2/g$. Mesopores and macropores were observed in the structure of CNTs.

Raman results showed the presence of structural defects in CNTs and no formation of SWNTs. It was also observed that $I_D/I_G$ ratio decreased with a decrease in the reaction temperature and inlet $C_2H_2$ composition in Ar.

In the light of all results above, it is recommended that the Co-Mo/$CaCO_3$ catalysts used for CNT production can be reduced in $H_2$ atmosphere before the nanotubes growth reaction in order to obtain metallic Co particles in catalyst. The synthesis time can be shorter than one hour to prevent the formation of amorphous carbon on the outer surface on nanotubes. Furthermore, different carbon precursors (e.g. propane, cyclohexane) and/or catalysts metal particles (e.g. Cu, Pt, W, Ti, Cr, ) and support materials (e.g. MCM-41) can be studied.

# REFERENCES


[1] Dai, L., "Carbon Nanotechnology: Recent Developments in Chemistry, Physics, Materials Science and Device Applications", 1st ed., Amsterdam: Elsevier Science, 2006.

[2] Mongillo, J., "Nanotechnology 101". Westport Conn.: Greenwood Press, 2007.

[3] O'Connell, M. J., "Carbon Nanotubes: Properties and Applications", 1st ed., Boca Raton, FL: CRC Press, 2006.

[4] Krüger, A., "Carbon Materials and Nanotechnology", 1st ed., Weinheim: Wiley-VCH, 2010.

[5] Harris, P. J. F., "Carbon Nanotube Science: Synthesis, Properties and Applications", 1st ed., New York: Cambridge University Press, 2009.

[6] Sharon, M., Sharon, M., "Carbon Nano Forms and Applications", 1st ed., McGraw-Hill Professional, 2009.

[7] Dresselhaus, M. S., Dresselhaus, G., Avouris, P., "Carbon nanotubes: synthesis, structure, properties, and applications", Berlin: Springer, 2001.

[8] Amorphous Carbon, http://en.wikipedia.org/wiki/Amorphous_carbon, Last Access Date, 15.10.2011.

[9] Booker, R. D., Boysen, E, "Nanotechnology For Dummies", 1st ed., Hoboken, NJ: Wiley, 2005.

[10] Endo, M., Iijima, S., Dresselhaus, M. S., "Carbon Nanotubes", 1st ed., New York: Pergamon, 1997.

[11] Meyyappan, M., "Carbon nanotubes: science and applications", Boca Raton, FL: CRC Press, 2005.

[12] Belin, T., Epron, F., "Characterization methods of carbon nanotubes: a review", *Materials Science and Engineering B*, vol. 119, no. 2, pp. 105-118, 2005.

[13] Daenen, M., De Fouw, R. D., Hamers, B., Janssen , P. G. A., Schouteden, K, Veld, M. A. J., "The wondrous world of carbon nanotubes", *Eindhoven*

*University of Technology*, 2003.

[14] Saito, R., "Physical Properties Of Carbon Nanotubes*"*, 1st ed., London: ICP, 1998.

[15] Tjong, S. C., "Carbon Nanotube Reinforced Composites: Metal and Ceramic Matrices*"*, 1st ed., Weinheim: Wiley-VCH, 2009.

[16] Jorio, A., Dresselhaus,G., Dresselhaus, M. S., "Carbon nanotubes: advanced topics in the synthesis, structure, properties and applications*",* Berlin: Springer, 2008.

[17] Reich, S., Thomsen, C., Maultzsch, J., "Carbon Nanotubes: Basic Concepts and Physical Properties*"*, 1st ed., Berlin: Wiley-VCH, 2004.

[18] Ebbesen, T. W., "Carbon Nanotubes: Preperation and Properties*"*, 1st ed., Boca Raton, FL: CRC-Press, 1996.

[19] Mhlanga, S. D., "Synthesis and study of carbon nanotubes and carbon spheres", PhD. Thesis, University of the Witwatersrand, Johannesburg, 2009.

[20] Shanov, V., Yun,Y. H., Schulz, M. J., "Synthesis and Characterization of Carbon Nanotube Materials", *Journal of the University of Chemical Technology and Metallurgy*, vol. 41, pp. 377-390, 2006.

[21] Li, Z., Dervishi, E., Xu, Y., Ma, X., Saini, V., Biris, A. S., Little, R., Biris, A. R., Lupu, D., "Effects of the Fe-Co interaction on the growth of multiwall carbon nanotubes", *The Journal of Chemical Physics*, vol.129, no. 7, 074712, 2008.

[22] Qingwen, L., Hao, Y., Yan, C., Jin, Z., Zhongfan, L., "A scalable CVD synthesis of high-purity single-walled carbon nanotubes with porous MgO as support material", *Journal of Materials Chemistry*, vol. 12, no. 4, pp. 1179-1183, 2002.

[23] Li, Q., Yan, H., Zhang, J., Liu, Z., "Effect of hydrocarbons precursors on the formation of carbon nanotubes in chemical vapor deposition", *Carbon*, vol. 42, no. 4, pp. 829-835, 2004.

[24] Dervishi, E., Li, Z., Biris, A. R., Lupu, D., Trigwell, S., Biris, A. S., "Morphology of Multi-Walled Carbon Nanotubes Affected by the Thermal Stability of the Catalyst System", *Chemistry of Materials*, vol. 19, no. 2, pp.

179-184, 2007.

[25] Li, Y., Zhang, X. B., Tao, X. Y., Xu, J. M., Huang, W.Z., Luo, J.H., Luo, Z.Q, Li, T., Liu, F., Bao, Y., Geise, H.J., "Mass production of high-quality multi-walled carbon nanotube bundles on a Ni/Mo/MgO catalyst", *Carbon*, vol. 43, no. 2, pp. 295-301, 2005.

[26] Liu, K., Jiang, K., Feng, C., Chen, Z., Fan, S., "A growth mark method for studying growth mechanism of carbon nanotube arrays", *Carbon*, vol. 43, no. 14, pp. 2850-2856, 2005.

[27] Yellampallı, S., "Quiescent Current Testing of CMOS Data Converters: Design, Fabrication and Testing*",* VDM Verlag, 2009.

[28] Kibria, A. K. M. F., Shajahan, M., Mo, Y. H., Kim, M. J., Nahm, K. S., "Long activity of Co-Mo/MgO catalyst for the synthesis of carbon nanotubes in large-scale and application feasibility of the grown tubes", *Diamond and Related Materials*, vol. 13, no. 10, pp. 1865-1872, 2004.

[29] Shajahan, M., Mo, Y. H., Kibria, A. K. M. F., Kim, M. J., Nahm, K. S., "High growth of SWNTs and MWNTs from $C_2H_2$ decomposition over Co-Mo/MgO catalysts", *Carbon*, vol. 42, no. 11, pp. 2245-2253, 2004.

[30] Couteau, E., Hernadi, K., Seo, J. W., Thien-Nga, L., Miko, C., Gaal, R., Forro, L., "CVD synthesis of high-purity multiwalled carbon nanotubes using $CaCO_3$ catalyst support for large-scale production", *Chemical Physics Letters*, vol. 378, no. 1-2, pp. 9-17, 2003.

[31] Kitiyanan, B., Alvarez, W. E., Harwell, J. H., Resasco, D. E., "Controlled production of single-wall carbon nanotubes by catalytic decomposition of CO on bimetallic Co-Mo catalysts", *Chemical Physics Letters*, vol. 317, no. 3-5, pp. 497-503, 2000.

[32] Alvarez, W. E., Kitiyanan, B., Borgna, A., Resasco, D. E., "Synergism of Co and Mo in the catalytic production of single-wall carbon nanotubes by decomposition of CO", *Carbon*, vol. 39, no. 4, pp. 547-558, 2001.

[33] Smajda, R., Mionic, M., Duchamp, M., Andresen, J. C., Forró, L., Magrez, A., "Production of high quality carbon nanotubes for less than $1 per gram", *Physica Status Solidi (c)*, vol. 7, no. 3-4, pp. 1236-1240, 2010.

[34] Dervishi, E., Li, Z., Biris, A. R., Lupu, D., Trigwell, S., Biris, A. S., "Morphology of multi-walled carbon nanotubes affected by the thermal stability of the catalyst system", Chem. Mater., vol.19, pp. 179-184, 2007.

[35] Colomer, J. F., Stephan, C., Lefrant, S., Tendeloo, G.V., Willems, I., Konya, Z., Fonseca, A., Laurent, C., Nagy, J.B., "Large-scale synthesis of single-wall carbon nanotubes by catalytic chemical vapor deposition (CCVD) method", *Chemical Physics Letters*, vol. 317, no. 1-2, pp. 83-89, 2000.

[36] Murakami, T., Hasebe, Y., Kisoda,K., Nishio,K., Isshiki, T., Harima, H., "Effective catalyst on $SiO_2$ in ethanol CVD for growth of single-walled carbon nanotubes", *Diamond and Related Materials*, vol. 17, no. 7-10, pp. 1467-1470, 2008.

[37] Gulino, G., Vieira, R., Amadou, J., Nguyen, P., Ledoux, M. J., Galvagno, S., Centi, G., Pham-Huu, C., "$C_2H_6$ as an active carbon source for a large scale synthesis of carbon nanotubes by chemical vapour deposition", *Applied Catalysis A: General*, vol. 279, no. 1-2, pp. 89-97, 2005.

[38] Magrez, A., Seo, Smajda , J. W., R., Mionić, M., Forró, L., "Catalytic CVD Synthesis of Carbon Nanotubes: Towards High Yield and Low Temperature Growth", *Materials*, vol. 3, no. 11, pp. 4871-4891, 2010.

[39] Mortazavi, S. Z., Reyhani, A., Iraji zad, A., "The effect of Pd addition to Fe as catalysts on growth of carbon nanotubes by TCVD method", *Applied Surface Science*, vol. 254, no. 20, pp. 6416-6421, 2008.

[40] Lyu, S. C., Liu, B. C., Lee, S. H., Park, C. Y., Kang, H. K., Yang, C. W., Lee, C. J., "Large-scale synthesis of high-quality single-walled carbon nanotubes by catalytic decomposition of ethylene", *J. Phys. Chem. B*, vol. 108, no. 5, pp. 1613-1616, 2004.

[41] Lee, C. J., Park, J., Yu, J. A., "Catalyst effect on carbon nanotubes synthesized by thermal chemical vapor deposition", *Chemical Physics Letters*, vol. 360, no. 3-4, pp. 250-255, 2002.

[42] Liu, B. C., Lyu, S. C., Jung, S. I., Kang, H. K., Yang, C. W., Park, J.W., Park, C. Y., Lee, C. J., "Single-walled carbon nanotubes produced by catalytic chemical vapor deposition of acetylene over Fe-Mo/MgO catalyst", *Chemical*

*Physics Letters*, vol. 383, no. 1-2, pp. 104-108, 2004.

[43] Kathyayini, H., Nagaraju, N., Fonseca, A., Nagy, J. B., "Catalytic activity of Fe, Co and Fe/Co supported on Ca and Mg oxides, hydroxides and carbonates in the synthesis of carbon nanotubes", *Journal of Molecular Catalysis A: Chemical*, vol. 223, no. 1-2, pp. 129-136, 2004.

[44] Kathyayini, H., Willems, I., Fonseca, A., Nagy, J. B., Nagaraju, N., "Catalytic materials based on aluminium hydroxide, for the large scale production of bundles of multi-walled (MWNT) carbon nanotubes", *Catalysis Communications*, vol. 7, no. 3, pp. 140-147, 2006.

[45] Li, Z., Dervishi, E., Xu, Y., Saini, V., Mahmood, M., Oshin, O. D., Biris, A. R., Biris, A. S., "Carbon nanotube growth on calcium carbonate supported molybdenum-transition bimetal catalysts", *Catal. Lett*., vol. 131, no. 3-4, pp. 356-363, 2009.

[46] Busnaina, A., "Nanomanufacturing Handbook*"*, 1st ed., CRC Press, 2006.

[47] Lowell, S., Shields, J. E., "Powder Surface Area and Porosity*"*, 3rd ed., New York: Springer, 1991.

[48] Costa, S., Borowiak-Palen, E., Kruszsyfiska, M., Bachmatiuk, A., Kalenczuk, R.J., "Characterization of Carbon nanotubes by Raman spectroscopy", *Materials Science-Poland*, vol. 26, No. 2, 20

[49] Li, Z., Little, R., Dervishi, E., Saini, V., Xu, Y., Biris, A. R., Lupu, D., Trigwell, S., Saini, D., Biris, A. S., "Micro-Raman spectroscopy analysis of catalyst morphology for Carbon", *Chemical Physics*, vol. 353, pp. 25-31, 2008.

[50] Shajahan, M., Kibria, A.K.M. F., "Growth Phenomena of Carbon Nanotubes Over Co-Mo/MgO Catalyst from the Decomposition of Acetylene", Bangladesh J. Sci. Ind. Res., vol. 42, 105-114, 2007.

[51] Herrera, J. E., Balzano, L., Borgna, A., Alvarez, W. E., Resasco, D.E., "Relationship between the Structure/Composition of Co–Mo Catalysts and Their Ability to Produce Single-Walled Carbon Nanotubes by CO Disproportionation", *Journal of Catalysis*, vol. 204, no. 1, pp. 129-145, 2001.

[52] Kelsall, R., Hamley, I. W., and M. Geoghegan, "Nanoscale Science and

Technology", 1st ed., Malden, MA: Wiley, 2005.

[53] Pradeep, T., "Nano: The Essentials", 1st ed., New Delhi: McGraw-Hill Professional, 2008.

# APPENDIX A

## CALCULATION OF COBALT (II) ACETATE TETRAHYDRATE AND AMMONIUM MOLYBDATE TETRAHYDRATE AMOUNTS

For impregnation, 19 g of $CaCO_3$ was weighed and the amount of Ca in catalyst was calculated using equations A.1 & A.2.

$$n_{CaCO_3} = m_{CaCO_3} / MW_{CaCO_3} \quad (A.1)$$

$$m_{Ca} = n_{CaCO_3} * MW_{Ca} \quad (A.2)$$

where $MW_{CaCO_3}$= 100.09 g/mol and $MW_{Ca}$= 40.078 g/mol

Then, 1 g of $(CH_3COO)_2Co\cdot 4H_2O$ and 1 g of $(NH_4)_6Mo_7O_{24}\cdot 4H_2O$ were weighed and the amount of Co and Mo in catalysts was calculated using equations A.3-A.4 & A.5-A.6, respectively.

$$n_{(CH_3COO)_2Co\cdot 4H_2O} = m_{(CH_3COO)_2Co\cdot 4H_2O} / MW_{(CH_3COO)_2Co\cdot 4H_2O} \quad (A.3)$$

$$m_{Co} = n_{(CH_3COO)_2Co\cdot 4H_2O} * MW_{Co} \quad (A.4)$$

where $MW_{(CH_3COO)_2Co\cdot 4H_2O}$ = 249.08 g/mol and $MW_{Co}$= 58.93 g/mol

$$n_{(NH_4)_6Mo_7O_{24}\cdot 4H_2O} = m_{(NH_4)_6Mo_7O_{24}\cdot 4H_2O} / MW_{(NH_4)_6Mo_7O_{24}\cdot 4H_2O} \quad (A.5)$$

$$m_{Mo} = n_{(NH_4)_6Mo_7O_{24}\cdot 4H_2O} *7* MW_{Mo} \quad (A.6)$$

where $MW_{(NH_4)_6Mo_7O_{24}\cdot 4H_2O}$= 1235.86 g/mol and $MW_{Mo}$= 95.94 g/mol

Thereafter, the weight percents of Ca, Co and Mo were calculated using equation A.7

$$w_X = m_X / (m_{Ca}+m_{Co}+m_{Mo}) \quad \text{(A.7)}$$

where X = Ca, Co or Mo

The amount of Mo and Co sources used for the catalyst preparation is tabulated in Table A.1.

**Table A.1** The amount of compounds used for the catalyst preparation

| **Co wt. %** | **Mo wt.%** | **The amount of $(CH_3COO)_2Co\cdot 4H_2O$ (g)** | **The amount of $(NH_4)_6Mo_7O_{24}\cdot 4H_2O$ (g)** |
|---|---|---|---|
| 2.82 | 6.47 | 1 | 1 |
| 6.47 | 2.82 | 2.30 | 0.44 |
| 6 | 1 | 2.82 | 0.20 |

# APPENDIX B

# VOLUMETRIC FLOW RATE CALIBRATION CURVES FOR ARGON AND ACETYLENE MASS FLOW CONTROLLERS

## B.1 Calibration Curve for Argon Mass Flow Controller

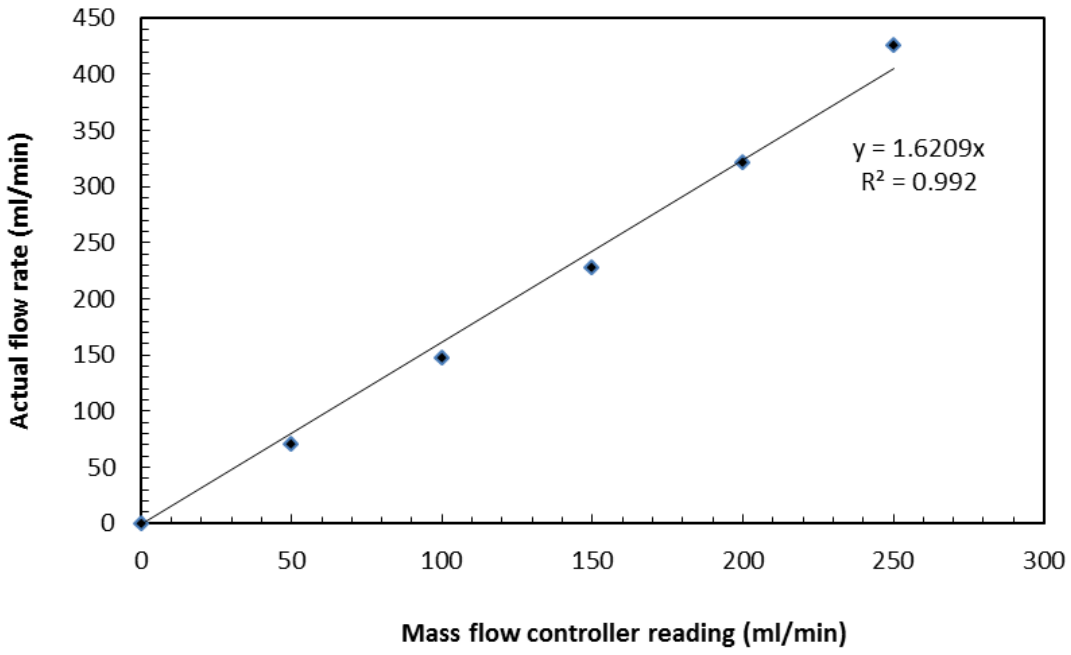


**Figure B.1** Volumetric flow rate calibration curve for argon mass flow controller.

## B.2 Calibration Curve for Acetylene Mass Flow Controller

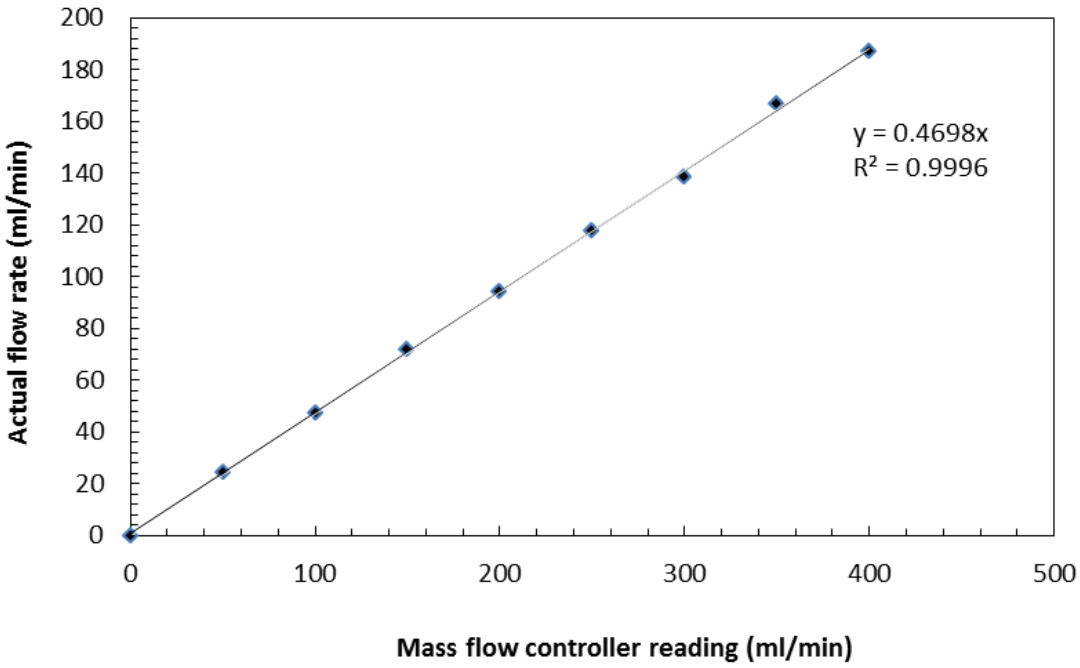


**Figure B.2** Volumetric flow rate calibration curve for acetylene mass flow controller.

# APPENDIX C

## TGA AND DTA PROFILES OF THE SYNTHESIZED CATALYSTS

Thermogravimetric analysis is a thermal analysis technique used to measure the weight change in a material as a function of temperature and time in inert or oxidative atmospheres, or in vacuum (nitrogen, helium, air). TGA analysis is carried out by increasing the temperature of the material gradually and plotting weight percent against temperature. It is widely used for both qualitative and quantitative analyses of all types of solid materials (organic or inorganic) [22].

TGA measurements are generally used to determine the composition of materials and to predict their thermal stability in a temperature range from 25°C to 1000°C. The characterization of materials showing weight loss or gain due to decomposition, oxidation, or dehydration is done by this technique. Also, it is used to distinguish different carbon species according to their combustion temperatures [22].

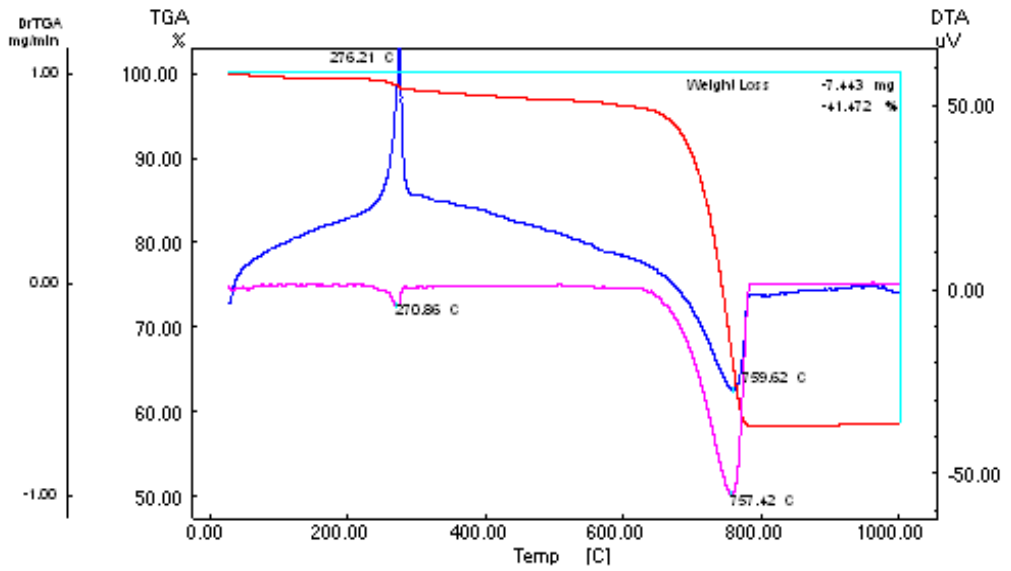


**Figure C.1** TGA and DTA profiles of the uncalcined catalyst with a Co:Mo ratio of 0.44 (red: TGA; blue: DTA).

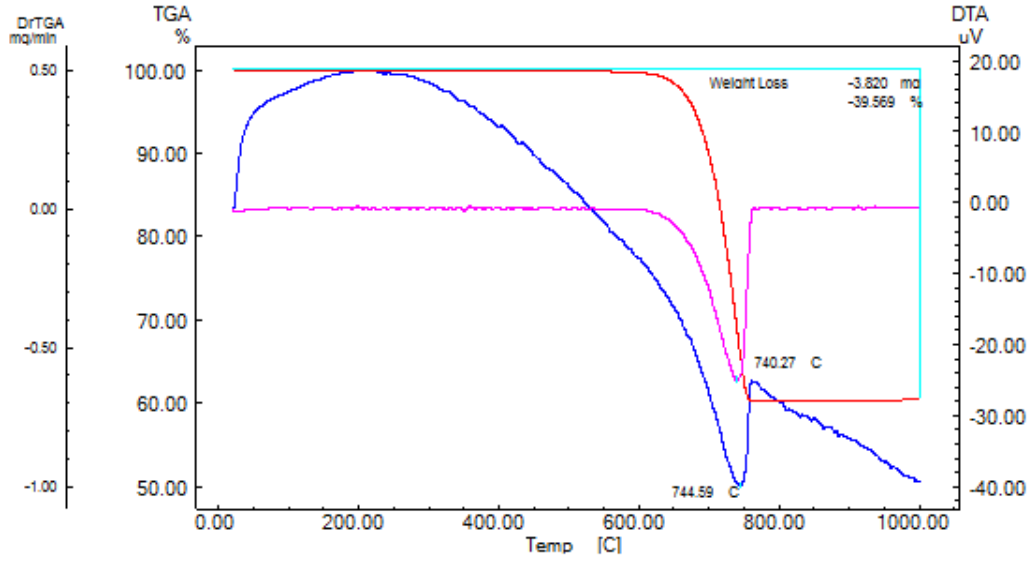


**Figure C.2** TGA and DTA profiles of the catalyst with a Co:Mo ratio of 0.44 and a calcination temperature of 500˚C (red: TGA; blue: DTA).

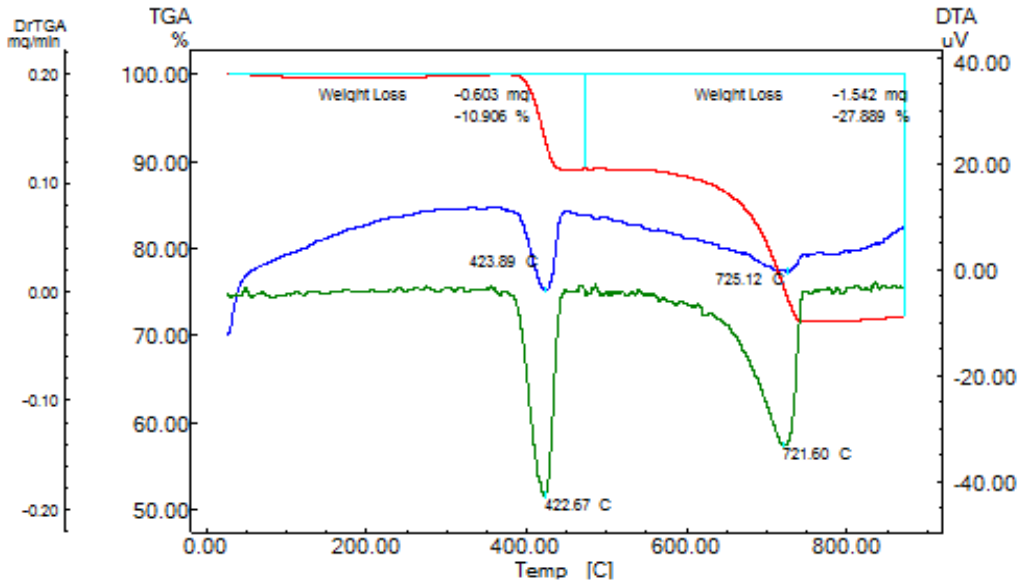


**Figure C.3** TGA and DTA profiles of the catalyst with a Co:Mo ratio of 0.44 and a calcination temperature of 700˚C (red: TGA; blue: DTA).

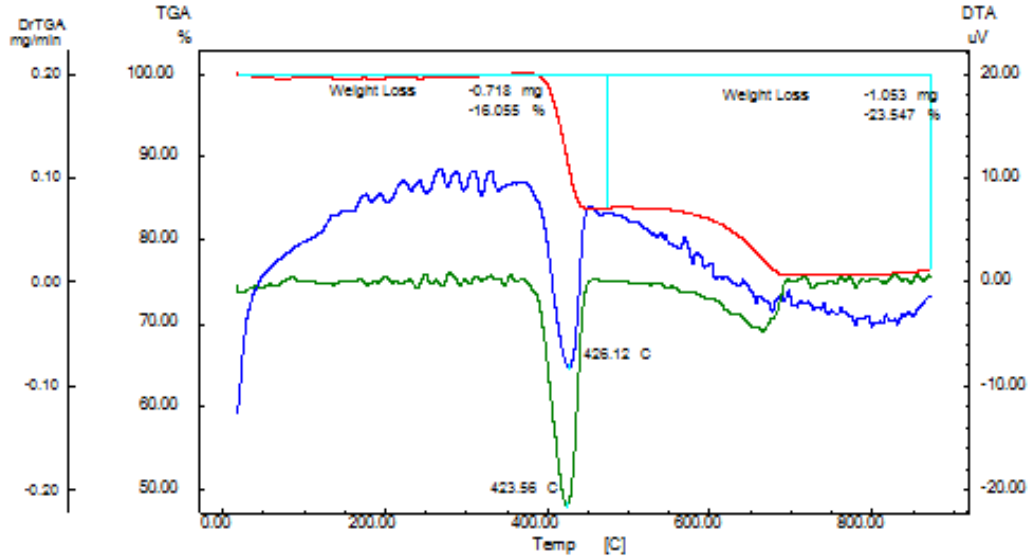


**Figure C.4** TGA and DTA profiles of the catalyst with a Co:Mo ratio of 0.44 and a calcination temperature of 750˚C (red: TGA; blue: DTA).

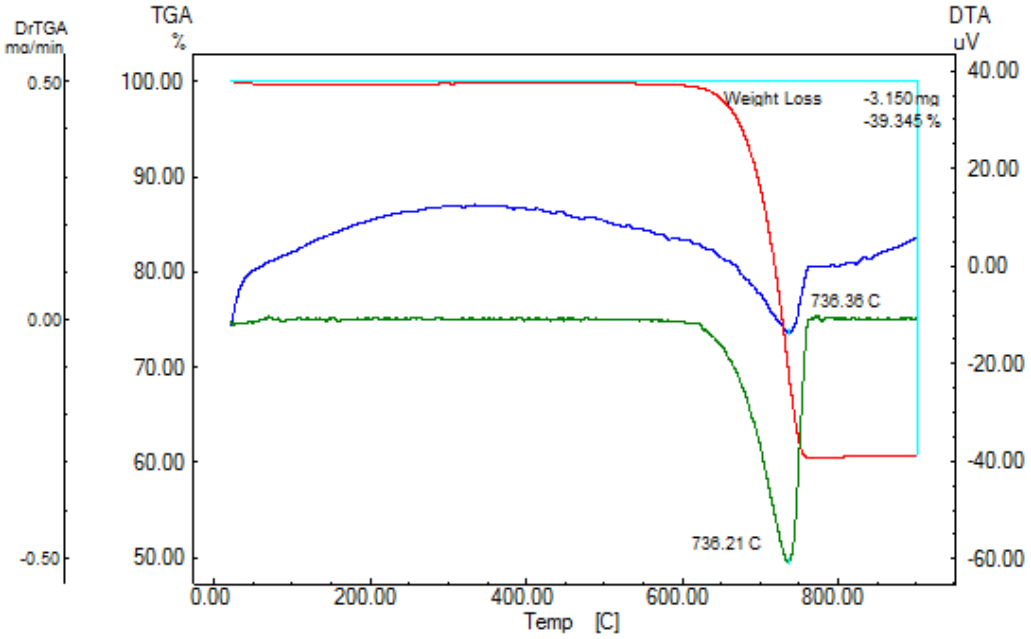


**Figure C.5** TGA and DTA profiles of the catalyst with a Co:Mo ratio of 2.30 and a calcination temperature of 500˚C (red: TGA; blue: DTA).

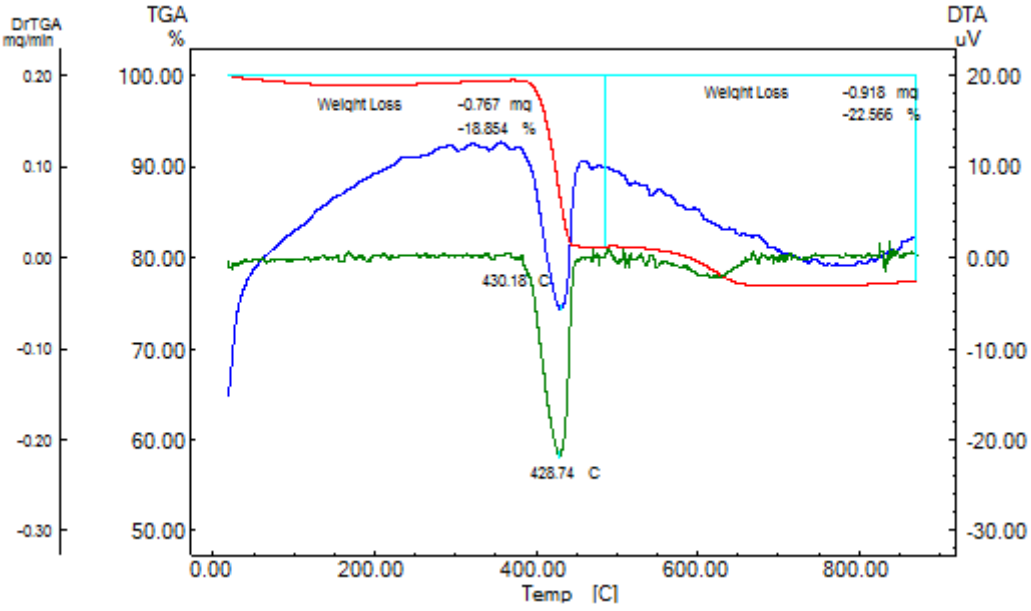


**Figure C.6** TGA and DTA profiles of the catalyst with a Co:Mo ratio of 2.30 and a calcination temperature of 700˚C (red: TGA; blue: DTA).

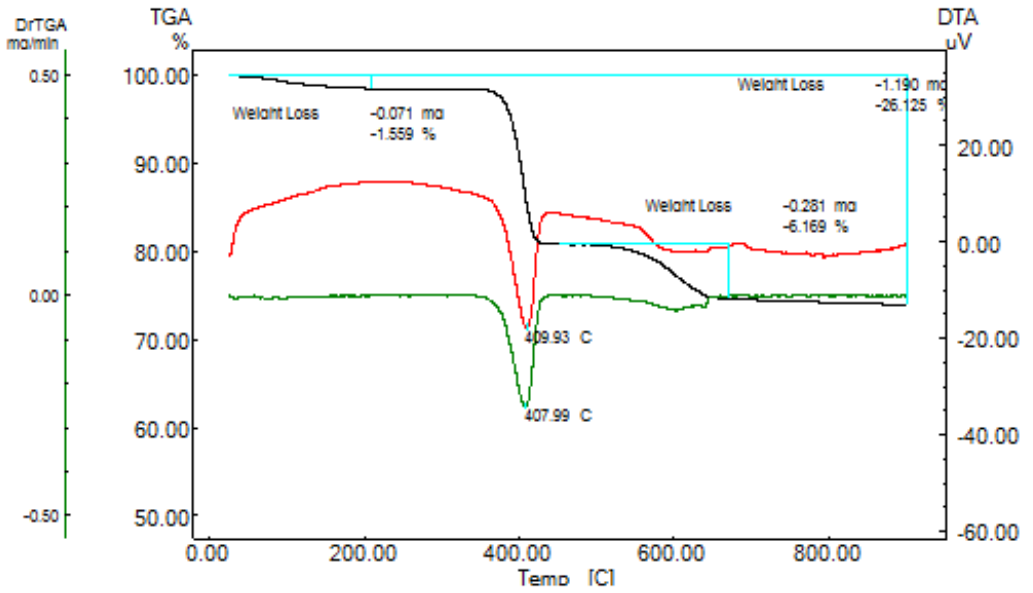


**Figure C.7** TGA an DTA profiles of the catalyst with a Co:Mo ratio of 2.30 and a calcination temperature of 750˚C (black: TGA; red: DTA).

# APPENDIX D

## X-RAY DIFFRACTION

X-ray Diffraction is a rapid and non-destructive surface analysis providing information on structures, phases, crystal orientations, and other structural parameters, such as average grain size, crystallinity, strain, and crystal defects. It gives detailed information about the chemical composition and crystallographic structure of materials and thin films. In addition, the interlayer spacing, the structural strain and impurities are determined with the help of XRD. Unknown solids are usually identified by X-ray diffraction which is vital to studies in geology, environmental science, material science, engineering and biology. It is also used to measure sample purity [52].

The basis of XRD is the observation of the scattered intensity of an X-ray beam that hits a sample as a function of incident and scattered angle, polarization, and wavelength or energy [52].

## D.1 XRD Patterns for Pure and Co-Mo Impregnated $CaCO_3$ Materials

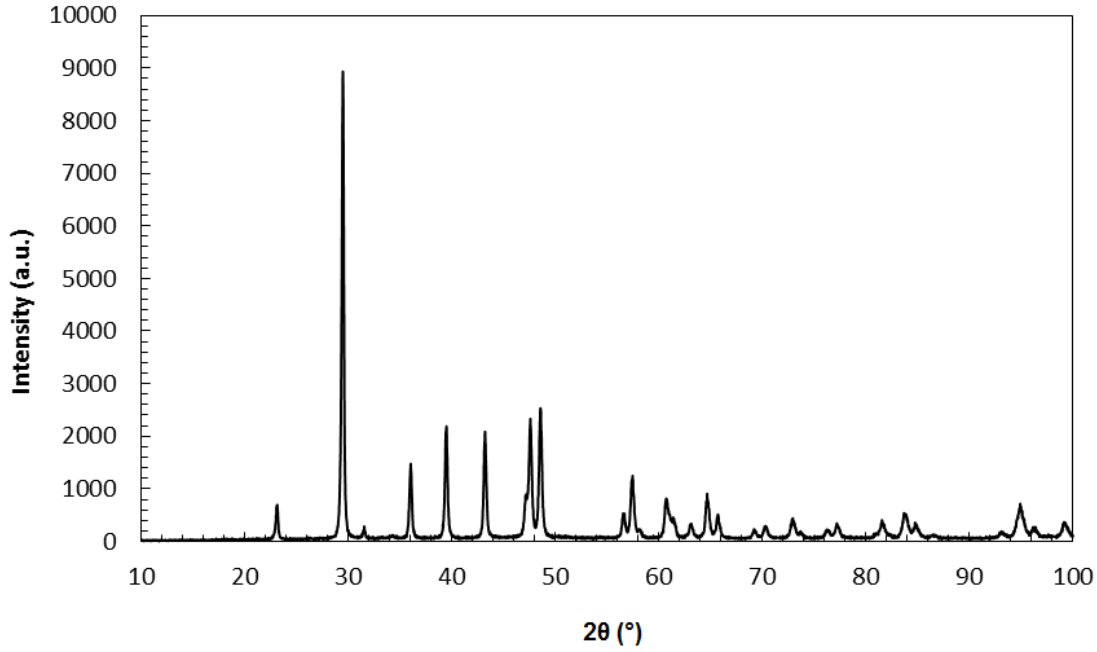


**Figure D.1.1** XRD pattern of pure $CaCO_3$.

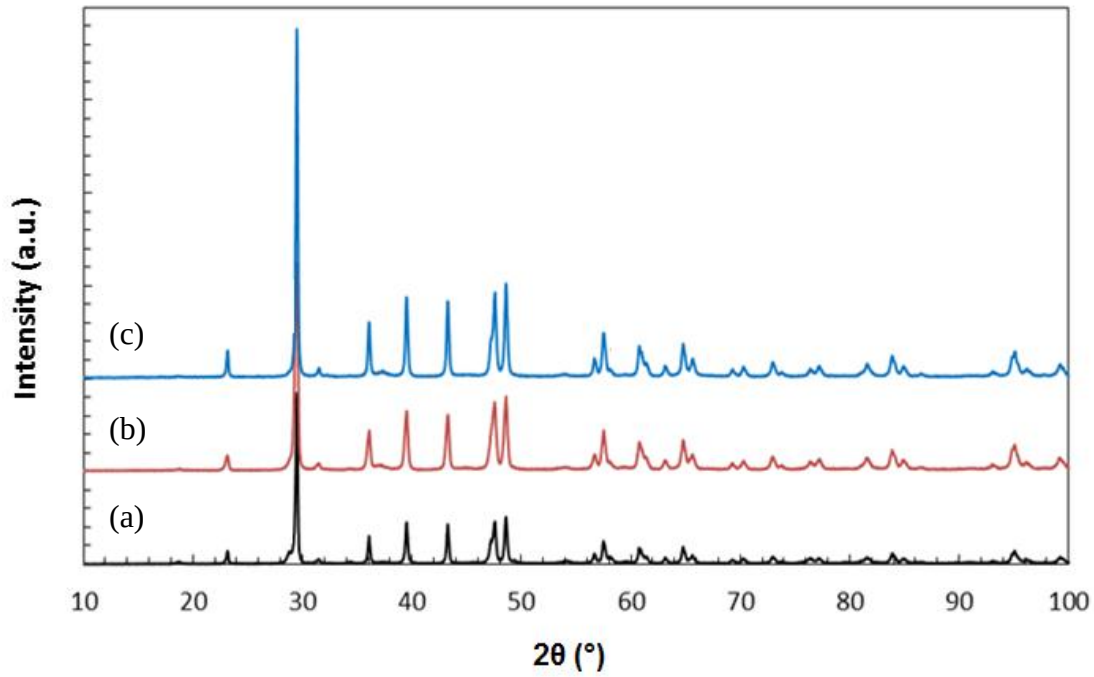


**Figure D.1.2** XRD patterns of the catalysts with different Co:Mo ratios: (a) 0.44, (b) 2.30, (c) 6 which were calcined at 500˚C.

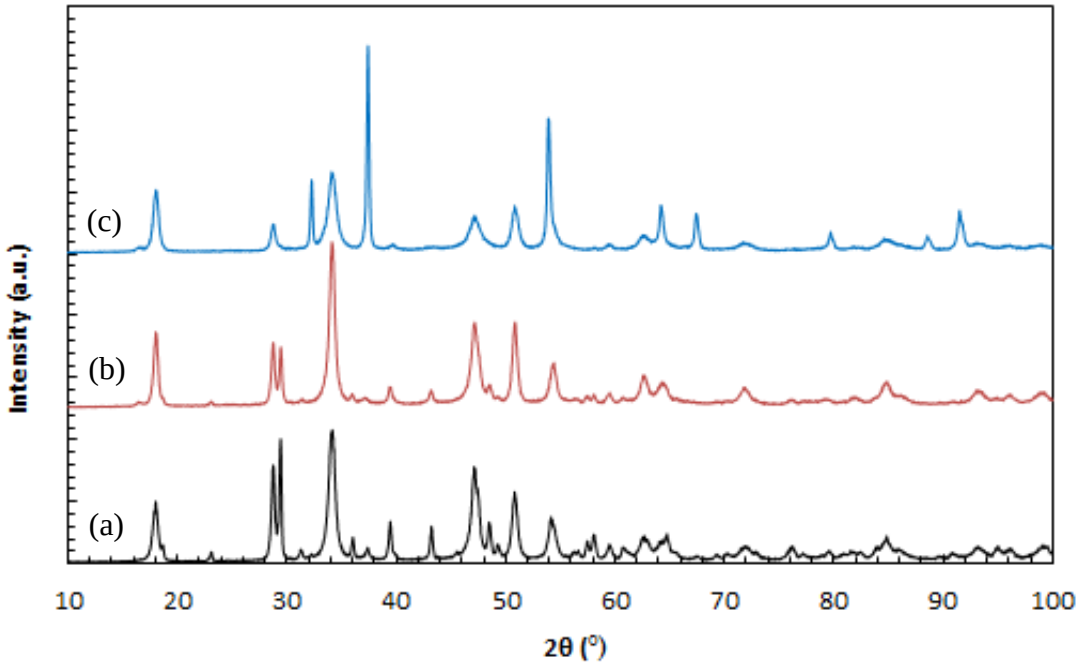


**Figure D.1.3** XRD patterns of the catalysts with different Co:Mo ratios: (a) 0.44, (b) 2.30, (c) 6 which were calcined at 700˚C.

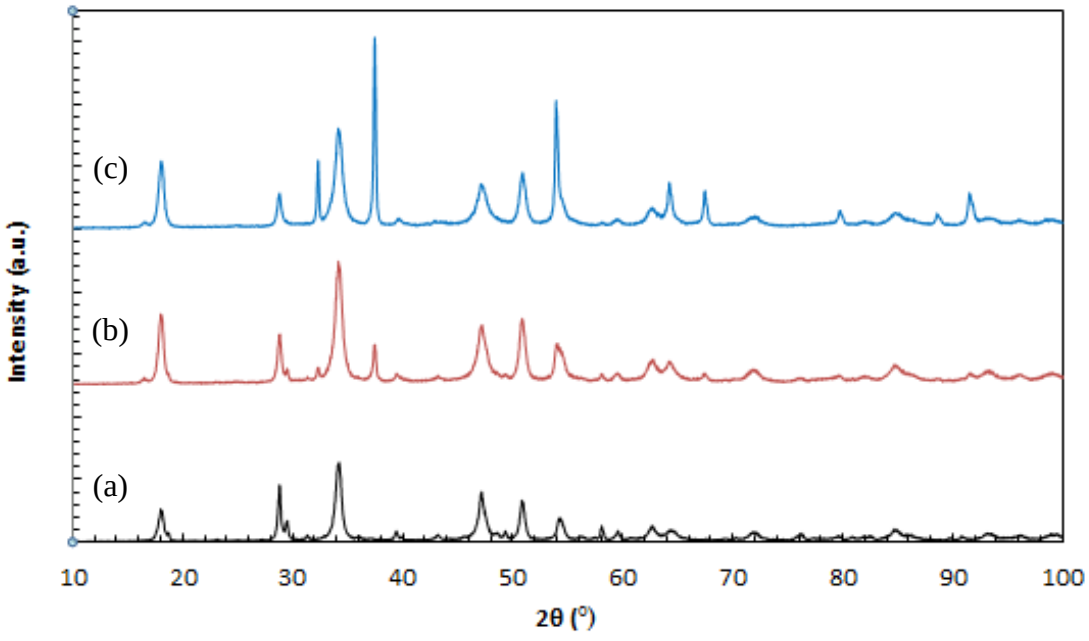


**Figure D.1.4** XRD patterns of the catalysts with different Co:Mo ratios: (a) 0.44, (b) 2.30, (c) 6 which were calcined at 750˚C.

## D.2 XRD Patterns for the Synthesized CNTs

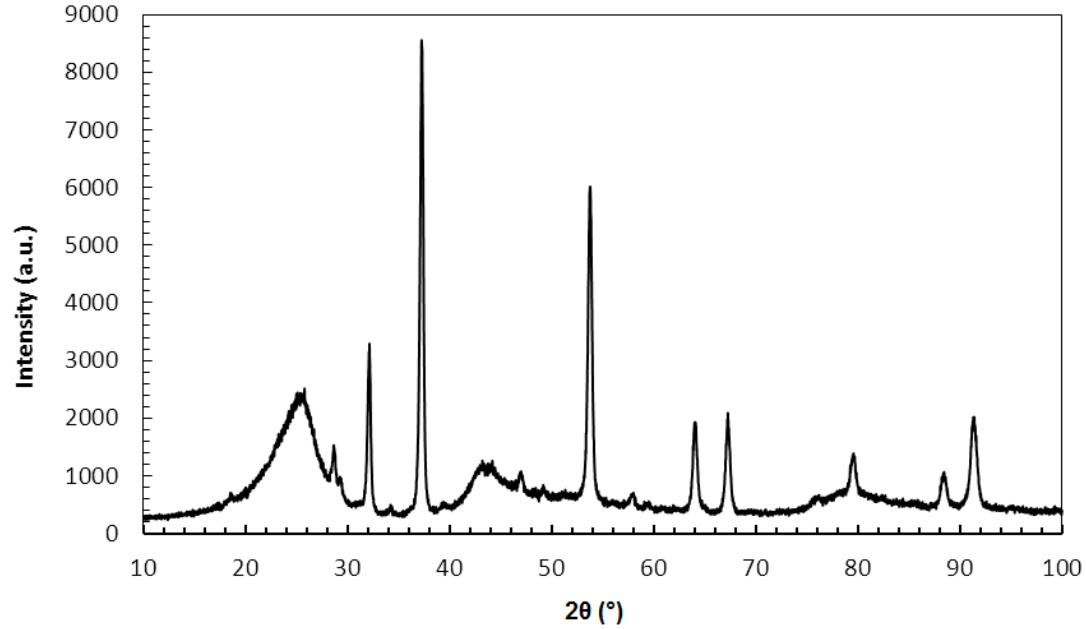


**Figure D.2.1** XRD pattern of purified CNTs produced at 700˚C over Co-Mo/$CaCO_3$ catalyst (Co:Mo= 0.44; $T_{cal}$= 750ºC; 25% $C_2H_2$ in Ar).

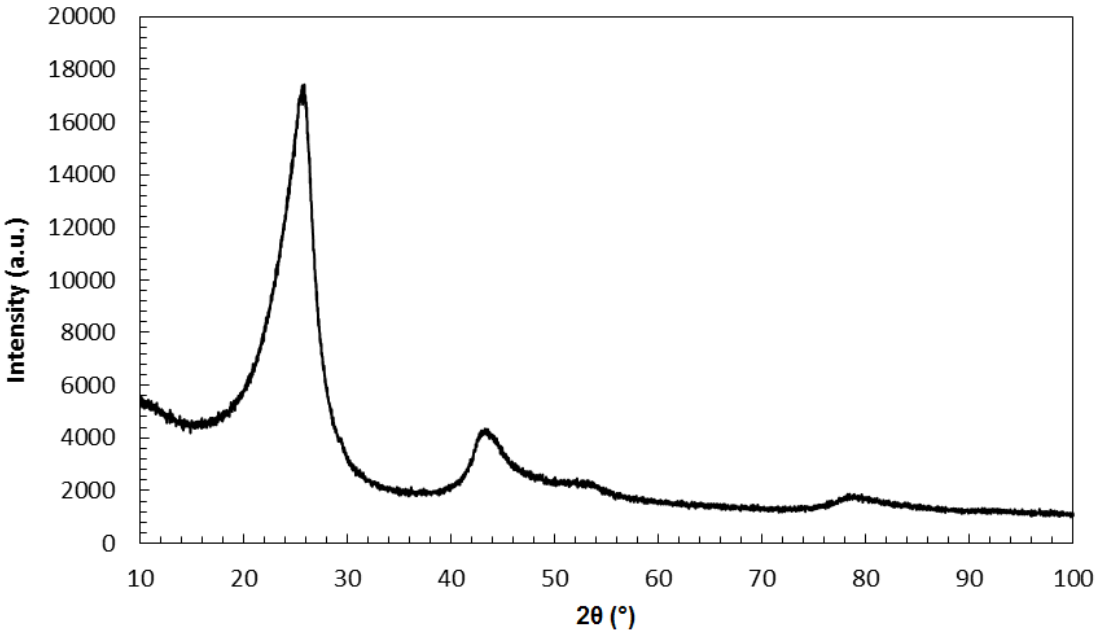


**Figure D.2.2** XRD pattern of purified CNTs produced at 700˚C over Co-Mo/$CaCO_3$ catalyst (Co:Mo= 6; $T_{cal}$= 700ºC; 25% $C_2H_2$ in Ar).

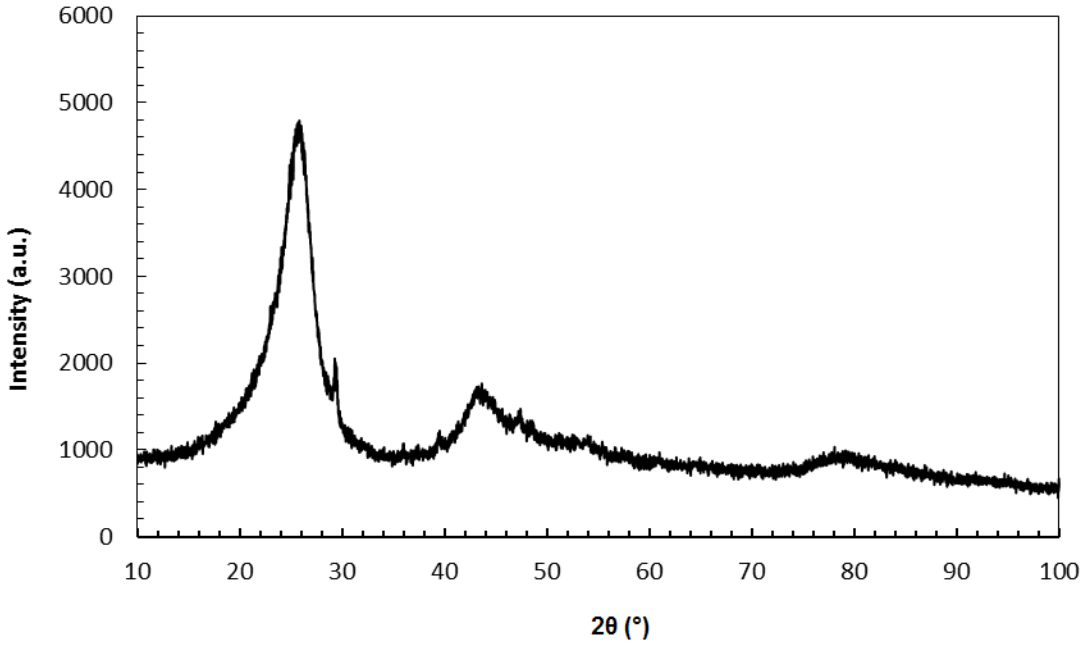


**Figure D.2.3** XRD pattern of purified CNTs produced at 500˚C over Co-Mo/$CaCO_3$ catalyst (Co:Mo= 6; $T_{cal}$= 750ºC; 25% $C_2H_2$ in Ar).

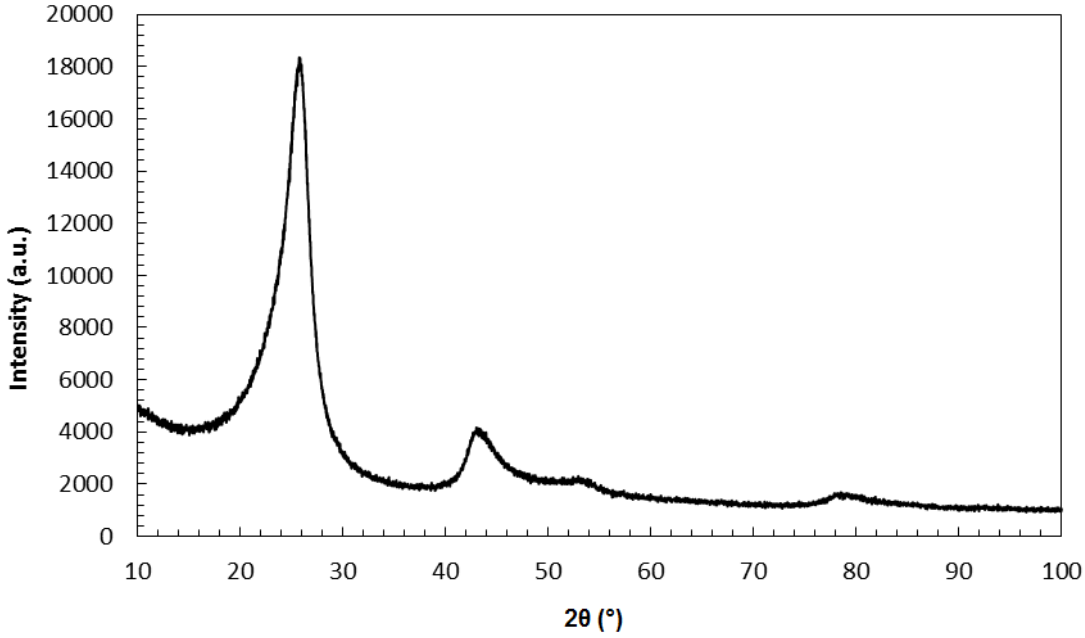


**Figure D.2.4** XRD pattern of purified CNTs produced at 650˚C over Co-Mo/$CaCO_3$ catalyst (Co:Mo= 6; $T_{cal}$= 750ºC; 25% $C_2H_2$ in Ar).

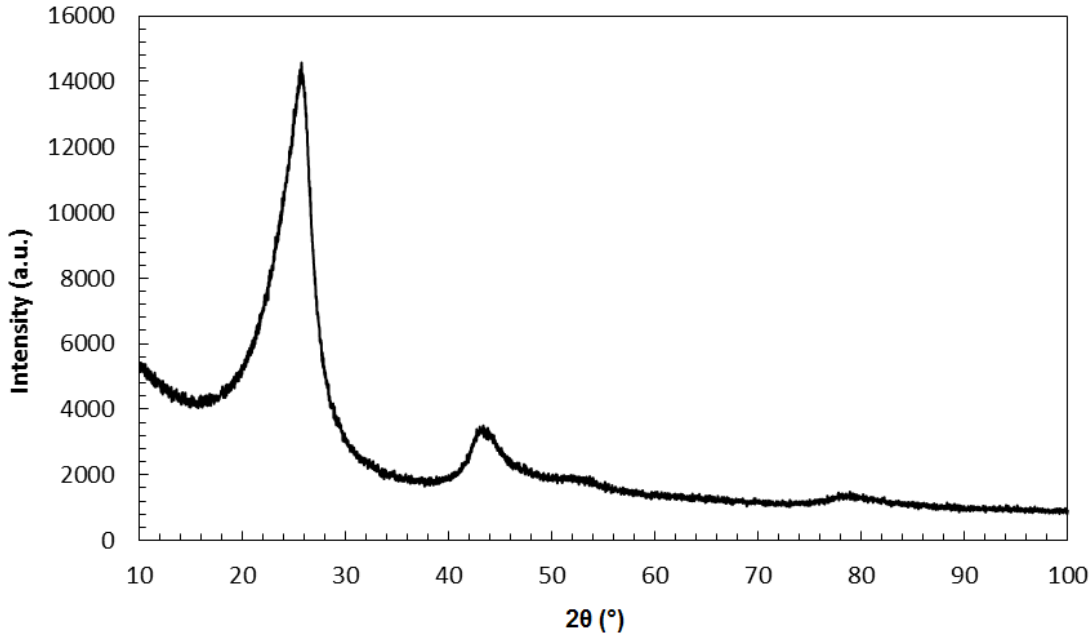


**Figure D.2.5** XRD pattern of purified CNTs produced at 700˚C over Co-Mo/$CaCO_3$ catalyst (Co:Mo= 6; $T_{cal}$= 750ºC; 25% $C_2H_2$ in Ar).

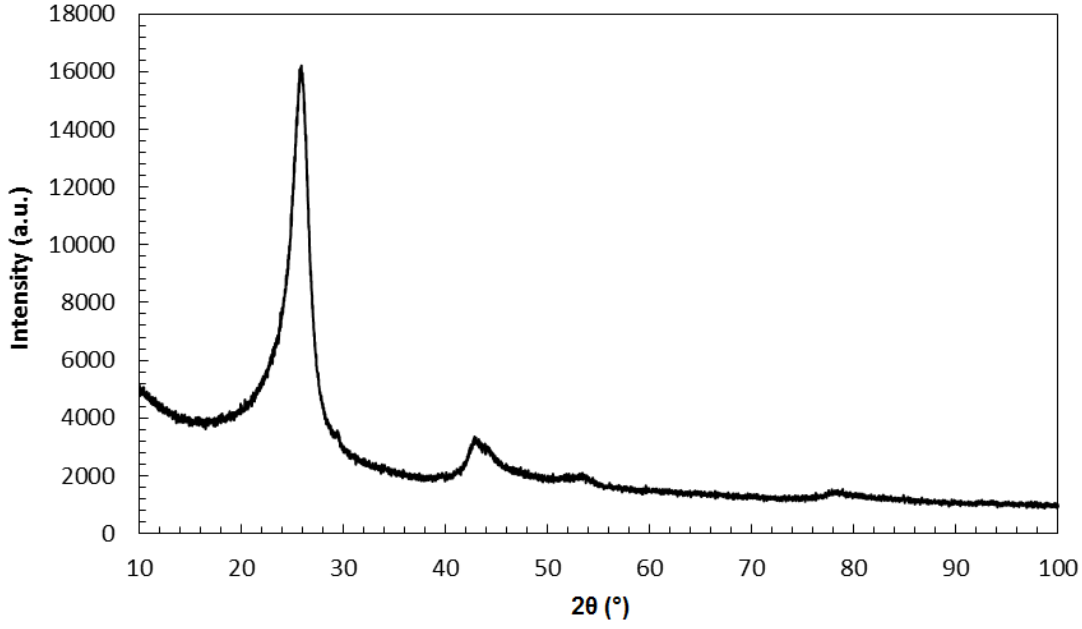


**Figure D.2.6** XRD pattern of purified CNTs produced at 700˚C over Co-Mo/$CaCO_3$ catalyst (Co:Mo= 6; $T_{cal}$= 750ºC; 10% $C_2H_2$ in Ar).

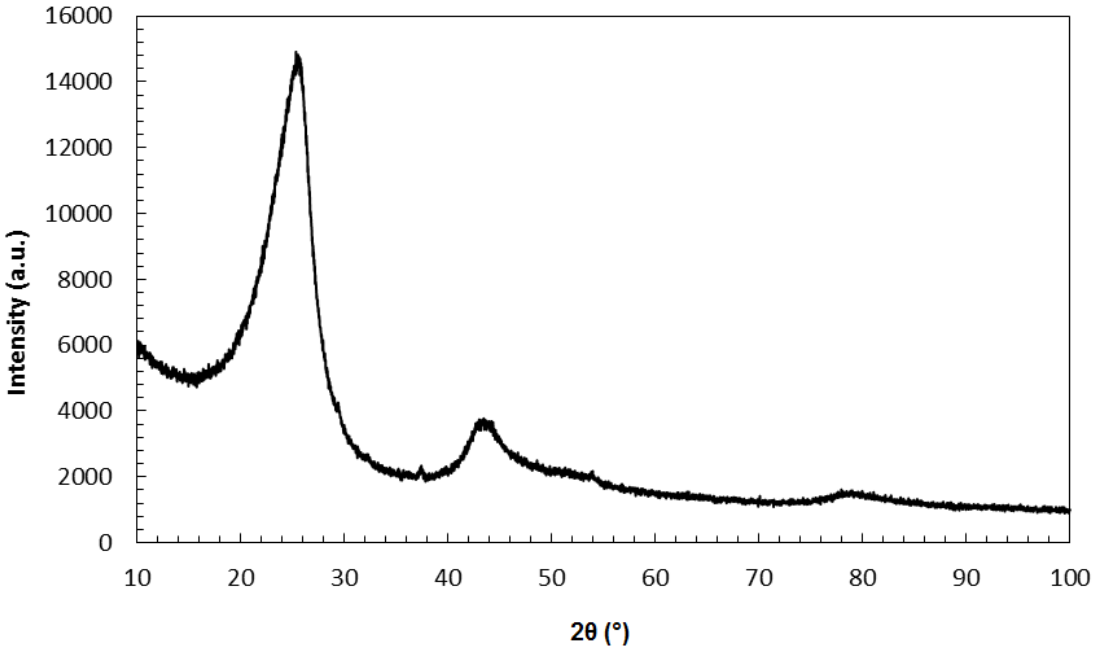


**Figure D.2.7** XRD pattern of purified CNTs produced at 700˚C over Co-Mo/$CaCO_3$ catalyst (Co:Mo= 6; $T_{cal}$= 750ºC; 30% $C_2H_2$ in Ar).

## D.3 XRD Data of Synthesized Materials and Reference Compounds

**Table D.3.1** XRD data for pure $CaCO_3$

| **2θ** | **d** | **$I/I_0$** |
|---|---|---|
| 23.10 | 3.8471 | 8 |
| 29.46 | 3.0294 | 100 |
| 31.52 | 2.8360 | 3 |
| 36.00 | 2.4927 | 17 |
| 39.44 | 2.2828 | 26 |
| 43.18 | 2.0934 | 24 |
| 47.12 | 1.9271 | 10 |
| 47.56 | 1.9103 | 28 |
| 48.54 | 1.8740 | 31 |
| 56.54 | 1.6263 | 7 |
| 57.38 | 1.6045 | 15 |
| 58.10 | 1.5863 | 3 |
| 60.68 | 1.5249 | 10 |
| 61.04 | 1.5168 | 6 |
| 61.40 | 1.5087 | 6 |
| 63.04 | 1.4734 | 5 |
| 64.62 | 1.4411 | 11 |
| 65.68 | 1.4204 | 7 |
| 69.18 | 1.3568 | 3 |
| 70.26 | 1.3386 | 4 |
| 72.88 | 1.2968 | 6 |
| 73.68 | 1.2847 | 3 |
| 76.22 | 1.2481 | 3 |
| 77.20 | 1.2347 | 5 |
| 81.54 | 1.1796 | 5 |
| 83.68 | 1.1548 | 7 |
| 84.78 | 1.1426 | 5 |
| 94.90 | 1.0456 | 8 |
| 96.16 | 1.0352 | 4 |
| 99.14 | 1.0119 | 5 |

**Table D.3.2** XRD data for the catalyst with a Co:Mo ratio of 0.44 and a calcination temperature of 500˚C

| **2θ** | **d** | **$I/I_0$** |
|---|---|---|
| 18.54 | 4.7814 | 3 |
| 23.14 | 3.8406 | 8 |
| 28.76 | 3.1016 | 8 |
| 29.48 | 3.0274 | 100 |
| 31.46 | 2.8413 | 4 |
| 34.00 | 2.6347 | 3 |
| 36.06 | 2.4887 | 17 |
| 39.50 | 2.2795 | 27 |
| 43.26 | 2.0897 | 25 |
| 47.18 | 1.9248 | 15 |
| 47.54 | 1.9111 | 27 |
| 48.56 | 1.8733 | 31 |
| 56.66 | 1.6232 | 7 |
| 57.48 | 1.6020 | 15 |
| 58.06 | 1.5873 | 5 |
| 60.76 | 1.5231 | 12 |
| 61.06 | 1.5163 | 6 |
| 61.42 | 1.5083 | 5 |
| 63.14 | 1.4713 | 4 |
| 64.76 | 1.4383 | 12 |
| 65.62 | 1.4216 | 6 |
| 70.26 | 1.3386 | 4 |
| 72.94 | 1.2959 | 6 |
| 76.36 | 1.2461 | 4 |
| 77.16 | 1.2352 | 4 |
| 81.56 | 1.1793 | 5 |
| 83.86 | 1.1527 | 8 |
| 84.86 | 1.1417 | 4 |
| 94.82 | 1.0463 | 8 |
| 95.04 | 1.0444 | 8 |
| 99.20 | 1.0115 | 6 |

**Table D.3.3** XRD data for the catalyst with a Co:Mo ratio of 0.44 and a calcination temperature of 700˚C

| **2θ** | **d** | **$I/I_0$** |
|---|---|---|
| 18.00 | 4.9240 | 44 |
| 18.66 | 4.7513 | 13 |
| 23.08 | 3.8504 | 9 |
| 28.74 | 3.1037 | 73 |
| 29.40 | 3.0355 | 91 |
| 31.24 | 2.8554 | 10 |
| 34.12 | 2.6256 | 100 |
| 36.02 | 2.4913 | 19 |
| 37.36 | 2.4050 | 12 |
| 39.42 | 2.2839 | 31 |
| 43.20 | 2.0924 | 28 |
| 45.48 | 1.9928 | 5 |
| 47.10 | 1.9279 | 74 |
| 47.46 | 1.9141 | 53 |
| 48.50 | 1.8754 | 33 |
| 49.28 | 1.8476 | 15 |
| 50.80 | 1.7958 | 54 |
| 54.12 | 1.6932 | 35 |
| 54.40 | 1.6852 | 28 |
| 56.62 | 1.6242 | 10 |
| 57.44 | 1.6030 | 18 |
| 58.04 | 1.5878 | 24 |
| 59.50 | 1.5523 | 15 |
| 60.70 | 1.5245 | 14 |
| 62.60 | 1.4827 | 20 |
| 62.98 | 1.4746 | 17 |
| 64.10 | 1.4516 | 16 |
| 64.72 | 1.4391 | 23 |
| 71.60 | 1.3168 | 12 |
| 71.90 | 1.3121 | 13 |
| 72.18 | 1.3077 | 12 |
| 75.78 | 1.2542 | 10 |
| 76.18 | 1.2486 | 14 |
| 79.54 | 1.2041 | 10 |
| 83.84 | 1.1530 | 13 |
| 84.54 | 1.1452 | 18 |
| 84.82 | 1.1421 | 20 |
| 85.92 | 1.1303 | 11 |
| 93.00 | 1.0619 | 13 |
| 94.96 | 1.0451 | 13 |
| 99.16 | 1.0118 | 14 |

**Table D.3.4** XRD data for the catalyst with a Co:Mo ratio of 0.44 and a calcination temperature of 750˚C

| **2θ** | **d** | **$I/I_0$** |
|---|---|---|
| 18.06 | 4.9078 | 40 |
| 18.72 | 4.7362 | 12 |
| 28.80 | 3.0974 | 76 |
| 29.46 | 3.0294 | 27 |
| 31.32 | 2.8536 | 10 |
| 32.84 | 2.7250 | 7 |
| 34.18 | 2.6211 | 100 |
| 36.02 | 2.4913 | 8 |
| 39.40 | 2.2851 | 14 |
| 43.22 | 2.0915 | 10 |
| 45.52 | 1.9910 | 8 |
| 47.12 | 1.9271 | 66 |
| 48.56 | 1.873 | 12 |
| 49.32 | 1.8462 | 15 |
| 50.84 | 1.7945 | 54 |
| 54.16 | 1.6921 | 32 |
| 54.42 | 1.6846 | 30 |
| 56.26 | 1.6338 | 9 |
| 58.06 | 1.5873 | 23 |
| 59.54 | 1.5514 | 15 |
| 62.64 | 1.4818 | 21 |
| 63.98 | 1.4540 | 13 |
| 64.30 | 1.4475 | 16 |
| 64.54 | 1.4427 | 14 |
| 64.82 | 1.4372 | 12 |
| 71.66 | 1.3159 | 12 |
| 72.24 | 1.3067 | 11 |
| 75.80 | 1.2539 | 9 |
| 76.18 | 1.2486 | 13 |
| 79.54 | 1.2041 | 9 |
| 80.82 | 1.1882 | 8 |
| 81.94 | 1.1748 | 7 |
| 82.46 | 1.1687 | 9 |
| 84.02 | 1.1509 | 8 |
| 84.66 | 1.1439 | 17 |
| 84.96 | 1.1406 | 14 |
| 85.90 | 1.1305 | 10 |
| 90.84 | 1.0814 | 8 |
| 93.18 | 1.0603 | 12 |
| 93.62 | 1.0565 | 9 |
| 98.96 | 1.0133 | 11 |

**Table D.3.5** XRD data for the catalyst with a Co:Mo ratio of 2.30 and a calcination temperature of 500˚C

| **2θ** | **d** | **$I/I_0$** |
|---|---|---|
| 22.97 | 3.8687 | 7 |
| 28.66 | 3.1122 | 5 |
| 29.33 | 3.0427 | 100 |
| 31.30 | 2.8555 | 3 |
| 35.93 | 2.4974 | 18 |
| 39.35 | 2.2879 | 28 |
| 43.12 | 2.0962 | 26 |
| 47.38 | 1.9172 | 32 |
| 47.43 | 1.9153 | 30 |
| 48.43 | 1.8780 | 34 |
| 56.68 | 1.6227 | 4 |
| 57.36 | 1.6051 | 18 |
| 58.05 | 1.5876 | 3 |
| 60.59 | 1.5270 | 13 |
| 61.13 | 1.5148 | 6 |
| 61.38 | 1.5092 | 4 |
| 63.05 | 1.4732 | 3 |
| 64.59 | 1.4418 | 13 |
| 65.47 | 1.4245 | 6 |
| 70.16 | 1.3403 | 4 |
| 72.78 | 1.2984 | 6 |
| 76.23 | 1.2480 | 3 |
| 77.08 | 1.2363 | 5 |
| 81.44 | 1.1808 | 5 |
| 83.69 | 1.1547 | 9 |
| 84.84 | 1.1419 | 3 |
| 94.89 | 1.0457 | 11 |
| 96.14 | 1.0354 | 3 |
| 99.01 | 1.0129 | 4 |

**Table D.3.6** XRD data for the catalyst with a Co:Mo ratio of 2.30 and a calcination temperature of 700˚C

| **2θ** | **d** | **$I/I_0$** |
|---|---|---|
| 18.04 | 4.9132 | 45 |
| 18.52 | 4.7870 | 8 |
| 23.00 | 3.8637 | 6 |
| 28.74 | 3.1037 | 39 |
| 29.44 | 3.0315 | 36 |
| 34.14 | 2.6241 | 100 |
| 35.98 | 2.4940 | 9 |
| 39.42 | 2.2839 | 14 |
| 43.18 | 2.0934 | 12 |
| 47.12 | 1.9271 | 52 |
| 47.40 | 1.9164 | 39 |
| 48.52 | 1.8747 | 15 |
| 50.82 | 1.7951 | 54 |
| 54.32 | 1.6874 | 27 |
| 57.36 | 1.6051 | 8 |
| 58.04 | 1.5878 | 9 |
| 59.48 | 1.5528 | 9 |
| 60.56 | 1.5277 | 8 |
| 62.62 | 1.4823 | 20 |
| 64.04 | 1.4528 | 14 |
| 64.30 | 1.4475 | 17 |
| 64.66 | 1.4403 | 14 |
| 71.44 | 1.3194 | 10 |
| 71.76 | 1.3143 | 13 |
| 71.92 | 1.3117 | 12 |
| 75.96 | 1.2517 | 8 |
| 84.80 | 1.1423 | 17 |
| 86.16 | 1.1278 | 9 |
| 92.80 | 1.0637 | 10 |
| 93.06 | 1.0614 | 11 |
| 93.54 | 1.0572 | 10 |
| 94.86 | 1.0460 | 7 |
| 96.02 | 1.0364 | 9 |
| 98.86 | 1.0140 | 10 |

**Table D.3.7** XRD data for the catalyst with a Co:Mo ratio of 2.30 and a calcination temperature of 750˚C

| **2θ** | **d** | **$I/I_0$** |
|---|---|---|
| 17.94 | 4.9404 | 33 |
| 28.61 | 3.1176 | 39 |
| 32.12 | 2.7844 | 10 |
| 33.92 | 2.6407 | 100 |
| 37.23 | 2.4132 | 30 |
| 39.26 | 2.2929 | 6 |
| 42.96 | 2.1036 | 5 |
| 46.97 | 1.9330 | 46 |
| 49.96 | 1.8241 | 4 |
| 50.63 | 1.8015 | 50 |
| 53.74 | 1.7043 | 29 |
| 55.18 | 1.6632 | 3 |
| 59.27 | 1.5578 | 6 |
| 62.41 | 1.4868 | 16 |
| 64.07 | 1.4522 | 15 |
| 67.19 | 1.3921 | 6 |
| 71.68 | 1.3156 | 9 |
| 79.42 | 1.2057 | 4 |
| 84.49 | 1.1458 | 12 |
| 85.26 | 1.1374 | 7 |
| 85.73 | 1.1323 | 5 |
| 91.44 | 1.0759 | 5 |
| 92.95 | 1.0624 | 6 |
| 95.76 | 1.0385 | 4 |
| 98.90 | 1.0138 | 5 |

**Table D.3.8** XRD data for the catalyst with a Co:Mo ratio of 6 and a calcination temperature of 500˚C

| **2θ** | **d** | **$I/I_0$** |
|---|---|---|
| 18.54 | 4.7819 | 3 |
| 23.22 | 3.8687 | 8 |
| 28.90 | 3.1122 | 3 |
| 29.56 | 3.0427 | 100 |
| 31.58 | 2.8555 | 3 |
| 34.00 | 2.6347 | 3 |
| 36.14 | 2.4974 | 15 |
| 39.57 | 2.2879 | 23 |
| 43.33 | 2.0962 | 22 |
| 47.33 | 1.9172 | 11 |
| 47.65 | 1.9153 | 24 |
| 48.66 | 1.8780 | 27 |
| 56.72 | 1.6227 | 5 |
| 57.57 | 1.6051 | 13 |
| 58.18 | 1.5876 | 3 |
| 60.82 | 1.5270 | 8 |
| 61.14 | 1.5148 | 5 |
| 61.36 | 1.5092 | 3 |
| 64.84 | 1.4418 | 9 |
| 65.65 | 1.4245 | 4 |
| 70.34 | 1.3403 | 3 |
| 73.00 | 1.2984 | 4 |
| 77.29 | 1.2363 | 3 |
| 81.63 | 1.1808 | 3 |
| 83.93 | 1.1547 | 5 |
| 84.96 | 1.1419 | 3 |
| 95.18 | 1.0457 | 7 |

**Table D.3.9** XRD data for the catalyst with a Co:Mo ratio of 6 and a calcination temperature of 700˚C

| **2θ** | **d** | **$I/I_0$** |
|---|---|---|
| 18.06 | 4.9079 | 33 |
| 28.86 | 3.0911 | 13 |
| 32.35 | 2.7652 | 34 |
| 34.17 | 2.6219 | 37 |
| 37.50 | 2.3964 | 100 |
| 39.78 | 2.2642 | 2 |
| 43.49 | 2.0792 | 2 |
| 47.25 | 1.9222 | 14 |
| 50.91 | 1.7922 | 19 |
| 53.99 | 1.6970 | 64 |
| 59.49 | 1.5526 | 2 |
| 62.70 | 1.4806 | 6 |
| 64.30 | 1.4476 | 20 |
| 67.50 | 1.3865 | 17 |
| 71.76 | 1.3143 | 3 |
| 72.07 | 1.3094 | 3 |
| 79.79 | 1.2010 | 8 |
| 84.71 | 1.1433 | 4 |
| 85.47 | 1.1351 | 3 |
| 88.63 | 1.1026 | 6 |
| 91.57 | 1.0747 | 18 |
| 92.88 | 1.0630 | 2 |
| 93.50 | 1.0576 | 2 |
| 95.98 | 1.0367 | 2 |
| 98.90 | 1.0138 | 2 |

**Table D.3.10** XRD data for the catalyst with a Co:Mo ratio of 6 and a calcination temperature of 750˚C

| **2θ** | **d** | **$I/I_0$** |
|---|---|---|
| 17.94 | 4.9404 | 34 |
| 28.76 | 3.1016 | 20 |
| 32.28 | 2.7709 | 35 |
| 34.16 | 2.6226 | 55 |
| 37.44 | 2.4000 | 100 |
| 39.60 | 2.2740 | 6 |
| 42.90 | 2.1064 | 5 |
| 43.42 | 2.0824 | 5 |
| 47.14 | 1.9263 | 25 |
| 49.26 | 1.8483 | 5 |
| 50.86 | 1.7938 | 31 |
| 53.94 | 1.6984 | 74 |
| 55.44 | 1.6460 | 6 |
| 59.50 | 1.5523 | 6 |
| 62.60 | 1.4827 | 12 |
| 64.22 | 1.4491 | 28 |
| 67.44 | 1.3876 | 24 |
| 71.50 | 1.3184 | 7 |
| 72.04 | 1.3098 | 7 |
| 79.72 | 1.2018 | 12 |
| 84.66 | 1.1439 | 9 |
| 85.22 | 1.1378 | 8 |
| 85.78 | 1.1318 | 7 |
| 88.58 | 1.1031 | 10 |
| 91.54 | 1.0750 | 24 |
| 92.82 | 1.0635 | 6 |
| 93.66 | 1.0562 | 6 |
| 96.04 | 1.0362 | 6 |
| 98.42 | 1.0174 | 6 |

**Table D.3.11** XRD data for as-synthesized CNTs grown at 700˚C over the catalyst with a Co:Mo ratio of 6 and a calcination temperature of 750˚C

| **2θ** | **d** | **$I/I_0$** |
|---|---|---|
| 18.660 | 4.7513 | 20 |
| 20.980 | 4.2308 | 22 |
| 22.000 | 4.0369 | 27 |
| 24.780 | 3.5900 | 40 |
| 25.420 | 3.5010 | 39 |
| 26.360 | 3.3783 | 33 |
| 28.180 | 3.1641 | 32 |
| 28.700 | 3.1079 | 36 |
| 31.200 | 2.8643 | 16 |
| 32.160 | 2.7810 | 42 |
| 34.240 | 2.6167 | 16 |
| 37.320 | 2.4075 | 100 |
| 41.180 | 2.1903 | 16 |
| 43.880 | 2.0616 | 21 |
| 46.940 | 1.9341 | 39 |
| 49.240 | 1.8490 | 19 |
| 53.800 | 1.7025 | 80 |
| 55.640 | 1.6505 | 21 |
| 57.960 | 1.5898 | 21 |
| 59.640 | 1.5561 | 16 |
| 64.080 | 1.4520 | 34 |
| 67.320 | 1.3897 | 31 |
| 75.800 | 1.2539 | 19 |
| 79.540 | 1.2041 | 25 |
| 87.160 | 1.1174 | 15 |
| 88.440 | 1.1045 | 21 |
| 91.400 | 1.0763 | 35 |

**Table D.3.12** XRD data for purified CNTs produced at 700 ˚C grown over the catalyst with a Co:Mo ratio of 6 and a calcination temperature of 700˚C at inlet acetylene composition of 25%

| **2θ** | **d** | **$I/I_0$** |
|---|---|---|
| 26.14 | 3.407 | 100 |
| 43.58 | 2.075 | 17 |
| 53.09 | 1.724 | 11 |
| 78.38 | 1.219 | 3 |

**Table D.3.13** XRD data for purified CNTs produced at 650 ˚C grown over the catalyst with a Co:Mo ratio of 6 and a calcination temperature of 750˚C at inlet acetylene composition of 25%

| **2θ** | **d** | **$I/I_0$** |
|---|---|---|
| 25.96 | 3.429 | 100 |
| 45.68 | 1.984 | 20 |
| 52.22 | 1.750 | 11 |
| 79.00 | 1.211 | 6 |

**Table D.3.14** XRD data for purified CNTs produced at 700 ˚C grown over the catalyst with a Co:Mo ratio of 6 and a calcination temperature of 750˚C at inlet acetylene composition of 25%

| **2θ** | **d** | **$I/I_0$** |
|---|---|---|
| 26.11 | 3.411 | 100 |
| 43.14 | 2.095 | 19 |
| 53.40 | 1.714 | 4 |
| 77.98 | 1.224 | 2 |

**Table D.3.15** XRD data for purified CNTs produced at 700 ˚C grown over the catalyst with a Co:Mo ratio of 6 and a calcination temperature of 750˚C at inlet acetylene composition of 10%

| **2θ** | **d** | **$I/I_0$** |
|---|---|---|
| 25.84 | 3.445 | 100 |
| 43.18 | 2.093 | 13 |
| 53.82 | 1.702 | 3 |
| 78.13 | 1.222 | 3 |

**Table D.3.16** XRD data for purified CNTs produced at 700 ˚C grown over the catalyst with a Co:Mo ratio of 6 and a calcination temperature of 750˚C at inlet acetylene composition of 30%

| **2θ** | **d** | **$I/I_0$** |
|---|---|---|
| 25.54 | 3.485 | 100 |
| 43.23 | 2.091 | 21 |
| 53.50 | 1.710 | 4 |
| 78.81 | 1.235 | 2 |

**Table D.3.17** XRD data for cubic CaO

| **Catalog No: 48-1467**<br>**CaO (Cubic)**<br>**Rad: CuKa1**<br>**Lambda: 1.5406** | | | | | |
|---|---|---|---|---|---|
| **2θ** | **d** | **$I/I_0$** | **h** | **k** | **l** |
| 32.200 | 2.7777 | 40 | 1 | 1 | 1 |
| 37.360 | 2.4051 | 100 | 2 | 0 | 0 |
| 53.860 | 1.7008 | 51 | 2 | 2 | 0 |
| 64.160 | 1.4504 | 17 | 3 | 1 | 1 |
| 67.380 | 1.3887 | 14 | 2 | 2 | 2 |
| 79.660 | 1.2026 | 5 | 4 | 0 | 0 |
| 88.530 | 1.1036 | 7 | 3 | 3 | 1 |
| 91.470 | 1.0757 | 14 | 4 | 2 | 0 |

**Table D.3.18** XRD data for hexagonal $Ca(OH)_2$

| **Catalog No: 04-0733**<br>**$Ca(OH)_2$ (Hexagonal)**<br>**Rad: CuKa1**<br>**Lambda: 1.5406** | | | | | |
|---|---|---|---|---|---|
| **2θ** | **d** | **$I/I_0$ *** | **h** | **k** | **l** |
| 18.089 | 4.9001 | 74 | 0 | 0 | 1 |
| 28.662 | 3.1120 | 23 | 1 | 0 | 0 |
| 34.088 | 2.6281 | 100 | 1 | 0 | 1 |
| 47.123 | 1.9270 | 42 | 1 | 0 | 2 |
| 50.794 | 1.7960 | 36 | 1 | 1 | 0 |
| 54.336 | 1.6870 | 21 | 1 | 1 | 1 |
| 62.538 | 1.4840 | 13 | 2 | 0 | 1 |
| 64.226 | 1.4490 | 13 | 1 | 1 | 2 |
| 71.777 | 1.3140 | 8 | 2 | 0 | 2 |
| 84.721 | 1.1432 | 11 | 2 | 1 | 1 |
| 93.229 | 1.0599 | 12 | 2 | 1 | 2 |
| 98.826 | 1.0143 | 7 | 3 | 0 | 1 |

* $I/I_0$ values less than 7 were not included.

**Table D.3.19** XRD data for hexagonal Co

| **Catalog No: 89-4308**<br>**Co (Hexagonal)**<br>**Rad: CuKa1**<br>**Lambda: 1.5406** | | | | | |
|---|---|---|---|---|---|
| **2θ** | **d** | **$I/I_0$** | **h** | **k** | **l** |
| 41.589 | 2.1698 | 27 | 1 | 0 | 0 |
| 44.264 | 2.0446 | 29 | 0 | 0 | 2 |
| 47.394 | 1.9166 | 100 | 1 | 0 | 1 |
| 62.351 | 1.4880 | 11 | 1 | 0 | 2 |
| 75.891 | 1.2527 | 10 | 1 | 1 | 0 |
| 83.729 | 1.1542 | 10 | 1 | 0 | 3 |

**Table D.3.20** XRD data for cubic CoO

| **Catalog No: 75-0419**<br>**CoO (Cubic)**<br>**Rad: CuKa1**<br>**Lambda: 1.5406** | | | | | |
|---|---|---|---|---|---|
| **2θ** | **d** | **$I/I_0$** | **h** | **k** | **l** |
| 34.103 | 2.6269 | 100 | 1 | 1 | 1 |
| 39.582 | 2.2750 | 22 | 2 | 0 | 0 |
| 57.220 | 1.6087 | 34 | 2 | 2 | 0 |
| 68.318 | 1.3719 | 22 | 3 | 1 | 1 |
| 71.813 | 1.3135 | 3 | 2 | 2 | 2 |
| 85.248 | 1.1375 | 3 | 4 | 0 | 0 |

**Table D.3.21** XRD data for monoclinic $CoMoO_4$

| **Catalog No: 25-1434**<br>**CoMoO4 (Monoclinic)**<br>**Rad: CuKa1**<br>**Lambda: 1.5406** | | | | | |
|---|---|---|---|---|---|
| **2θ** | **d** | **$I/I_0$ *** | **h** | **k** | **l** |
| 14.159 | 6.2501 | 70 | 1 | 1 | 0 |
| 16.014 | 5.5300 | 20 | 1 | 1 | 1 |
| 18.906 | 4.6901 | 10 | 2 | 0 | 1 |
| 21.498 | 4.1301 | 10 | 1 | 1 | 1 |
| 23.707 | 3.7501 | 20 | 0 | 2 | 1 |
| 25.063 | 3.5502 | 60 | 0 | 0 | 2 |
| 28.512 | 3.1281 | 100 | 2 | 2 | 0 |
| 32.267 | 2.7721 | 55 | 2 | 2 | 2 |
| 32.852 | 2.7241 | 40 | 1 | 3 | 1 |
| 38.302 | 2.3481 | 25 | 1 | 3 | 2 |
| 40.777 | 2.2111 | 25 | 4 | 0 | 0 |
| 42.780 | 2.1121 | 12 | 0 | 4 | 1 |
| 43.340 | 2.0861 | 60 | 3 | 3 | 0 |
| 43.670 | 2.0711 | 10 | 2 | 2 | 2 |
| 45.837 | 1.9781 | 10 | 4 | 2 | 0 |
| 46.993 | 1.9321 | 40 | 1 | 3 | 3 |
| 52.714 | 1.7351 | 30 | 5 | 1 | 0 |
| 55.476 | 1.6550 | 15 | 1 | 5 | 1 |
| 55.658 | 1.6501 | 25 | 4 | 2 | 4 |
| 56.515 | 1.6270 | 20 | 4 | 4 | 1 |
| 56.935 | 1.6160 | 25 | 0 | 4 | 3 |
| 57.874 | 1.5920 | 12 | 1 | 1 | 4 |
| 59.555 | 1.5510 | 35 | 3 | 5 | 1 |
| 61.209 | 1.5130 | 35 | 1 | 5 | 2 |
| 62.821 | 1.4780 | 25 | 6 | 2 | 3 |

* $I/I_0$ values less than 10 were not included.

**Table D.3.22** XRD data for tetragonal $CaMoO_4$

| **Catalog No: 29-0351**<br>**$CaMoO_4$ (Tetragonal)**<br>**Rad: CuKa1**<br>**Lambda: 1.5406** | | | | | |
|---|---|---|---|---|---|
| **2θ** | **d** | **$I/I_0$ *** | **h** | **k** | **l** |
| 18.625 | 4.7603 | 25 | 1 | 0 | 1 |
| 28.774 | 3.1002 | 100 | 1 | 1 | 2 |
| 31.247 | 2.8602 | 14 | 0 | 0 | 4 |
| 34.329 | 2.6102 | 16 | 2 | 0 | 0 |
| 39.310 | 2.2901 | 10 | 2 | 1 | 1 |
| 39.817 | 2.2621 | 6 | 1 | 1 | 4 |
| 45.471 | 1.9931 | 6 | 2 | 1 | 3 |
| 47.069 | 1.9291 | 30 | 2 | 0 | 4 |
| 49.266 | 1.8481 | 14 | 2 | 2 | 0 |
| 54.090 | 1.6941 | 14 | 1 | 1 | 6 |
| 56.212 | 1.6351 | 6 | 2 | 1 | 5 |
| 58.031 | 1.5881 | 20 | 3 | 1 | 2 |
| 59.510 | 1.5521 | 10 | 2 | 2 | 4 |
| 75.793 | 1.2541 | 8 | 2 | 0 | 8 |
| 76.150 | 1.2491 | 12 | 3 | 1 | 6 |
| 79.545 | 1.2041 | 6 | 3 | 3 | 2 |
| 80.836 | 1.1881 | 6 | 4 | 0 | 4 |

* $I/I_0$ values less than 6 were not included.

**Table D.3.23** XRD data for monoclinic $MoO_3$

| **Catalog No: 89-1554**<br>**$MoO_3$ (Monoclinic)**<br>**Rad: CuKa1**<br>**Lambda: 1.5406** | | | | | |
|---|---|---|---|---|---|
| **2θ** | **d** | **$I/I_0$ *** | **h** | **k** | **l** |
| 23.101 | 3.8470 | 100 | 0 | 1 | 1 |
| 24.998 | 3.5592 | 51 | 2 | 0 | 0 |
| 33.369 | 2.6830 | 9 | 0 | 2 | 0 |
| 33.802 | 2.6496 | 15 | 2 | 1 | 1 |
| 34.658 | 2.5861 | 12 | 2 | 1 | 1 |
| 42.144 | 2.0499 | 6 | 2 | 2 | 0 |
| 47.019 | 1.9311 | 5 | 0 | 2 | 2 |
| 51.297 | 1.7796 | 5 | 4 | 0 | 0 |
| 53.376 | 1.7151 | 5 | 2 | 2 | 2 |

* $I/I_0$ values less than 5 were not included.

**Table D.3.24** XRD data for hexagonal $Mo_2C$

| **Catalog No: 89-3014**<br>**$Mo_2C$ (Hexagonal)**<br>**Rad: CuKa1**<br>**Lambda: 1.5406** | | | | | |
|---|---|---|---|---|---|
| **2θ** | **d** | **$I/I_0$ *** | **h** | **k** | **l** |
| 34.459 | 2.6006 | 100 | 1 | 0 | 0 |
| 38.026 | 2.3645 | 23 | 0 | 0 | 2 |
| 52.247 | 1.7495 | 54 | 1 | 0 | 2 |
| 61.732 | 1.5015 | 15 | 1 | 1 | 0 |
| 72.655 | 1.3003 | 7 | 2 | 0 | 0 |
| 74.851 | 1.2675 | 12 | 1 | 1 | 2 |
| 85.075 | 1.1394 | 9 | 2 | 0 | 2 |

* $I/I_0$ values less than 7 were not included.

**Table D.3.25** XRD data for orthorhombic $Mo_2C$ (89-2669)

| **Catalog No: 89-2669**<br>**$Mo_2C$ (Orthorhombic)**<br>**Rad: CuKa1**<br>**Lambda: 1.5406** | | | | | |
|---|---|---|---|---|---|
| **2θ** | **d** | **$I/I_0$ *** | **h** | **k** | **l** |
| 34.471 | 2.5997 | 21 | 0 | 2 | 1 |
| 38.067 | 2.3620 | 23 | 2 | 0 | 0 |
| 39.535 | 2.2776 | 100 | 1 | 2 | 1 |
| 52.288 | 1.7482 | 15 | 2 | 2 | 1 |
| 61.759 | 1.5009 | 15 | 0 | 4 | 0 |
| 69.769 | 1.3469 | 14 | 3 | 0 | 2 |
| 74.903 | 1.2668 | 14 | 2 | 2 | 3 |
| 75.203 | 1.2624 | 7 | 1 | 3 | 3 |
| 75.849 | 1.2533 | 10 | 1 | 0 | 4 |

* $I/I_0$ values less than 7 were not included.

**Table D.3.26** XRD data for orthorhombic $Mo_2C$ (71-0242)

| **Catalog No: 71-0242**<br>**$Mo_2C$ (Orthorhombic)**<br>**Rad: CuKa1**<br>**Lambda: 1.5406** | | | | | |
|---|---|---|---|---|---|
| **2θ** | **d** | **$I/I_0$ *** | **h** | **k** | **l** |
| 34.317 | 2.6110 | 20 | 0 | 2 | 1 |
| 34.440 | 2.6020 | 17 | 0 | 0 | 2 |
| 38.000 | 2.3660 | 32 | 2 | 0 | 0 |
| 39.491 | 2.2801 | 100 | 1 | 0 | 2 |
| 52.125 | 1.7533 | 16 | 2 | 2 | 1 |
| 61.379 | 1.5093 | 8 | 0 | 4 | 0 |
| 61.617 | 1.5040 | 15 | 0 | 2 | 3 |
| 69.577 | 1.3501 | 14 | 3 | 2 | 1 |
| 74.513 | 1.2724 | 6 | 2 | 4 | 0 |
| 74.729 | 1.2693 | 15 | 2 | 2 | 3 |
| 74.956 | 1.2660 | 7 | 1 | 3 | 3 |
| 75.479 | 1.2585 | 10 | 1 | 4 | 2 |
| 75.766 | 1.2545 | 7 | 1 | 0 | 4 |
| 75.766 | 1.2545 | 7 | 1 | 0 | 4 |

* $I/I_0$ values less than 6 were not included.

# APPENDIX E

# EDS RESULTS FOR THE SYNTHESIZED CATALYSTS AND CNTS

In order to characterize the elemental composition the sample is bombarded by an electron beam and X-rays emitted from the sample are detected. X-rays which are characteristic of the elements present on the sample are produced because of the effect of the electron beam on the sample. The characteristic X-rays of different elements are separated by an EDS detector. Qualitative and quantitative analysis, elemental mapping, and line profile analysis are possible with EDS [53]. EDS spectra of the synthesized catalysts are given in Figures E.1-E.5. EDS spectra of the carbon nanotubes produced over Co-Mo/$CaCO_3$ catalysts are given in Figures E.6-E.14.

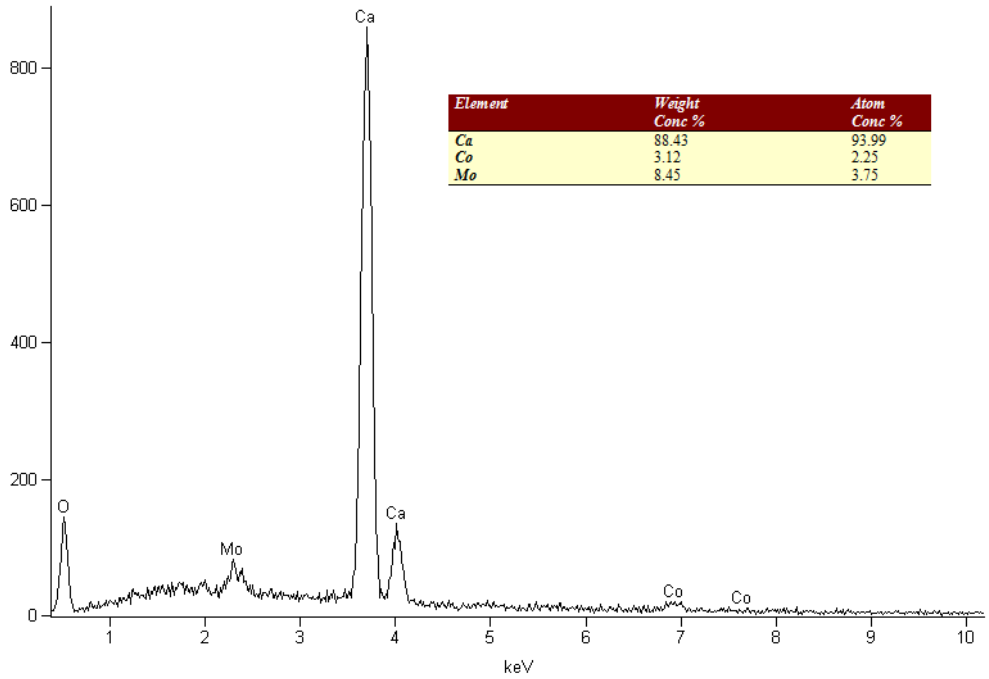


**Figure E.1** EDS spectrum of the catalyst with a Co:Mo ratio of 0.44 and a calcination temperature of 500˚C.

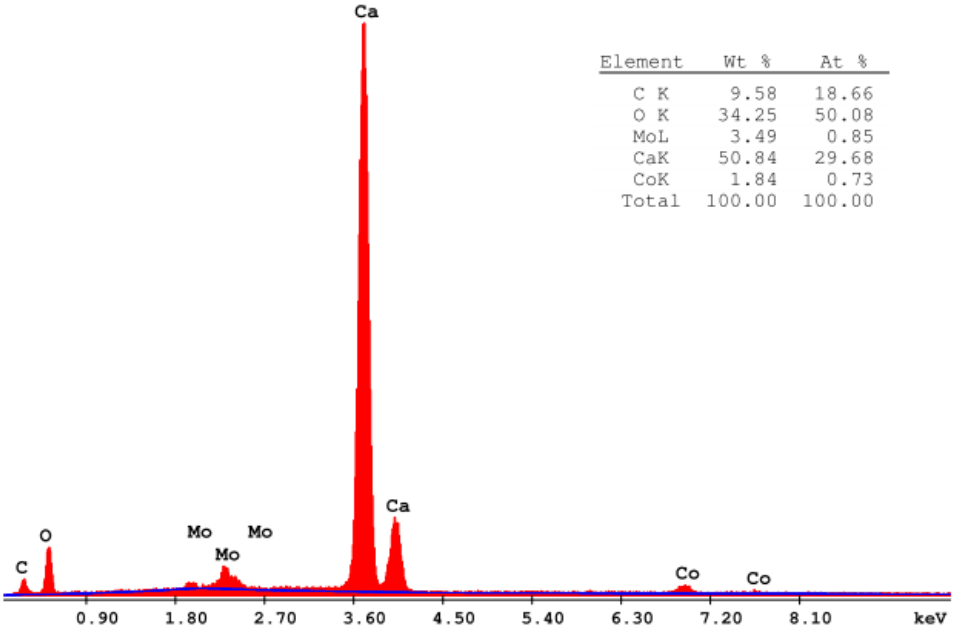


**Figure E.2** EDS spectrum of the catalyst with a Co:Mo ratio of 0.44 and a calcination temperature of 700˚C.

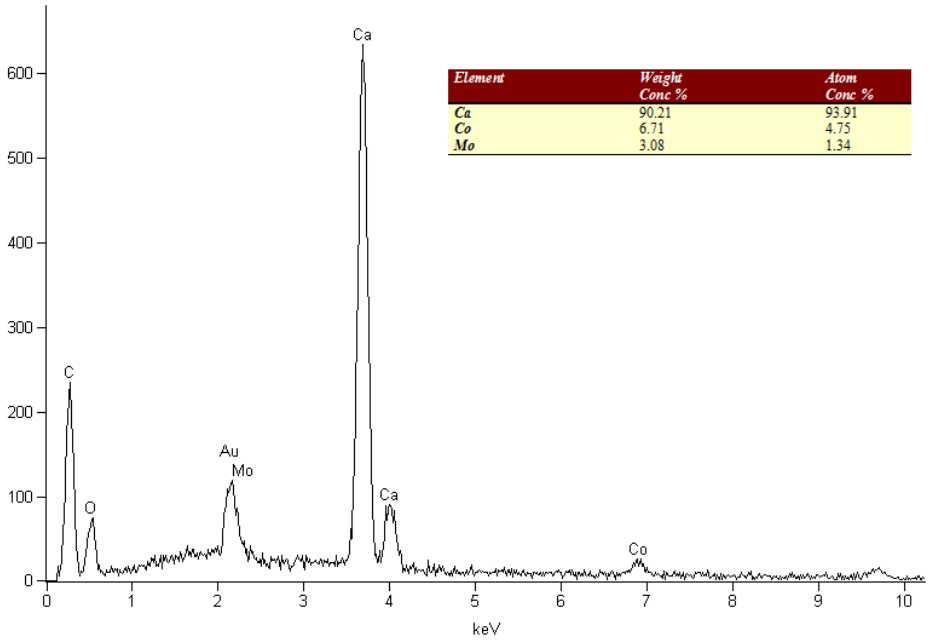


**Figure E.3** EDS spectrum of the catalyst with a Co:Mo ratio of 2.30 and a calcination temperature of 500˚C.

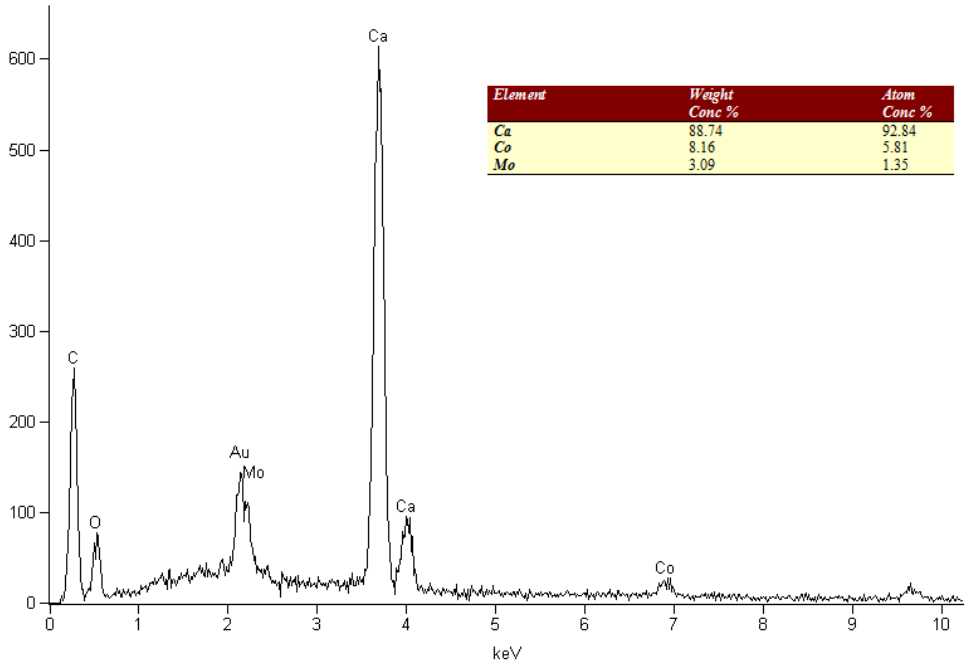


**Figure E.4** EDS spectrum of the catalyst with a Co:Mo ratio of 2.30 and a calcination temperature of 700˚C.

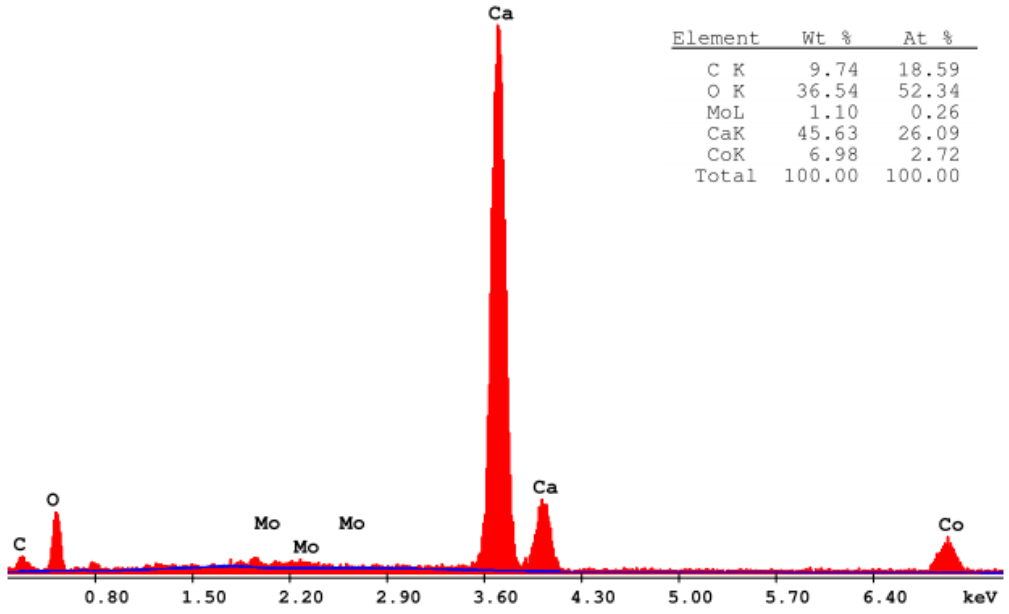


**Figure E.5** EDS spectrum of the catalyst with a Co:Mo ratio of 6 and a calcination temperature of 700˚C.

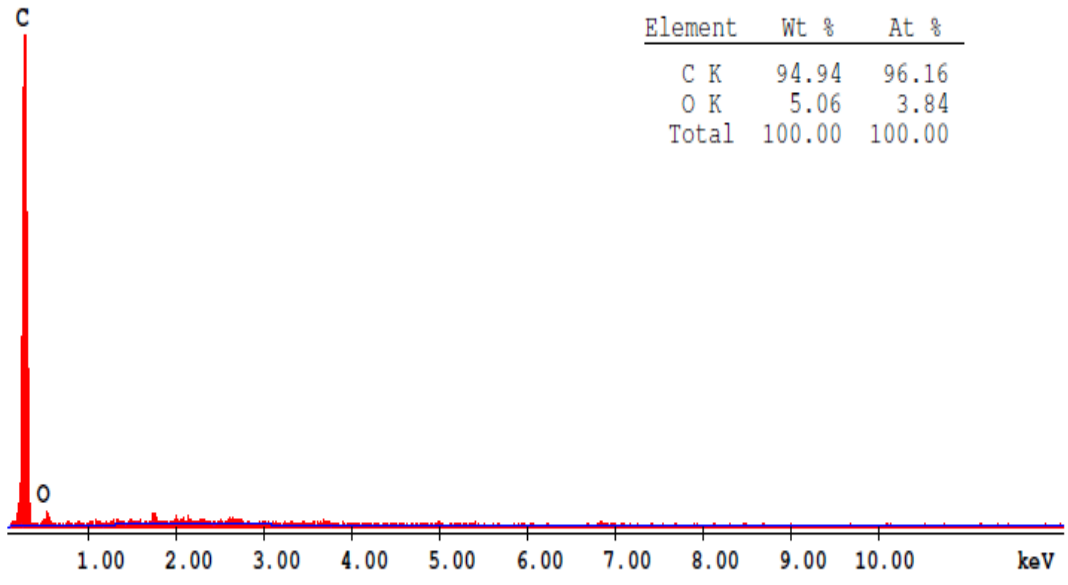


**Figure E.6** EDS spectrum of the carbon nanotubes produced at 600˚C over the catalyst with a Co:Mo ratio of 0.44 and a calcination temperature of 750˚C at an inlet $C_2H_2$ composition of 25% in Ar.

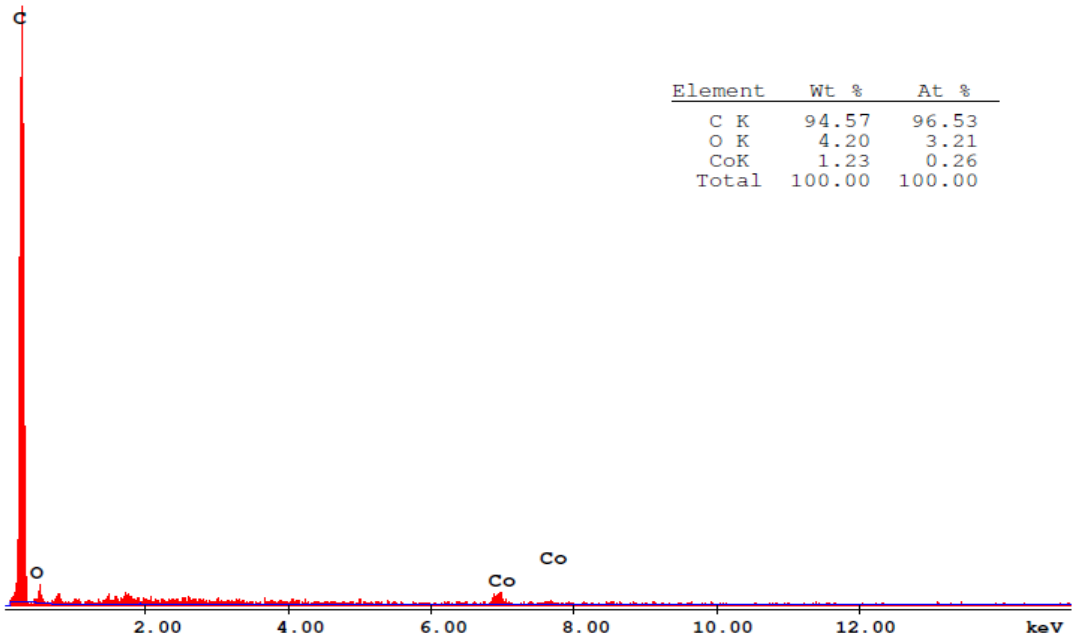


| Element | Wt % | At % |
|---|---|---|
| C K | 94.57 | 96.53 |
| O K | 4.20 | 3.21 |
| CoK | 1.23 | 0.26 |
| Total | 100.00 | 100.00 |

**Figure E.7** EDS spectrum of the carbon nanotubes produced at 500˚C over the catalyst with a Co:Mo ratio of 0.44 and a calcination temperature of 700˚C at an inlet $C_2H_2$ composition of 25% in Ar.

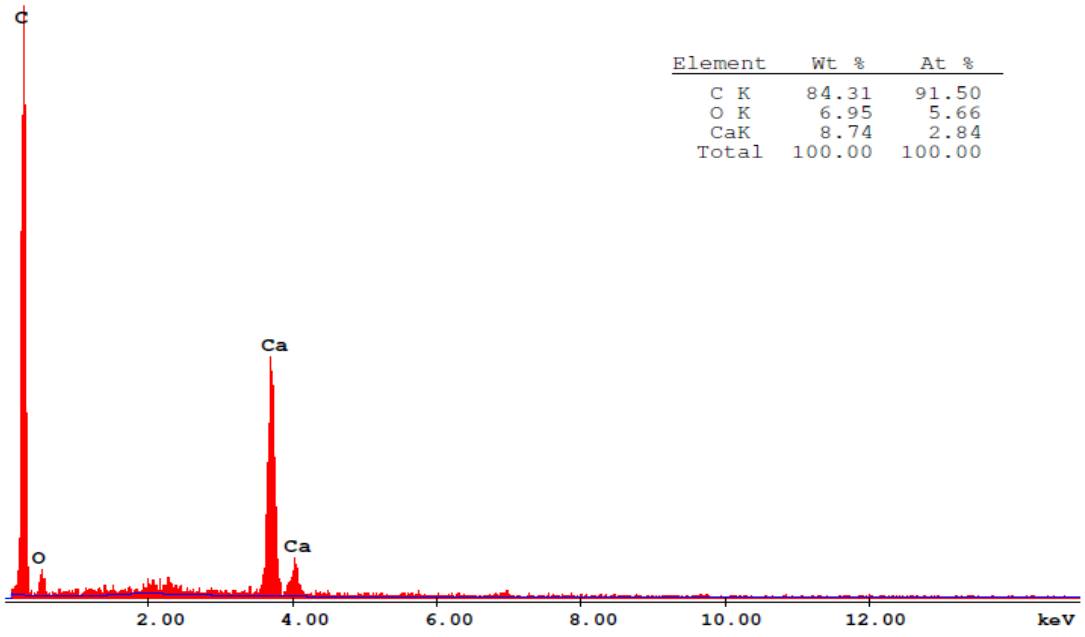


| Element | Wt % | At % |
|---|---|---|
| C K | 84.31 | 91.50 |
| O K | 6.95 | 5.66 |
| CaK | 8.74 | 2.84 |
| Total | 100.00 | 100.00 |

**Figure E.8** EDS spectrum of the carbon nanotubes produced at 700˚C over the catalyst with a Co:Mo ratio of 0.44 and a calcination temperature of 500˚C at an inlet $C_2H_2$ composition of 25% in Ar.

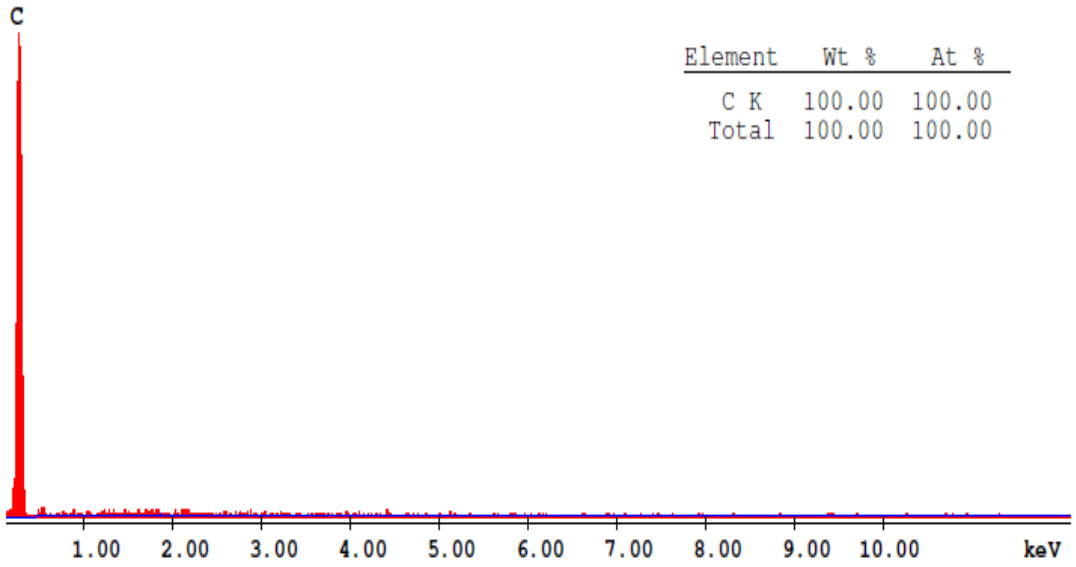


**Figure E.9** EDS spectrum of the carbon nanotubes produced at 500˚C over the catalyst with a Co:Mo ratio of 2.30 and a calcination temperature of 750˚C at an inlet $C_2H_2$ composition of 25% in Ar.

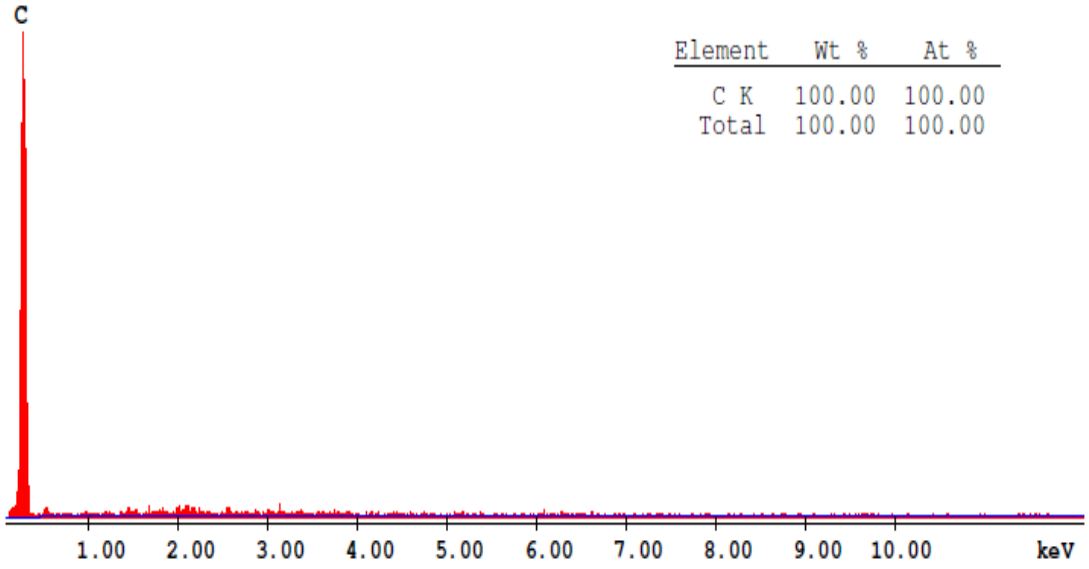


**Figure E.10** EDS spectrum of the carbon nanotubes produced at 600˚C over the catalyst with a Co:Mo ratio of 2.30 and a calcination temperature of 750˚C at an inlet $C_2H_2$ composition of 25% in Ar.

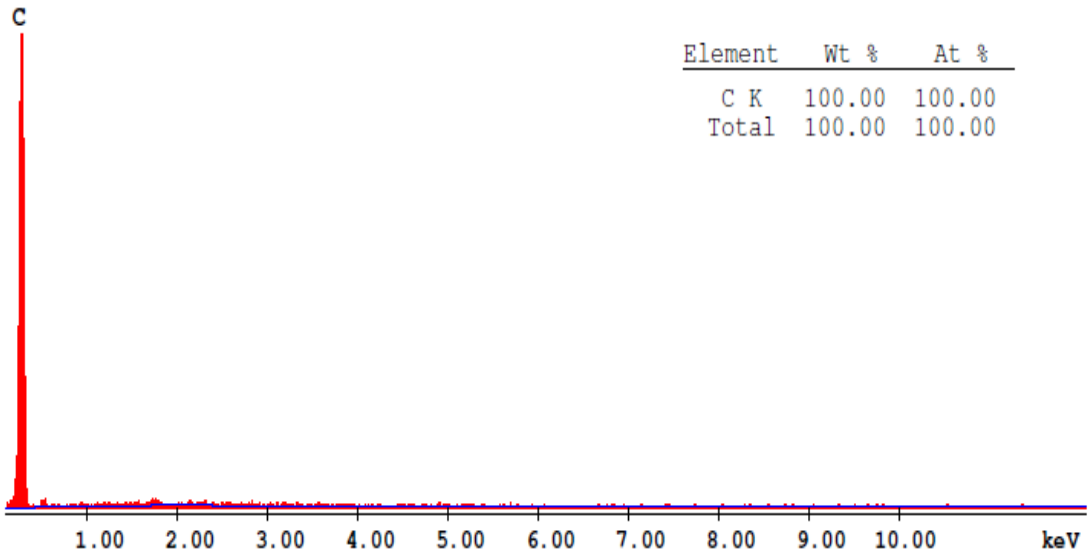


**Figure E.11** EDS spectrum of the carbon nanotubes produced at 650˚C over the catalyst with a Co:Mo ratio of 2.30 and a calcination temperature of 750˚C at an inlet $C_2H_2$ composition of 25% in Ar.

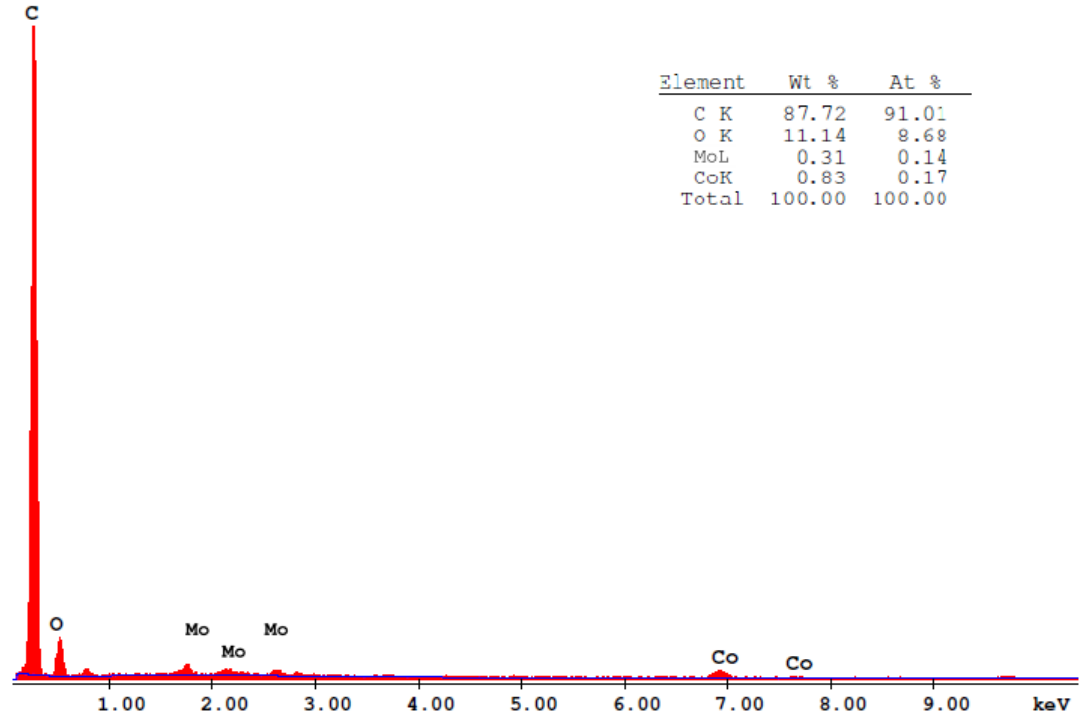


**Figure E.12** EDS spectrum of the carbon nanotubes produced at 500˚C over the catalyst with a Co:Mo ratio of 6 and a calcination temperature of 750˚C at an inlet $C_2H_2$ composition of 25% in Ar.

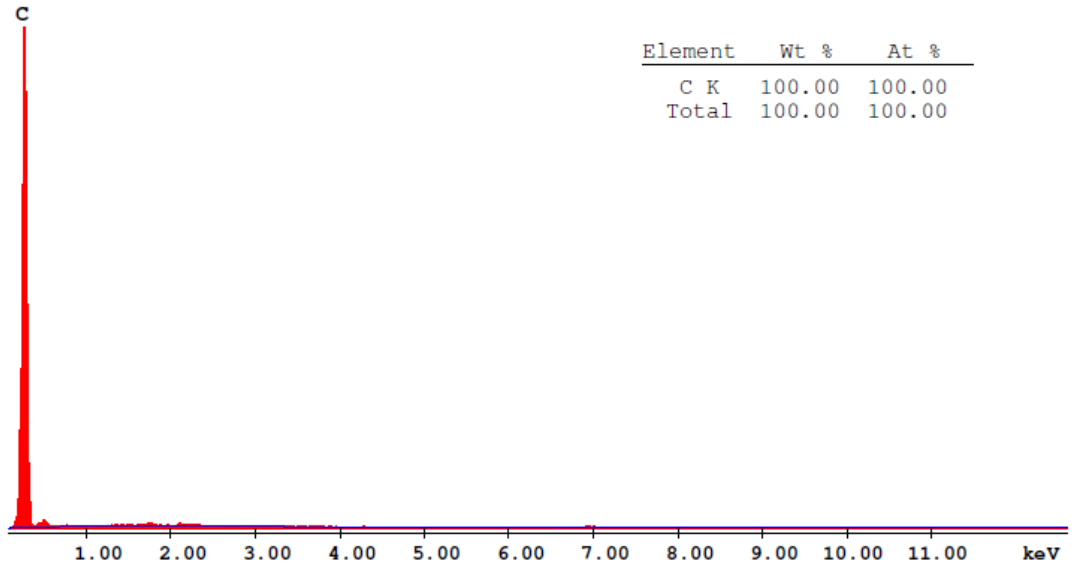


**Figure E.13** EDS spectrum of the carbon nanotubes produced at 700˚C over the catalyst with a Co:Mo ratio of 6 and a calcination temperature of 750˚C at an inlet $C_2H_2$ composition of 20% in Ar.

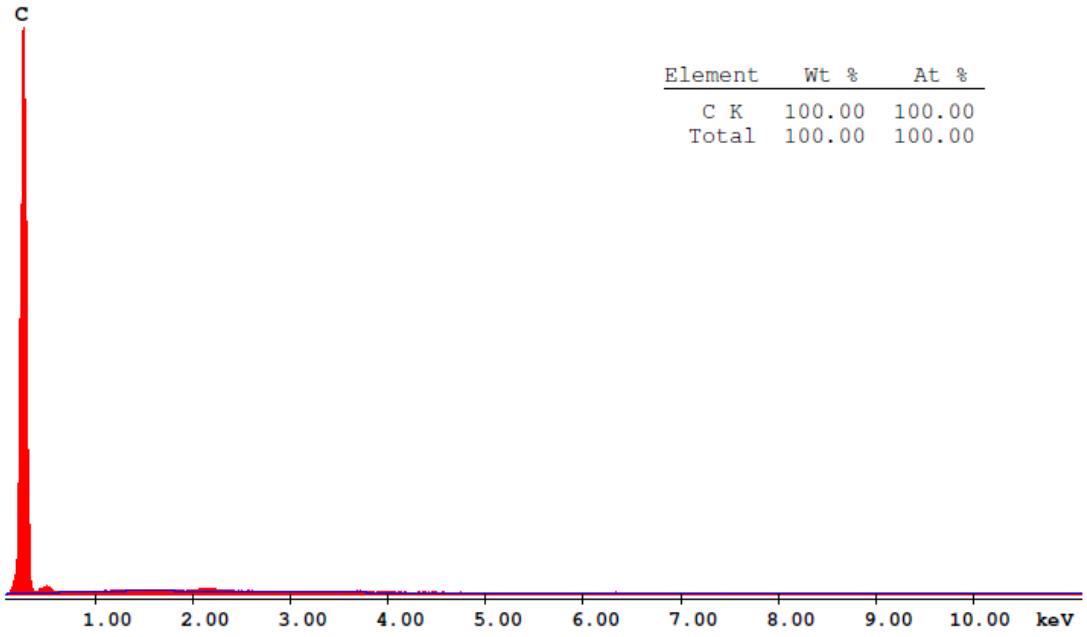


**Figure E.14** EDS spectrum of the carbon nanotubes produced at 700˚C over the catalyst with a Co:Mo ratio of 6 and a calcination temperature of 750˚C at an inlet $C_2H_2$ composition of 30% in Ar.

# APPENDIX F

# X-RAY PHOTOELECTRON SPECTROSCOPY

X-ray photoelectron spectroscopy (XPS) is a quantitative surface chemical analysis technique used to obtain the elemental composition of the surface (top 1-10 nm) chemical and electronic state of the elements present at the surface of the material.

To investigate the chemical composition of surfaces X-ray photons are used as the primary beam. In this technique, the material to be analyzed is irradiated by a beam of X-rays. At the same time, the kinetic energy of collected electrons and the number of electrons escaping from the surface of the material are measured [52].

Each element has a unique binding energy which is used to identify the elemental composition of the sample. Binding energies which are experimentally determined are characteristics of specific elements. Therefore these energies are used for the identification of the characteristic peaks belonging to a material with unknown elemental composition. Hence, the presence of a specific element within the material is proved by the presence of peaks at specific energies. Moreover, the concentration of the element is associated with the intensity of the peaks which provides a quantitative analysis of the surface composition. Additionally, XPS also distinguishes different chemical bonding configurations as well as different elements [52].

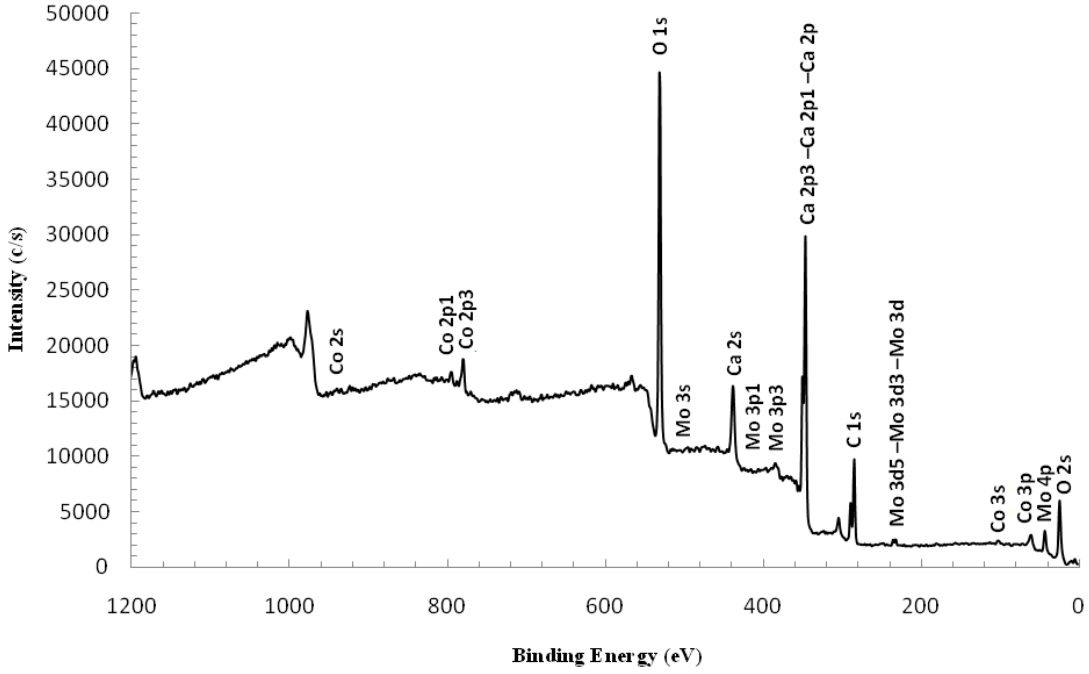


**Figure F.1** XPS spectrum of the catalyst with a Co:Mo ratio of 2.30 and a calcination temperature of 700˚C.

# APPENDIX G

## SEM IMAGES OF THE SYNTHESIZED CNTS

SEM is one of the most widely used analysis technique in academic and industrial areas since it provides rapid and high-resolution imaging with extreme details. It is a crucial technique for the investigation and the analysis of nanomaterials due to its capability of direct imaging, It is commonly used because of its versatility, its various modes of imaging, easy sample preparation, and easy interpretation of the images. SEM which utilizes secondary electrons and back-scattered electrons to investigate the sample is useful for imaging the surface and subsurface of micro- and nanostructures. Moreover, morphological properties of carbon nanotubes can be studied using SEM [52, 53]. SEM images of CNTs grown over Co-Mo/$CaCO_3$ catalysts are given in Figure G.1-G.16.

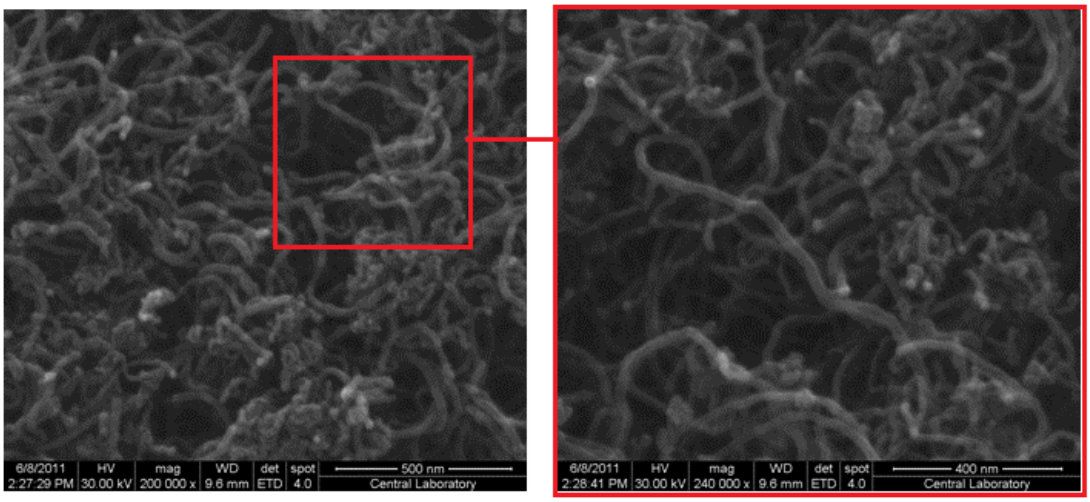


(a) (b)

**Figure G.1** SEM images of CNTs grown over the catalyst with a Co:Mo ratio of 0.44 and a calcination temperature of 700˚C at a synthesis temperature of 500˚C at an inlet acetylene composition of 25% in argon (a) 200,000x magnification (b) 240,000x magnification.

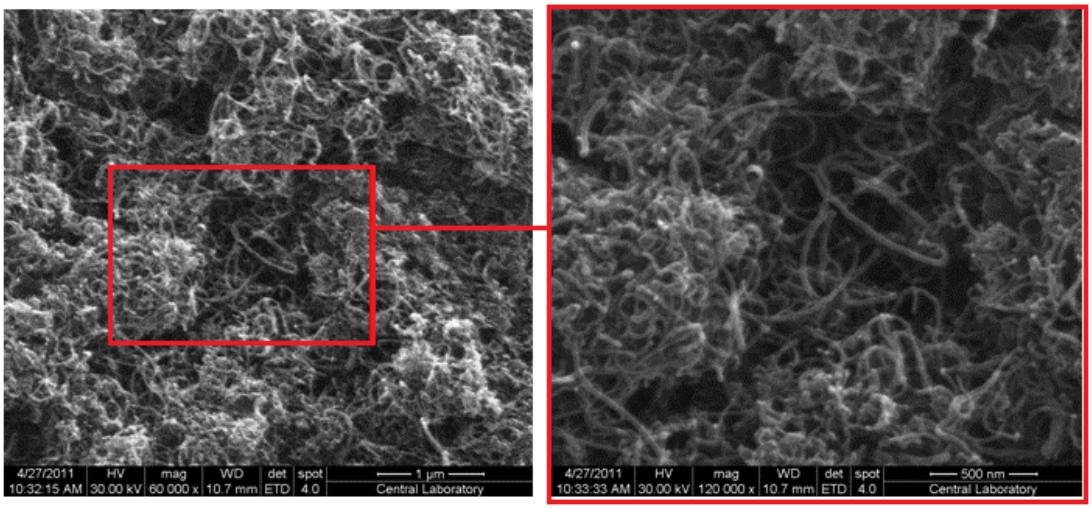


(a) (b)

**Figure G.2** SEM images of CNTs grown over the catalyst with a Co:Mo ratio of 0.44 and a calcination temperature of 700˚C at a synthesis temperature of 600˚C at an inlet acetylene composition of 25% in argon (a) 60,000x magnification (b) 120,000x magnification.

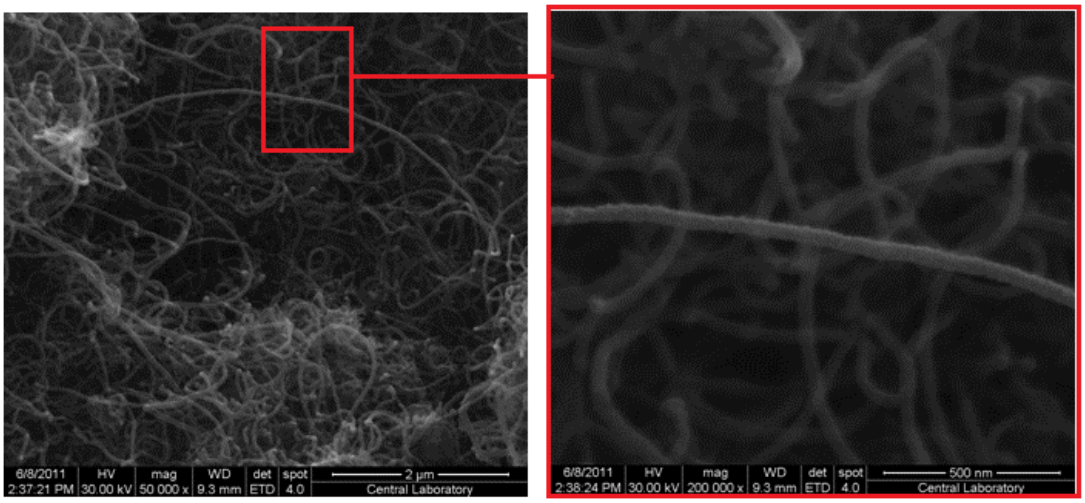


(a) (b)

**Figure G.3** SEM images of CNTs grown over the catalyst with a Co:Mo ratio of 0.44 and a calcination temperature of 700˚C at a synthesis temperature of 650˚C at an inlet acetylene composition of 25% in argon (a) 50,000x magnification (b) 200,000x magnification.

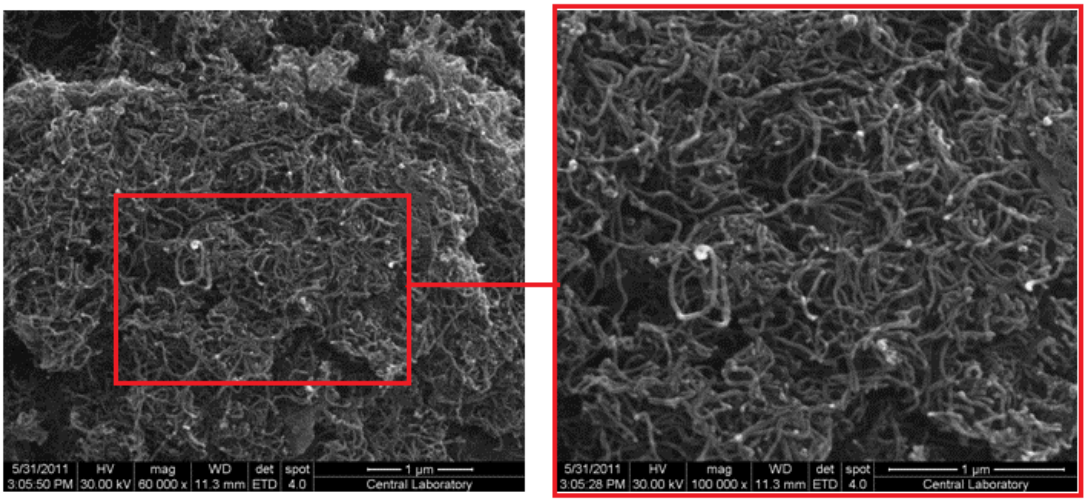


(a) (b)

**Figure G.4** SEM images of CNTs grown over the catalyst with a Co:Mo ratio of 2.30 and a calcination temperature of 750˚C at a synthesis temperature of 500˚C at an inlet acetylene composition of 25% in argon (a) 60,000x magnification (b) 100,000x magnification.

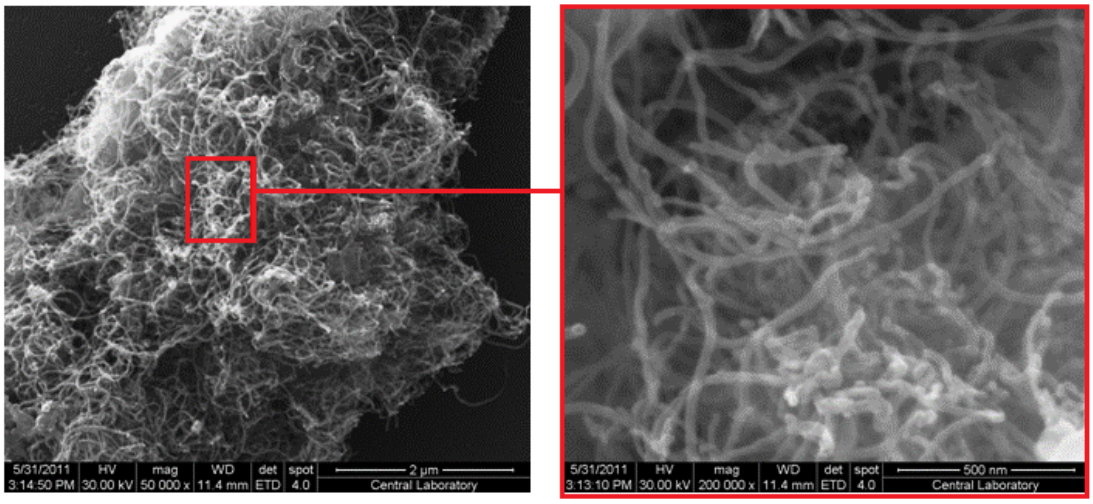


(a) (b)

**Figure G.5** SEM images of CNTs grown over the catalyst with a Co:Mo ratio of 2.30 and a calcination temperature of 750˚C at a synthesis temperature of 600˚C at an inlet acetylene composition of 25% in argon (a) 50,000x magnification (b) 200,000x magnification.

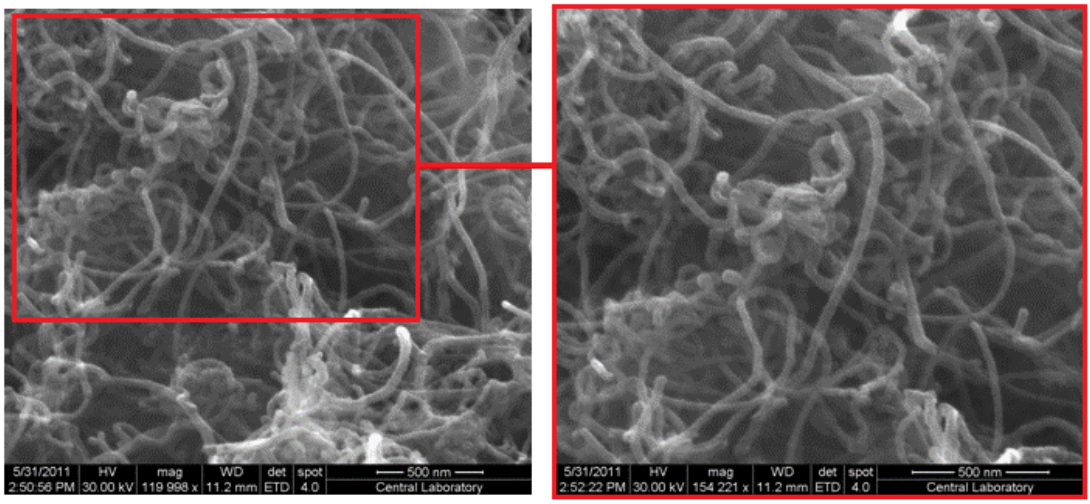


(a) (b)

**Figure G.6** SEM images of CNTs grown over the catalyst with a Co:Mo ratio of 2.30 and a calcination temperature of 750˚C at a synthesis temperature of 650˚C at an inlet acetylene composition of 25% in argon (a) 120,000x magnification (b) 154,000x magnification.

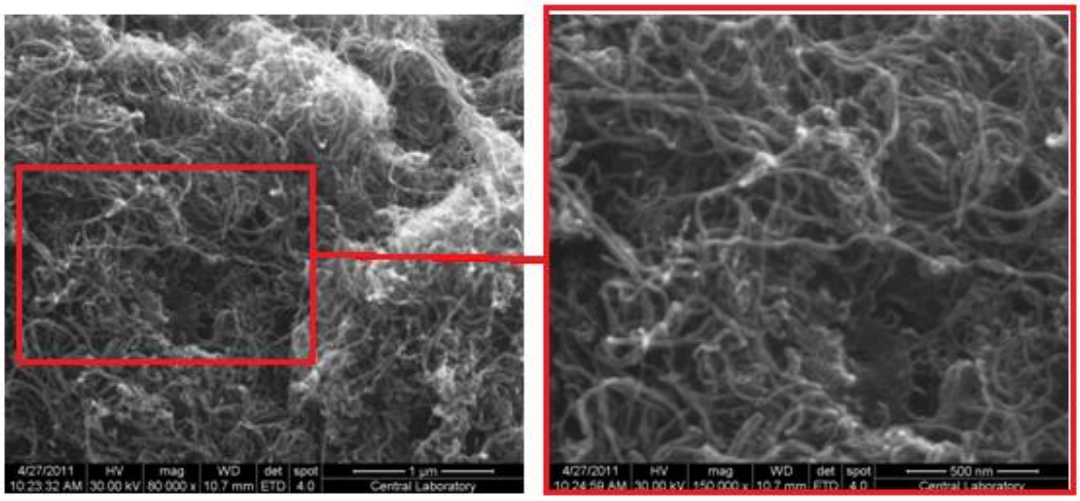

(a) (b)

**Figure G.7** SEM images of CNTs grown over the catalyst with a Co:Mo ratio of 2.30 and a calcination temperature of 700˚C at a synthesis temperature of 500˚C at an inlet acetylene composition of 25% in argon (a) 80,000x magnification (b) 150,000x magnification.

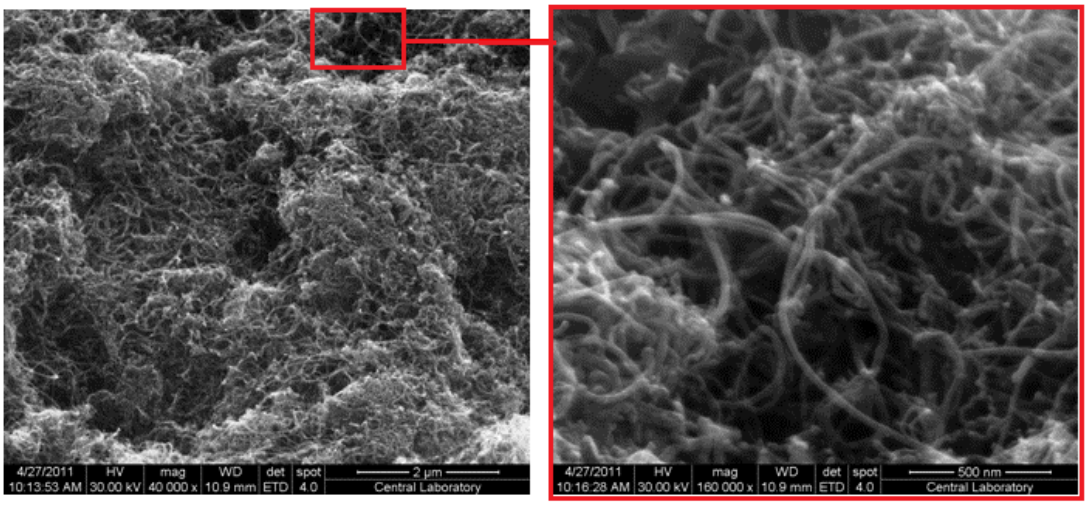

(a) (b)

**Figure G.8** SEM images of CNTs grown over the catalyst with a Co:Mo ratio of 2.30 and a calcination temperature of 700˚C at a synthesis temperature of 600˚C at an inlet acetylene composition of 25% in argon (a) 40,000x magnification (b) 160,000x magnification.

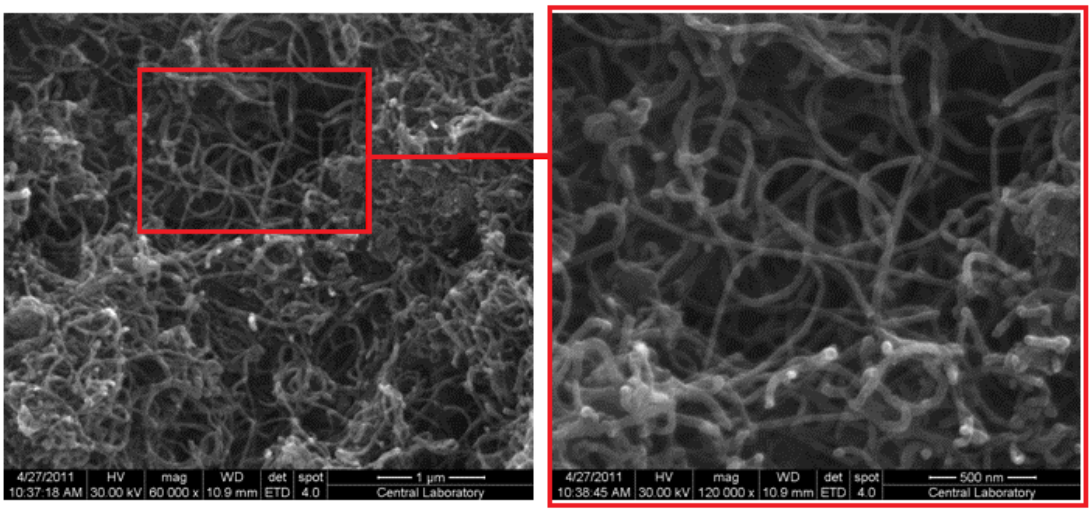


(a) (b)

**Figure G.9** SEM images of CNTs grown over the catalyst with a Co:Mo ratio of 2.30 and a calcination temperature of 700˚C at a synthesis temperature of 650˚C at an inlet acetylene composition of 25% in argon (a) 60,000x magnification (b) 120,000x magnification.

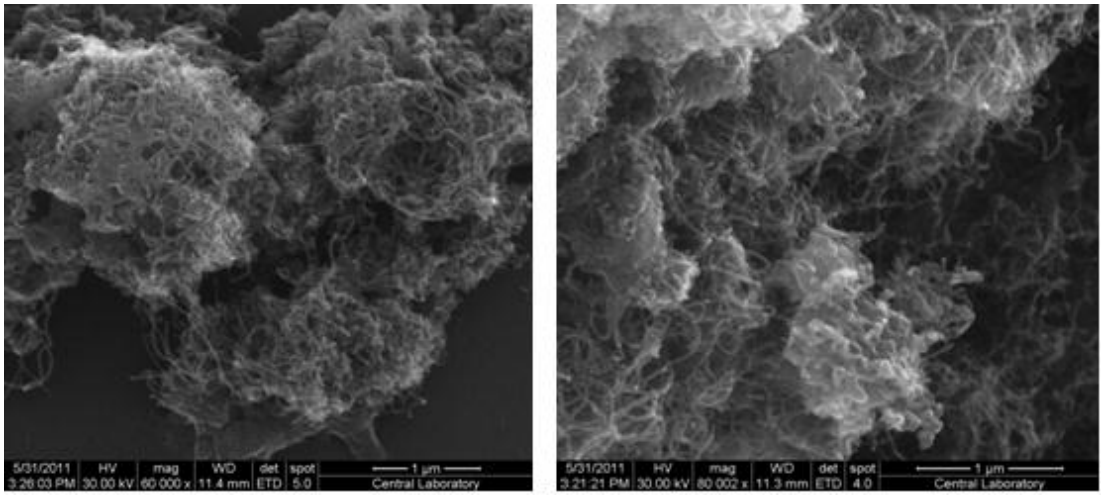


(a) (b)

**Figure G.10** SEM images of CNTs grown over the catalyst with a Co:Mo ratio of 6 and a calcination temperature of 750˚C at a synthesis temperature of 500˚C at an inlet acetylene composition of 25% in argon (a) 60,000x magnification (b) 80,000x magnification.

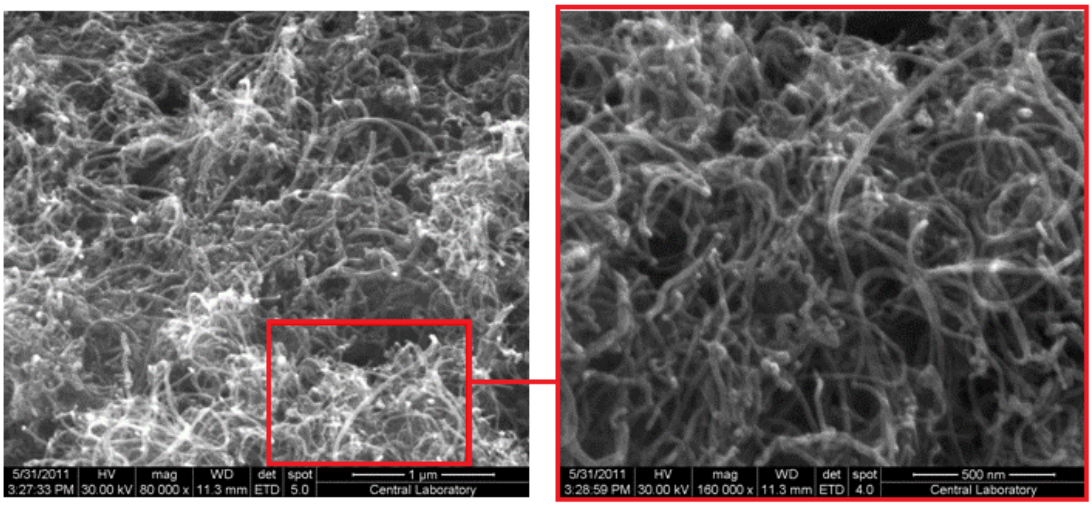


(a) (b)

**Figure G.11** SEM images of CNTs grown over the catalyst with a Co:Mo ratio of 6 and a calcination temperature of 750˚C at a synthesis temperature of 600˚C at an inlet acetylene composition of 25% in argon (a) 80,000x magnification (b) 160,000x magnification.

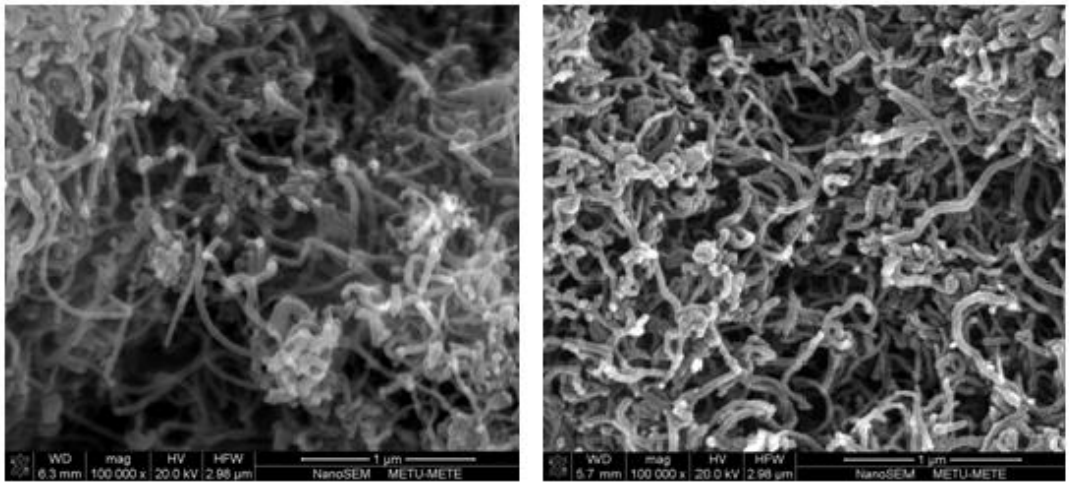


(a) (b)

**Figure G.12** SEM images of CNTs grown over the catalyst with a Co:Mo ratio of 6 and a calcination temperature of 750˚C at a synthesis temperature of 650˚C at an inlet acetylene composition of 25% in argon (a) 100,000x magnification (b) 100,000x magnification.

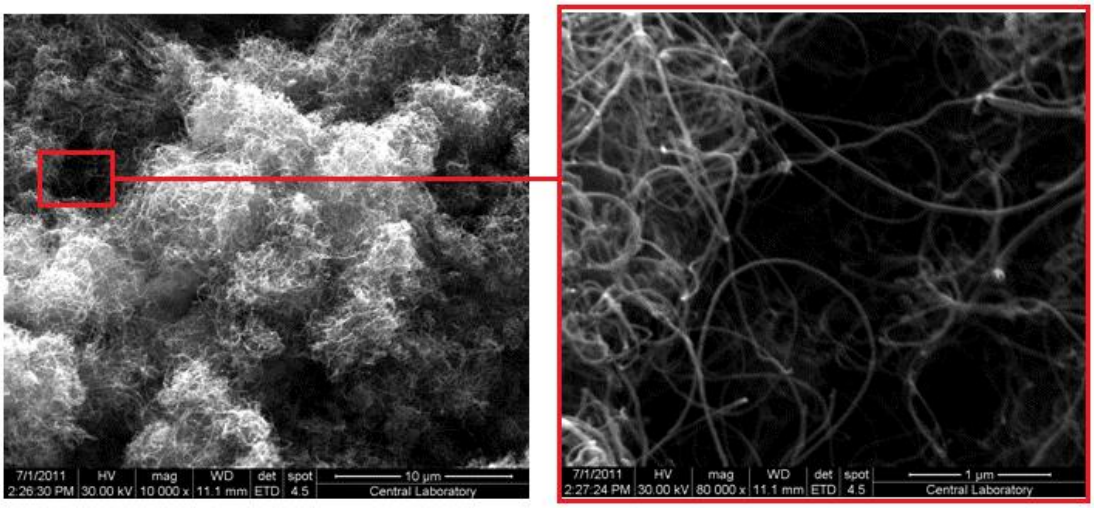


(a) (b)

**Figure G.13** SEM images of CNTs grown over the catalyst with a Co:Mo ratio of 6 and a calcination temperature of 750˚C at a synthesis temperature of 700˚C at an inlet acetylene composition of 10% in argon (a) 10,000x magnification (b) 80,000x magnification.

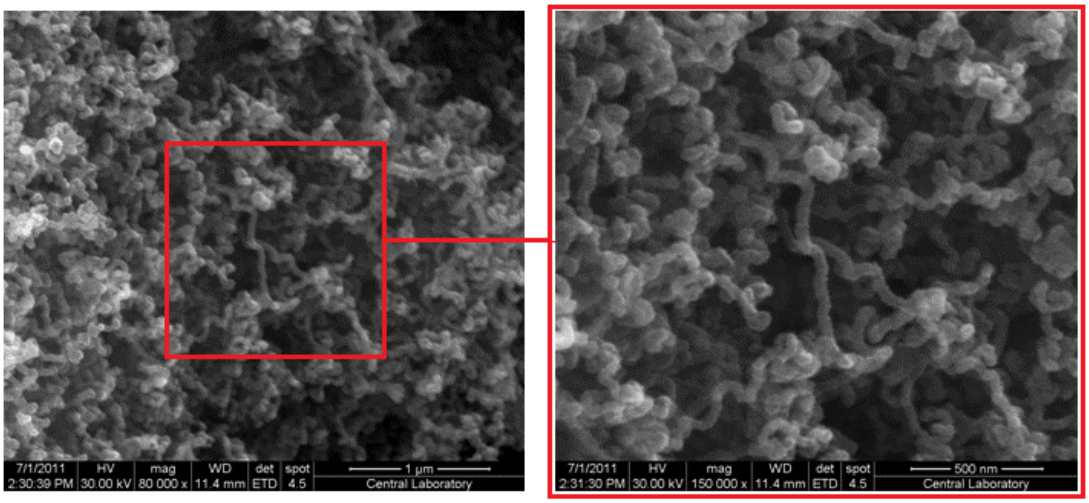


(a) (b)

**Figure G.14** SEM images of CNTs grown over the catalyst with a Co:Mo ratio of 6 and a calcination temperature of 750˚C at a synthesis temperature of 700˚C at an inlet acetylene composition of 15% in argon (a) 80,000x magnification (b) 150,000x magnification.

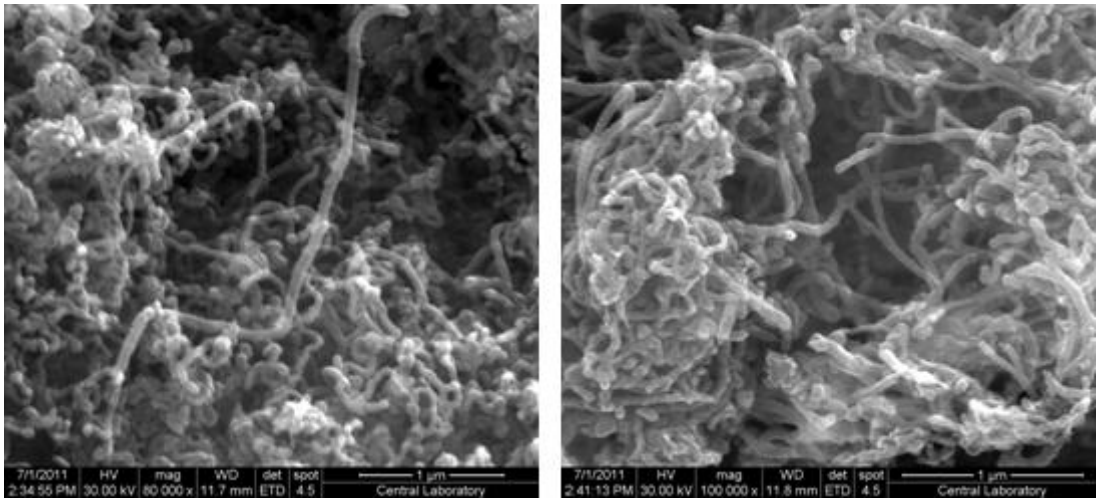


(a) (b)

**Figure G.15** SEM images of CNTs grown over the catalyst with a Co:Mo ratio of 6 and a calcination temperature of 750˚C at a synthesis temperature of 700˚C at an inlet acetylene composition of 20% in argon (a) 80,000x magnification (b) 100,000x magnification.

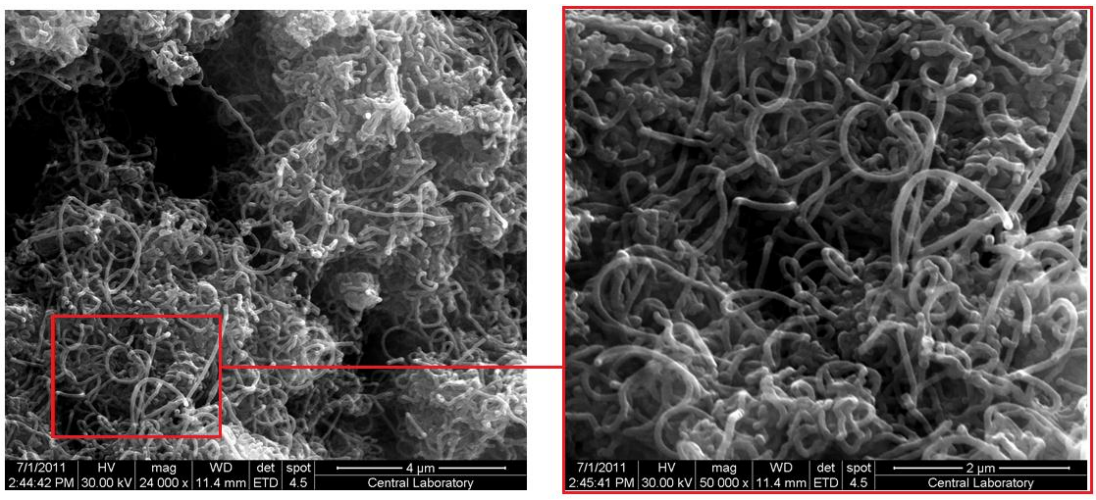


(a) (b)

**Figure G.16** SEM images of CNTs grown over the catalyst with a Co:Mo ratio of 6 and a calcination temperature of 750˚C at a synthesis temperature of 700˚C at an inlet acetylene composition of 30% in argon (a) 24,000x magnification (b) 50,000x magnification.

# APPENDIX H

# EXPERIMENTAL DATA FOR CNT PRODUCTION

## H.1 Experimental Data of CNT Synthesis

**Table H.1.1** Product weights after CNT synthesis experiment

| **Catalyst Co:Mo wt. ratio** | **$T_{cal}$ (˚C)** | **$T_{rxn}$ (˚C)** | **$C_2H_2$ composition in Ar (%)** | **$W_{products}$ (g)** |
|---|---|---|---|---|
| 0.44 | 500 | 700 | 25 | 0.0246 |
| 0.44 | 700 | 500 | 25 | 0.0646 |
| 0.44 | 700 | 600 | 25 | 0.0760 |
| 0.44 | 700 | 650 | 25 | 0.0825 |
| 0.44 | 700 | 700 | 25 | 0.0591 |
| 0.44 | 750 | 500 | 25 | 0.0728 |
| 0.44 | 750 | 600 | 25 | 0.0848 |
| 0.44 | 750 | 700 | 25 | 0.2932 |
| 2.30 | 500 | 700 | 25 | 0.2756 |
| 2.30 | 700 | 500 | 25 | 0.0674 |
| 2.30 | 700 | 600 | 25 | 0.2003 |
| 2.30 | 700 | 650 | 25 | 0.4818 |
| 2.30 | 700 | 700 | 25 | 0.4183 |

**Table H.1.1** Product weights after CNT synthesis experiment (cont'd)

| **Catalyst Co:Mo wt. ratio** | **$T_{cal}$ (˚C)** | **$T_{rxn}$ (˚C)** | **$C_2H_2$ composition in Ar (%)** | **$W_{products}$ (g)** |
|---|---|---|---|---|
| 2.30 | 750 | 500 | 25 | 0.0644 |
| 2.30 | 750 | 600 | 25 | 0.0478 |
| 2.30 | 750 | 650 | 25 | 0.5034 |
| 2.30 | 750 | 700 | 25 | 0.531 |
| 6 | 500 | 700 | 25 | 0.267 |
| 6 | 700 | 700 | 25 | 0.6474 |
| 6 | 750 | 500 | 25 | 0.0928 |
| 6 | 750 | 600 | 25 | 0.3652 |
| 6 | 750 | 650 | 25 | 0.6876 |
| 6 | 750 | 700 | 25 | 0.7629 |
| 6 | 750 | 700 | 25 | 0.7543 |
| 6 | 750 | 700 | 10 | 0.2543 |
| 6 | 750 | 700 | 15 | 0.2899 |
| 6 | 750 | 700 | 20 | 0.3408 |
| 6 | 750 | 700 | 30 | 1.0298 |

## H.2 Blank Experimental Data

**Table H.2.1** Weights of the catalysts after the blank experiment

| **Co:Mo wt. ratio** | **$T_{cal}$(˚C)** | **$T_{rxn}$ (˚C)** | **$W_{catalyst}$ (g)** |
|---|---|---|---|
| 0.44 | 500 | 700 | 0.0284 |
| 0.44 | 700 | 600 | 0.0319 |
| 0.44 | 700 | 700 | 0.0280 |
| 0.44 | 750 | 600 | 0.0324 |
| 0.44 | 750 | 700 | 0.0295 |
| 2.30 | 500 | 700 | 0.0291 |
| 2.30 | 700 | 600 | 0.0340 |
| 2.30 | 700 | 700 | 0.0313 |
| 2.30 | 750 | 600 | 0.0329 |
| 2.30 | 750 | 700 | 0.0303 |
| 6 | 500 | 700 | 0.0287 |
| 6 | 700 | 700 | 0.0306 |
| 6 | 750 | 600 | 0.0336 |
| 6 | 750 | 700 | 0.0278 |

# APPENDIX I

## TEM IMAGES OF THE SYNTHESIZED CNTS

Transmission electron microscope is an important electron microscopic technique in which transmitted electrons are used to obtain an image of the sample. It is a useful tool for direct imaging the internal microstructure of ultrathin specimens. In addition to extraordinary image resolution TEM also provides the characterization of crystallographic phase and crystallographic orientation. Moreover, elemental maps and images highlighting elemental contrast are possible at EDS mode and dark field mode, respectively [53].

TEM is powerful technique to gain information about the morphology of CNTs, the diameters, the number of walls, and the distance between the walls. It is possible to determine the structure, size, and shape of nanotubes with the help of the TEM [20]. The inner cavity of carbon nanotubes is also observed by TEM. Hence, it is also used to distinguish carbon nanotubes from other carbonaceous products (e.g. carbon particles and nanofibers).

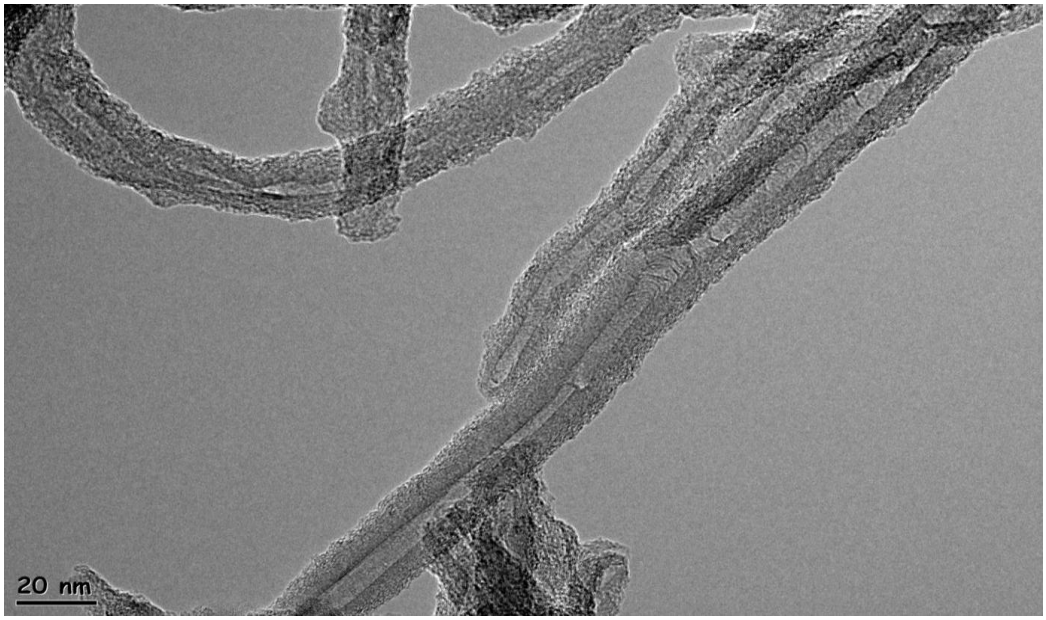


(a)

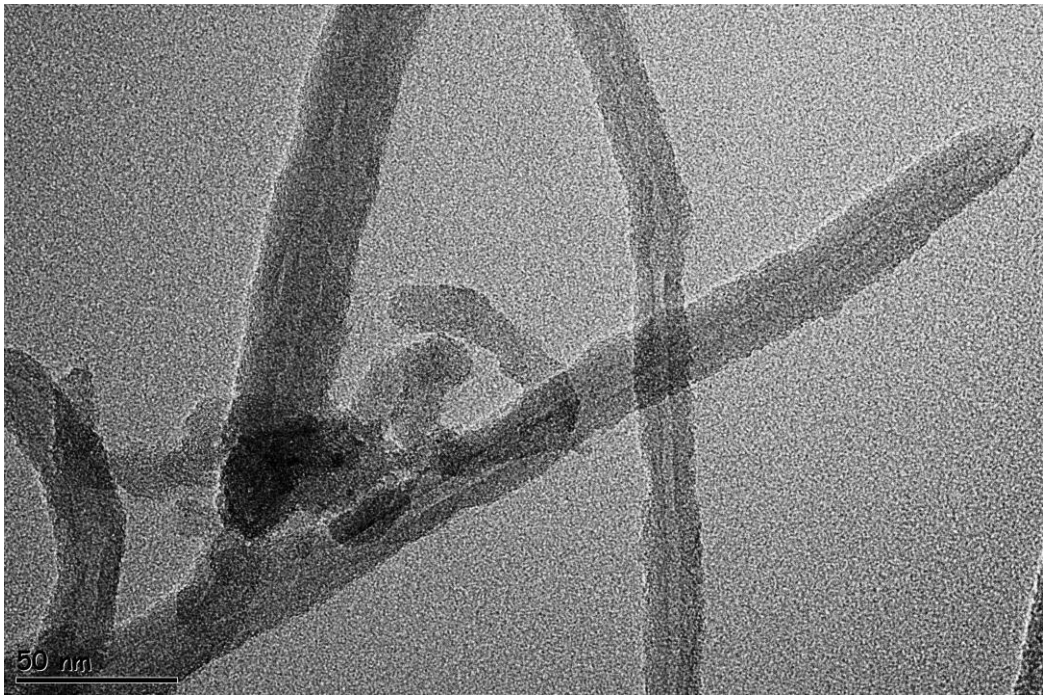


(b)

**Figure I.1** TEM image of purified CNT bundles grown at 600˚C over the catalyst with a Co:Mo ratio of 6 and a calcination temperature of 750˚C at different magnifications (a) & (b).

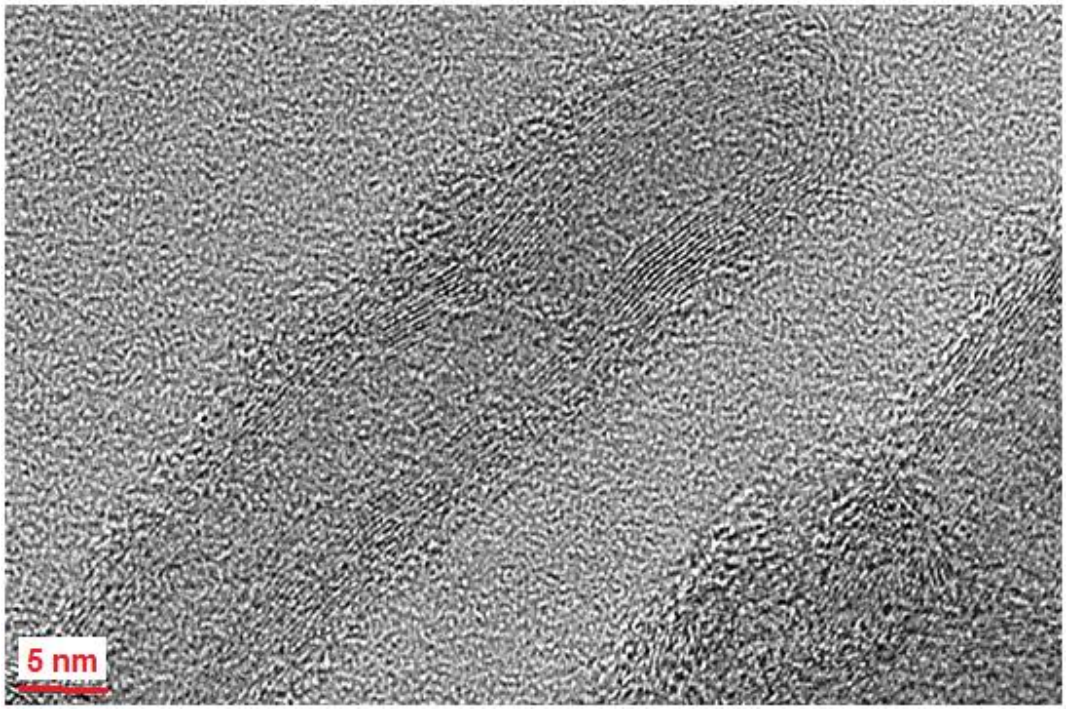


**Figure I.2** High Resolution TEM image of a closed-tip CNT grown at 600˚C over the catalyst with a Co:Mo ratio of 6 and a calcination temperature of 750˚C.

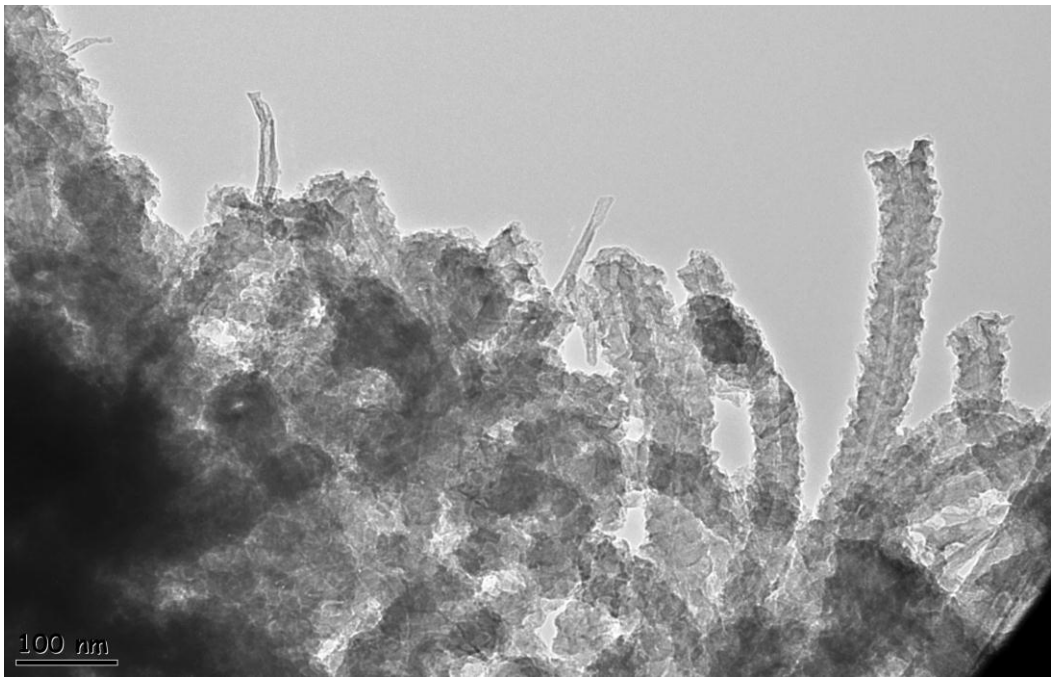


**Figure I.3** High Resolution TEM image of CNTs grown at 700˚C over the catalyst with a Co:Mo ratio of 6 and a calcination temperature of 750˚C.

# APPENDIX J

## RAMAN SPECTROSCOPY

Raman spectroscopy is used for the determination of the chemical structure of a sample and for the identification of the compounds. Raman spectroscopy is a fast, simple, sensitive, and non-destructive analysis and does not require a sample preparation. Raman provides both qualitative and quantitative analyses.

Raman is based on the inelastic scattering of monochromatic light which is generally from a laser source in the visible, near infrared, or near ultraviolet range. The basis of Raman spectroscopy is the measuring molecular vibrations which are specific to the chemical bonds and symmetry of molecules. Hence, it provides a fingerprint used for the identification of a molecule. Qualitative analysis is performed by spectral library searching because of the fact that Raman spectra are unique for each molecule. On the other hand, the measure of the relative intensities of bands which are directly proportional to the relative concentrations of the compounds can provide quantitative analysis of a mixture [20].

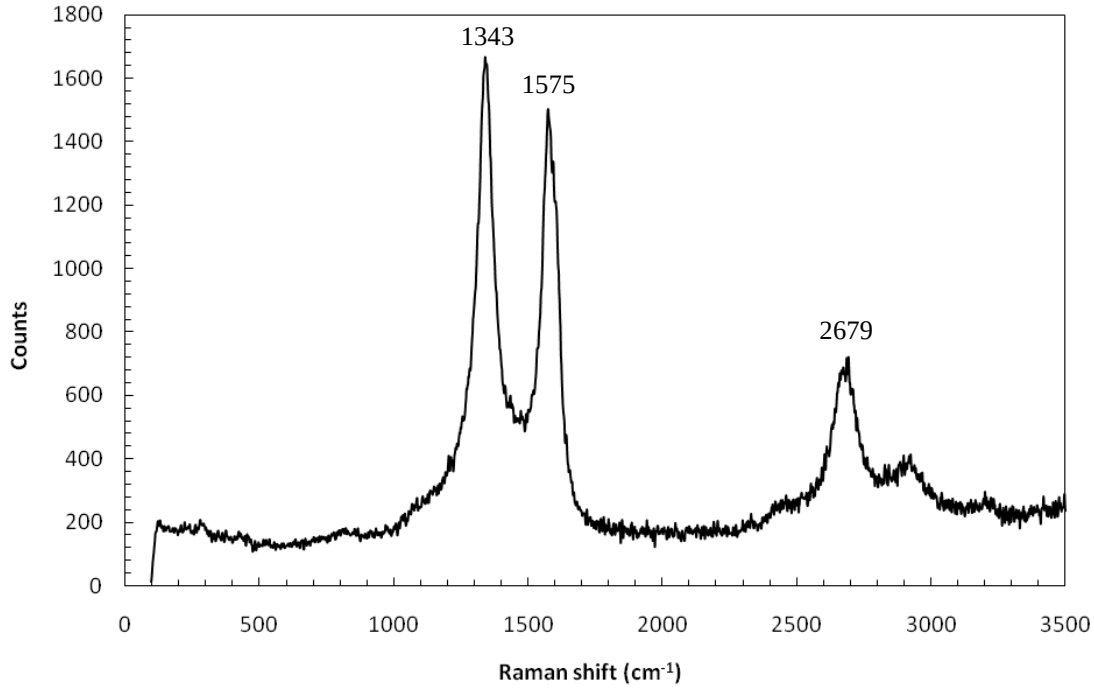


**Figure J.1** Raman spectrum of the MWNTs produced at 600˚C on the catalyst with a Co:Mo ratio of 6 and a calcination temperature of 750˚C (25% $C_2H_2$ in Ar)**.**

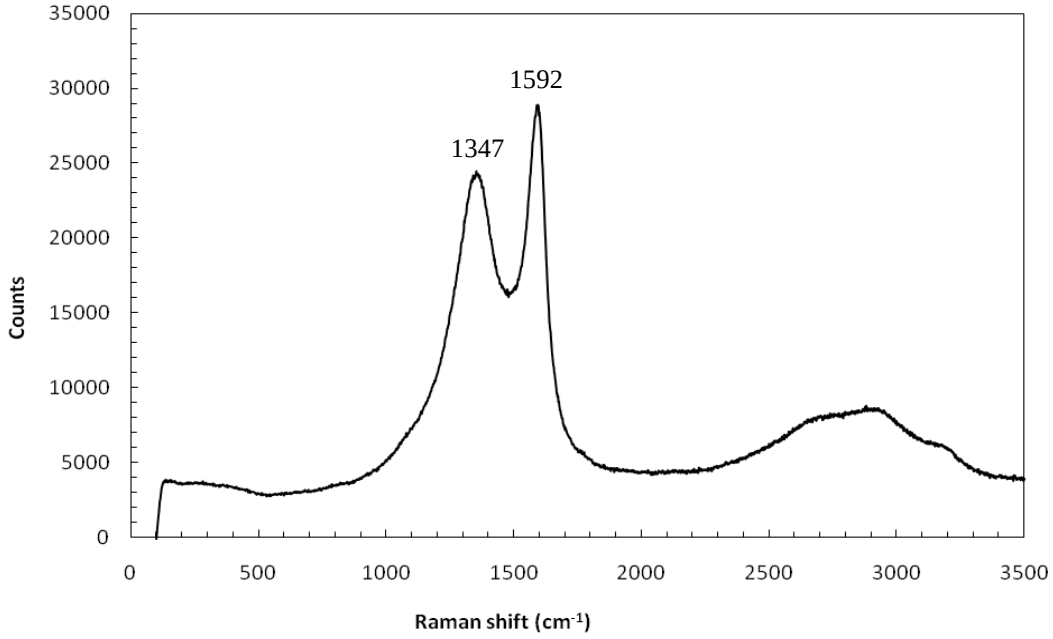


**Figure J.2** Raman spectrum of the MWNTs produced at 500˚C on the catalyst with a Co:Mo ratio of 6 and a calcination temperature of 750˚C (25% $C_2H_2$ in Ar).

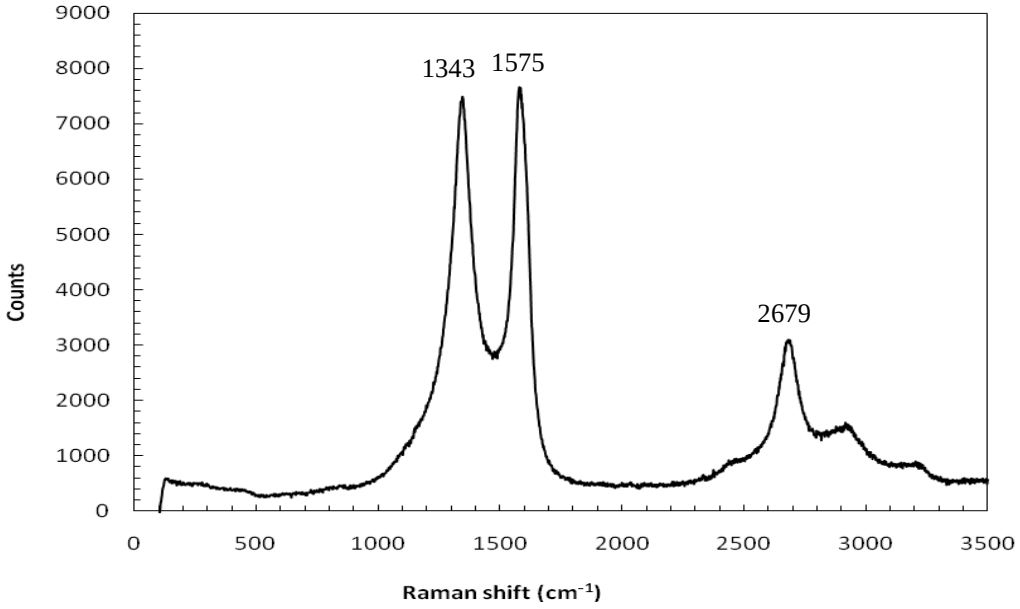


**Figure J.3** Raman spectrum of the MWNTs produced at 700˚C on the catalyst with a Co:Mo ratio of 2.30 and a calcination temperature of 750˚C (25% $C_2H_2$ in Ar).

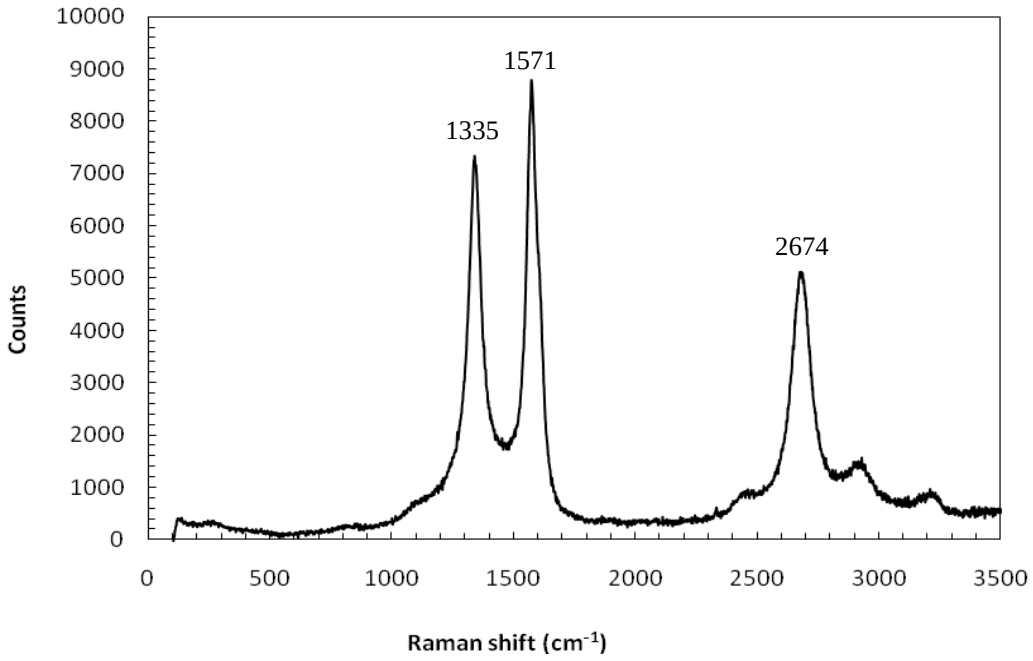


**Figure J.4** Raman spectrum of the MWNTs produced at 700˚C and at an acetylene concentration of 10% on the catalyst with a Co:Mo ratio of 6 and a calcination temperature of 750˚C.